Array-Based Vapor Sensing Using Conductive Carbon Black-Polymer Composite Thin Film Detectors

Thesis by

Erik J. Severin

In Partial Fulfillment of the Requirements

for the Degree of

Doctor of Philosophy

California Institute of Technology

Pasadena, California

1999

(Submitted May 28, 1999)

Acknowledgments

"I may not have gone where I intended to go, but I think I have ended up where I intended to be" - Douglas Adams

There are many people who have helped me finish this thesis, either by giving me moral encouragement, professional advice, or helping to perform experiments. In particular, I have had a few key mentors who have guided me along this path. First, I need to acknowledge Mrs. Leslie Warner, my high school English teacher and drama coach, for recognizing in me a potential that I thought only I could see. She was the first teacher who believed in my ability to excel, and her reaffirmation of my potential was a great boost. Thanks Mrs. Warner! Another person who was instrumental to my success was Professor Fred Stocker, my college advisor and organic chemistry professor at Macalester College (St. Paul, MN). Like Mrs. Warner, his belief in me and assumption that I would do well, kept me striving to produce my best work. He was the first person to encourage me to apply for graduate school, and, in particular, schools of Caltech's caliber. I owe my attendance here to Dr. Stocker because he believed in me when I did not. Thanks Dr. Stocker! Additionally, I owe a huge debt to Dr. Mark Lonergan, who was a post-doc in our group during my first two years, for his instruction in the art of conducting research and his faith in me. Additionally, Mark helped define this project in its early stages. He pushed the scientific discussion to a high intellectual level and had a long-range vision of what could be done with this system. Thanks Mark! Of course, I must thank my advisor, Professor Nathan Lewis. His encouragement and faith in my abilities motivated me to rise to the occasion and do my best. Nate's unwavering support when others disregarded me was invaluable to my completing this thesis. Thanks Nate! Finally, or perhaps primarily, I must acknowledge my mother. It was her ability to see what could be, rather than what was, that taught me I could rise above my situation and attend one of the highest caliber chemistry departments in the country. Thanks mom!

Other people worked on this project with me and have contributed to its breadth and depth. Brett Doleman was a fellow graduate student on the project and made contributions to data analysis and comparisons to mammalian olfaction; Dr. Bob Sanner, a research fellow, worked with us for a year and contributed to combinatorial uses of polymers and to chiral discrimination; Dr. Greg Sotzing, a post-doc, has worked with us for the last two years and has initiated new detector technologies and contributed to the temperature dependence studies; Shawn Briglin is a new graduate student on the project and to whom the torch is passed. Good Luck!

I kept these words posted at my desk to help me keep perspective on life:

Success

"To laugh often and much; to win the respect of intelligent people and the affection of children; to earn the appreciation of honest critics and endure the betrayal of false friends; to appreciate beauty, to find the best in others; to leave the world a little better; whether by a healthy child, a garden patch or a redeemed social condition; to know even one life has breathed easier because you have lived. This is the meaning of success." -Ralph Waldo Emerson

Dedicated to my mother, Kathleen Severin,

and my father, Fredrick Severin (1928-1992)

Abstract

A simple, broadly responsive detector array, based on polymer-carbon black composites that can detect, classify, and quantify various vapors and vapor mixtures is described. The individual detector elements of the array are constructed from films consisting of carbon black particles dispersed into insulating organic polymers. The carbon black provides an electrically conductive network in the films, whereas the different organic polymers are the source of chemical diversity between elements in the detector array. Swelling of the polymer upon exposure to a vapor increases the electrical resistance of the film by disrupting the conductive network of carbon black particles, thereby providing a simple means for monitoring the presence of a vapor. The dc electrical resistance change of an individual composite is shown to be consistent with the predictions of percolation theory. The differing gas-solid partition coefficients between vapor analytes for the various polymers of the detector array produce a characteristic pattern of resistance changes for each analyte. The response of these detectors is linear with variations in analyte concentration, allowing quantification as well as identification of a test analyte. This type of detector array can be used to discriminate different classes of analyte molecules (such as aromatics from alcohols) as well as those within a particular class (such as benzene from toluene and methanol from ethanol). Additionally, by using polymers with chiral subunits, enantiomerically different vapors can be discriminated. Principle component data analysis is used to identify and quantify airborne analytes and the relative compositions of simple gas mixtures. Integration of the electrical resistance signals with data analysis software has made sensing and analysis functions possible in a compact, low-power, simple vapor sensor device.

Table of Contents

List of Figures and Tables

Chapter 1

Introduction

Of the five mammalian senses (sight, hearing, touch, taste, and smell), there exists technology today which mimics three. The camera acts as an artificial eye, the microphone acts as an artificial ear, and there are pressure sensors to replicate the sense of touch. These technologies are quite old and have seen huge leaps in resolution and miniaturization in the last 20 years with the realization of transistor technology. However, notable in their absence are the ability to mimic taste and smell.

Many researchers believe that the sense of taste is really a combination of response from receptors on the tongue and from the olfactory bulb, with the primary sensation of flavor due to our sense of smell.[1] In the human olfactory system the sensitivity to odor intensity is poor; however, the loss of sensitivity is compensated for by an excellent power to discriminate similar complex odors.[2] Often slight differences in relative amounts of constituents between complex mixtures will cause those mixtures to have distinguishable odors.

The human nose, in the form of trained panels, is still the primary "instrument" used in many industries to evaluate the smell (and quality) of products such as perfumes, foodstuffs, and beverages. Additionally, dogs are employed by military and police agencies to detect illicit substances because of the superb canine sensitivity. Both groups, however, are subject to fatigue and are expensive to maintain. A valuable technological contribution would be a device with the ability to mimic the sense of smell. To design such a device we take our inspiration from the biological system.

I. Mammalian Olfaction

Mammalian nose receptors do not work exclusively in a "Lock and Key" fashion, but are more generally responsive to all analytes across chemical families. It is believed that the brain processes a composite pattern of these variable magnitude responses that occur across the olfactory epithelium.[1,3] This conclusion is intuitive in part because we know from experience that mammals can smell things that have not been present in an isolated form before this century. For example, dogs are able to detect the vapor signatures from sources such as cocaine and TNT. It seems unlikely that dogs have felt evolutionary pressure to develop receptors to these substances.

Instead, a pattern recognition approach has been proposed in which the brain classifies partial responses from many olfactory receptors as patterns associated with a particular odor signature.

Experimental evidence supporting the "pattern of response" approach to mammalian olfaction has recently been obtained. In these studies, mice were genetically altered with blue marker genes on isolated olfactory genes so that when the olfactory gene was expressed, the neurons that activate a specific odor receptor would be colored blue. In this way researchers could trace the connection between the odor receptor in the epithelium and the olfactory bulb in the brain.[3,4] It was shown that the blue axons stretching from olfactory neurons, which were randomly distributed across the epithelium, projected to only two glomeruli in the olfactory bulb of the brain. Because the glomeruli in the olfactory bulb are differentially sensitive to specific odors, and because their positions are defined in the bulb, a two-dimensional map of odor receptor response is mapped by the brain. It is believed that a particular analyte will activate a characteristic combination (a pattern) of these glomeruli in the bulb.[3] This indicates that olfactory sensing works as an array-based system where the olfactory receptors are the individual detectors and the brain does the pattern recognition.

In 1998, researchers were able to isolate an individual olfactory bulb receptor.[5] This receptor was addressed electrochemically to monitor its response to vapor presentations of various analytes. It was found that the receptor produced varying responses (a pattern) to a series of 50 analytes, rather than only responding to one particular compound.[5] Both the genetic work and the behavior of specific receptors are strong evidence that the mammalian olfactory system takes a pattern recognition approach to odor identification both in the organization of the receptors and glomeruli and in the mechanism of odor recognition at the receptor level. This does not, however, preclude the possibility of other analyte-specific receptors.

II. Sensor Criteria

Chemical sensors have been developed with particular sensitivities to particular analytes. This mimics the sense of smell or taste only for particular, limited applications. One early example of this was the pH meter which was developed by Arnold Beckman. Other examples include the

oxygen sensor in automobiles, and carbon monoxide detectors found in some fire detectors. The limit of this approach, however, is that new sensors must be developed for each analyte.

Non-specific detectors that can measure physical properties of molecules, such as the mass to charge ratio in the case of mass spectroscopy, and combustion properties in flame ionization detection have been in existence for years. These types of detectors are limited, however, by their general response to all analytes, since they only indicate that an analyte is present but not necessarily *which* analyte is present. Hence, these types of devices must be coupled to a separation technology such as gas chromatography in order to be used to identify analytes.

A single, non-specific detector cannot identify a particular analyte completely; however, with an array of differentially sensitive detectors, this is possible. Pattern recognition using the response by an array of non-specific detectors is a strategy for sensor development being used more and more over the last ten years, and seems to follow the example of biology outlined above.

When developing a new type of sensor to mimic the sense of smell, there are basic design criteria that should be met. Primarily, a new sensor must have an easily transduced signal. Complex signal analysis will limit the potential applicability of a developed system. Additionally, complex signals will suffer greater signal degradation during transmission. For example, devices that collect an electromagnetic spectrum are likely to be expensive to operate and the data will be more susceptible to noise. For the system described in this thesis, the response signal is a simple dc resistance that is quite robust. Moreover, the technology for monitoring and measuring resistance has been well established for all of this century.

The developed sensor must have reproducible and reversible responses. In a pattern recognition approach to sensing, analytes are assigned identities by the similarity of the array response pattern to libraries of stored response patterns. Reproducible responses ensure that an analyte of interest will be assigned correctly. Reproducibility also applies to fabrication since the ability to fabricate the elements of the sensor, so they perform in a manner consistent with previous copies, is critical to reduce training time for each device made. Reversibility of response is important for sensor longevity. The alternative to a reversible sensor is a "one exposure"

disposable sensor, only having use in critical applications with infrequent exposure events, thereby justifying the cost of continually replacing sensors. However, for the system detailed in this thesis, the goal was to develop a long-use sensor.

The device must be broadly responsive to analytes that cut across chemical classes in order to mimic the mammalian sense of smell and avoid the limited scope of analyte-specific sensors. This point is key to the pattern recognition approach to sensing. In such a device, each element of the array will respond to most analyte presentations, but to different degrees. Provided that chemical interactions form the basis of an array element's response, this strategy essentially probes the chemical variability between analytes in one step. Not only does this strategy identify the analyte, it can provide chemical information concerning an unknown analyte based upon the relative responses between detector elements of known composition. For instance, a polar unknown will cause a larger response in sensors with a strong dipole, unknowns with the ability to hydrogen bond will cause a larger response in sensor elements wth hydrogen bonding ability, etc. Currently, this amount of information is only available by performing multiple chromatography experiments with solid and mobile phases that have diverse chemical properties. A sensor array with broadly responsive elements will provide this information in one step.

It is crucial to the widespread application of a sensor system that it be stable in many environments. The performance of devices that depend on sensitive electrical or chemical components will suffer in real world situations. Any sensor development program must keep eventual real world applicability in mind when pursuing technical solutions. Temperature dependence of analyte responses and signal variations due to analyte concentration variations must be understood. This will allow analyte response libraries to be generated at a few sets of temperatures and analyte concentrations but to be useful in a variety of real world conditions.

The ideal sensor will be inexpensive to fabricate and easy to miniaturize. Any sensor technology must be fieldable if its development is to be justified, and cost is always a factor in evaluating the production of a device. Widespread use of new sensors suffers if they are expensive to construct or operate unless they have been developed for specific critical applications

such as found in the US space program where cost is of less importance. Additionally, miniaturization of sensors is crucial to almost all possible applications to which new sensor technologies will be applied. The analytical field is saturated with large, $60K boxes that require a 120 V or 240 V power supply. Battery operated sensor systems will allow new applications of sensors that are unrealized with current technology, particularly in conjunction with the field of robotics.

Use of sensors in arrays to generate patterns of response is a technique that is gaining popularity and has been exploited since the early 1980s. The use of multi-element sensor systems for discrimination between analytes was reported for the first time by Dodd and Persaud, who used three tin oxide sensors with broad, overlapping specificity of response, to discriminate complex analytes.[6] However, successful use of this strategy has been demonstrated with various sensor systems. An overview of some of the main array-based sensor systems is presented below.

III. Sensor Technology

Metal oxide semiconductor (MOS) devices are inexpensive and robust sensors for combustible and toxic gases. The devices are quite simple in design, essentially amounting to chemically sensitive resistors. They consist of an electrically heated ceramic pellet onto which a thin porous film of metal oxide doped with various precious metals has been deposited. Gases interact with the surface and thereby affect the conductivity of the MOS film. The devices are run at elevated temperatures to achieve fast response/recovery times, to be reversible, and to eliminate interference with water. This results in high power consumption which can be a disadvantage of these devices. However, in some applications this is not a concern. For example, these devices are well suited to the high temperature environment of an engine's exhaust system where they are often used to monitor NO_X and SO_X polluting gases. The advantages of the MOS devices include low cost and relatively high sensitivity, particularly toward gaseous analytes (NO_X, CO, etc.) as compared to the polymer sorption devices described below. The disadvantages of MOS devices include the low diversity that can be incorporated, which reduces selectivity. Changes in the semiconductor structure lends some selectivity, as does varying the temperature; however

responses to similar analytes, such as a homologous series of alkanes, will be difficult to distinguish.

Polymer sorption devices make up the bulk of array-based sensor systems. A typical configuration of these devices consists of an electrical, acoustic, or optical transducer with an incorporated chemically selective layer, usually a polymer film. This polymer layer interacts with the analyte(s) of interest so that its physical properties change in a manner that is probed by the transducer. The sensitivity and selectivity of these devices depend on the degree of sorption by the analyte into the polymer layer. If the sorbed molecules sit on the surface of the selective layer, then adsorption has occurred, while if/when the molecules dissolve into the layer, then absorption has occurred. Sorption processes are involved in the response mechanism of all polymer-based gas phase chemical sensors.

A second and more subtle influence on the sensitivity and selectivity of these gas sensors is the manner by which transduction of an analytical signal is generated. The transduction method is unique to each sensor type and forms the bases of differences between technologies. For example, mass sensitive devices and certain conducting polymer systems can detect simple adsorption, while other conducting polymer composites and optical devices require absorption as well. Additionally, the conductive composite device detailed in this thesis relies on absorption of analyte molecules and can be described by percolation theory (chapter 2).

Since sorption events are central to the polymer based devices described below as well as the device detailed in this thesis, a brief description of the important considerations of the sorption process follows.

IV. Sorption into Polymer Devices

The partition coefficient, K, is a thermodynamic parameter that defines the equilibrium distribution of vapor between the gas phase and the sorbent phase at a specific temperature, as defined by

$$K = C_S/C_V \qquad (1.1)$$

with C_S representing the concentration in the polymer film, and C_V representing the concentration of analyte in the vapor phase. Figure 1.1 illustrates the sorption of vapor molecules from the gas phase into a sorbent thin film on a solid support such as a sensor device. The larger the partition coefficient, the greater the absorption of the analyte into the polymer film.

The response of the device, R, is proportional to the amount of analyte that has sorbed onto/into the polymer film

$$R \alpha C_S \qquad (1.2)$$

which is related to equation 1.1 by

$$R \alpha K(C_V) \qquad (1.3)$$

which shows the dependence of the response on the partition coefficient. Since both K and C_V can be known (K for many polymer/solvent combinations are recorded and there are procedures for determining this constant for new systems), the response to a given analyte is predictable to a first approximation. To the extent K is constant with analyte concentration, equation 1.3 indicates a linear relationship between the response by the device as a function of analyte concentration. This has been shown for the device detailed in this thesis (see chapter 3) and other polymer sorption systems.[7]

At equilibrium, the chemical potentials of the analyte in the vapor phase and the analyte in the sorbed phase will be equal. The chemical potential, μ, is related to the fraction of vapor pressure by

$$\mu = \mu^\circ + RT \ln(yx) \qquad (1.4)$$

and

$$P/P^\circ = \mathbf{a} = (yx) \qquad (1.5)$$

where μ° is the chemical potential of the analyte at its equilibrium vapor pressure, R is the gas constant, T is temperature, **a** is the activity of the analyte, y is the analyte activity coefficient, x is the mole fraction of the analyte in the sorbed phase at equilibrium, P is the partial pressure of the analyte exposed to the sorbing phase, and P° is the equilibrium vapor pressure of the analyte.[8] For analytes with similar activity coefficients, the response of sorption based detectors will depend, to

a first order, on the fractional vapor pressure at which the analyte is presented. This is a subtle, but important point. This indicates that a detector's response threshold is not a function of absolute concentration but instead depends on the degree the analyte is saturated in the sample. Analytes with low vapor pressures will still cause a response in the detector if they are present at a large enough percent of their equilibrium vapor pressure. This has ramifications for the detection of low vapor pressure materials such as some essential oils and organic solids like TNT or cocaine.

The process of absorption can be considered in terms of a model with endothermic and exothermic steps. The vapor molecules dissolving into a polymer layer are the solute, while the polymer is the solvent. The creation of a cavity in the solvent means disruption of attractive interactions between solvent molecules (the monomer units of the polymer) which is an endothermic process. When this cavity is filled with solute vapor molecules, attractive interactions between solute and solvent molecules are formed which is an exothermic process.

The properties of a molecule that dictate these interactions are called solubility properties, and include hydrogen bonding, dipole/dipole, dipole/induced dipole, and induced dipole-induced dipole (also called dispersion) interactions. Empirical, overall solubility parameters which encompass the influence of all these interactions have been defined but only provide rough guidance when determining the degree of sorption of an analyte into a polymer film. The closer in value the solubility factor of the polymer is to the analyte, the greater sorption that occurs.

The partition coefficient is related to the standard Gibbs free energy of solution of a gaseous solute, $\Delta G°$, by

$$\Delta G° = -RT (\ln K) \qquad (1.6)$$

which upon rearrangement yields

$$(\ln K) = (-\Delta G°/R)\cdot(1/T) \qquad (1.7)$$

indicating a linear dependence on (ln K) verses (1/T). Since K is proportional to the response it is also true that

$$(\ln R) = \mathbf{C}\cdot(1/T) \qquad (1.8)$$

(where **C** is a constant specific to the system) which is shown to be true for the device detailed in this thesis in chapter 5 and has been shown for other sorption devices.[9] This will generally be true for all the polymer sorption devices in which the transduction mechanism causes the response to be directly proportional to K.

Polymer sorption devices, in many ways, follow the rules and trends found in the chromatography literature. They are essentially inverse processes. In column chromatography, a long stationary phase has a small "plug" of analyte flowing over it. By contrast, in these polymer sorption devices, a small "plug" of sorbent material has a long (relatively) flow of analyte over it (Figure 1.2). In both chromatography and polymer sorption vapor detectors, the resolution between analytes will be related to the partition coefficients of the analytes. In the chromatography literature this is referred to as the selectivity factor, α, and is defined by

$$\alpha = K_a/K_b \qquad (1.9)$$

where K_a is the partition coefficient of the more sorbing species and K_b is the partition coefficient of the less sorbing species. By definition $\alpha \geq 1$. Equation 1.7 has yet to be shown to generally apply for any polymer sorption device, including the one detailed in this work, but it falls out of the theory described above.

In addition to the carbon black-polymer composite device detailed in this thesis, there are three other main polymer sorption technologies for vapor detection that have been developed. These are conductive polymer systems, polymer coated acoustic devices (SAW and QCM), and colorimetric systems. A brief discussion of each follow here and in chapter 2.

V. Sorption Based Sensors

Conducting polymer vapor detectors have been incorporated into arrays since the mid 1980s. They consist of a single conducting polymer film (either poly(pyrrole) or poly(aniline) or their alkylated derivatives) grown electrochemically across two electrodes between which the electrical resistance of the film is measured during exposure to an analyte. Certain chemical species can affect the intrinsic conductivity of the material through charge transfer events. In addition, the resistance of these devices changes with the polymer layer swelling and concomitant disruption of

conductive pathways. The materials that comprise elements of an array are usually chemically similar, with variation found in the alkyl sub-unit and the counter-ion of the doped polymer resulting in low chemical selectivity. The response of the these films is determined to a large extent by the electrochemical deposition conditions used to make the device. For example, the electrolyte/solvent system used in the deposition affects the detector response greatly. These materials are most sensitive to polar species such as the alcohols and amines, and show poor discrimination between non-polar lipophilic species. Additionally, these devices show response to the light gases such as NO_2 and NH_3. This type of response is unlikely to be due to absorption into the polymer matrix because of the partitioning arguments detailed above, but instead likely involves changes in the intrinsic conductivity due to adsorbed charge transfer species. This has been shown through optical absorption spectral changes upon exposure to electron-poor and electron-rich gaseous species.[7] Due to the complex nature of the transduction mechanism employed by these detectors, the responses to analyte vapors are not as predictable as the non-conducting polymer systems described below.

Acoustic devices used as sensors include the quartz crystal microbalance (QCM) and surface acoustic wave (SAW) devices. QCMs consist of a piezoelectric quartz crystal oscillator coated with a polymer film. The sorption of odor molecules onto/into the membrane results in a decrease in the resonant frequency of the shear mode oscillation (5-10 MHz) due to the increased mass. This frequency shift is the transduction method of the device and is used as the device output. The responses between oscillators can be modified by using different polymer layers on each resonator. Similar to QCMs are the SAW devices, which consist of interdigitated electrodes patterned onto a piezoelectric quartz substrate onto which a thin polymer film has been applied. An oscillating voltage (in the hundreds of MHz) is applied to the device which produces a surface oscillation in the quartz substrate. Sorption of analyte molecules onto/into the film increases the mass of the film and its elastic modules which perturbs the surface wave and leads to a shift in frequency. To compensate for ambient temperature and pressure effects, the detector is coupled to a reference oscillator which is protected from environmental effects. The frequency difference

between the reference SAW and the detector SAW is used as the device output. Again, differences in response between detectors are dictated by the differences in the coated polymer films. SAW devices are more sensitive than the QCMs to the presence of an analyte and to environmental fluctuations due to the higher frequencies at which they operate, but also have less robustness and an increased complexity.

Fiber optic colorimetric devices make use of the interaction between solvatochromic fluorescent dyes, such as Nile Red, imbedded into polymer beads, and the analyte vapor to which the beads are exposed. These dyes exhibit large shifts in their emission peak wavelength with changes in the polarity of the dye environment. The polymer beads are attached to the distal end of individual 2 μm optical fibers bundled together to form probes with diameters on the order of 500 μm. Each fiber usually contains one composite bead, the color change of which can be read remotely through the fiber optic with standard CCD technology. The high efficiency of optical fibers allows as much as several kilometers between the sensing end of the fiber and the measuring device with no electrical interference and little signal degradation. Different sensing elements are produced by immobilizing different dyes in polymer matrices of varying composition. The unique dye-polymer regions interact uniquely with various analytes causing differences in the fluorescent response by each particular dye-polymer pairing.[10]

VI. Data Analysis

Each of the techniques described above, as well as the device detailed in this thesis, make use of pattern recognition and data reduction techniques. One of the most popular, and the one used here, is Principal Component Analysis (PCA), described below.

Consider an array of discrete detectors where each sensor i produces a steady state response to an analyte j. The response of a set of n detectors to an analyte exposure can be represented by a vector, **X**, where each component of the vector corresponds to the response from an individual detector to that analyte, x_{ij},

$$\mathbf{X} = x_{1j}, x_{2j}, x_{3j}, ..., x_{nj} \qquad (1.10)$$

The response of an array of detectors to a set of m analytes can be regarded as a set of **X** vectors represented by a response matrix, **Y**.

$$\mathbf{Y} = \begin{matrix} (x_{11}, x_{21}, x_{31}, \ldots, x_{n1}) \\ (x_{12}, x_{22}, x_{32}, \ldots, x_{n2}) \\ (x_{1m}, x_{2m}, x_{3m}, \ldots, x_{nm}) \end{matrix} \qquad (1.11)$$

where each column refers to the individual discrete detectors and the rows represent exposures to individual analytes. If the detectors in a system are uniquely orthogonal, then all the off-diagonal elements of **Y** would be zero; however, in most array-based systems individual detectors will respond to a variety of odors with varying intensities. This matrix can be quite complex owing to the typical use of 10-20 detectors and hundreds of exposures. Each detector represents a dimension in "response space" so that a 20 detector array will produce data in 20-dimensional space. Therefore, data simplification techniques are used to visualize the variance in the data. Often, preprocessing of the data occurs before visualization techniques are employed depending on the information required of the data. These might include compensating for concentration fluctuations by a normalization procedure.

Principal component analysis (PCA) is the data simplification technique used to investigate the new detectors detailed in this thesis. PCA can be used to evaluate the response of an array of detectors to single or multi-component analytes. The method basically consists of expressing the response vectors **X** in terms of linear combinations of orthogonal vectors (called principal vectors or eigenvectors), each of which accounts for a certain amount of variance in the data, with each vector representing a smaller amount of variance. The scalar product of the principal vectors with the response vectors, **X**, gives the value of the principal component (or eigenvalue). The first principal component, with the largest eigenvalue, represents the largest variance in the data; the second principal component, with the next largest eigenvalue, represents the next largest amount of variance in the data, and so on.

There is often significant correlation between responses from different detectors to a set of analytes indicating that the majority of the information held in "response space" can be displayed

using a small number of principal vectors. Often principal components 1-3 are all that are needed to display the unique responses for 8-10 analytes exposed to 10-20 detectors.

In simple terms, PCA is the process of finding new axes through the response data such that the new axes contain the largest variance between data clusters. An illustration of this idea is shown in Figure 1.3. The data clusters in Figure 1.3 represent responses by two detectors (and drawn as orthogonal vectors, which is rare) to three analytes. These analytes are not resolved completely by either detector. There is overlap between data sets A and B for detector 1, and between data sets B and C for detector 2. However, a new, principal, vector can be drawn through the points such that all the clusters are separated when projected onto this vector.

PCA is a quite powerful data simplification technique and allows one to make sense out of what would otherwise be intractable amounts of data.

VII. References

1)Gardner, J. W.; Bartlett, P. N. *Sensors And Actuators B Chemical* **1994**, *18*, 211-220.

2)Gardner, J. W.; Hiines, E. L. *Pattern Analysis Techniques*; Kress-Rogers, E., Ed.; CRC Press, Inc.: New York, NY, 1997, pp 633-652.

3)Axel, R. *Scientific American* **1995**, *273*, 154 -159.

4)Buck, L.; Axel, R. *Cell* **1991**, *65*, 175-187.

5)Zhao, H. Q.; Ivic, L.; Otaki, J. M.; Hashimoto, M.; Mikoshiba, K.; Firestein, S. *Science* **1998**, *279*, 237-242.

6)Persaud, K.; Dodd, G. *Nature* **1982**, *299*, 352.

7)Persaud, K. C.; Travers, P. J. *Arrays of Broad Specificity Films for Sensing Volatile Chemicals*; Kress-Rogers, E., Ed.; CRC Press, Inc.: New York, NY, 1997, pp 563-592.

8)Doleman, B. J.; Severin, E. J.; Lewis, N. S. *Proceedings of the National Academy of Sciences of the United States of America* **1998**, *95*, 5442-5447.

9)Zellers, E. T.; Han, M. W. *Analytical Chemistry* **1996**, *68*, 2409-2418.

10)White, J.; Kauer, J. S.; Dickinson, T. A.; Walt, D. R. *Analytical Chemistry* **1996**, *68*, 2191-2202.

Figure 1.1: An illustration of the absorption of a vapor from the gas phase into a sorbent polymer film on an inert detector substrate.

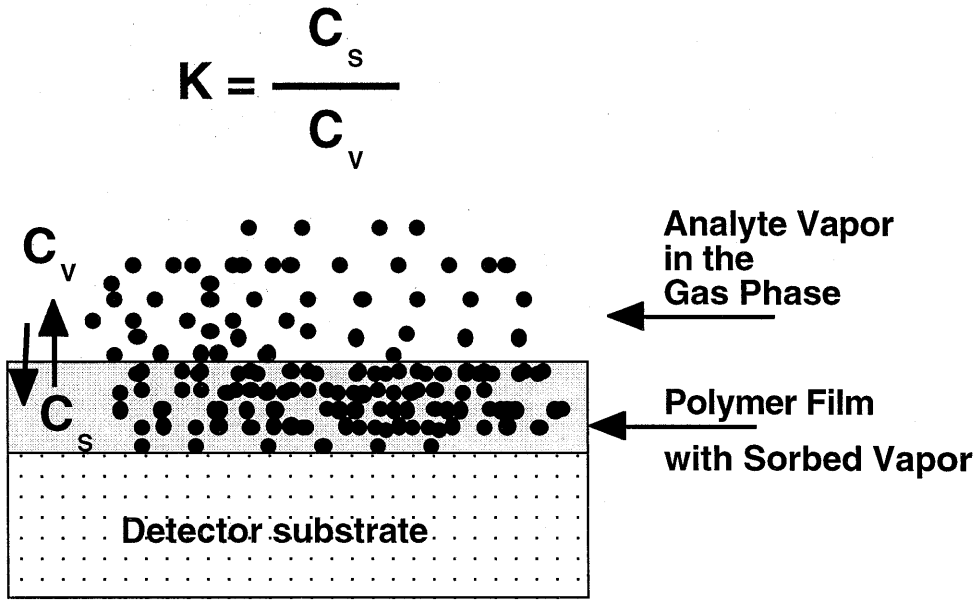
K = Cs / Cv
Cv
Cs
Analyte Vapor in the Gas Phase
Polymer Film with Sorbed Vapor
Detector substrate

Figure 1.1

Figure 1.2: An illustration of the connection between chromatography and polymer sorption devices. **A**) Chromatography scheme with an analyte "plug" and a long sorbent phase. **B**) Polymer sorption scheme with a short sorbent "plug" and a long flowing analyte stream.

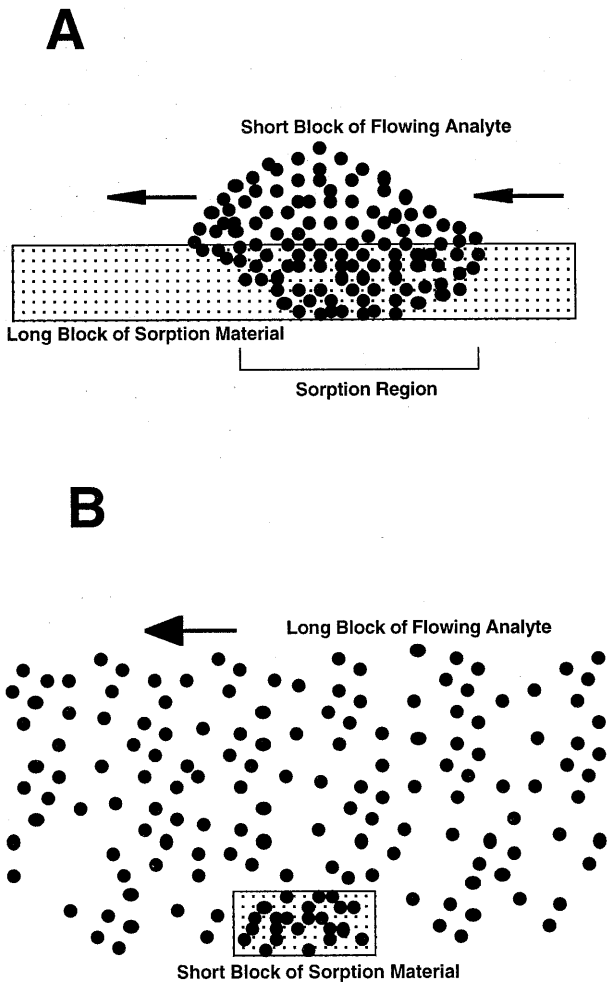
A
Short Block of Flowing Analyte
Long Block of Sorption Material
Sorption Region
B
Long Block of Flowing Analyte
Short Block of Sorption Material

Figure 1.2

Figure 1.3: An illustration of principal component analysis. The data clusters are shown as relative responses by two detectors. The data is not resolved completely by either detector. A principal component vector can be drawn such that when the data are projected onto that vector the data clusters are resolved.

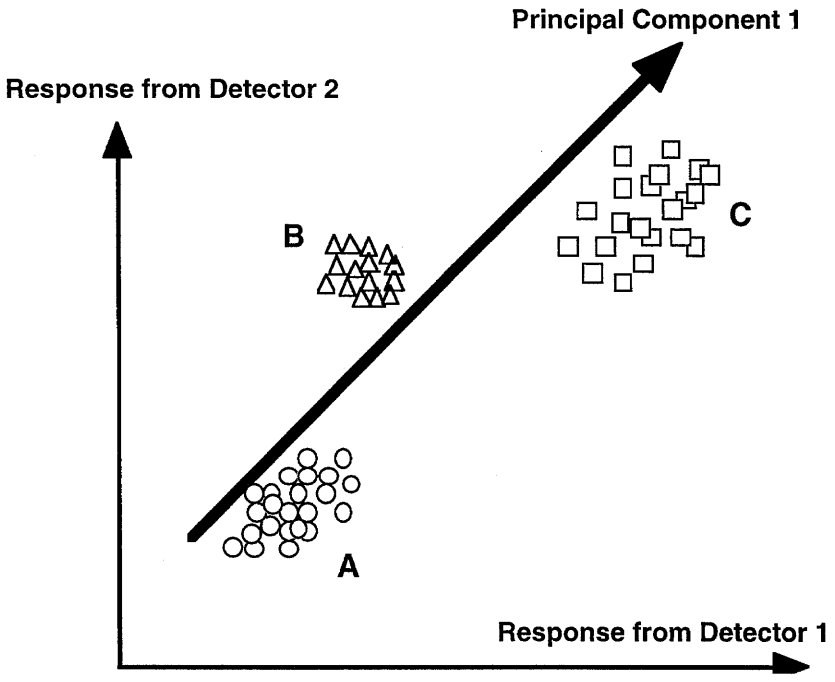
Principal Component 1
Response from Detector 2
B
C
A
Response from Detector 1

Figure 1.3

Chapter 2

Array-Based Vapor Sensing Using Chemically Sensitive, Carbon Black-Polymer Resistors

Abstract:

We describe herein the construction of a simple, low-power, broadly responsive vapor sensor. Carbon black-organic polymer composites have been shown to swell reversibly upon exposure to vapors. Thin films of carbon black-organic polymer composites have been deposited across two metallic leads, with swelling-induced resistance changes of the films signaling the presence of vapors. To identify and classify vapors, arrays of such vapor-sensing elements have been constructed, with each element containing the same carbon black conducting phase but a different organic polymer as the insulating phase. The differing gas-solid partition coefficients for the various polymers of the sensor array produce a pattern of resistance changes that can be used to classify vapors and vapor mixtures. This type of sensor array has been shown to resolve common organic solvents, including molecules of different classes (such as aromatics from alcohols) as well as those within a particular class (such as benzene from toluene and methanol from ethanol). The response of an individual composite to varying concentrations of solvent is shown to be consistent with the predictions of percolation theory. Accordingly, significant increases in the signals of array elements have been observed for carbon black-polymer composites that were operated near their percolation thresholds.

I. Introduction

Conventional approaches to chemical sensors have traditionally made use of a "lock-and-key" design, wherein a specific receptor is synthesized in order to bind strongly and highly selectively to the analyte of interest. A related approach involves exploiting a general physicochemical effect selectively toward a single analyte, such as the use of the ionic effect in the construction of a pH electrode. With both of these approaches, selectivity is achieved through precise chemical design of the receptor site. Such approaches are appropriate when a specific target compound is to be identified in the presence of controlled backgrounds and interferences. However, this type of approach requires the synthesis of a separate, highly selective sensor for each analyte to be detected. In addition, this type of approach is not particularly useful for analyzing, classifying, or assigning human value judgments to the composition of complex vapor mixtures such as perfumes, beers, foods, mixtures of solvents, etc.

An alternative approach to chemical sensing is closer conceptually to a design widely proposed for the mammalian sense of olfaction.[1,2] In such an approach, the strict "lock-and-key" design criterion of traditional sensing devices is abandoned. Instead, in this alternative sensor architecture, an array of incrementally different sensors is used, with every element in the sensor array chosen to respond to a number of different chemicals or classes of chemicals.[3-15] The elements of such an array should contain as much chemical diversity as possible, so that the array responds to the largest possible cross-section of analytes. Although in this design identification of an analyte cannot be accomplished from the response of a single sensor element, a distinct pattern of responses produced over the collection of sensors in the array could provide a fingerprint that would allow classification and identification of the analyte. The advantage of this approach is that it can yield responses to a variety of different analytes, including those for which the array was not originally designed. In addition, the broadly responsive sensors need not incorporate synthetically challenging, custom-designed, "lock-and-key" receptor sites in order to generate a response to an analyte. Also, an array of sensors naturally performs an integration to yield a unique signal for

complex but distinctive odors (e.g., cheeses, beers, etc.) without requiring that the mixture be broken down into its individual components prior to, or during, the analysis.

We describe herein a simple, broadly responsive sensor array, based on carbon black composites[16-18] and demonstrate that this array can classify, detect, and quantify various test vapors and vapor mixtures. The individual sensor elements are constructed from films consisting of carbon black particles dispersed into insulating organic polymers. The carbon black endows electrical conductivity to the films, whereas the different organic polymers are the source of chemical diversity between elements in the sensor array. Swelling of the polymer upon exposure to a vapor increases the resistance of the film, thereby providing an extraordinarily simple means for monitoring the presence of a vapor.[16,19-25] Since different polymer compositions are present on each sensor element, an array of elements responds to a wide variety of vapors (or complex mixtures of vapors) in a distinctive, identifiable fashion (Figure 2.1a). The electrical resistance signals that are output from the array can be readily integrated into software- or hardware-based neural network processors, allowing for an integration of sensing and analysis functions into a compact, low-power, simple vapor sensor.

Array-based vapor sensing has been demonstrated previously in several systems, including those using surface acoustic wave devices,[15,26-28] tin oxide sensors,[29-31] and conducting organic polymers.[32-34] In general, desirable design criteria for the elements of such an array are as follows: (1) they should readily transduce environmental information into an easily monitored signal, using a minimum of hardware and energy; (2) they should exhibit reversible, reproducible responses with a minimum of baseline drift; (3) they should be broadly tunable to respond in a predictable manner to a wide range of chemical species and concentrations; (4) they should be easily fabricated, preferably from inexpensive, commercially-available materials using well-established techniques; (5) they should permit miniaturization to facilitate the construction of compact sensors with a large number of elements; and (6) they should be robust and stable in many different environments. SnO_2 gas sensors[29-31] are among the most well-established sensing elements, and several commercial "electronic noses" have been based on SnO_2 arrays.[6] Although

such arrays yield diagnostic responses for several gases, the incomplete understanding of catalytic processes at the doped SnO_2 surface makes chemical control of the response properties, and thus deliberate introduction of desired chemical diversity into the array, difficult to accomplish. Surface acoustic wave (SAW) devices are extremely sensitive to the presence of vapors, but involve somewhat sophisticated electronics to sustain surface Rayleigh waves in the piezoceramic crystals. Chemical diversity in a SAW array can be readily attained by coating the SAW crystals with different polymer films having differing gas-solid partition coefficients towards a vapor of interest. To our knowledge, primarily because of the electronic complexity involved in a SAW device and the resulting engineering challenges associated with micromanufacturing large numbers of such systems into an integrated system, the largest SAW array reported to date contains approximately 12 sensor elements.[15,26-28] In contrast, over 1000 receptor genes have recently been discovered in the mammalian olfactory system, and it is therefore estimated that the dimensionality of smell in humans is approximately 10^3.[35] There is thus great intellectual interest in constructing sensor arrays that have large numbers of chemically distinct sensor elements so that a large number of diverse sensing tasks can be accommodated within one array structure, and to investigate fundamentally the behavior of systems that are functionally, if not structurally, analogous to the mammalian olfactory response. Conducting organic polymers have also been used to form sensor arrays,[32,33] and commercial "electronic nose" devices have recently been announced using poly(pyrroles).[36] However, since there are only a few classes of stable conducting polymers, and since to date the conducting polymers have been synthesized electrochemically to yield insoluble, intractable materials, additional variation in the array elements has been largely confined to changes in the counterion of the polymer or to the more synthetically challenging task of varying the substituents on the polymer backbone.

The scope of conducting polymer-based sensors has recently been broadened through the use of a set of polymer blends that possess a common conducting element, poly(pyrrole), for signal transduction, and a variety of insulating, swellable, organic polymers to achieve chemical diversity in the array.[34] These devices have been shown to function quite well, but the long-term

stability of poly(pyrrole) is of concern for practical use of such systems. The advantages of the approach described herein are that the conductive element is a very stable species, carbon black, and that chemical diversity in the sensor array can be readily obtained through the use of simply prepared, conventional organic polymers that function as the insulating phase of the carbon black composites. Individual carbon black composites have been widely explored as humidity sensors[16,20-22] and, to a somewhat lesser extent, as sensors for organic vapors or liquids such as gasoline.[19,23-25] To our knowledge, however, carbon black composites have yet to be incorporated into an array-based sensing configuration. In this paper, we demonstrate the feasibility of using carbon black-organic polymer composites in a broadly responsive, multi-component vapor sensor. We also demonstrate how the properties of these individual sensors can be tuned through variation in the insulating polymer and carbon black content of the composite films.

II. Experimental

A. Materials

The carbon black used in the composites was Black Pearls 2000 (BP2000), a furnace black material that was generously donated by Cabot Co. (Billerica, MA). The polymers used in the composites are listed in Table 2.1. All polymers were purchased from Polysciences Inc. or Aldrich Chemical Co. and were used as received. The solvents used in this study were toluene, benzene, ethyl acetate, methanol, ethanol, 2-propanol, hexane, chloroform and tetrahydrofuran (THF); all were reagent grade and were used as received from EM Scientific.

B. Apparatus

Standard glassware was used to construct a bubbler apparatus (to provide known partial pressures of various vapors) and a flow chamber to control the resulting gas stream. The bubblers were large test tubes (30 cm long with a 3 cm inside diameter) equipped with exit sidearms. To provide a pathway for gas flow, a glass tube terminated by a coarse filter frit was inserted into a rubber stopper and then placed into the top of each bubbler. The carrier gas was compressed air from the general lab source, and was neither filtered nor dehumidified. The measurements were

performed at room temperature, which was in the range 22±2 °C over the course of the experiments described herein. The carrier gas was introduced into the solvent through the porous ceramic frit, and the solvent-saturated gas mixture exited the bubbler via the sidearm of the glass tube. Saturation of the gas streams in our experimental apparatus was verified for the highest flow rates (1.0 L min^{-1}) used in this work through measurement of the rate of mass loss of liquid in the bubbler,[37] thus saturation conditions were assumed to have been obtained for the lower flow rates used in other experiments described in this work. The experimentally measured vapor pressures at the highest gas flow rate through the bubbler were within 2% of the values calculated from the literature[38] for the measured temperatures of the solvent in the bubblers during the period of gas flow. The experimentally measured vapor pressures, and corresponding solvent temperatures, were: acetone: 176 torr (19°C); benzene: 83 torr (22°C); chloroform: 158 torr (20°C); ethanol: 50 torr (22°C); ethyl acetate 82 torr (22°C); hexane: 114 torr (19°C); methanol: 102 torr (21°C); 2-propanol: 37 torr (22°C); toluene: 25 torr (23°C). The saturated vapor was carried out the sidearm of the bubbler, blended with a controlled background flow of pure carrier gas and then introduced into a sensing chamber. This chamber consisted of a glass tube (22 cm long with a 2.6 cm inside diameter) to which inlet and outlet sidearms had been attached. The sensing elements were introduced into the chamber through a 24/40 taper ground glass opening attached at one end of the chamber. The chamber was then sealed with a ground-glass stopper through which the electrical lead wires had been sealed. The gas flow rates were controlled with needle valves and stopcocks.

C. Fabrication of Substrates

Ceramic capacitors (22 nF, approx. 2 x 4 x 4 mm) from Kemet Electronics (Greenville, SC) were found to provide a very convenient electrical contact and physical support for the composite films of each sensor (see Figure 2.1b). First, the interdigitated electrodes inside the capacitor were exposed by using progressively finer grades of sandpaper and polishing paste to remove the top of the capacitor. During this process, the bulk of the material was removed with diamond-impregnated sanding paper on a sanding belt. The path of the grinding paper or paste was parallel to the interdigitated electrodes to avoid shorting the capacitor. Following the diamond

paper treatment, the capacitors were sanded on a disk sander using 3M Tri-M-ite Fre-Cut, Open Coat, 360 grit paper. The tops of the capacitors were then polished on a 48-1581-BXXR polishing wheel (Buehler LTD, Lake Bluff, IL) using 0.3 μm diameter Buehler α-alumina micropolish grit. After the polishing step, the capacitors were sonicated in acetone or 2-propanol for 5-10 min to remove any residual alumina. All capacitors that were used as sensors had an initial resistance after polishing of greater than 10 MΩ (greater than the upper measurement limit of our ohmmeter).

D. Fabrication of Composite Films and Individual Sensor Elements

Individual sensor elements were prepared by a single dip of the polished, cleaved capacitors into 10 mL solutions that contained 80 mg of dissolved polymer and 20 mg of suspended carbon black. After removal from the solution, any excess liquid was shaken off or blotted off, and the film was then dried in air prior to use. The solvent was generally THF, but benzene was the solvent for composites prepared from poly(ethylene - *co* - vinyl acetate) and poly(ethylene oxide), and dichloromethane was the solvent for composites made from poly(caprolactone). Prior to immersion of the capacitor, the solutions were sonicated for 5-10 min to aid in the suspension of the carbon black. Some studies were also performed using glass substrates instead of the ceramic capacitors described above. To prepare the glass substrates, two parallel bands of gold, 0.5-1.0 μm thick and separated by 5 mm, were deposited onto conventional 7.5 cm x 2.5 cm glass slides. The slides were then cut into strips to produce 0.7 cm x 2.5 cm pieces of glass, with each strip of glass having one pair of Au leads spaced 5 mm apart.

When glass substrates were used, a slightly different procedure was utilized to form the composite films. Appropriate aliquots (4-15 mL in volume depending on the final desired polymer concentration) of stock polymer solutions (6 mg mL^{-1}) were diluted to a volume of 15 mL using the same solvent as that in the stock solution. Carbon black was added to this solution until the total mass of polymer and carbon black was 100 mg. Two glass substrates were then dipped back to back (the front being the side with the gold leads) into this solution. The slides were held with a forceps, dipped into the solution, and removed quickly (0.1-0.5 s). The slides were dipped

several times with 5-10 s of air drying between dips. Studies using glass substrates were only performed with poly(ethylene - *co* - vinyl acetate) (PEVA, 82% (w / w) ethylene) or poly(*N*-vinylpyrrolidone) (PVP) carbon black composites. The PEVA slides were dipped 4 times, while the PVP slides were dipped 10 times into the fabrication solution.

At the lowest carbon black loadings studied, the composite films of PVP and PEVA appeared speckled under 40X magnification, with the largest carbon black aggregates being ≈30 μm in length and irregular in shape. With increasing carbon black loading, the aggregate size increased until eventually the films appeared uniformly black under 40X magnification. Profilometry data obtained using a Dektak 3030 profilometer (Sloan Technology Corp., Santa Barbara, CA) on these films showed average film thicknesses ranging from 0.2 - 2 μm.

E. Measurements

To determine the response of the sensor elements to various vapors, the dc resistance of each sensor was determined as a function of time. Resistance measurements were performed using a simple two-point configuration. Sensors fabricated with the capacitor supports were plugged directly into a 40 pin bus strip that was then connected to a multiplexing ohmmeter via a ribbon cable. The resistances of the composite films on glass substrates were monitored similarly except that the gold leads on the glass slides were pressure-contacted with flat-jawed alligator clips.

Generally, resistance data were acquired using a Hydra 2620A Data Acquisition Unit (John Fluke Mfg. Co.) interfaced to a personal computer. All of the prepared samples had resistances less than the 10 MΩ limit of the Hydra 2620A. In some cases, however, swelling increased the sample resistance to above 10 MΩ. In these cases, resistance measurements were performed using a Princeton Applied Research model 173 potentiostat or a Hewlett Packard model 6024 dc power supply (to apply a known potential) and a Keithley model 177 multimeter (to measure the resulting current across the resistive sensor element). In a few test cases, electrical resistance measurements were also made in a four-point configuration, and these data indicated that, in our experimental configuration, vapor-induced changes in contact resistance were minimal compared to the vapor-induced changes in the resistivity of the sensor films.

To initiate an experiment, the sensors were placed into the glass chamber and a background flow of compressed air was introduced until the resistance of the sensors stabilized. Solvent vapor streams of various concentrations and compositions were then passed over the sensors. The flow rates in the bubblers were controlled using flow meters obtained from Gilmont Instruments, Inc., with the lower and upper limits of the flow meters being either 0.2 L min^{-1} and 15.0 L min^{-1}, 0.0010 L min^{-1} and 0.280 L min^{-1}, 0.0015 L min^{-1} and 0.310 L min^{-1}, or 0.0048 L min^{-1} and 0.673 L min^{-1} respectively. Analyte gas flows were kept low enough (< 1 L min^{-1}) to ensure that the vapor was saturated with solvent prior to dilution with the background gas. In a typical experiment, resistance data on the sensor array elements were collected for 1 min (to serve as a baseline), followed by a 0.25 - 1.5 min collection during exposure to the solvent vapor stream, and then were followed by a 5 min recovery time.

III. Results

A. Sensor Element Response Characteristics

Figure 2.2 shows the resistance change of two carbon black-polymer composite films during repeated, periodic exposures to a test solvent vapor. The resistances of the films increased when the solvent vapor was present and then returned to their original baseline values after the vapor flow was discontinued. For example, Figure 2.2a shows data for fifteen sequential exposures of a PEVA (poly(ethylene - *co* - vinyl acetate, 82% (w / w) ethylene)-carbon black composite film to 1.1 ppt (ppt = part per thousand (v/v)) of benzene in air; Figure 2.2b shows similar data for the exposure of a PVP (poly(*N*-vinylpyrrolidone))-carbon black composite film to 1.5 ppt methanol in air. For the PEVA composite, resistance changes of 8.7 ± 0.2 kΩ (0.77% of the baseline value) were observed for exposure to benzene vapor; for the PVP composite, resistance changes of 2.95 ± 0.07 kΩ (2.28% of the baseline value) were observed for exposure to methanol. The form of the time response of these sensors were representative of all sensor elements studied in this work, with response times under these experimental conditions generally varying from <2 s to 4 s for the film thicknesses used in this study (2 s was the minimum time resolution of the multiplexing ohmmeter in this experiment). As can be seen from the data of

Figure 2.2, the baseline resistance value drifted by approximately <0.02% for the PEVA composite and <0.15% for the PVP composite over a 20 min time period. These relative resistance changes and baseline drift rates were representative of the behavior of all sensor elements studied in this work under these experimental conditions.

It was of interest to examine the dependence of the signal response on the conductor/insulator ratio of a sensor element film. If the film composition could be manipulated so that solvent-induced swelling forced the film across its percolation threshold, very large resistance changes might be observed upon introduction of low concentrations of solvent vapor. Such a change should also produce a nonlinear signal vs. vapor concentration response, with the greatest sensitivity to vapor near the percolation threshold. Figure 2.3 displays such data for two PEVA-carbon black composite sensor elements, one fabricated from a 15% (w/w) carbon black-PEVA mixture and the other from a 50% (w/w) carbon black-PEVA mixture. The data in Figure 2.3 are semilog plots of the partial pressure dependence of the maximum relative differential resistance signals, $\Delta R_{max,\infty}/R$, where R is the baseline resistance of the film prior to exposure to the solvent and $\Delta R_{max,\infty}$ is the maximum differential resistance signal that was observed in response to an extended exposure of the sensor to the specified partial pressure of solvent vapor. During exposure to benzene vapor, both sensor elements clearly displayed maximum relative differential resistance responses that were a function of the partial pressure, P, of the solvent. Below $P/P^* \approx 0.81$ (P^* = saturation partial pressure = 114 ppt benzene under ambient conditions), the concentration dependencies of the responses of the two films were of similar form, with an approximately linear response observed at the lowest vapor concentrations (see Figure 2.3 inset). Above $P/P^* \approx 0.81$, the response profile of the 50% (w/w) carbon black-PEVA film remained continuous, but a significant increase in response was observed for the 15% (w/w) carbon black-PEVA film, consistent with swelling passing the latter material through its percolation threshold.

A further investigation into the effect of changing the conductor/insulator ratio of a sensor film was performed using a series of PVP and PEVA films with varying stoichiometries. Figure 2.4 shows the responses of the PVP films to 11 ppt methanol and of the PEVA films to 9 ppt

benzene; baseline conductances for these sensors are also shown. The error bars on the conductance values are estimates based on the deviation between four or five composite films fabricated at each composition, and the error bars of the $\Delta R_{max,\infty}/R$ values are based on the deviation between the responses of these four or five sensors to four exposures each. As the carbon black contents of the films were lowered toward their respective percolation thresholds, the baseline conductances of the composites decreased. Furthermore, the magnitude of the maximum relative differential resistance response, $\Delta R_{max,\infty}/R$, observed in response to introduction of a constant partial pressure of analyte increased as the conductor/insulator ratio decreased. The increase in response was significant, with $\Delta R_{max,\infty}/R$ varying by a factor of five in response to changes in the carbon black content of the composite. Even larger improvements are expected with further reduction in the carbon black content, but to date, we have only studied films having initial baseline resistances less than the 10 MΩ limit of our multiplexing ohmmeter.

B. Array-Based Vapor Sensing

1. Response Patterns for Various Vapors

Although each individual sensor element had a characteristic relative differential resistance response, such data from an isolated sensor element would only be useful in a controlled environment that contained a single, known gas species. In more complex situations, data from a number of different sensors would be required. For this purpose, resistance data were obtained for arrays of carbon black-polymer composite sensor elements during exposure to various chemically different gaseous species.

To evaluate the performance of a modestly sized sensor array, a set of 17 carbon black-polymer composites was fabricated, with each sensor element having a different polymer in the composite (see Table 2.1). Modified capacitors served as substrates for the composite films in the sensor array. Air (at a flow rate of 1 L min^{-1}) saturated with one of nine common organic solvents: acetone, benzene, chloroform, ethanol, ethyl acetate, hexane, 2-propanol, methanol, or toluene was combined with a background air flow (6 L min^{-1}) and the mixture then introduced into a chamber containing the sensor array. This produced the following concentrations of each solvent:

acetone: 40±2 ppt; benzene: 16.4±0.7 ppt; chloroform: 34±2 ppt; ethanol: 10.0±0.4 ppt; ethyl acetate 16.0±0.6 ppt; hexane: 26±1 ppt; methanol: 21.2±0.8 ppt; 2-propanol: 7.5±0.3 ppt; toluene: 4.9±0.2 ppt. Solvent vapors were introduced for 60 s, in random order, six times each (except for acetone, for which only three exposures were performed), over a total period of 10 h. Between vapor exposures, the sensors were exposed only to the solvent-free background flow (air) for a minimum of 6 min, although shorter recovery times could have been employed in most cases. The data obtained from this experiment are summarized in Table 2.2.

Figure 2.5 displays the normalized, relative differential resistance data for this array during exposure to three representative solvents: methanol, ethyl acetate and benzene. These three solvents have similar vapor pressures (113, 85, and 87 torr at 296 K, respectively) but the solvents clearly differ in their chemical properties. To facilitate comparison between various sensors, a normalized signal, S'_{sj}

$$S'_{sj} = \frac{\Delta R_{sj,\max} / R_j}{\sum_s (\Delta R_{sj,\max} / R_j)}, \qquad (1.1)$$

has been plotted, where s = methanol, ethyl acetate, or benzene, j is the sensor number, R_j is the baseline resistance of sensor j before exposure to the solvent, and $\Delta R_{sj,max}$ is the largest differential resistance change observed for the jth sensor during the 60 sec exposure to solvent s. For the film thicknesses and solvent concentrations used in this series of experiments, almost none of the sensors reached equilibrium so the recorded $\Delta R_{sj,max}$ value also incorporated temporal aspects of the resistance response of the array. Nevertheless, the histogram in Figure 2.5 clearly shows that the differential resistance response patterns generated by these solvents at this test pressure can be easily distinguished from each other using this modestly-sized sensor array.

The error bars in Figure 2.5 represent the standard error over the various exposures to each solvent (Table 2.2). These experiments were conducted at much higher vapor concentrations than those in Figure 2.2. At these higher concentrations, small decreases in responses and/or shifts in

baselines were observed upon repeated solvent exposures of certain composites, but the small baseline shifts could be compensated for electronically if so desired and such minor shifts did not preclude the use of the sensor array, even under these stressing conditions, to separate the various vapors based on their array responses. The error bars depicted in Figure 2.5 reflect this effect, and also incorporate errors due to instabilities in our flow system and random errors in the resistance measurements. The presence of impurities in the background air stream, such as oil vapor from the compressed air source used to provide the carrier gas flow, would only minimially affect the data of Figure 2.5 since any signals arising from the presence of such impurities would be present in the resistance readings taken before and after exposure to the test vapors. Additionally, a slow baseline drift was also noted for most sensors. Over a three-month period under ambient conditions, the baseline resistances of the composites in our 17-element array increased an average of 16%, with the maximum increase being 55% (for poly(vinyl chloride - *co* - vinyl acetate)) and the minimum being <1% (poly(methyl vinyl ether - *co* - maleic anhydride), although this baseline drift did not significantly affect the $\Delta R/R$ performance of the sensor array.

2. *Principal Component Analysis for Data Reduction of an Array Response*

A more quantitative approach to evaluating the performance of the sensor array is provided by principal component analysis. Principal component analysis transforms multivariate data sets into a coordinate space that allows for the variance in the data to be represented in the minimum number of dimensions. The vectors in this new coordinate set are the principal components of the data stream, and the separation between various vapors (e.g., various presentations to the array) is therefore readily visualized in this transformed data space.[39,40]

The principal components are linear combinations of descriptors (in our case, the relative differential resistance responses):

$$\mathbf{P} = \mathbf{DC}, \qquad (1.2)$$

where $\mathbf{D} = \{d_{ij}\}$ and $\mathbf{P} = \{p_{ij}\}$ are m x n matrices and $\mathbf{C} = \{c_{ij}\}$ is an n x n matrix containing the coefficients of the linear combination. For a sensor array (with n sensors) exposed m times to various analytes, d_{ij} represents the response of the jth sensor to the ith exposure and p_{ij} the jth principal component for the ith exposure. The power of principal component analysis stems from the fact that the coefficient matrix, **C**, (containing as its columns the eigenvectors of the covariance matrix $\mathbf{D}^T\mathbf{D}$) is chosen such that the principal components are mutually orthogonal, even though the original descriptors may have been heavily correlated.

Prior to performing principal component analysis, the data from the 17-element sensor array were normalized and autoscaled. The maximum differential resistance change for the jth sensor to the ith exposure, $\Delta R_{ij,max}$, was normalized by the sum of the responses for all 17 sensors to that same exposure to produce a value S_{ij}:

$$S_{ij} = \frac{\Delta R_{ij,\max}}{\sum_j \Delta R_{ij,\max}} \qquad (1.3)$$

where S_{ij} is the normalized signal. This normalization involves a summation over the entire array for a given exposure rather than over a collection of exposures for a given sensor, as in eq 2.1. The normalization of eq 2.3 helps correct for differences in the exposure concentrations, which are a consequence of the solvents' differing vapor pressures. In the limit of linear response, the normalization process assures that the solvents are not being distinguished on the basis of their concentrations alone. The normalized maximum relative differential resistance changes were then autoscaled, resulting in a set of descriptors, d_{ij}, that were defined as:

$$d_{ij} = \frac{S_{ij} - \bar{S}_j}{\sigma_j} \qquad (1.4)$$

Here, $\bar{S}_j$ and σ_j are the mean and standard deviation, respectively, of all of the normalized signal responses of sensor j to the entire range of solvents. This autoscaling procedure provides a means of accounting for differences in the dynamic ranges of the sensors. After normalizing and autoscaling, the data were transformed into principal component space. The principal components were numbered in accord with the amount of variance they contained: the lower the number, the more variance contained along that direction in principal component space.

The first five principal components (Figure 2.6) contained greater than 98% of the total variance in the data. The patterned areas in Figure 2.6 encompass all of the responses of the array that were produced during the repeated exposures to each specified vapor. The representation in principal component space clearly shows not only that, at the test concentrations used in this work, the carbon black-polymer composite array can readily distinguish nonpolar from polar solvents (e.g., benzene or toluene from methanol or acetone) but also illustrates that such an array can readily distinguish members of a related class of materials (e.g., methanol from ethanol from 2-propanol, or benzene from toluene). A notable feature of this type of sensing device is that the sensor elements were not designed *a priori* to have specific responses to any particular vapor or class of vapors, yet the array could nevertheless separate a broad range of chemical species having relatively subtle differences in their chemical/physical properties.

3. Array Response to Mixtures

The ability of our sensor array to analyze vapor mixtures was also of interest. To explore this property, the sensor array was exposed to varying vapor concentrations of ethanol and methanol, and then to mixtures of these two vapors. To accomplish this, varying flow rates of air saturated with methanol and/or air saturated with ethanol were mixed into a 10 L min^{-1} vapor-free air flow. For the mixtures, both the total flow rate of the methanol/ethanol analyte stream and the relative amounts of methanol to ethanol in the stream were varied. In the analysis of these data, the maximum relative differential resistance changes from the sensor array, $\Delta R_{max}/R$, were not normalized according to eq 2.3 since the concentration dependence was also of significance in these experiments. Instead, the data (presented in Table 2.3) were simply autoscaled according to

eq 2.4 and then transformed into principal component space. In these experiments, the variation in the analyte flow rates of the various mixtures at a given total analyte concentration was so small relative to the background flow rate that autoscaling of the data was still valid.

The first two principal components of this data set (containing 94% of the total variance in the data) are shown in Figure 2.7. The sensor array could distinguish methanol from ethanol at any of the concentrations studied and was also able to quantify the concentration of these vapors. In addition, for the mixtures, the data defined two distinct (pseudo-linear) paths that spanned the region between the responses of the pure components. Each path contained the data for a given total analyte flow rate, and the position along either path indicated the methanol/ethanol ratio of the mixture. Hence, the sensor array was also able to quantify the absolute concentration of each species in this binary mixture over the tested concentration range.

IV. Discussion

A. Classification and Identification of Vapors Using the Carbon Black-Organic Polymer Chemiresistor Array

1. General Features of the Chemiresistor Array

The success of modestly-sized arrays of chemically sensitive resistors in the detection and classification of vapors underscores the advantages of an approach to chemical sensing that utilizes broadly responsive sensing elements. The use of a common conducting phase, combined with the use of conventional insulating organic polymers to achieve the differential swelling properties of the various sensor elements, allows fabrication of such arrays from readily available, stable 2.materials. An additional attractive feature of the present system is the simplicity of the signal transduction process. A chemical sorption event is directly transduced into an electrical resistance signal that can be readily integrated with inexpensive, conventional, signal processing circuitry.

Despite the lack of chemical specificity in the binding of an analyte to an individual array element, the carbon black-polymer composite chemiresistor array discriminated between a variety of vapors, some of which displayed very subtle chemical differences. This array also was able to identify and quantify the vapor mixture tested in this initial study. In fact, the 17-element carbon

black-based sensor array was able to distinguish all of the nine test analytes from each other at the specific test concentrations used in this work, even though this test set required distinguishing molecules from very different classes, such as alcohols from aromatics, as well as those within a particular class, such as benzene from toluene or methanol from ethanol from 2-propanol.

The ability to resolve various vapors is quantified by their separation in principal component space. The best resolved vapors generally showed the largest separation in the early principal components, i.e., in those components containing the most variance in the data. For exposure of our array to the nine test analytes at the test concentrations used in this work, the first five principal components (shown in Figure 2.6) contained 49%, 25%, 17%, 4%, 2%, and 1%, respectively, of the total variance. The positions of the various data points in the principal component space depicted in Figure 2.6 therefore need to be scaled by the relative magnitudes of each principal component in order to obtain a true visualization of the resolving power of the sensor array. The greatest resolution was observed between the polar compounds, which were distinguished in the first three dimensions of principal component space (Figure 2.6a). This is reasonable because nearly all of the sensor elements were reasonably polar, with many being able to participate in hydrogen bonding, so gas-solid interactions based on polarity dominated the binding of the various analytes into the composite films of the sensor array. The more non-polar molecules were separated collectively from the polar compounds in the first three principal components, but separation of the non-polar compounds from each other was based on more subtle effects. These effects only become evident through an analysis of the higher principal components of the sensor array response (see Figure 2.6b). Of course, principal component analysis is a purely statistical approach to data reduction, and a neural network could easily be trained, without additional array design, to assign an increased weighting to the response of certain sensors if the primary function of the array were, for example, to separate benzene from toluene. Even restricting the data evaluation to principal component analysis, resolution of non-polar analytes should improve significantly with the incorporation of additional sensor elements having composite films fabricated from carbon black and non-polar organic polymers.

Ideally, the swelling-induced relative differential resistance response of each of the chemiresistors could be related to solubility parameters that correlate with the partition coefficients for binding of a given vapor into a given polymer film. Such a correlation has been drawn for the swelling of a commercial carbon black-polymer composite with a variety of saturated vapors.[23] For some of our chemiresistors, the relative differential resistance response did indeed track with the extent of swelling predicted by solubility parameters. For other chemiresistors, however, the agreement between maximum relative differential resistance changes and solubility parameters was poor. There was some difficulty in drawing definitive conclusions from our experiments because the vapor concentrations for the nine solvents were different (thus requiring correction based on linear response) and because the short exposure times used to investigate the array responses to various vapors did not permit equilibrium to be reached on the sensor elements at the test concentrations and composite film thicknesses used in this study. However, as long as the exposure period was maintained constant, the data of Figures 2.5 and 2.6 show that the various vapors could be distinguished even without reaching an equilibrium differential resistance signal (which could be obtained in a specified time period through use of thinner films, if so desired). The data of Figure 2.5 do qualitatively show the selectivity of the sensors for different solvents and demonstrate that these responses agree with simple chemical ideas. For instance, the $\Delta R_{max}/R$ response of the protic poly(4-vinyl phenol) composite, sensor #1, to methanol was 55 times greater than that its response to benzene. The situation is reversed for one of the non-polar sensor elements, PEVA (sensor #16), with benzene producing a 42 times larger $\Delta R_{max}/R$ signal than methanol. Note that although it is possible to analyze the data of Table 2.2 to ascertain which subset of sensor elements provided the "best" discrimination for a given pair of vapors, this assessment is very task-dependent (i.e., the "best" subset of sensors for separating benzene from toluene are different from the "best" subset of sensors for separating methanol from ethanol and are different yet again from the "best" subset of sensors for separating benzene and toluene in the presence of methanol or ethanol, etc.), so this type of evaluation has not been performed extensively at this time.

Further improvements in the resolving power of the sensor array are expected when the temporal information provided by each solvent is incorporated into the data analysis algorithm. The time course of the resistance change is a potentially valuable additional discriminant because it will reflect the diffusion rate of a vapor into a particular film.[41] In fact, the concentration of $CHCl_3$ or CCl_4 above a poly(vinyl chloride)-carbon black composite has been determined previously on the basis of temporal response information alone and potentially can take advantage of data involving specific molecular interactions that affect the binding and diffusion kinetics of various analytes into the sensor elements.[25] We are currently investigating the best means by which test analytes can be classified by our sensor array; however, since it is unlikely that a single algorithm will be optimal for all tasks on a given sensor array, we have not pursued this scenario-specific analysis extensively at the present time.

2. *Identification of Mixtures and Distinguishing Unknowns from Mixtures of Previously Identified Vapors*

The identification and quantification of methanol/ethanol mixtures by the sensor array highlights further the potential power of array-based sensing, provided that linearity is maintained or that extensive calibration runs are performed over nonlinear response regions. Determining both the ratio of components in, and the total concentration of, a binary mixture necessarily requires more than a single degree of freedom. Although such additional degrees of freedom could be achieved with a single sensor, for instance by using temporal information, they are much more easily incorporated into a multi-component architecture such as in the array structure described herein. The data of Figure 2.7 also show that, for methanol/ethanol mixtures, the separation between methanol and ethanol vapors in principal component space is maintained for several different concentrations of these vapors both separately and in binary mixtures. Of course, evaluation of the quantitative changes in separation factors in principal component space that might occur for all possible analytes of interest at all possible concentration ranges of practical interest is beyond the scope of this initial investigation. Clearly, the separation ability of such arrays

contemplated for any specific practical application must be evaluated for the task of concern under application-specific conditions.

A particularly interesting question that naturally arises in the context of environmental monitoring is whether a sensor array can distinguish a chemically distinct species from a mixture of vapors for which the array response has been previously investigated. A multi-linear regression was thus performed to determine if the array response of a given member of our collection of test solvents could be expressed as a linear combination of the responses of the other test solvents. In this evaluation, the best fit parameters, $\boldsymbol{a} = \{a_1, a_2, \ldots, a_8\}$, to the following system of linear equations were determined using a constrained multi-linear regression:[42]

$$a_1\mathbf{r}_1 + a_2\mathbf{r}_2 + \ldots + a_8\mathbf{r}_8 = \mathbf{r}_9. \qquad (1.5)$$

The column vector, $\mathbf{r}_i$, contained the maximum relative differential resistance responses of the 17 sensors to a particular solvent, and the index 9 indicated the solvent to be expressed as a linear combination of the other eight vapors. In the limit of linear response, the coefficients, $\boldsymbol{a}$, are proportional to the partial pressures of the solvents. Consequently, there is a limited range of physically relevant values of $\boldsymbol{a}$. For example, coefficients that represent mixtures containing negative concentrations of any vapor are non-physical and can be rejected. Similarly, if one knew the total vapor concentration, or had some independently determined, physically realistic constraints on the mass balance or on the concentrations of any of the components in the mixture, additional ranges of $\boldsymbol{a}$ could be identified as invalid solutions to the problem of concern and thus also rejected.

In determining the best fit to eq 2.5 with our sensor array, the coefficients $\boldsymbol{a}$ were merely constrained to remain positive, since negative coefficients for our data set implied negative pressures. No other constraints, either on the total pressure of the system or on the pressure limits of a particular species, were applied. Using only this simple constraint criterion, seven of the test solvents at the test concentrations used in this work could be conclusively identified as unique

species that were not mixtures of the other solvents. For example, Figure 2.8 demonstrates the best fit for ethyl acetate in terms of the responses of the array to the other vapors in the test set. The best fit pattern to the ethyl acetate response was generated by a mixture of acetone, benzene and chloroform (840 : 82 : 1). Although this mixture could account for the response of several sensor elements, the complete pattern could not be satisfactorily matched over the entire array. Similar behavior was observed for acetone, chloroform, ethanol, hexane, 2-propanol, and methanol in our system.

Benzene and toluene were the only two solvents that produced responses at the test concentration under study which could be modeled as a linear combination of the maximum relative differential resistance response patterns generated by the other solvents in our test set. For example, the fingerprint of benzene could be successfully modeled as a linear combination of the response produced by toluene combined with responses arising from small concentrations of the other solvents. Use of further information in the data produced by the chemiresistor array, such as the temporal response of the resistance signals, might resolve even these remaining ambiguities. The ability to distinguish chemically distinct species from mixtures of other vapors is a much stronger indication of the information content of the sensor array responses than simply separating individual analytes of similar concentrations, since the inclusion of mixtures and varying analyte concentrations as possible allowed solutions introduces many more degrees of freedom in fitting the data produced by exposure to the unknown vapor. The ability to distinguish chemically distinct test vapors from any physically realistic mixtures of other predetermined vapors further demonstrates the potential of carbon black-organic polymer sensor arrays for environmental monitoring, where the identification of foreign matter is often crucial.

We also note that for many applications that require evaluation of the constancy of complex vapor mixtures, such as for example quality control applications of foodstuffs, linearity of the sensor array response to analyte concentration is not particularly important, whereas constancy of signal response and signal/noise limits are more critical. In contrast, other vapor detection applications might demand different performance specifications. Although it is clear that these

polymer composite chemiresistor materials make promising candidates for sensor arrays, it is not clear at this point which applications are best matched to the performance factors that can be achieved from these types of systems.

B. Response Mechanisms of Individual Carbon Black-Polymer Composite Sensor Elements

1. Correlations Between Resistance Changes and Predictions of Percolation Theory

The resistivity vs. carbon black content of carbon black-organic polymer composites is well described by percolation theory.[16,18,43-45] At low carbon black loadings, the composites are insulators because no connected pathway of conductive particles exists across the material. As the carbon black content is increased, a sharp transition occurs in which the resistivity of the composite can decrease dramatically (by up to 10 orders of magnitude) with a small variation in the carbon black concentration. At this transition point, designated as the percolation threshold, a connected pathway of carbon black particles is formed. A consistent explanation of the differential resistance response of our sensor elements to solvent vapor is that swelling disrupts the conduction pathways, thereby resulting in an increased resistance of the composite film.

More quantitatively, percolation theory predicts that the resistivity of a carbon black-organic polymer composite, ρ, will be given by:[23,43]

$$\rho=\frac{(z-2)\rho_c\rho_m}{A+B+[(A+B)^2+2(z-2)\rho_c\rho_m]^{1/2}}, \qquad (1.6a)$$

where

$$A=\rho_c[-1+(z/2)(1-(v_c/f))], \qquad (1.6b)$$

$$B=\rho_m[(zv_c/2f)-1], \qquad (1.6c)$$

and where ρ_c is the resistivity of the carbon black, ρ_m is the resistivity of the polymer matrix, v_c is the volume fraction of carbon black in the composite, z is the coordination number of the carbon black particles, and f is their total packing fraction ($v_c \leq f$). The volume fraction of carbon black in the composite at the percolation threshold, v_p, is given by $2f/z$. Figure 2.9 displays the theoretical prediction of eq 2.6 for a hypothetical composite having $v_p = 0.33$ and $\rho_m / \rho_c = 10^{11}$,

under the assumption that swelling does not affect the volume of the conductive element but only changes the total volume, V. In this situation, swelling of the insulating phase will produce a relative volume change, $\Delta V/V$, of the film.

In Figure 2.9, two primary response regions can be identified. For volume changes small enough that the carbon black volume fraction in the swollen composite, v_c^{sw}, remains greater than v_p, swelling reduces, but does not eliminate, connected conductance pathways in the film. The relative differential resistance response in this regime is pseudo-linear over a reasonable volume range of the composite (c.f. Figure 2.9 inset). However, for swelling-induced volume changes such that $v_c > v_p > v_c^{sw}$, the resistivity of the swollen film is predicted to be much larger than that of the denser, unswollen composite material.

Experimentally, profiles such as those in Figure 2.9 can be related to the maximum relative differential resistance response data under at least two separate experimental protocols: (1) measuring the time dependence of the resistance change upon swelling by a given solvent vapor, or (2) determining the resistance changes after reaching equilibrium in response to exposure to a series of different concentrations of a given vapor. For swelling of individual carbon black-organic polymer composites by organic liquids or vapors, approach (1) has been demonstrated previously to generate time-dependent resistance changes that are in qualitative agreement with the predictions of Figure 2.9.[24] This approach only can be applied when the resistivity of the carbon-black composite is spatially uniform during the swelling process; i.e., when the diffusion rate of vapor through the film is much greater than the rate of swelling of the composite. In the work described herein, approach (2) has been adopted since it allows a comparison of theory with the maximum relative differential resistance response observed under equilibrium conditions, $\Delta R_{max,\infty}/R$ (Figure 2.3). The similar functional form of the predicted response (Figure 2.9) and the experimental data (Figure 2.3) argues strongly that the swelling-induced relative differential resistance responses of the carbon black-polymer composite chemiresistors are dominated by a percolation mechanism. Note that in our experiments, only those composites having the lowest carbon black loadings, and exposed to the highest vapor concentrations (i.e., the 15% PEVA

chemiresistor exposed to air that was nearly saturated with benzene) swelled sufficiently to ensure that $v_c > v_p > v_c^{sw}$. This behavior is also in agreement with the theoretical predictions of Figure 2.9, in which the swelling required to reach the critical increase in resistance is predicted to be the lowest for the composite with the lowest initial conducting phase content.

The majority of the studies reported herein were restricted to composites in swelling environments where v_c^{sw} remained greater than v_p. For conductive composites swelling in the range $v_c^{sw} > v_p$, percolation theory predicts that the maximum relative differential resistance signal produced at equilibrium in response to a given level of swelling will increase with decreasing carbon black content. This behavior is illustrated in Figure 2.10 using eq 2.6 with $\rho_m/\rho_c = 10^{11}$, $v_p = 0.33$ and assuming a constant 1% swelling for the various measurements. Comparison of Figure 2.4 with Figure 2.10 demonstrates that the PEVA and PVP composites investigated herein behaved in qualitative agreement with the predictions of percolation theory for films in which $v_c^{sw} > v_p$. Thus, the magnitude of the $\Delta R_{max,\infty}/R$ response to a given swelling change can be manipulated through carbon black content even for composites operating under conditions in which $v_c^{sw} > v_p$.

2. Sensitivity Estimates for Vapor Detection Using Carbon Black-Polymer Composite Chemiresistor Arrays

From the data in Figures 2.3 and 2.4, it is possible to estimate the ultimate sensitivities possible with the sensing approaches discussed above. The largest maximum relative differential resistance signal observed in response to a change in partial pressure, ΔP, of a test vapor is expected for a composite having its stoichiometry poised such that the slightest swelling will pass the material through the percolation threshold. Although none of the composites synthesized in this work met this criterion, the sharp increase in response observed for the 15% PEVA composite above $P/P^* = 0.81$ can be used to estimate the partial pressure dependence of the maximum relative differential resistance response expected for such a situation (Figure 2.3). Increasing the benzene pressure from $P/P^* = 0.81$ to 0.84 corresponded to the introduction of an additional 3.4 ppt of benzene. The composite resistance increased by a factor of five in response to this change in vapor

pressure, implying that $(\Delta R_{max,\infty}/R)/\Delta P$ would be greater than 100% per ppt, i.e., >1 ppt^{-1} (assuming a linear resistance vs. swelling response over this range of swelling). This is much larger than the $(\Delta R_{max,\infty}/R)/\Delta P$ response observed for swelling of composites having $v_c^{sw}>v_p$. For example, the 15% PEVA sensor's response to 10 ppt of benzene was 10%, yielding a $(\Delta R_{max,\infty}/R)/\Delta P$ response of 0.01 ppt^{-1}. Data for the other sensor/solvent combinations studied in this work (for a 60 s exposure period) can be obtained by scaling these sensitivity values by the relative responses displayed by each sensor/solvent system (Table 2.2).

Of course, the useable information arising from a sensor element is not a function of the signal amplitude alone but depends instead on the signal/noise ratio. Shurmer *et al.* have discussed the ultimate sensitivity attainable with resistance-based vapor sensors in the limit of Johnson or white noise.[46] For application in arrays, the lower limit on the measurable voltage was placed at ten times the noise voltage. For a $(\Delta R_{max,\infty}/R)/\Delta P$ value of 0.25 ppt^{-1}, typical of SnO_2 vapor sensors, the calculated lower detection limit was 1 ppb (ppb = part per billion (v/v)) of solvent vapor. Empirically, however, somewhat higher sensitivity limits of 10-100 ppb were estimated from experimental data using SnO_2 vapor sensors at a signal/noise level of 10:1. Using the same approach as Shurmer *et al.*, the 1 ppt^{-1} $(\Delta R_{max,\infty}/R)/\Delta P$ response of our carbon black composites predicts a lower vapor detection limit of 0.25 ppb at a signal/noise of 10:1 in the most favorable case where the sensor and amplifier noise is purely limited by Johnson noise. For comparison, composites in which $v_c^{sw} > v_p$, i.e., those for which swelling does not induce the composite to cross its percolation threshold, the observed responses of ≈0.01-ppt^{-1} imply Johnson-noise-limited vapor detection levels of ≈ 25 ppb at a signal/noise ratio of 10:1.

The above limits can, of course, only be taken as crude estimates that might be obtained under optimized conditions. The actual signal/noise limits will depend on the acceptable 2.power levels that can be used in the measurement, thermal and temporal drifts, the validity of linear response (especially given the extrapolations made above), and on the other sources of noise such as interference or 1 / f noise, which is characteristic of carbon black-composite resistors.[47] We have performed some sensitivity studies with our current equipment, and observe that the

achievable measurement resolution, rather than noise, limits our sensitivity at present. For example, for a circuit with a 40 kΩ base resistance, our dc resistance measurement resolution is currently 0.025%. For a 55% carbon black - PVP chemiresistor having such a baseline resistance and having its noise less than our measurement resolution, we have been able to sense 70 ppm (ppm = part per million (v/v)) levels of methanol (through a 0.05% maximum relative differential resistance change). This measurement was recorded without the possible sensitivity benefits afforded by working very near the percolation threshold. We are currently fully characterizing the noise in our chemiresistors and improving our measurement techniques to thoroughly investigate the sensitivity limits attainable with carbon black composite films.

An advantage of using sensing elements whose conductivity is dominated by percolation is that their sensing properties can be readily controlled through changes in the composition of the composite. By working near the percolation threshold, such that v_c^{sw} drops below v_p at the slightest swelling, very good sensitivity could, in principle, be achieved in response to small changes in vapor pressure (with a loss of linearity in the resistance vs. vapor concentration profile, however, for a large range of vapor concentrations). Another approach would be to use composites with stoichiometries such that v_c^{sw} passed through v_p after some amount of swelling. The focus here would not be on measuring the actual resistance of the composite as v_c^{sw} dropped below v_p; rather, it would be on determining if v_c^{sw} becomes less than v_p upon swelling. In other words, each composite would provide a binary piece of data that, when coupled with many composites of differing stoichiometries, would determine the degree of swelling. Of course, the resolution of such a system depends on the number of stoichiometries included. Consequently, the size of an array including many different types of polymers might become prohibitively large unless the film deposition process can be automated and miniaturized. The final approach suggested by the form of $\Delta R/R$ vs. $\Delta V/V$ shown in Figure 2.9, and the one used in our sensor array, is to use composites such that v_c^{sw} remains greater than v_p upon swelling. Although this may not afford the sensitivity of exclusively using composites with v_c slightly above v_p, the lower resistivities of the composites utilized herein permit the utilization of thin films to obtain rapid

response times, allow operating in the linear response range in order to utilize the principle of superposition to analyze unknown patterns produced by the array, and allow use of a relatively inexpensive multiplexing digital multimeter to monitor the data arising from the array elements.

V. Conclusions

A broadly responsive, easily monitored vapor sensor has been developed using thin film, carbon black-polymer composites. The chemiresistor elements have been shown to give distinctive, low-power, dc, signal patterns in response to the presence of test concentrations of various organic solvent vapors. The response mechanism of the sensors has been shown to agree qualitatively with predictions of percolation theory. An understanding of the response mechanism allows for the sensor response signals to be deliberately tuned to a desirable range by changing the nature and abundance of the insulating polymer and/or the abundance of carbon black in the sensor film. This type of sensor is inexpensive and easily fabricated. Furthermore, the ease with which it can be modified as well as customized for specific chemical and environmental monitoring tasks makes it potentially attractive for such applications.

VI. References

(1) Reed, R. R. *Neuron* **1992**, *8*, 205.

(2) Lancet, D.; Ben-Arie, N. *Curr. Biol.* **1993**, *3*, 668.

(3) Zaromb, S.; Stetter, J. R. *Sens. Actuators* **1984**, *6*, 225.

(4) Lundstrom, I.; Erlandsson, R.; Frykman, U.; Hedborg, E.; Spetz, A.; Sundgren, H.; Welin, S.; Winquist, F. *Nature* **1991**, *352*, 47.

(5) Shurmer, H. V.; Gardner, J. W. *Sens. Actuators B* **1992**, *8*, 1.

(6) Gardner, J. W.; Bartlett, P. N. *Sens. Actuators B* **1994**, *18*, 211.

(7) Abe, H.; Yoshimura, T.; Kanaya, S.; Takahashi, Y.; Miyashita, Y.; Sasaki, S. *Anal. Chim. Acta* **1987**, *194*, 1.

(8) Abe, H.; Kanaya, S.; Takahashi, Y.; Sasaki, S. I. *Anal. Chim. Acta* **1988**, *215*, 155.

(9) Amato, I. *Science* **1991**, *251*, 1431.

(10) Newman, A. R. *Anal. Chem.* **1991**, *63*,

(11) *Sensors and Sensory Systems for an Electronic Nose*; Gardner, J. W.; Barlett, P. N., Ed.; Kluwer Academic Publishers: Dordrecht, 1992.

(12) Ishida, H.; Suetsugu, K.; Nakamoto, T.; Moriizumi, T. *Sens. Actuators A* **1994**, *45*, 153.

(13) Nakamoto, T.; Fukuda, A.; Moriizumi, T.; Asakura, Y. *Sens. Actuators B* **1991**, *3*, 221.

(14) Nakamoto, T.; Sasaki, S.; Fukuda, A.; Moriizumi, T. *Sens. Materials* **1992**, *4*, 111.

(15) Nakamoto, T.; Fukuda, A.; Moriizumi, T. *Sens. Actuators B* **1993**, *10*, 85.

(16) Norman, R. H. *Conductive Rubbers and Plastics*; Elsevier: Amsterdam, 1970.

(17) *Carbon Black-Polymer Composites*; Sichel, E. K., Ed.; Marcel Dekker, Inc.: New York, 1982.

(18) Medalia, A. I. *Rubber Chem. Tech.* **1986**, *59*, 432.

(19) Ford, C. J. In U.S. Patent 2,691,134, 1951

(20) Newton, R. G. *J. Rubber Res.* **1946**, *15*, 35.

(21) Sands, A. G.; McDowell, M. V. *Rubber Age, New York* **1956**, *80*, 500.

(22) Boyd, J.; Bulgin, D. *J. Text. Inst. Proc.* **1957**, *48*, 66.

(23) Lundberg, B.; Sundqvist, B. *J. Appl. Phys.* **1986**, *60*, 1074.

(24) Ruschau, G. R.; Newnham, R. E.; Runt, J.; Smith, B. E. *Sens. Actuators* **1989**, *20*, 269.

(25) Talik, P.; Zabkowskawaclawek, M.; Waclawek, W. *J. Mater. Sci.* **1992**, *27*, 6807.

(26) Ballantine, D. S.; Rose, S. L.; Grate, J. W.; Wohltjen, H. *Anal. Chem.* **1986**, *58*, 3058.

(27) Grate, J. W.; Abraham, M. H. *Sens. Actuators B* **1991**, *3*, 85.

(28) Grate, J. W.; Rosepehrsson, S. L.; Venezky, D. L.; Klusty, M.; Wohltjen, H. *Anal. Chem.* **1993**, *65*, 1868.

(29) Gardner, J. W.; Shurmer, H. V.; Corcoran, P. *Sens. Actuators B* **1991**, *4*, 117.

(30) Gardner, J. W.; Shurmer, H. V.; Tan, T. T. *Sens. Actuators B* **1992**, *6*, 71.

(31) Corcoran, P.; Shurmer, H. V.; Gardner, J. W. *Sens. Actuators B* **1993**, *15*, 32.

(32) Shurmer, H. V.; Corcoran, P.; Gardner, J. W. *Sens. Actuators B* **1991**, *4*, 29.

(33) Pearce, T. C.; Gardner, J. W.; Friel, S.; Bartlett, P. N.; Blair, N. *Analyst* **1993**, *118*, 371.

(34) Freund, M. S.; Lewis, N. S. *Proc. Natl. Acad. Sci. U.S.A.* **1995**, *92*, 2652.

(35) Axel, R. *Scientific American* **1995**, *273*, 154.

(36) Freemantle, M. *Chemical and Engineering News* **1995**, p. 30.

(37) Atkins, P. W. *Physical Chemistry;* 5 ed.; W. H. Freeman and Co.: 1994.

(38) Yaws, C. L. *Handbook of Vapor Pressure*; Gulf Publishing Co.: Houston, TX, 1994; Vol. 1-3.

(39) Hecht, H. G. *Mathematics in Chemistry: An Introduction to Modern Methods*; Prentice Hall: Englewood Cliffs, NJ, 1990.

(40) Gardner, J. W. *Sens. Actuators B* **1991**, *4*, 109.

(41) Crank, J.; Park, G. S. *Diffusion in Polymers*; Academic Press: London, 1968.

(42) Spath, H. *Mathematical Algorithms For Linear Regression*; Academic Press: Boston, 1991.

(43) Kirkpatrick, S. *Rev. Mod. Phys.* **1973**, *45*, 574.

(44) Jachym, B. J. In *Carbon Black - Polymer Composites*; E. K. Sichel, Ed.; Marcel Dekker, Inc.: New York, 1982; pp 103.

(45) Reboul, J. P. In *Carbon Black-Polymer Composites*; E. K. Sichel, Ed.; Marcel Dekker, Inc.: New York, 1982; pp 79.

(46) Shurmer, H. V.; Corcoran, P.; James, M. K. *Sens. Actuators B* **1993**, *16*, 256.

(47) Brophy, J. J. *Basic Electronics for Scientists*; McGraw-Hill: New York, 1972.

Table 2.1: Insulating polymers used in composite detector films

Designator	Polymer
1	poly(4-vinyl phenol)
2	poly(styrene - co - allyl alcohol), 5.7% hydroxyl
3	poly(α-methylstyrene)
4	poly(vinyl chloride - co - vinyl acetate), 10% vinyl acetate
5	poly(vinyl acetate)
6	poly(N -vinylpyrrolidone)
7	poly(carbonate bisphenol A)
8	poly(styrene)
9	poly(styrene - co - maleic anhydride), 50% styrene
10	poly(sulfone)
11	poly(methyl methacrylate)
12	poly(methyl vinyl ether - co - maleic anhydride)
13	poly(vinyl butyral)
14	poly(vinylidene chloride - co - acrylonitrile), 80% vinylidene chloride
15	poly(caprolactone)
16	poly(ethylene - co- vinyl acetate), 82% ethylene
17	poly(ethylene oxide)

Table 2.2: Relative differential resistance changes ($\Delta R/R$), in percent, for each sensor element exposed to nine solvents. The numbers of the sensor elements correspond to the polymer composites indicated in Table 2.1. Values are averages of six exposures to each solvent, except for acetone, for which only three exposures were performed. Errors are in parentheses.

Table 2.2

Element ->	1	2	3	4	5	6
toluene	0.13(9)	0.3(1)	1.2(2)	0.4(2)	0.05(2)	0.63(6)
methanol	10.(1)	1.6(1)	1.9(1)	0.37(3)	1.05(3)	16.(1)
isopropanol	0.23(9)	0.17(2)	0.52(9)	0.08(3)	0.02(2)	1.6(5)
hexane	0.06(3)	0.13(3)	0.8(2)	0.28(7)	0.01(2)	0.18(6)
ethyl acet.	1.2(1)	0.66(7)	2.2(2)	0.76(6)	0.14(3)	2.1(4)
ethanol	2.3(7)	0.4(1)	1.3(3)	0.11(5)	0.09(2)	5.(2)
chloroform	0.45(7)	0.70(8)	2.2(3)	0.9(2)	0.35(8)	5.(1)
benzene	0.20(6)	0.35(8)	1.4(4)	0.50(9)	0.09(3)	1.0(2)
acetone	4.179(1)	0.990(1)	3.2880(2)	0.6663(7)	0.1915(3)	2.751(2)

Element ->	7	8	9	10	11	12
toluene	1.9(4)	2.3(2)	0.07(4)	1.4(2)	1.3(5)	0.08(4)
methanol	1.2(1)	0.82(5)	2.3(2)	3.5(5)	2.0(2)	2.3(4)
isopropanol	0.6(1)	0.52(6)	0.06(2)	0.6(1)	0.7(2)	0.08(3)
hexane	0.9(2)	1.4(2)	0.03(2)	0.7(2)	0.6(2)	0.01(2)
ethyl acet.	3.6(7)	4.9(6)	0.39(3)	4.0(5)	3.4(1)	0.31(8)
ethanol	0.9(2)	0.7(2)	0.4(1)	1.6(6)	1.3(3)	0.4(1)
chloroform	3.7(2)	6.9(7)	0.26(5)	3.4(4)	6.(1)	0.15(6)
benzene	2.2(5)	3.0(3)	0.10(3)	1.9(2)	1.7(5)	0.07(3)
acetone	5.619(8)	5.648(5)	0.7723(2)	4.942(9)	3.476(2)	0.5135(6)

Element ->	13	14	15	16	17
toluene	0.07(3)	0.9(2)	4.2(2)	19.(1)	1.47(6)
methanol	0.75(4)	1.3(1)	1.2(1)	0.9(2)	0.74(6)
isopropanol	0.02(2)	0.21(6)	0.9(2)	1.5(4)	0.3(1)
hexane	0.05(3)	0.22(5)	1.1(1)	16.0(9)	0.70(4)
ethyl acet.	0.07(4)	2.2(2)	3.3(2)	7.3(6)	0.88(9)
ethanol	0.02(4)	0.7(2)	0.9(3)	1.1(4)	0.5(1)
chloroform	0.08(6)	1.3(3)	15.(2)	56.(6)	5.(1)
benzene	0.06(4)	1.01(8)	5.3(3)	21.(1)	1.5(1)
acetone	0.0782(6)	2.8883(3)	2.9408(3)	4.313(2)	0.7998(3)

Table 2.3: Relative differential resistance changes ($\Delta R/R$), in percent, for each sensor element exposed to methanol/ethanol mixtures. The numbers of the sensor elements correspond to the polymer composites indicated in Table 2.1; sensor element number 1 was defective at this point and is therefore not included in this tabulation. The concentrations of the components of the mixtures are given in parts per thousand (ppt).

Table 2.3

Exp.	ppt MeOH	ppt EtOH	# 2	# 3	# 4	# 5	# 6	# 7	# 8	# 9
1	8.4(3)	0	0.892	1.142	0.332	0.679	4.194	0.653	0.49	1.401
2	7.1(3)	0	0.803	1.023	0.332	0.594	3.695	0.579	0.429	1.278
3	5.9(2)	0.53(3)	0.804	0.957	0.193	0.566	3.493	0.55	0.417	1.091
4	4.8(2)	1.06(6)	0.625	0.877	0.249	0.396	2.957	0.49	0.417	0.841
5	3.5(1)	1.65(9)	0.535	0.824	0.166	0.424	2.719	0.49	0.368	0.717
6	2.26(9)	2.3(1)	0.491	0.878	0.235	0.283	2.546	0.505	0.393	0.592
7	1.13(5)	2.8(1)	0.402	0.744	0.138	0.17	2.071	0.446	0.343	0.374
8	0	3.3(2)	0.223	0.638	0.152	0.028	1.656	0.416	0.319	0.218
9	0	3.9(2)	0.268	0.718	0.222	0.057	1.833	0.431	0.319	0.249
10	0	2.7(1)	0.223	0.585	0.125	0.057	1.478	0.342	0.27	0.249
11	5.7(2)	0	0.714	0.904	0.332	0.509	3.197	0.505	0.368	1.154
12	0	2.0(1)	0.223	0.452	0.083	0.028	1.246	0.297	0.221	0.125
13	3.6(1)	0.34(2)	0.268	0.479	0.083	0.141	1.363	0.297	0.221	0.312
14	2.9(1)	0.67(4)	0.313	0.559	0	0.17	1.54	0.282	0.27	0.437
15	2.16(9)	1.01(5)	0.357	0.612	0.208	0.198	1.719	0.312	0.27	0.53
16	1.44(6)	1.35(7)	0.447	0.692	0.166	0.283	1.956	0.372	0.295	0.624
17	0.72(3)	1.69(9)	0.536	0.745	0.18	0.396	2.313	0.401	0.344	0.749
18	4.3(2)	0	0.581	0.745	0.166	0.396	2.43	0.431	0.344	0.905
19	2.9(1)	0	0.447	0.612	0.236	0.283	1.896	0.312	0.27	0.686
20	1.47(6)	0	0.313	0.426	0.055	0.198	1.186	0.238	0.172	0.374
21	0	1.36(7)	0.179	0.399	0.097	0.028	0.89	0.223	0.246	0.031
22	0	0.69(4)	0.089	0.24	0.055	0	0.534	0.119	0.123	0.062

Exp.	ppt MeOH	ppt EtOH	# 10	# 11	# 12	# 13	# 14	# 15	# 16	# 17
1	8.4(3)	0	0.909	0.764	0.403	0.312	0.738	0.873	0.386	0.617
2	7.1(3)	0	0.815	0.669	0.293	0.349	0.708	0.798	0.361	0.561
3	5.9(2)	0.53(3)	0.796	0.628	0.183	0.342	0.615	0.778	0.337	0.532
4	4.8(2)	1.06(6)	0.682	0.519	0.11	0.134	0.574	0.664	0.313	0.436
5	3.5(1)	1.65(9)	0.644	0.491	0.146	0.193	0.534	0.664	0.361	0.437
6	2.26(9)	2.3(1)	0.607	0.437	0.073	0.089	0.472	0.627	0.385	0.428
7	1.13(5)	2.8(1)	0.569	0.382	0.11	0.149	0.37	0.627	0.385	0.386
8	0	3.3(2)	0.493	0.328	0.037	0.03	0.205	0.59	0.433	0.376
9	0	3.9(2)	0.531	0.355	0.11	0.104	0.205	0.705	0.481	0.408
10	0	2.7(1)	0.417	0.3	0.037	0.045	0.185	0.534	0.313	0.301
11	5.7(2)	0	0.721	0.573	0.183	0.386	0.678	0.724	0.337	0.506
12	0	2.0(1)	0.341	0.219	0.11	0.015	0.185	0.42	0.265	0.27
13	3.6(1)	0.34(2)	0.379	0.246	0.037	0.164	0.247	0.458	0.265	0.291
14	2.9(1)	0.67(4)	0.379	0.273	0.11	0.074	0.308	0.477	0.265	0.279
15	2.16(9)	1.01(5)	0.418	0.328	0.147	0.104	0.411	0.438	0.24	0.311
16	1.44(6)	1.35(7)	0.494	0.41	0.073	0.104	0.493	0.496	0.24	0.332
17	0.72(3)	1.69(9)	0.57	0.437	0.183	0.268	0.431	0.553	0.24	0.375
18	4.3(2)	0	0.569	0.465	0.183	0.238	0.514	0.553	0.264	0.374
19	2.9(1)	0	0.418	0.328	0.11	0.164	0.452	0.476	0.192	0.289
20	1.47(6)	0	0.266	0.191	0.11	0.178	0.247	0.267	0.144	0.193
21	0	1.36(7)	0.304	0.191	0.074	0.045	0.206	0.324	0.216	0.192
22	0	0.69(4)	0.19	0.109	0.037	0.045	0.062	0.19	0.12	0.128

Figure 2.1: (a) Schematic of a chemiresistor sensor array and the response profiles generated by such an array. In this work, an array of 17 conducting carbon black-polymer composites has been used (the polymers of the composites are listed in Table 2.1). The resistance of each composite is monitored and observed to increase upon swelling by organic vapors. The open arrow in the schematic is a time marker corresponding to the introduction of solvent vapor and the solid arrow to its removal. The maximum relative differential resistance changes ($\Delta R_{max}/R$) for the elements of the array during exposure to the test vapor provide a fingerprint that can be used to classify various analytes. (b) Schematic showing a cleaved capacitor substrate.

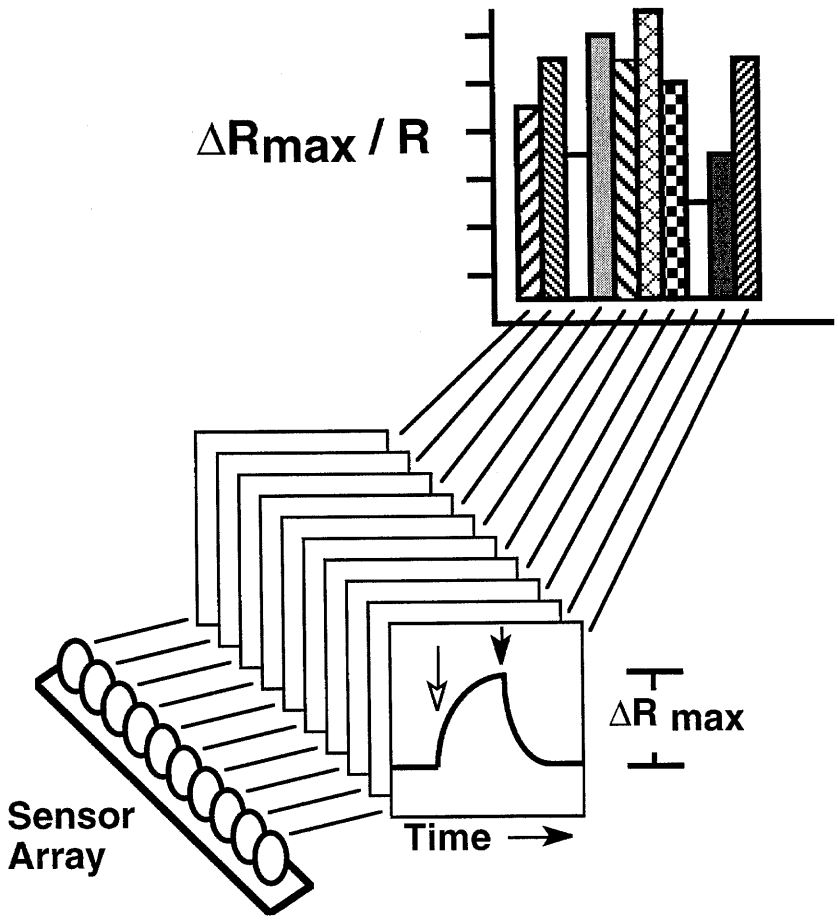

Figure 2.1a

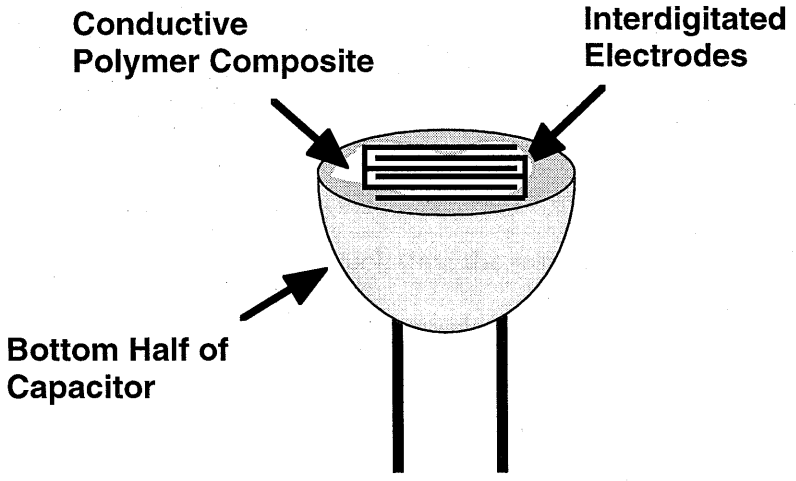
Conductive
Polymer Composite
Interdigitated
Electrodes
Bottom Half of
Capacitor

Figure 2.1b

Figure 2.2: The resistances, *R*, of carbon black composites of (a) PEVA and (b) PVP upon 15 repeated exposures to benzene (at 1.1 ppt) and methanol (at 1.5 ppt), respectively. The PEVA composite was fabricated from a 15% (w/w) carbon black mixture and the PVP composite from a 45% (w/w) carbon black mixture. Both composite films were deposited onto glass slides. The exposure periods were for 15 s during which time the resistances increased as shown. These exposures were interlaced between recovery periods in which the resistances decreased. These traces demonstrate the good reproducibility and stability that can be achieved with carbon black composites.

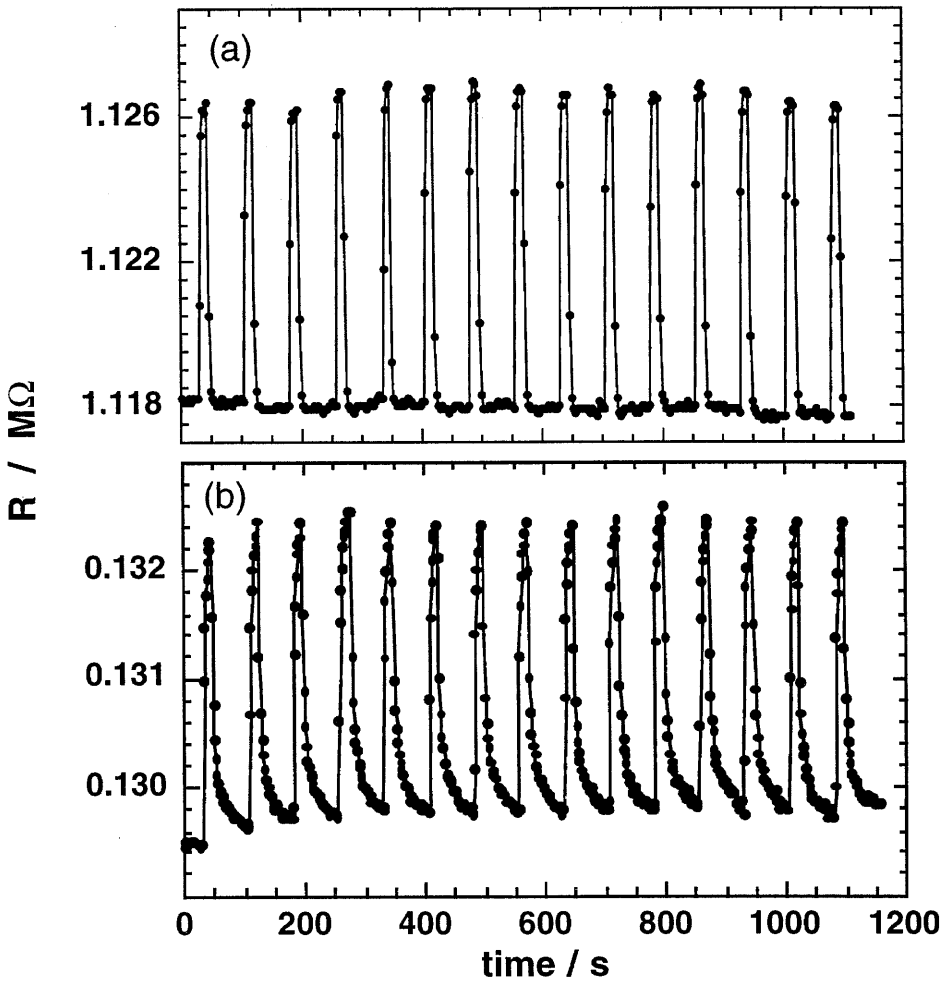
(a)
1.126
1.122
1.118
(b)
0.132
0.131
0.130
R / MΩ
0
200
400
600
800
1000
1200
time / s

Figure 2.2

Figure 2.3: The maximum relative differential resistance changes, $\Delta R_{max,\infty}/R$, for two carbon black composites of PEVA (thin films on glass substrates) in response to varying partial pressures, P, of benzene. The exposure times for different concentrations of benzene varied, but in each case they were sufficient for the chemiresistor to realize its maximum resistance change in response to the test vapor. P^* is the vapor pressure of benzene under ambient conditions, and the legend indicates the carbon black content of the fabrication solution. The film with the lower carbon black content passed through its percolation threshold upon swelling, resulting in a sharp increase in the relative differential resistance change at $P/P^* \approx 0.81$. The film with the greater carbon black content did not exhibit such critical behavior, in accord with expectations that the composite with the higher volume fraction of the conductive component should require more swelling to cross through its percolation threshold. The inset shows the data at low partial pressures on a linear scale to demonstrate the approximately linear dependence of $\Delta R_{max,\infty}/R$ on ΔP in this regime.

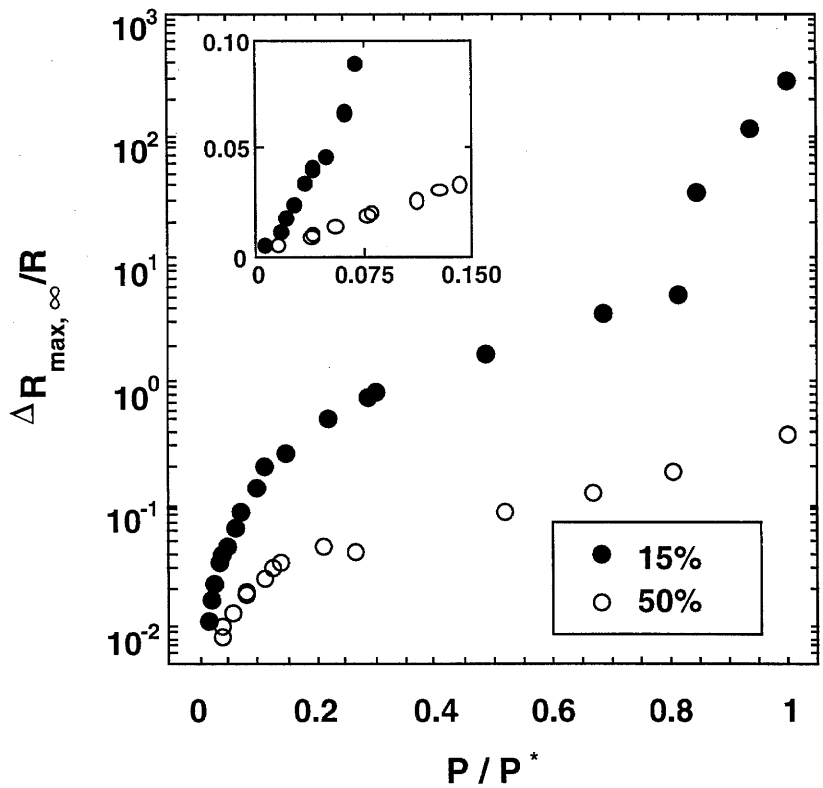
10^3
10^2
10^1
10^0
10^{-1}
10^{-2}
$\Delta R_{max,\infty}/R$
0.10
0.05
0
0
0.075
0.150
15%
50%
0
0.2
0.4
0.6
0.8
1
P / P*

Figure 2.3

Figure 2.4: The maximum relative differential resistance changes ($\Delta R_{max,\infty}/R$, solid circles, left axis) and baseline conductances (G, open circles, right axis) for (a) PEVA- and (b) PVP-carbon black composites (thin films on glass substrates) as a function of carbon black content. For the PEVA sensors, the maximum relative differential resistance changes are those observed in response to 9 ppt benzene; for the PVP sensors, they are those observed in response to 11 ppt methanol. The error bars on the conductance values are estimates based on the deviation between four or five composite films fabricated at each composition, and the error bars of the $\Delta R_{max,\infty}/R$ values are based on the deviation between the responses of these four or five sensors to four exposures each. At carbon black concentrations below those shown, the baseline resistances of the composites were too high to be measured by the multiplexing ohmmeter (>10 MΩ) used in monitoring the array-based sensor.

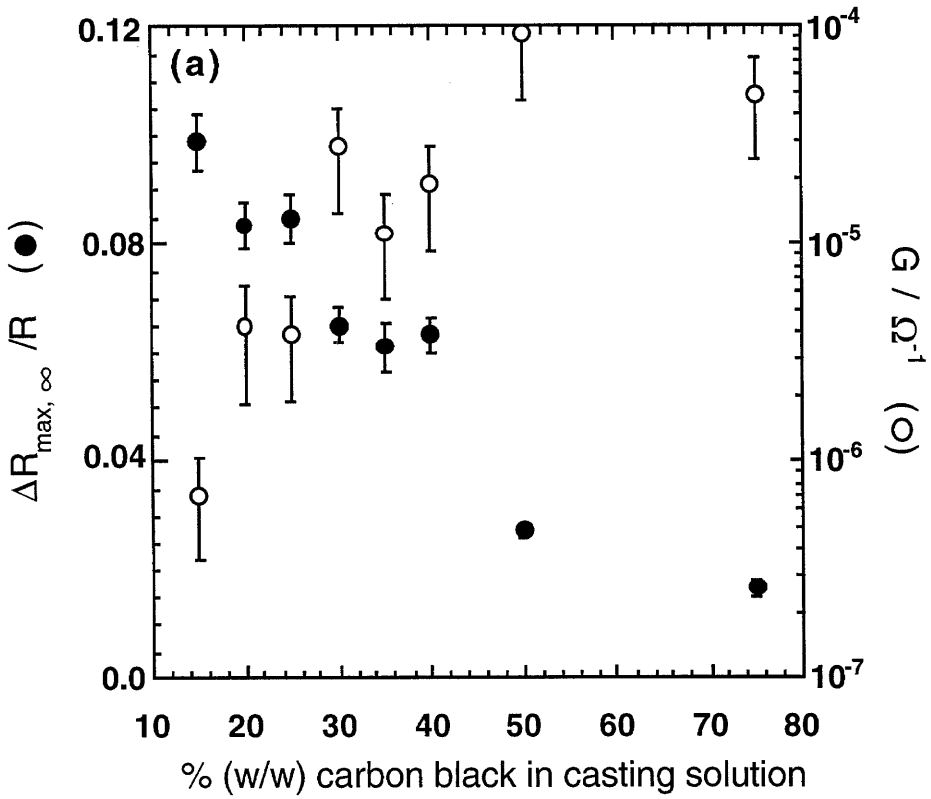
(a)
0.12
0.08
0.04
0.0
$\Delta R_{max,\infty}/R$ (●)
10^{-4}
10^{-5}
10^{-6}
10^{-7}
G / Ω^{-1} (○)
10
20
30
40
50
60
70
80
% (w/w) carbon black in casting solution

Figure 2.4a

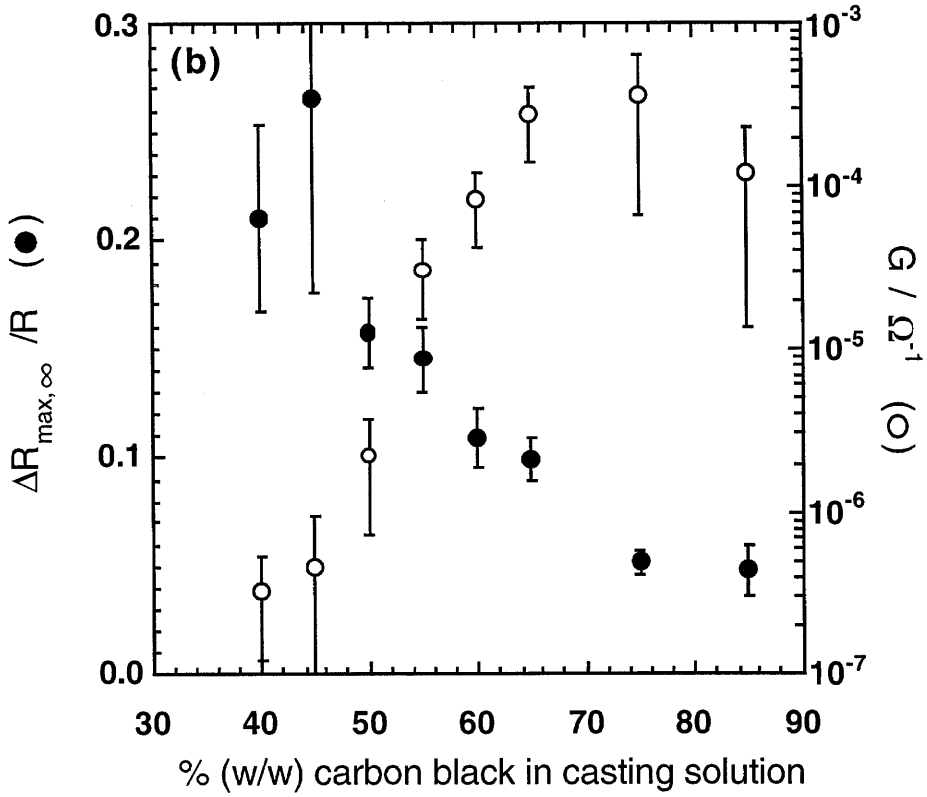
(b)
0.3
0.2
0.1
0.0
$\Delta R_{max,\infty}/R$ (●)
10^{-3}
10^{-4}
10^{-5}
10^{-6}
10^{-7}
G / Ω^{-1} (○)
30
40
50
60
70
80
90
% (w/w) carbon black in casting solution

Figure 2.4b

Figure 2.5: The normalized signal response, S', of the 17 chemiresistors in the array (see Table 2.1) for 60 s exposures to methanol, ethyl acetate, and benzene. The concentrations of each solvent vapor were: benzene: 16.4±0.7 ppt; ethyl acetate 16.0±0.6 ppt; methanol: 21.2±0.8 ppt. Each recorded S value is the average of six separate exposures (Table 2.2). As a visualization aid, each sensor's relative differential resistance response was individually normalized by dividing the $\Delta R_{max}/R$ value observed for exposure to a particular vapor by the sum of that sensor's $\Delta R_{max}/R$ responses to methanol, ethyl acetate, and benzene. The normalization factors (in %) are given parenthetically following the sensor numbers. For instance, for sensor #1, $\Delta R_{max}/R$ was 0.12 (i.e., 12%) in response to methanol. The fingerprints for the three solvents are clearly different, demonstrating the ability of this array to distinguish these vapors.

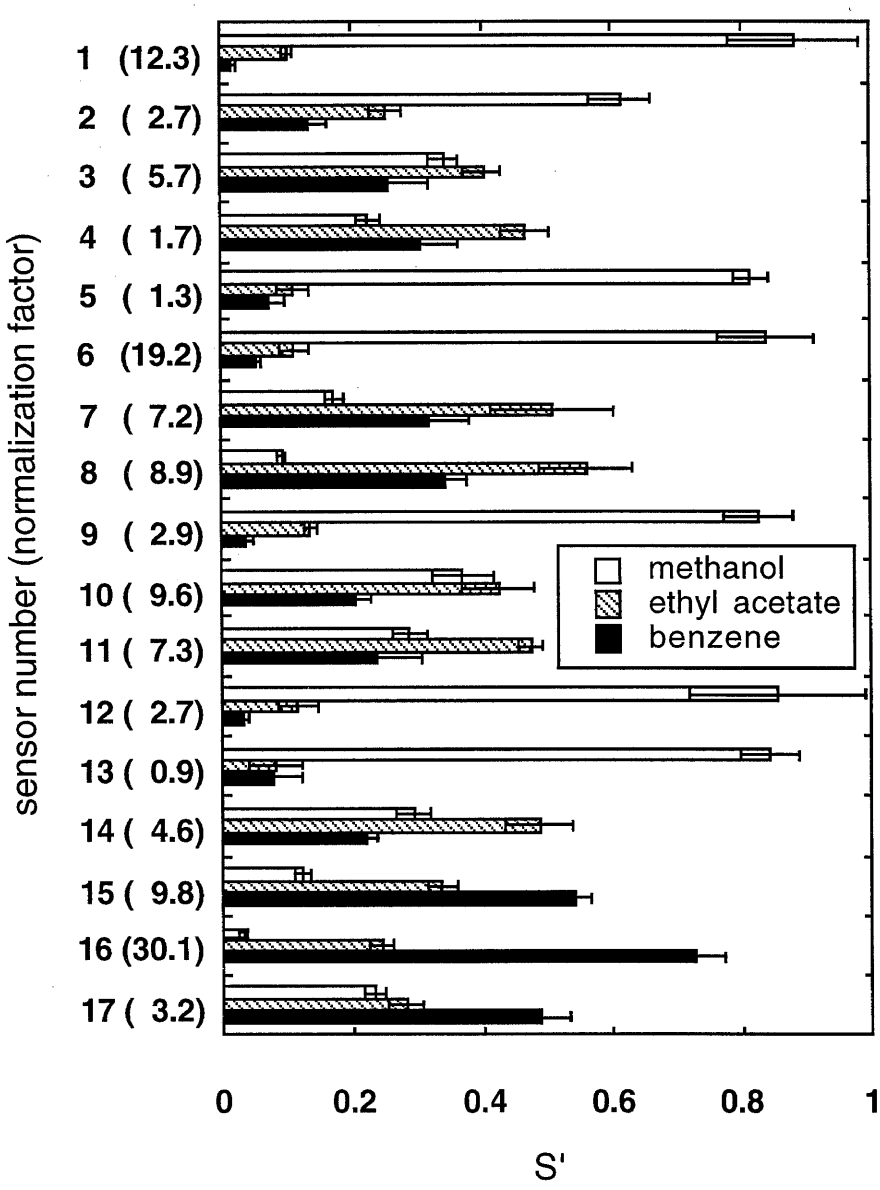
1 (12.3)
2 (2.7)
3 (5.7)
4 (1.7)
5 (1.3)
6 (19.2)
7 (7.2)
8 (8.9)
9 (2.9)
10 (9.6)
11 (7.3)
12 (2.7)
13 (0.9)
14 (4.6)
15 (9.8)
16 (30.1)
17 (3.2)
sensor number (normalization factor)
methanol
ethyl acetate
benzene
0
0.2
0.4
0.6
0.8
1
S'

Figure 2.5

Figure 2.6: The results from the exposure of the 17-element array to nine solvents as represented in (a) the first three dimensions of principal component space, and (b) the third, fourth and fifth dimensions of principal component space. These five principal components contain over 98% of the total variance in the data. The concentrations of each solvent vapor were: acetone: 40±2 ppt; benzene: 16.4±0.7 ppt; chloroform: 34±2 ppt; ethanol: 10.0±0.4 ppt; ethyl acetate 16.0±0.6 ppt; hexane: 26±1 ppt; methanol: 21.2±0.8 ppt; 2-propanol: 7.5±0.3 ppt; toluene: 4.9±0.2 ppt. Each patterned region contains six points corresponding to six exposures of each solvent (Table 2.2), except for acetone which only contained data for three exposures. The unresolved region in PC1-PC2-PC3 space contains the responses to benzene, chloroform, hexane, and toluene. Each loci of points for each solvent occupies a unique region of principal component space, indicating that the array distinguished all nine test analytes.

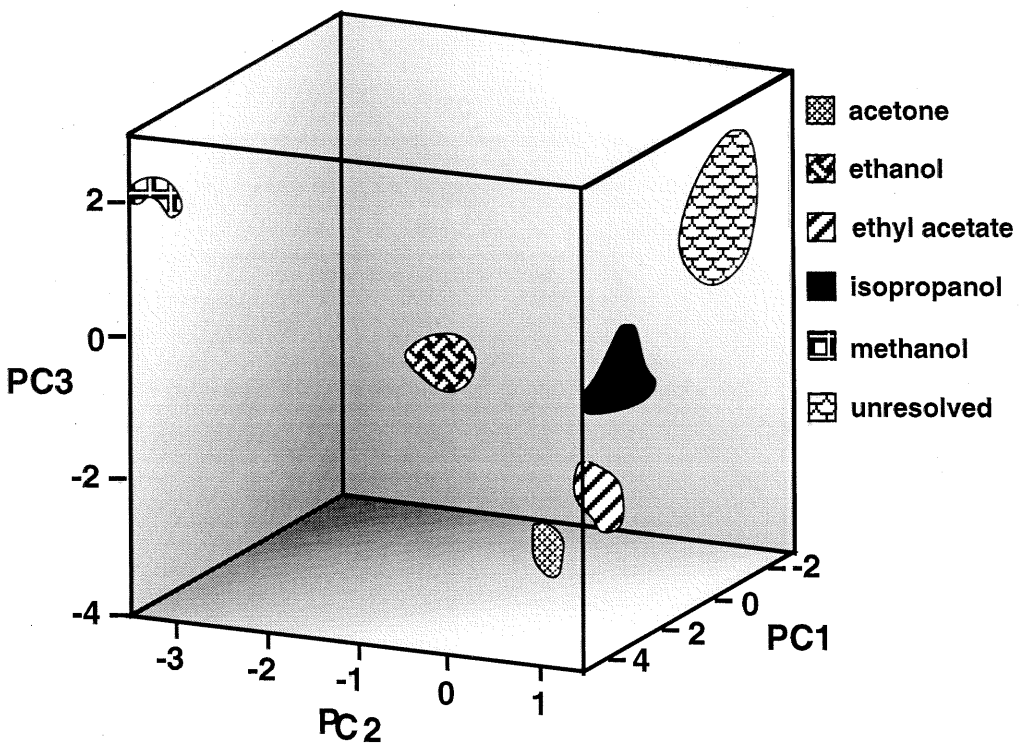
acetone
ethanol
ethyl acetate
isopropanol
methanol
unresolved
PC3
2
0
-2
-4
-3
-2
-1
0
1
PC2
-2
0
2
4
PC1

Figure 2.6a

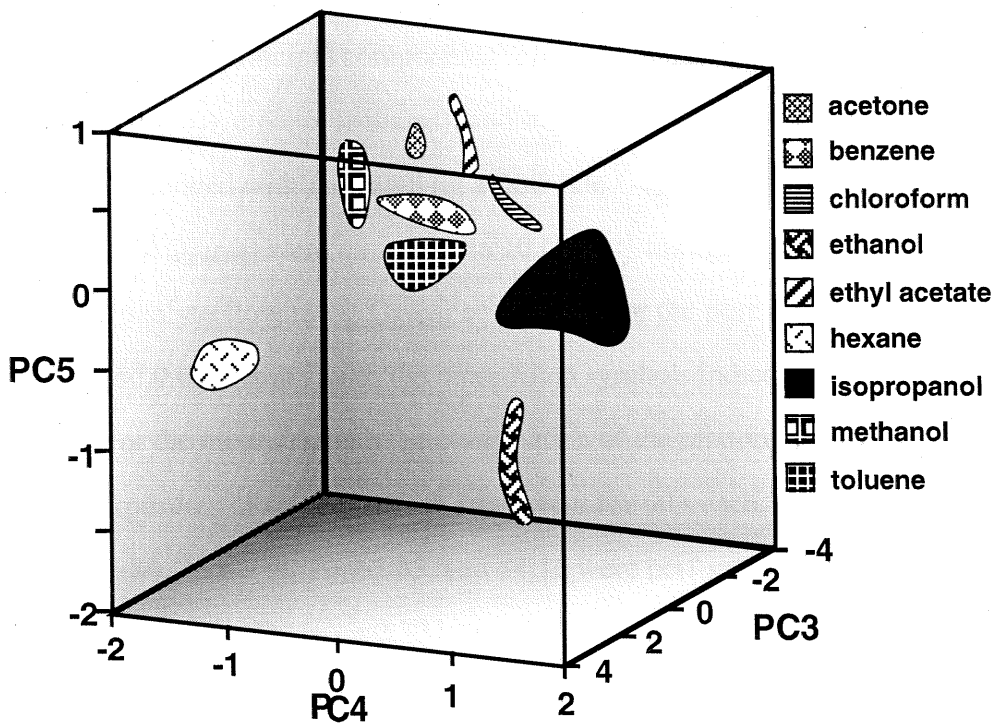
acetone
benzene
chloroform
ethanol
ethyl acetate
hexane
isopropanol
methanol
toluene
PC5
1
0
-1
-2
PC4
-2
-1
0
1
2
PC3
-4
-2
0
2
4

Figure 2.6b

Figure 2.7: The first two principal components resulting from the exposure of a 16-element array to methanol (circles), ethanol (squares), and mixtures of the two (+ and **X**). To expose the sensor, an air flow saturated with methanol (at a flow rate Q_{MeOH}) and/or one saturated with ethanol (at a flow rate Q_{EtOH}) were mixed into a 10 L min^{-1} background flow passing over the sensor array. The analyte flow rates, Q_{EtOH} or Q_{MeOH}, for the pure solvents were 0.10, 0.20, 0.30, 0.40, 0.50, and 0.60 L min^{-1} with the more filled symbols indicating the direction of increasing flow. For the mixtures, both the composition of the mixture and its total concentration were varied and exposures of solvents to the array were for 60 s each. Exposures with Q_{MeOH} : Q_{EtOH} ratios of 16:84, 33:67, 50:50, 67:33, and 84:16 were performed at two different total analyte flow rates: $Q_{MeOH} + Q_{EtOH}$ = 0.30 L min^{-1} or 0.50 L min^{-1} . The direction of increasing mole fraction of methanol in the vapor mixture, χ_M, is indicated. In the limit of linear response, the mixtures are expected to fall on one of the two dotted lines, depending on the total analyte flow rate.

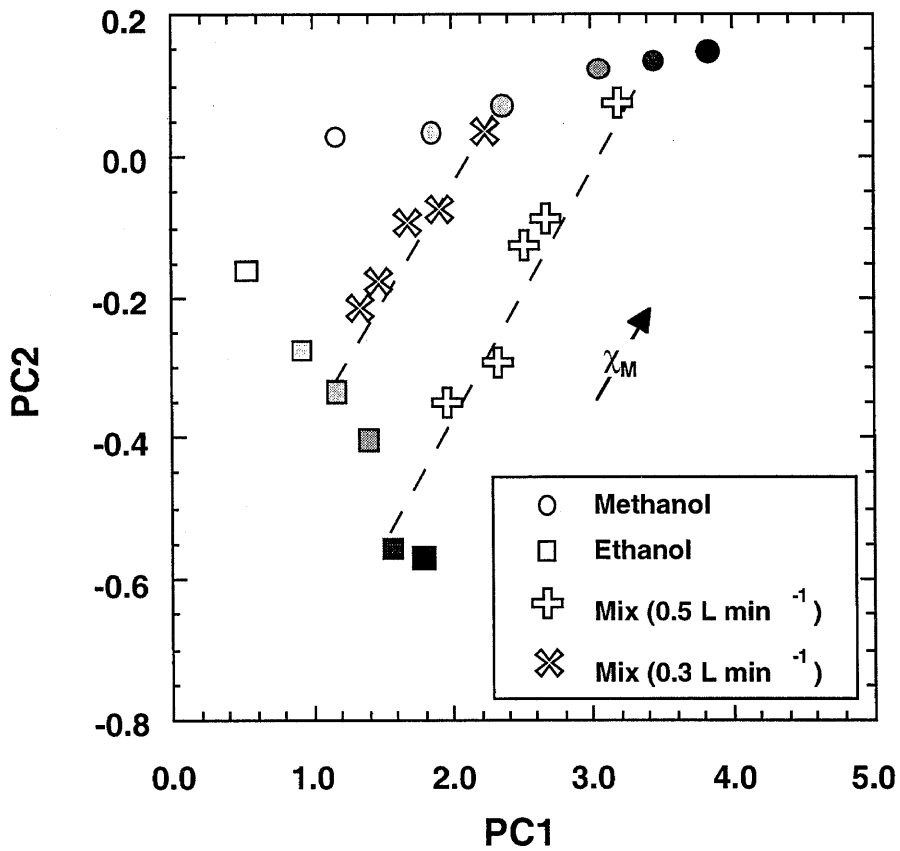
0.2
0.0
-0.2
-0.4
-0.6
-0.8
PC2
0.0
1.0
2.0
3.0
4.0
5.0
PC1
χ_M
Methanol
Ethanol
Mix (0.5 L min $^{-1}$)
Mix (0.3 L min $^{-1}$)

Figure 2.7

Figure 2.8: A histogram comparing the maximum relative differential resistance responses of the 17 sensors during a 60 s exposure to ethyl acetate to those predicted for a hypothetical mixture of acetone, benzene, and chloroform (840 : 82 : 1). This mixture represents the best fit from a multi-linear regression where the maximum relative differential resistance responses to ethyl acetate were modeled as a linear combination of the responses observed during a 60 s exposure to each of the other eight solvents (see eq 2.6 and associated text). Although the maximum relative differential resistance response of some of the sensors could be accounted for, the entire fingerprint could not be satisfactorily modeled. The error bars on the observed data correspond to the variance in responses of similarly prepared sensors.

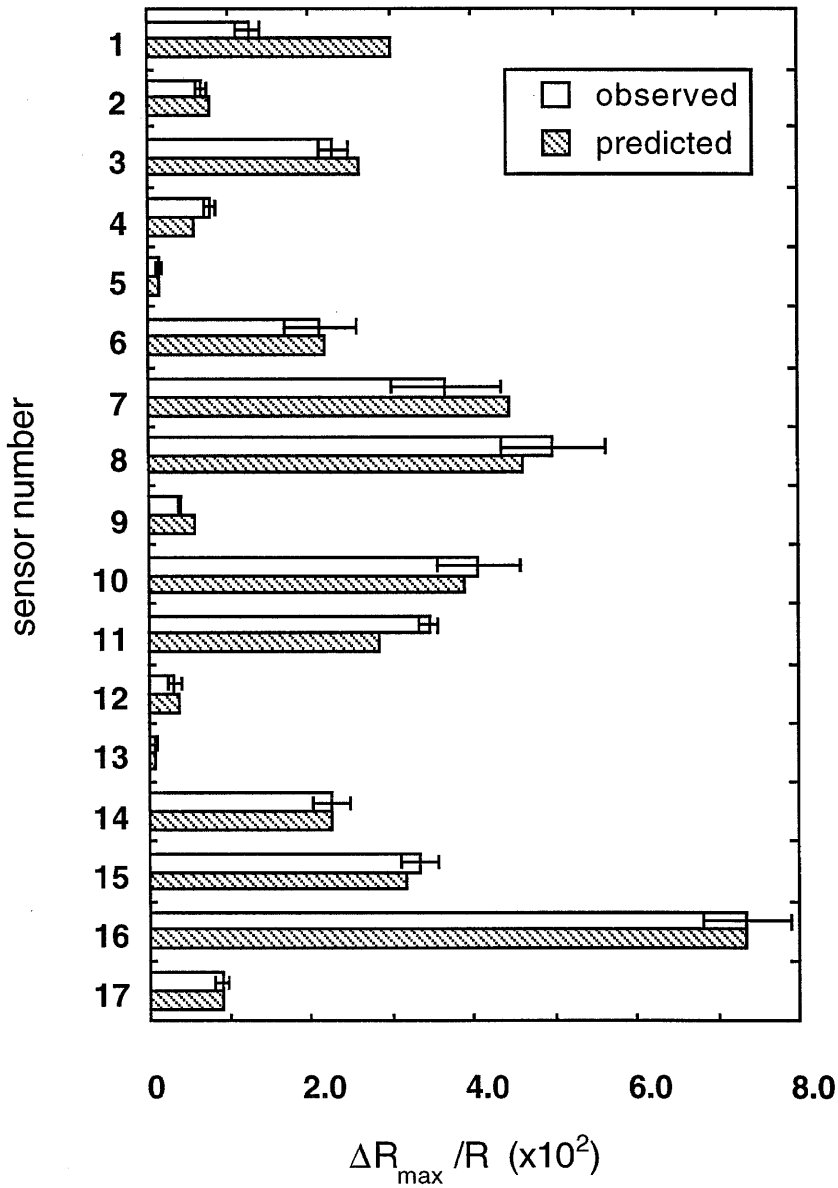
observed
predicted
sensor number
1
2
3
4
5
6
7
8
9
10
11
12
13
14
15
16
17
0
2.0
4.0
6.0
8.0
ΔR max /R (x10²)

Figure 2.8

Figure 2.9: The relative differential resistance change, $\Delta R/R$, predicted by percolation theory (see eq 2.5 and associated text) as a function of the relative volume change, $\Delta V/V$, of a carbon black-polymer composite upon swelling. The volume of carbon black is assumed to be unaffected by swelling and the polymer matrix is assumed to have a conductivity 11 orders of magnitude lower than that of carbon black. The three separate lines are for composites with differing initial volume percentages of carbon black, as indicated. The percolation threshold for the system is at $v_c = 0.33$. The total volume change results in a change in the effective carbon black content, v_c^{sw}. When v_c^{sw} drops below the percolation threshold, a sharp increase in response is observed. Of course, the position of this sharp increase depends on the value of v_c. The inset shows the resistance change on a linear scale for swelling in the region where v_c^{sw} remains greater than its value at the percolation threshold. Comparison of this figure with Figure 2.3 shows the qualitative agreement between the observed response and the predictions of percolation theory.

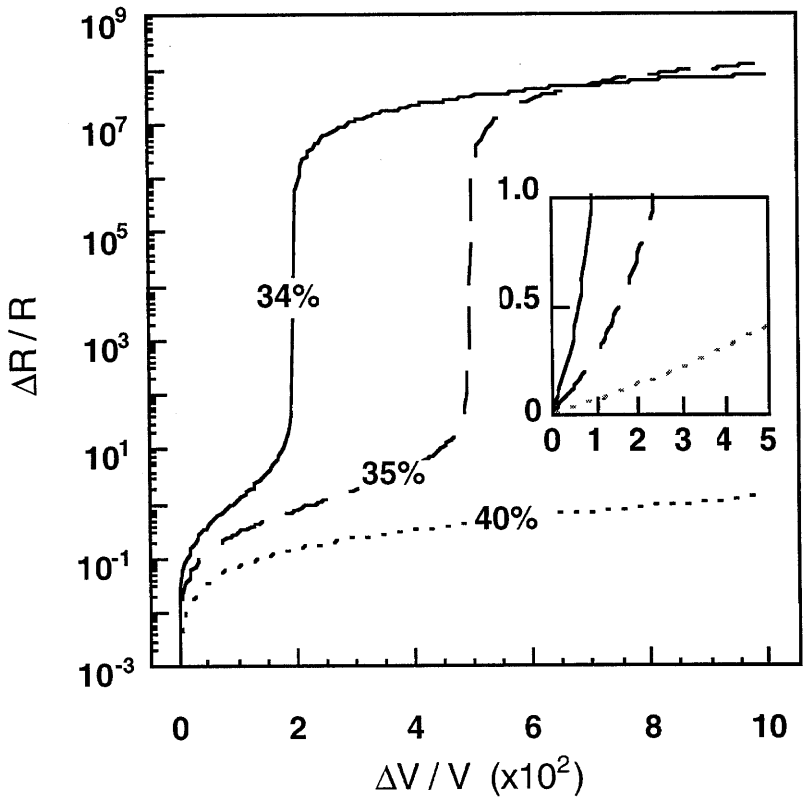
10^9
10^7
10^5
10^3
10^1
10^{-1}
10^{-3}
ΔR / R
34%
35%
40%
1.0
0.5
0
0 1 2 3 4 5
0 2 4 6 8 10
ΔV / V (x10^2)

Figure 2.9

Figure 2.10: The baseline conductivity, σ_i, and relative differential resistance response, $\Delta R/R$, to 1% swelling predicted by percolation theory (see eq 2.5 and associated text) as a function of the initial volume fraction of carbon black, v_c. As in Figure 9, v_p =0.33 and $\rho_m / \rho_c = 10^{11}$. The baseline conductivities are normalized by the conductance of pure carbon black, σ_c. The 1% swelling in this range of compositions is such that the effective carbon black content always remains above the percolation threshold. Comparison of this figure with Figure 2.4 demonstrates the qualitative agreement between percolation theory and the observed $\Delta R_{max}/R$ responses for the carbon black composites studied in this work.

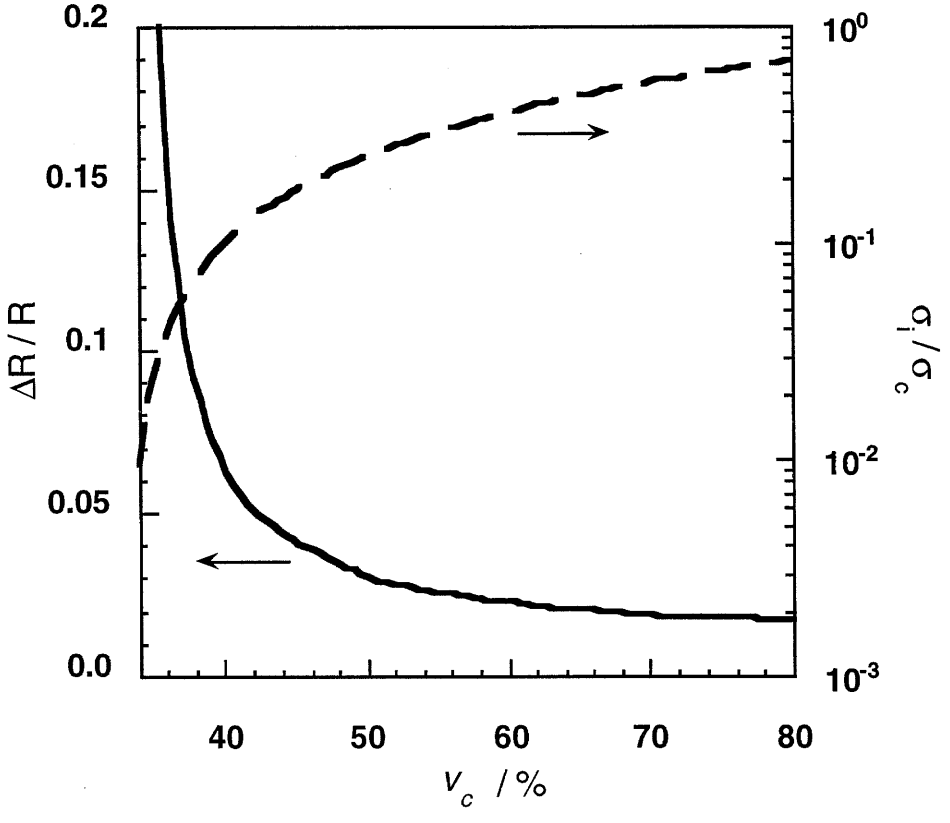

Figure 2.10

Chapter 3

An Investigation of the Concentration Dependence and Response to Analyte Mixtures of Carbon Black-Insulating Organic Polymer Composite Vapor Detectors

Abstract:

The responses relative to an air background of carbon black/polymer composite vapor detectors have been determined as a function of the concentration of a homologous series of alcohols (n-$C_nH_{2n+1}OH$, $1 \leq n \leq 8$), a homologous series of alkanes (n-C_nH_{2n+2}, $5 \leq n \leq 10$ and $n=12,14$), and a set of diverse solvent vapors. In all cases the steady-state relative differential resistance responses of the carbon black/polymer composite vapor detectors were well-described by a linear relationship with respect to the analyte partial pressure, at least over the tested concentration range ($P/P^\circ = 0.005$-0.03 where P° is the vapor pressure of the analyte). When two vapors in air were simultaneously presented to the detectors, the steady-state relative differential resistance response relative to an air background was the sum of the steady-state relative differential resistance responses obtained when each analyte was exposed separately to the carbon black/polymer composite detectors under study. Similarly, when an analyte was exposed to the detectors on top of a background level of another analyte, the steady-state relative differential resistance responses of the array of detectors were very close to those obtained when the test analyte was exposed to the detectors only in the presence of background air. The initial training requirements from the array response output data of such detectors are minimized because the steady-state relative differential resistance response pattern produced by the analyte of concern can be associated uniquely with that odor, under the conditions explored in this work.

I. Introduction

Arrays of several types of vapor detectors are actively being explored to produce an "electronic nose".[1-5] In this type of system architecture, no individual detector is highly selective towards an individual analyte, as would be the case in the traditional "lock and key" approach to chemical sensing. Instead, each detector responds to many analytes, and each analyte elicits a response from many detectors. The resulting odor signature from the array of broadly cross responsive detectors is used to classify, and in some cases quantify, the analyte of concern. Detector modalities that have been employed in this architecture include surface acoustic wave (SAW) devices,[6-9] tin oxide detectors,[10-12] electrically conductive organic polymers,[2,13,14] coated fiber optic detectors,[15] polymer-coated micromirrors,[16,17] quartz crystal microbalances (QCMs),[18,19] and carbon black-polymer composite chemiresistors.[1]

These types of broadly responsive detector arrays can be useful in at least two generic categories of sensing tasks. In one mode of operation, the array is only required to sense changes in an odor relative to a known prior condition. The changes of interest may have many different physical and/or chemical origins, some of which may not be anticipated in advance, but all of which should optimally be probed by the vapor detector array. This mode of operation is useful for applications in quality control and quality assurance of foodstuffs, fragrances, consumer goods, and similar applications.[14,20-22] For such purposes, the detector response need only be reproducible from trial to trial, and no constraints on the form of the detector response are necessarily required to perform the task at hand.

In another operational mode, a detector array could be used to identify a signature of an odor in the field based on a comparison of the array response to the response signature that was recorded and stored for that analyte during a prior training/calibration run.[23-25] Such applications might include providing a warning when a particular odor becomes present above a certain concentration level in the vapor phase, tracking and/or localization of an odor in the environment, or determining the concentration of an analyte in a simple, but relatively time-independent, effluent mixture. In these types of applications, it is highly advantageous to utilize detectors that have a

linear output signal in response to variations in the concentration of a particular odor, so that the pattern type allows identification of the odor while the pattern height can be straightforwardly related to the odor concentration. It is even more advantageous if the array response to the odor of concern is the same in the absence and presence of other odors. In this fashion, the initial training requirements from the array response output data are minimized because the pattern produced by the analyte of concern can be associated uniquely with that odor regardless of the changing environmental conditions under which the analysis is performed.

Prior work in our laboratory has demonstrated that insulating organic polymers interspersed with domains of electrical conductors can provide chemically sensitive detector materials that can be used to produce an "electronic nose" array.[1,2] The conducting polymer composites have been formed using either organic, inorganic, or carbonaceous materials as the conducting phase. Sorption of organic solvent vapors into these types of detectors produces a characteristic, reversible resistance change in the detector element.[1] Because every organic polymer will have a characteristic gas/polymer partition coefficient in response to the presence of a particular odor, a collection of insulating organic polymers provides a diversity in detector materials that produces the diagnostic response pattern of the detector array. Under certain circumstances, analysis of the pattern of signals produced by the detector array then allows information on odor classification and concentration to be extracted through signal processing methods.[26]

In this work, we describe the results of an extensive set of experiments designed to investigate the behavior of arrays of conductive polymer composite detectors when presented with a broadly construed, generic set of test organic vapors at varying analyte concentrations. In addition, we have probed the response when the detectors are exposed to various concentrations of members of homologous series of alkanes or alcohols. Additionally, the detector response properties have been investigated during exposure to various binary vapor mixtures to ascertain whether an array response pattern for a pure odor is transferable, weighted by the mole fraction of its vapor in an analyte mixture, to binary mixtures of analytes. Finally, we describe the results of

experiments in which a small but rapidly changing odor concentration has been superimposed upon a relatively slowly-varying baseline odor concentration.

II. Experimental

A. Materials

The carbon black used in the composites was Black Pearls 2000 (BP2000), a furnace black material that was generously donated by Cabot Co. (Billerica, MA). The polymers used in the composites are (listed as detector #, polymer): 1, poly(4-vinyl phenol); 2, poly(styrene-co-allyl alcohol), 5% hydroxy; 3, poly(α-methylstyrene); 4, poly(vinyl chloride-co-vinyl acetate), 10% vinyl acetate; 5, poly(N-vinylpyrrolidone); 6, poly(vinyl acetate); 7, poly(methyl vinyl ether-co-maleic anhydride); 8, poly(carbonate bisphenol A); 9, poly(styrene); 10, poly(styrene-co-maleic anhydride), 50% styrene; 11, poly(vinyl butyral); 12, poly(sulfone); 13, poly(methyl methacrylate); 14, poly(vinylidene chloride-co-acrylonitrile), 80% vinylidene chloride; 15, poly(caprolactone); 16, poly(ethylene-co-vinyl acetate), 82% ethylene; 17, poly(ethylene oxide); 18, poly(butadiene), 36% cis-1,4, 55% trans-1,4, 9% vinyl-1,2; 19, poly(epichlorohydrin); 20, poly(styrene-co-butadiene), 28% Styrene; 21, addition product of sodium menthoxide to poly(pentafluorostyrene); 22, (+) isopinocampheol derivatized poly(p-chloromethylstyrene); 23, poly(fluorostyrene); 24, poly(styrene-co-isoprene) (Figure 3.1). All polymers were purchased from Polysciences Inc. or Aldrich Chemical Co. and were used as received, except polymers 20-23, which were kindly supplied by Prof. Robert H. Grubbs of Caltech. The solvents used in this study all were reagent grade and were used as received.

B. Fabrication of Detectors

Two substrates were used for the detectors. In one configuration, two parallel bands of gold, 50-100 nm thick and separated by either 1 mm or 5 mm, were deposited onto conventional 7.5 cm x 2.5 cm glass slides (Corning Inc.). The slides were then cut into strips to produce 0.7 cm x 2.5 cm pieces of glass, with each strip of glass having one pair of Au leads spaced 1 or 5 mm apart. In the second configuration, a commercial surface mounting breadboard was slightly modified to be used as the substrate. The commercial product ("Surfboards") consisted of parallel

leads of metal deposited onto the circuit board material. These leads were soldered to pins that were on 0.10" centers. The commercial product was cut into pairs of leads and was then coated with the composite films.

The detector films were made from a solution of the polymer into which carbon black had been suspended. 160 mg of one of the insulating polymers (Figure 3.1) was dissolved in 20 mL of tetrahydrofuran, and carbon black (40 mg) was then suspended in this solution, to produce a composition of 80% polymer and 20% carbon black by weight of solids. The solvent was generally tetrahydrofuran, benzene or methylene chloride, depending on solubility of the polymer. The solutions were sonicated for 5 min to suspend the carbon black. Aromatics and chlorinated solvents yielded very good suspensions of the carbon black. A single solution that contained the polymer and the carbon black was used to prepare all the detectors of a given composition that were used in this work. An aliquot of the suspension was spin coated, at 1000 rpm, onto a glass substrate using a Headway (Garland, TX) spin coater, and the resulting film was allowed to dry in air. Multiple coatings of the suspension were applied to each substrate to yield detectors having resistance values of approximately a few hundred kΩ. For the fiberglass substrates, the film was applied by dip coating the substrate two or three times until the desired resistance was achieved. Before use, the detectors were dried in open air and then were placed in air flowing at 20 L/min for 12-24 hours.

C. Instrumentation and Apparatus

An automated flow system consisting of LabVIEW software, a Pentium computer, and electronically-controlled solenoid valves and mass flow controllers was used to produce and deliver selected concentrations of solvent vapors to the detectors.[27] To obtain the desired analyte concentration, a stream of carrier gas was passed through a bubbler that had been filled with the solvent of choice. Saturation of the carrier gas with the solvent vapor was verified through measurement of the rate of mass loss of the solvent in the bubbler.[28] The vapor-saturated carrier gas was then diluted with pure carrier gas through the use of mass flow controllers (MKS Instruments, Inc). Calibrations of the flow system using a flame ionization detector (Model 300

HFID, California Analytical Instruments, Inc.) verified that the analyte concentrations delivered to the sensors were those expected from the settings of the mass flow controllers.

The carrier gas for all experiments was oil-free air, obtained from the general compressed air lab source, containing 1.10 ± 0.15 ppth (parts per thousand) of water vapor. The air was filtered to remove particulates, but deliberately was not dehumidified nor otherwise purified. Fluctuations in laboratory temperature, 21.5 ± 1.5 °C, could cause an ≈10% error in setting and controlling the vapor concentrations between nominally identical exposures over the course of the data collection analyzed in this work. No temperature control of the apparatus or of the carbon black-polymer composite detectors was performed.

D. Measurements

The dc electrical resistance of each detector was monitored in response to the presence of various test vapors and mixtures of vapors. Resistance measurements were performed using a simple two-point configuration across the gold leads that bridged the sensing element. The detectors were multiplexed through a Keithley model 7001 channel switcher to a Keithley model 2002 multimeter that measured the dc resistance of each detector once every 3 - 5 seconds, with the exact time interval depending on the particular experiment.

To initiate an experiment, the detectors were placed into the flow chamber and a background flow of compressed air was introduced until the resistance of the detectors stabilized. Each exposure consisted of a three-step process that began with 60 s of air flow to achieve a smooth baseline resistance. After this period, the detectors were exposed to solvent vapor at a controlled concentration in flowing air. The solvent exposure was then followed by a flow of clean air for a time equal to the total exposure time, to restore the baseline resistance values. For the linearity studies, the 60 s baseline period was followed by 240 s of exposure to the test analyte. To probe the dependence of the detector response on the order of presentation, in some measurements of the mixture studies, the exposure phase consisted of parts. In the sequential mixture measurements, the first analyte (denoted as s_1) was exposed for 120 s, at which time the second solvent, s_2, was introduced and exposed for an additional 120 s. During the exposure of

the second analyte, the first analyte was continually flowing (this protocol is denoted as s_1, s_1 $+s_2$). In the measurements when a mixture of two analytes was exposed simultaneously to the sensors (denoted $s_1 + s_2$), the two analytes of the mixture were presented to the detectors for a total of 240 s.

In studies of mixtures, the eight bubblers of the system were divided into two banks of four bubblers each. One mass flow controller was present for "bank A" and one for "bank B" (Table 1). One-way valves ensured that significant gas back flow did not occur during the experiments. Analytes in the same solvent bank could not be exposed simultaneously to the detectors. Therefore, 16 pairs of solvents were available for use in the first set of mixture studies. In the second mixture study only six solvents were used, three in each bank, so nine solvent pairs were available. The detectors used for the eight-solvent experiment were formed from polymers 1-18, 21, 23 (Figure 3.1). The detectors used for the six-solvent experiment, the alcohol linearity study, and the alkane linearity study, were formed using polymers 8, 12, 15-24 (Figure 3.1). In all experiments, one copy of each type of detector was used.

In both the 8-solvent and 6-solvent mixture experiments, the detectors were exposed to individual solvents (s_1), to pairs of solvents presented simultaneously ($s_1 + s_2$), and to one solvent followed by addition of another solvent (s_1, $s_1 + s_2$) (Table 2). The individual solvents and the pre-selected pairs of s_1, s_2 solvents were exposed to the detectors at analyte concentrations that corresponded to 0.5, 1.0, and 1.5 % of each solvent's vapor pressure, P°. In the 6-solvent experiment, individual solvents were additionally presented at 2.0 and 2.5 % of P°. Solvents forming every compositionally distinct binary mixture were permuted in their order of presentation to the detectors, so that for each solvent pair (one from bank A and one from bank B), the trials included the exposure protocol s_A, s_A+s_B as well as the exposure protocol s_B, s_B+s_A. In both experimental runs, 27 unique mixture protocols were investigated for each solvent pair (Table 2). Each unique exposure protocol, for each type of mixture and pure analyte presentation, was repeated 5 times. The 8-solvent experiment thus contained 2280 total exposures (8 solvents, 3 concentrations, 5 repeats of each for the individual solvent exposures, 6 x 8 x 5 simultaneous

mixture exposures, and 16 x 8 x 2 x 5 sequential mixture exposures). The 6-solvent experiment contained 1365 total exposures (6 x 5 x 5 individual solvent exposures, 3 x 9 x 5 simultaneous mixture exposures, and 9 x 6 x 2 x 5 sequential mixture exposures). Within each experiment, every exposure was assigned a randomly generated index number using the Microsoft Excel random number generator. The exposures were then presented to the detector array in ascending order of the assigned index values.

In the studies designed to quantify the detector response as a function of analyte concentration, two homologous series of vapors, one consisting of straight chain alcohols and the other of straight chain alkanes, were exposed to the detectors. The alcohols used were: methanol, ethanol, 1-propanol, 1-butanol, 1-pentanol, 1-hexanol, 1-heptanol, and 1-octanol. In a separate run, n-pentane, n-hexane, n-heptane, n-octane, n-nonane, n-decane, n-dodecane, and n-tetradecane were used. In another, related set of experiments, the broad test set of solvents used in the studies of mixtures (Table 1) was exposed to the detectors over a wider concentration range ($0.005\ P° \leq P \leq 0.03\ P°$) than was used in the runs to determine the detector's response to mixtures of these particular solvent vapors. Additionally, one run with the straight chain alcohols was performed using vapor concentrations that were in the range $0.01\ P° \leq P \leq 0.06\ P°$. In each of these experiments, each unique presentation of an analyte was repeated 10 times, with the entire presentation order (within a run) randomized with respect to solvents, concentrations of solvents, and repeated exposures to a solvent.

E. Data Processing

Although the resistance of each detector was sampled once every 3 - 5 seconds during each exposure, only the maximum relative differential resistance change, $\Delta R_{js,max}/R_{jb,air}$, was used in analysis of the data. Where $\Delta R_{js,max}$, produced by exposure to an individual solvent, is the maximum resistance change of the j^{th} detector during exposure to solvent s, and $R_{jb,air}$ is the baseline resistance of the j^{th} detector exposed to the initial 60 s period of exposure to background air. In the mixture studies when solvents were exposed sequentially to the detectors, three separate relative differential resistance readings were calculated from the data from each exposure protocol

s_1,s_1+s_2. The initial baseline value of the j^{th} detector was denoted as $R_{jb,air}$, the steady-state resistance value during exposure to solvent s_1 was denoted as $R_{j,s1}$, and the steady-state resistance value during exposure to solvent s_2 in the presence of s_1 was denoted as $R_{j,s1+s2}$. The steady-state maximum relative differential resistance change observed upon exposure of the first solvent to the j^{th} detector, $\Delta R_{j,s1,max}/R_{jb,air}$, was calculated using $\Delta R_{j,s1,max} = R_{j,s1} - R_{jb,air}$. The maximum relative differential resistance change upon exposure to the second solvent was calculated using $R_{j,s1}$ as the baseline resistance value for exposure to solvent s_2. Thus, $\Delta R_{j,s2,max}/R_{jb,s1} = (R_{j,s1+s2} - R_{j,s1})/R_{j,s1}$. Finally, the total maximum relative differential resistance change observed as a result of exposure of the j^{th} detector to solvents s_1 and s_2 relative to the initial air baseline resistance of this detector, $\Delta R_{j,s1,s1+s2,max}/R_{jb,air}$, was calculated as $\Delta R_{j,s1,s1+s2}/R_{jb,air} = (R_{j,s1+s2} - R_{jb,air})/R_{jb,air}$. Sample responses for a single exposure and for a sequential mixture exposure are shown in Figure 3.2.

For these solvents and detectors, the exposure time was sufficiently long that the maximum response value, $\Delta R_{js,max}/R_{jb}$, was a very good approximation to the change in the steady-state resistance value of the detectors in response to the specified analyte concentration relative to the baseline resistance of the detector in an air background flow alone. Examples of the temporal dependence of individual carbon black-insulating polymer composite detectors are shown in Figure 3.2. For some exposures in the 8-solvent system, the value R_{jb,s_1} had not completely reached steady state. Therefore, to calculate $\Delta R_{js2,max}/R_{jb,s_1}$ in those cases, the slope of the resistance values 30 s prior to the start of the exposure was calculated and subtracted from the R_{js_2} values. If this correction were not made, then the detector's response to s_2 would have been overestimated.

III. Results

A. Linearity of Detector Response for Pure Odors

Figure 3.3a displays the maximum relative differential resistance data, $\Delta R_{js,max}/R_{jb,air}$, for a 12-element conducting organic polymer composite detector array towards a series of test analytes when each analyte was maintained at a partial pressure, P, in air equal to 3% of its vapor pressure, P°, at 22°C. Each analyte can be seen to produce a distinct $\Delta R_{js,max}/R_{jb,air}$ response pattern on the

array of conducting polymer composite detectors. Principal component analysis was used in order to aid visualization of the differences between $\Delta R_{js,max}/R_{jb,air}$ patterns produced by the various analytes. Figure 3.3b presents the $\Delta R_{js,max}/R_{jb,air}$ data in principal component space, with the axes representing the first and second principal components of the data set. All analytes were well-separated from each other based on the differences between their characteristic $\Delta R_{js,max}/R_{jb,air}$ response patterns on the array of detectors.

The concentration of each analyte was then varied over six even steps in the range 0.005 $P°\leq P\leq 0.03\ P°$. Figure 3.4 depicts the responses of a few representative detectors to all of the test solvent vapors. The data were well-fit by a linear dependence of $\Delta R_{js,max}/R_{jb,air}$ on $P/P°$ over the $P/P°$ ranges probed in this experiment. A summary of the correlation coefficients calculated for these lines is presented in Table 4. For some sensor-analyte combinations the correlation coefficients were low because the sensor exhibited only a very small response to the analyte. For example, poly(sulfone) had a small response to non-polar solvents and so the correlations coefficients for these presentations are low. Similarly, essentially no response was exhibited by poly(sulfone) to dodecane.

Figure 3.5 presents the concentration-dependent $\Delta R_{js,max}/R_{jb,air}$ response data for the entire detector array in principal component space. For each test vapor, the analytes produced a unique signal response pattern, with the pattern direction in principal component space diagnostic of the analyte and the pattern height proportional to the analyte concentration in the vapor phase. This behavior is further illustrated by normalization of the detector response patterns with respect to analyte concentration according to eq 2.1.

$$S_{js} = \frac{\Delta R_{js,max} / R_{jb,air}}{\sum_j \left[\Delta R_{js,max} / R_{jb,air} \right]} \qquad (2.1)$$

where S_{js} is the normalized signal for 12 detector films exposed to benzene, chloroform, and nitrobenzene each presented at $P/P° = 0.005 - 0.03$ in six even steps. As can be seen from Figure

3.6a-c , the characteristic S_{js} pattern of each test vapor was maintained, within experimental error, as the analyte concentration was varied.

Additional experiments were performed using a homologous series of alkanes, and then using a homologous series of alcohols, as test analytes. Figures 3.7 and 3.8 display the $\Delta R_{js,max}/R_{jb,air}$ values for selected detectors. The statistical information on these runs is summarized in Table 4. Again the data were well-fit by a linear dependence of $\Delta R_{js,max}/R_{jb,air}$ on P/P° over the P/P° range probed in these experiments.

Figure 3.9a shows that all of the test alcohols could all be distinguished from one another visually in principal component space when the responses of all detectors in the array are considered. Additionally, like the analytes in the broad test set, the normalized patterns of $\Delta R_{js,max}/R_{jb,air}$ were essentially invariant as the analyte concentration was varied. Identical behavior was observed for the alkanes, as seen in Figure 3.9b. Thus, the $\Delta R_{js,max}/R_{jb,air}$ pattern type is diagnostic of the analyte and the pattern height indicates the concentration of each of these analytes, at least under the conditions of these test runs.

B. Detector Response to Analytes in the Presence of Background Odors

The response of the detectors to various test vapors was also investigated when the detectors were first exposed to, and then maintained in the presence of, a fixed concentration of another solvent vapor. Figure 3.10 exhibits the $\Delta R_{js,max}/R_{jb,air}$ values displayed by poly(ethylene-co-vinyl acetate) and poly(caprolactone) detectors in response to varying concentrations of heptane in the range $0.005\ P° \leq P \leq 0.025\ P°$, relative to an air background gas flow. The responses for heptane vapor at $0.005\ P° \leq P \leq 0.015\ P°$ in air were then recorded when the detector was exposed to the analyte gas stream in the presence of a constant background gas that consisted of air with either 2-propanol, benzene, or cyclohexanone at P/P° = 0.005, 0.010, and 0.015 for each background gas. As displayed in Figure 3.10, $\Delta R_{jheptane,max}/R_{jb,s1}$ and $\Delta R_{jheptane,max}/R_{jb,air}$ were essentially constant for s_1 = benzene, cyclohexanone, 2-propanol at the three values of P/P°. Figure 3.11 shows the same result in principal component space for the responses of the entire array of detectors, illustrating that this behavior is characteristic of the

response pattern in the detector array as well as of the individual detectors displayed in Figure 3.10.

C. Detector Response to Binary Analyte Mixtures

Figure 3.12a shows the $\Delta R_{s2,max}/R_{jb,s1}$ and $\Delta R_{s1,s1+s2,max}/R_{jb,air}$ values of a carbon black-poly(ethylene oxide) detector to mixtures of benzene and heptane, and Figure 3.12b shows the $\Delta R_{s2,max}/R_{jb,s1}$ and $\Delta R_{s1,s1+s2,max}/R_{jb,air}$ values of a carbon black-poly(epichlorohydrin) detector to mixtures of chloroform and methanol. For both of these detectors for both the $\Delta R_{s2,max}/R_{jb,s1}$ and $\Delta R_{s1,s1+s2,max}/R_{jb,air}$ values, s_1 and s_2 were each presented to the detectors at P/P° = 0.005, 0.010, and 0.015.

Figure 3.12 shows that the linear dependence of $\Delta R_{js,max}/R_{jb}$ on P/P° exhibited by an individual detector was maintained when the analyte was a constituent of a binary solvent mixture. The lines that have been drawn in Figure 3.12 to connect the data points also correspond to the change in response that would be expected based on the $\Delta R_{js,max}/R_{jb,air}$ behavior of the detector when presented with corresponding changes in the concentration of the individual solvent vapor in an air background. Additionally, the total $\Delta R_{js1+s2,max}/R_{jb,air}$ response to two solvents relative to a background air baseline was independent of whether the two solvents were exposed simultaneously or sequentially to the detector. Furthermore, in the case of sequential solvent vapor exposures, the maximum relative differential response values for a given solvent were independent of the order in which the solvents were presented to the detector. Figure 3.13 shows similar data, in principal component space, that was produced by an entire array of carbon black-polymer composite detectors during individual analyte exposure, and simultaneous and sequential exposures of binary mixtures of benzene and nitrobenzene. Similar behavior was observed for all nine binary mixtures explored in this work (see section II. D for a description of the binary mixtures explored).

IV. Discussion

A. Linearity of Detector Response vs. Analyte Concentration

The linearity in $\Delta R_{js,max}/R_{jb}$ response of the conducting organic polymer composite detectors vs. the concentration of a pure analyte is readily understood based on the signal transduction mechanism of these types of vapor detectors. Sorption of the vapor into the detector leads to swelling of the polymer, which then produces an increase in the electrical resistance through the network of conducting regions in the composite film. Although the absolute $\Delta R_{js,max}$ of the composite is sensitive to the fractional loading of the conductive filler in the insulating polymer of the conductive material,[29-31] the relative swelling of the film in response to the presence of an analyte vapor should remain constant provided that the filler material does not significantly affect the properties of the insulating portion of the composite. Under such conditions, the ratiometric quantity $\Delta R_{js,max}/R_{jb}$ is expected to be the key parameter that characterizes the response of conducting polymer composite vapor sensors to various analytes of interest. The present work quantitatively confirms these expectations.

Based on the expectations discussed above, for small fractional film swellings, the observed $\Delta R_{js,max}/R_{jb}$ response should be a linear function of the concentration of the vapor that partitions into the film. This appears to be the case for the solvents studied during the course of this work. This type of behavior has been observed for poly(pyrrole) conducting polymer vapor sensors,[32] and for vapor sensors that monitor the capacitance change of dielectric polymer films in response to the presence of vapor analytes, where again the response is a linear function of the analyte concentration.[33-35] Polymer films that are exposed to analytes that either bind very strongly to the polymer, or that induce significant structural distortions in the chains of the polymeric material, could certainly produce a saturation of the detector response at concentrations well below the saturated vapor pressure of the analyte; however, such behavior was not observed for any of the solvents or detectors explored in this work.

For mixtures, as long as the concentration of analyte molecules is dilute in the polymer film, the linear swelling relationship as a function of the analyte concentration in the vapor phase is expected to be a good microscopic description of the signal transduction properties of the detectors when exposed to combinations of these same gaseous analytes. Thus, the swelling response of a

polymer to binary analyte mixtures is expected to be a weighted linear combination of the response to the individual analytes in the vapor phase. Previous work in our laboratory has shown that the fraction of the partial pressure of the odor, as opposed to the concentration of the odor, is the key variable in determining the response of the carbon black organic polymer composite vapor detectors.[36] Thus, to first order, the response of a polymer composite detector array to a mixture of solvents should be readily obtained by calculating the fractional composition of the constituents in the mixture relative to their individual vapor pressures under the experimental test conditions of concern. This additive behavior is, in fact, in excellent accord with experimental observations for the response of the conducting polymer composite arrays to the binary mixtures studied during the course of this work.

B. Implications for Algorithm Development/Pattern Recognition Requirements

All architectures that rely on array-based sensing require some type of training set and signal processing algorithm in order to classify and/or identify an analyte upon presentation to the detector array. In this respect, the performance and range of applicability of such detector arrays is intimately coupled to the data reduction algorithms and computational capabilities that are required to achieve the sensing task of concern.

The minimum possible training set, and the minimum requirements on computational capabilities to analyze a mixture or to classify and/or identify a particular analyte, are clearly achieved when the detector response is a linear function of the analyte concentration and when the differential detector response to the analyte of concern is independent of whether or not other analytes are present in the environment. Both of these conditions were met for the carbon black organic polymer composite chemiresistor response characteristics over the ranges of concentrations and for the ranges of analyte/background concentrations that were explored during the course of this study. This behavior contrasts with the properties reported for tin oxide chemiresistors[37] or for dye-impregnated organic polymer coatings on fiber optics,[5,37] whose responses are nonlinear with analyte concentration and/or with variations in environmental background. Such nonlinearities imply that significantly more computational resources and algorithm development

will be required to achieve similar system performance in varying background environments or when an analyte concentration is to be quantified either alone or in a mixture of vapors. The exact tradeoffs imposed by more complex data reduction and more involved computational requirements, relative to the opportunity to exploit possibly increased information content of a richly varying signal response pattern, will be array and task specific, and will require a detailed analysis for the specific task of interest.

For odors that are more complex compositionally than simple binary or ternary mixtures of analytes, it could be envisioned that a single array-based detector response fingerprint would not be sufficient to produce a unique vector decomposition of the mixture into the signatures of each of the components of a training set of vapors. Thus, one response pattern might not be sufficient to provide a unique solution to the chemical composition of the odor mixture of concern. It is likely that, even for complex odors, useful information will be obtained, however, if some temporal or spatio-temporal variation in the composition of the odor is present. Under such conditions, changes in detector response can be identified with individual portions of the analyte based on their differential response patterns relative to the integrated baseline response of the odor on the detector array. The detector response characteristic that is least demanding on the signal processing and computational resources under such circumstances is when the pattern for an analyte remains linearly proportional to the analyte concentration regardless of the composition, or concentration, of the other components of the background ambient. This behavior was observed experimentally for the conducting polymer composite detectors for the various solvents and background ambient vapors evaluated in this work.

V. Conclusions

Under the conditions of this study, carbon black-organic polymer composite vapor detectors displayed a linear steady-state relative differential resistance signal in response to changes in the concentration of analyte vapor in the gas phase. This behavior was observed relative to either an air background or relative to a background that contained an organic solvent vapor in air. Moreover, the steady-state relative differential resistance response patterns produced by an array of

carbon black-polymer composite detectors upon exposure to a test series of binary mixtures of analytes were the arithmetic sums of the maximum relative differential resistance responses that were obtained upon independent exposure of the array to each individual component of the mixture. This behavior implies that, under our test conditions, a relatively simple algorithm and training set, based on identifying a solvent vapor through its pattern type and quantifying the vapor concentration through the pattern height, would be sufficient to identify and quantify the test vapors and test vapor mixtures studied in this work.

VII. References

1)Lonergan, M. C.; Severin, E. J.; Doleman, B. J.; Beaber, S. A.; Grubbs, R. H.; Lewis, N. S. *Chemistry of Materials* **1996**, *8*, 2298.

2)Freund, M. S.; Lewis, N. S. *Proceedings of the National Academy of Sciences of the United States of America* **1995**, *92*, 2652-2656.

3)Grate, J. W.; Klusty, M.; McGill, R. A.; Abraham, M. H.; Whiting, G.; Andonian-Haftvan, J. *Analytical Chemistry* **1992**, *64*, 610-624.

4)Gardner, J. W.; Bartlett, P. N. *Sensors And Actuators B Chemical* **1994**, *18*, 211-220.

5)Walt, D. R.; Dickinson, T.; White, J.; Kauer, J.; Johnson, S.; Engelhardt, H.; Sutter, J.; Jurs, P. *Biosensors & Bioelectronics* **1998**, *13*, 697.

6)Nakamoto, T.; Fukuda, A.; Moriizumi, T. *Sensors and Actuators B* **1993**, *10*, 85-90.

7)Ballantine, D. S.; Rose, S. L.; Grate, J. W.; Wohltjen, H. *Analytical Chemistry* **1986**, *58*, 3058-3066.

8)Grate, J. W.; Abraham, M. H. *Sensors and Actuators B* **1991**, *3*, 85-111.

9)Grate, J. W.; Martin, S. J.; White, R. M. *Analytical Chemistry* **1993**, *65*, A987-A996.

10)Gardner, J. W.; Barlett, P. N. *Sensors and Sensory Systems for an Electronic Nose*; Kluwer Academic Publishers: Dordrecht, 1992.

11)Gardner, J. W.; Shurmer, H. V.; Corcoran, P. *Sensors And Actuators B Chemical* **1991**, *4*, 117-121.

12)Corcoran, P.; Shurmer, H. V.; Gardner, J. W. *Sensors And Actuators B Chemical* **1993**, *15*, 32-37.

13)Shurmer, H. V.; Corcoran, P.; Gardner, J. W. *Sensors And Actuators B Chemical* **1991**, *4*, 29-33.

14)Pearce, T. C.; Gardner, J. W.; Friel, S.; Bartlett, P. N.; Blair, N. *Analyst* **1993**, *118*, 371-377.

15)White, J.; Kauer, J. S.; Dickinson, T. A.; Walt, D. R. *Analytical Chemistry* **1996**, *68*, 2191-2202.

16)Butler, M. A.; Ricco, A. J.; Buss, R. *Journal of the Electrochemical Society* **1990**, *137*, 1325-1326.

17)Hughes, R. C.; Ricco, A. J.; Butler, M. A.; Pfeifer, K. B. *Journal of Biochemistry and Biotechnology* **1993**, *41*, 77-85.

18)Slater, J. M.; Paynter, J. *Analyst* **1994**, *119*, 191-195.

19)Slater, J. M.; Watt, E. J. *Analyst* **1991**, *116*, 1125-1130.

20)Schweizerberberich, P. M.; Vaihinger, S.; Gopel, W. *Sensors And Actuators B Chemical* **1994**, *18*, 282-290.

21)Gardner, J. W.; Shurmer, H. V.; Tan, T. T. *Sensors And Actuators B Chemical* **1992**, *6*, 71-75.

22)Shurmer, H. V.; Gardner, J. W.; Chan, H. T. *Sensors And Actuators* **1989**, *18*, 361-371.

23)Charlesworth, J. M.; Riddell, S. Z.; Mathews, R. J. *Journal Of Applied Polymer Science* **1993**, *47*, 653.

24)Nieuwenhuizen, M. S.; Harteveld, J. L. N. *Sensors and Actuators, A-Physical* **1994**, *44*, 219.

25)Grate, J. W.; Rosepehrsson, S. L.; Venezky, D. L.; Klusty, M.; Wohltjen, H. *Analytical Chemistry* **1993**, *65*, 1868.

26)Doleman, B. J.; Lonergan, M. C.; Severin, E. J.; Vaid, T. P.; Lewis, N. S. *Anal. Chem.* **1998**, *70*, 4177-4190.

27)Severin, E. J. *Ph.D. Thesis*; California Institute of Technology: Pasadena, CA, 1999.

28)Atkins, P. W. *Physical Chemistry*; W.H. Freeman and Co.: New York, NY, 1994.

29)Anderson, J. E.; Adams, K. M.; Troyk, P. R. *Journal of Non-Crystalline Solids* **1991**, *131*, 587-592.

30)Godovski, D. Y.; Koltypin, E. A.; Volkov, A. V.; Moskvina, M. A. *Analyst* **1993**, *118*, 997-999.

31)Kirkpatrick, S. *Reviews of Modern Physics* **1973**, *45*, 574-588.

32)Persaud, K. C.; Travers, P. J. *Arrays of Broad Specificity Films for Sensing Volatile Chemicals*; Kress-Rogers, E., Ed.; CRC Press, Inc.: New York, NY, 1997, pp 563-592.

33)Ralston, A. R.; Tobin, J. A.; Bajikar, S. A.; Denton, D. D. *Sensors and Actuators B-Chemical* **1994**, *22*, 139.

34)Boltshauser, T.; Leme, C. A.; Baltes, H. *Sensors and Actuators B-Chemical* **1993**, *15*, 75.

35)Denton, D. D.; Senturia, S. D.; Anolik, E. S.; Scheider, D. *Digest of Technical Papers, 3rd Int. Conf. on Solid-State Sensors and Actuators (Transducers '85)* **1985**, 202-205.

36)Doleman, B. J.; Severin, E. J.; Lewis, N. S. *Proceedings of the National Academy of Sciences of the United States of America* **1998**, *95*, 5442-5447.

37)Harsanyi, G. *Polymer Films in Sensor Applications*; Technomic Pub. Co., Inc.: Basel, Switzerland, 1995.

Figure 3.1: Structures of the polymers used in this work. Listed as detector, polymer: 1, poly(4-vinyl phenol); 2, poly(styrene-co-allyl alcohol), 5% hydroxy; 3, poly(α-methylstyrene); 4, poly(vinyl chloride-co-vinyl acetate), 10% vinyl acetate; 5, poly(N-vinylpyrrolidone); 6, poly(vinyl acetate); 7, poly(methyl vinyl ether-co-maleic anhydride); 8, poly(bisphenol A carbonate); 9, poly(styrene); 10, poly(styrene-co-maleic anhydride), 50% styrene; 11, poly(vinyl butyral); 12, poly(sulfone); 13, poly(methyl methacrylate); 14, poly(vinylidene chloride-co-acrylonitrile), 80% vinylidene chloride; 15, poly(caprolactone); 16, poly(ethylene-co-vinyl acetate), 82% ethylene; 17, poly(ethylene oxide); 18, poly(butadiene), 36% cis-1,4, 55% trans-1,4, 9% vinyl-1,2, 19, poly(epichlorohydrin); 20, poly(styrene-co-butadiene), 28% Styrene; 21, addition product of sodium menthoxide to poly(pentafluorostyrene); 22, (+) isopinocampheol derivatized poly(p-chloromethylstyrene); 23, poly(fluorostyrene); 24, poly(styrene-co-isoprene)

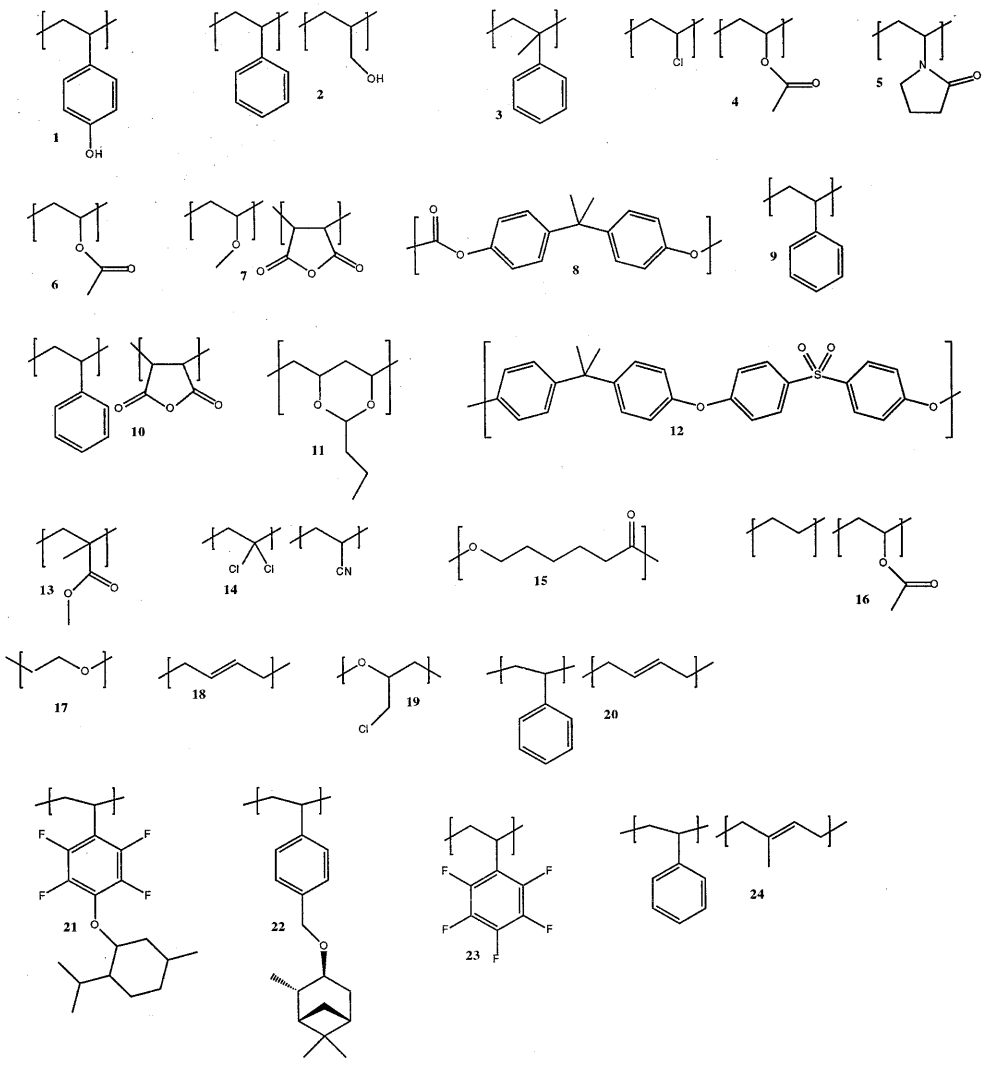
1
OH
2
OH
3
4
Cl
5
N
6
7
8
9
10
11
12
13
14
Cl
Cl
CN
15
16
17
18
19
Cl
20
21
F
22
23
24

Figure 3.1

Figure 3.2: Representative differential resistance responses for three types of vapor presentations to a poly(ethylene-co-vinyl acetate)-carbon black composite vapor detector. **A**) Exposure to benzene at P/P° = 0.02 ($\Delta R_{js_1,max}$ indicated by arrow 1) followed by exposure to benzene at P/P° = 0.02 and chloroform at P/P° = 0.02 ($\Delta R_{js_2,max}$ indicated by arrow 2). The combined response, $\Delta R_{js_1,max} + \Delta R_{js_2,max}$, is indicated by arrow 5. **B**) Exposure to chloroform at P/P° = 0.02 ($\Delta R_{js_1,max}$ indicated by arrow 3) followed by exposure to chloroform at P/P° = 0.02 and benzene at P/P° = 0.02 ($\Delta R_{js_2,max}$ indicated by arrow 4). The combined response, $\Delta R_{js_1,max} + \Delta R_{js_2,max}$, is also indicated by arrow 5. Arrow 1 ≈ Arrow 4; Arrow 3 ≈ Arrow 2. **C**) Benzene at P/P° = 0.02 and chloroform at P/P° = 0.02 both presented simultaneously to the detector (response, $\Delta R_{js_1+s_2,max}$ is again indicated by arrow 5).

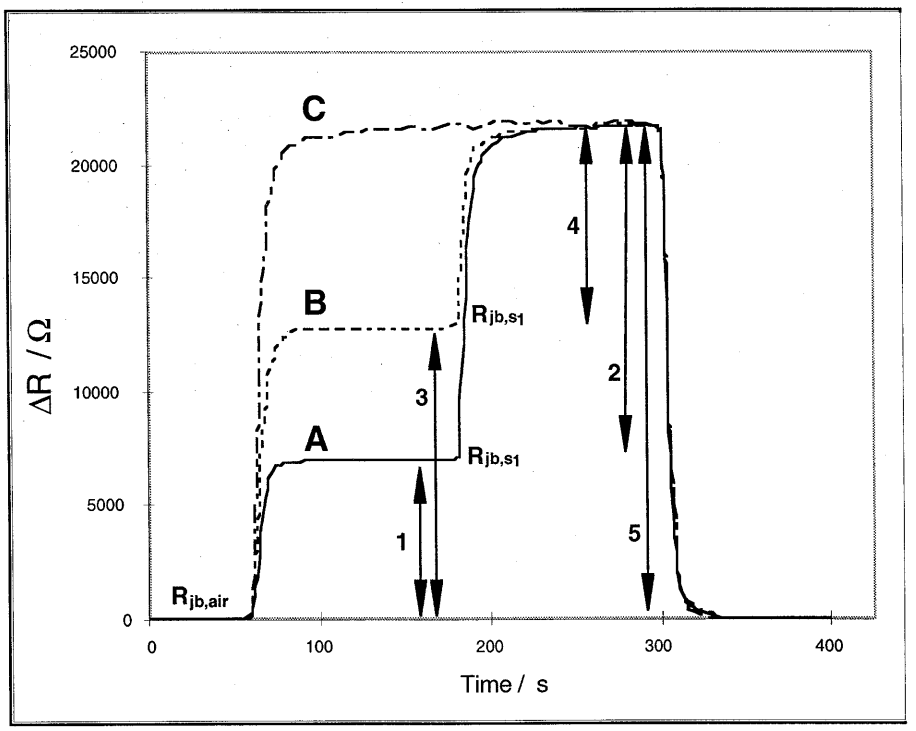
25000
20000
15000
10000
5000
0
ΔR / Ω
0
100
200
300
400
Time / s
C
B
A
$R_{jb,s1}$
$R_{jb,s1}$
$R_{jb,air}$
1
2
3
4
5

Figure 3.2

Figure 3.3: **A**) A histogram of the maximum relative differential resistance response of 12 carbon black-polymer composite detectors exposed to n-heptane, cyclohexanone, benzene, chloroform, nitrobenzene, and 2-propanol each presented at $P/P^{\circ} = 0.03$ in air. Each analyte was presented 10 times to the array, with the order of presentation randomized over all repetitions of all test solvents. **B**) Results from the exposures described in (**A**) as represented by the first two dimensions of principal component-space, which contain 96% of the total variance in the data. The ellipsoids contain 95% of the data for each analyte in principal component space.

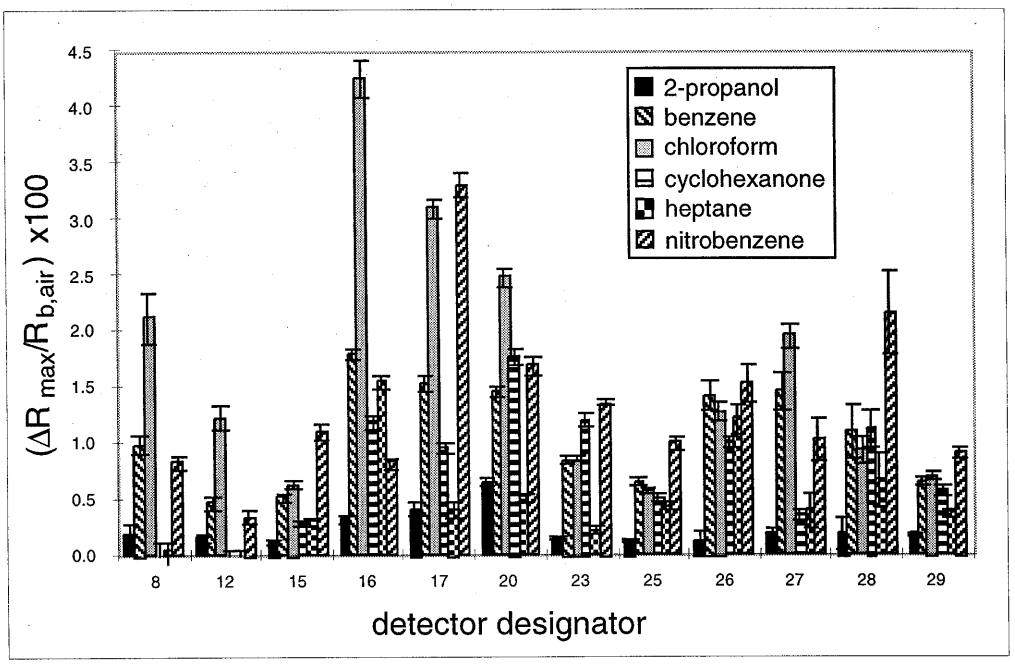
4.5
4.0
3.5
3.0
2.5
2.0
1.5
1.0
0.5
0.0
(ΔR max/Rb,air) x100
2-propanol
benzene
chloroform
cyclohexanone
heptane
nitrobenzene
8
12
15
16
17
20
23
25
26
27
28
29
detector designator

Figure 3.3a

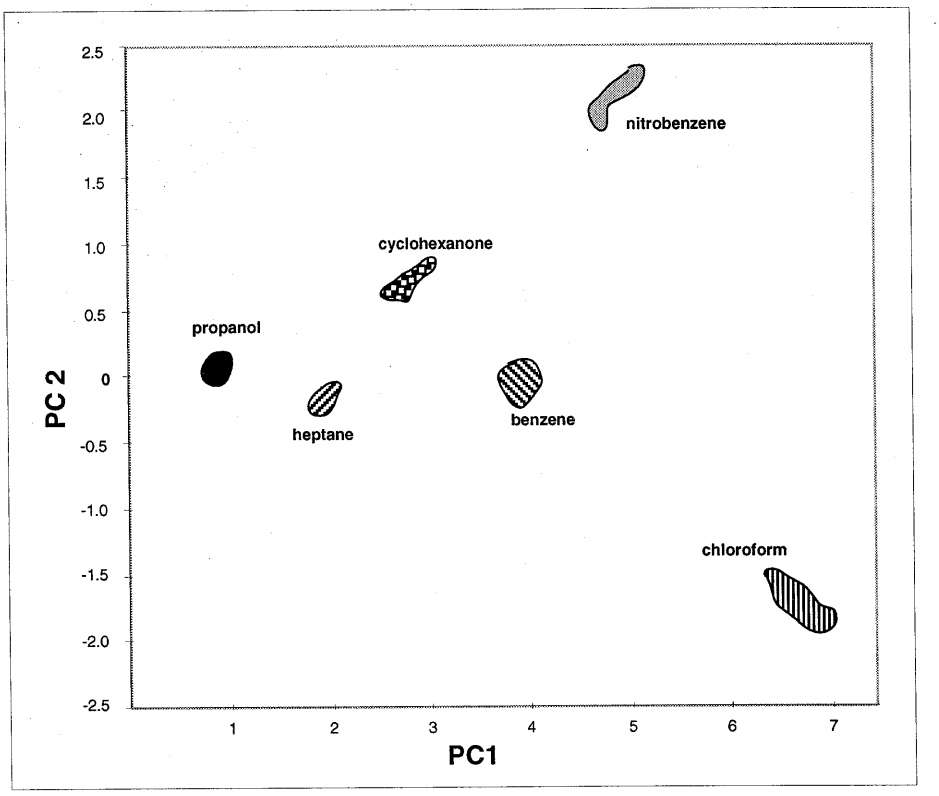
2.5
2.0
1.5
1.0
0.5
0
-0.5
-1.0
-1.5
-2.0
-2.5
PC 2
1
2
3
4
5
6
7
PC1
nitrobenzene
cyclohexanone
propanol
heptane
benzene
chloroform

Figure 3.3b

Figure 3.4: Average maximum relative differential resistance responses, $\Delta R_{js,max}/R_{jb,air}$, of composite detector films consisting of carbon black and: **A**) Poly(ethylene-co-vinyl acetate), **B**) Poly(epichlorohydrin), **C**) Poly(butadiene), when exposed to n-heptane, cyclohexanone, benzene, chloroform, nitrobenzene, and 2-propanol, each at P/P° = 0.005 to 0.03 in air in six even steps. Each analyte was presented 10 times to the array, with the order of presentation randomized over all repetitions of all test solvents. The error bars represent 1σ values computed from 10 exposures at each P/P°.

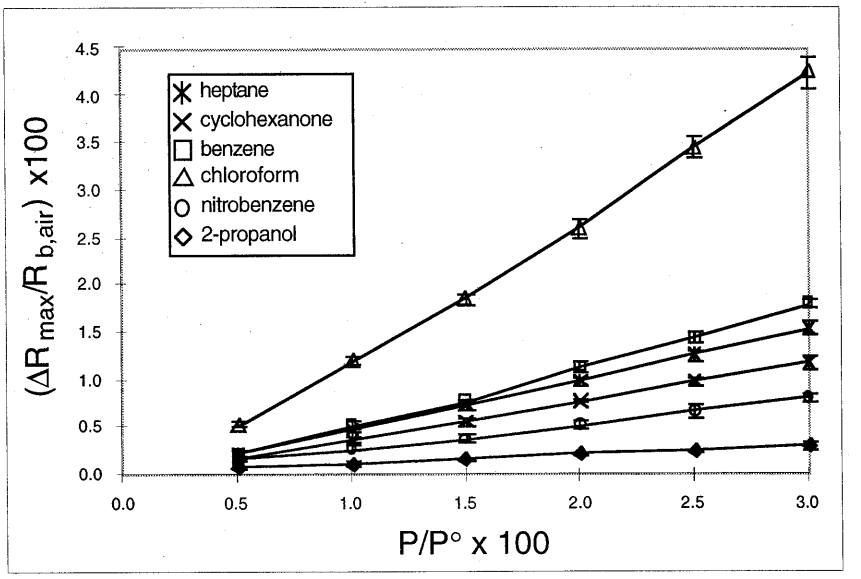
heptane
cyclohexanone
benzene
chloroform
nitrobenzene
2-propanol
(ΔR max/R b,air) x100
P/P° x 100
4.5
4.0
3.5
3.0
2.5
2.0
1.5
1.0
0.5
0.0
0.0
0.5
1.0
1.5
2.0
2.5
3.0

Figure 3.4a

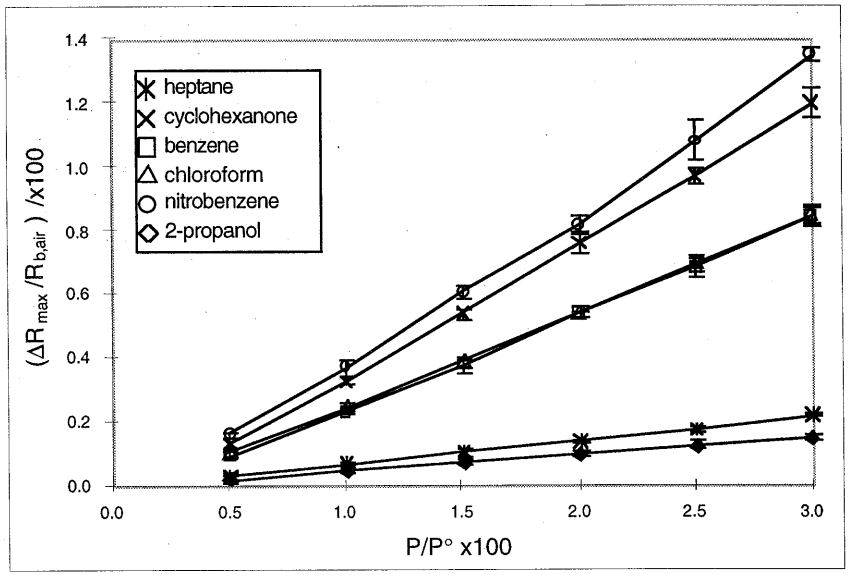
heptane
cyclohexanone
benzene
chloroform
nitrobenzene
2-propanol
(ΔRmax /Rb,air) /x100
P/P° x100
0.0
0.2
0.4
0.6
0.8
1.0
1.2
1.4
0.5
1.0
1.5
2.0
2.5
3.0

Figure 3.4b

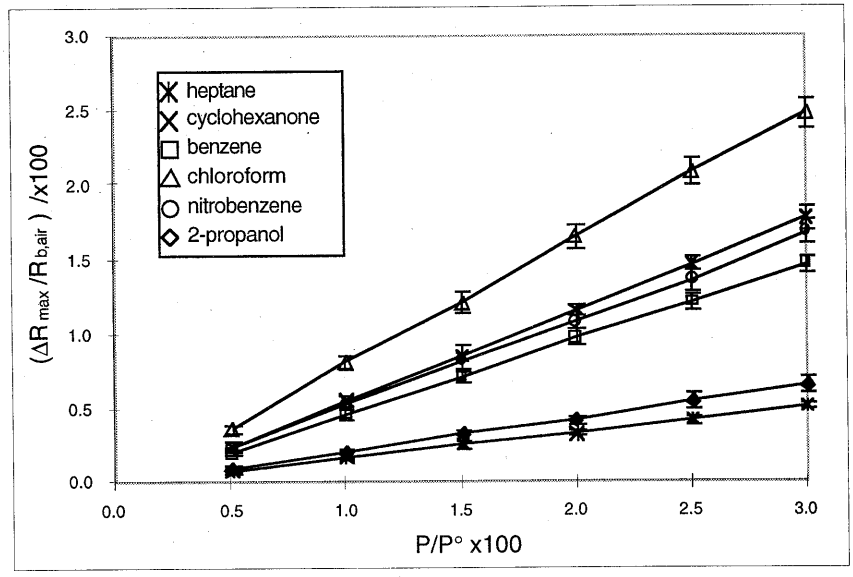
3.0
2.5
2.0
1.5
1.0
0.5
0.0
0.0
0.5
1.0
1.5
2.0
2.5
3.0
(ΔR max /R b,air) /x100
P/P° x100
heptane
cyclohexanone
benzene
chloroform
nitrobenzene
2-propanol

Figure 3.4c

Figure 3.5: Data in principal component space from a 12-detector array exposed to n-heptane, cyclohexanone, benzene, chloroform, nitrobenzene, and 2-propanol each at $P/P^{\circ} = 0.005$ to 0.03 in air in six even steps. The first three principal components depicted contained 98% of the total variance in the data. The ellipsoids contain 95% of the data for each analyte. Each analyte was presented 10 times to the array, with the order of presentation randomized over all repetitions of all test solvents.

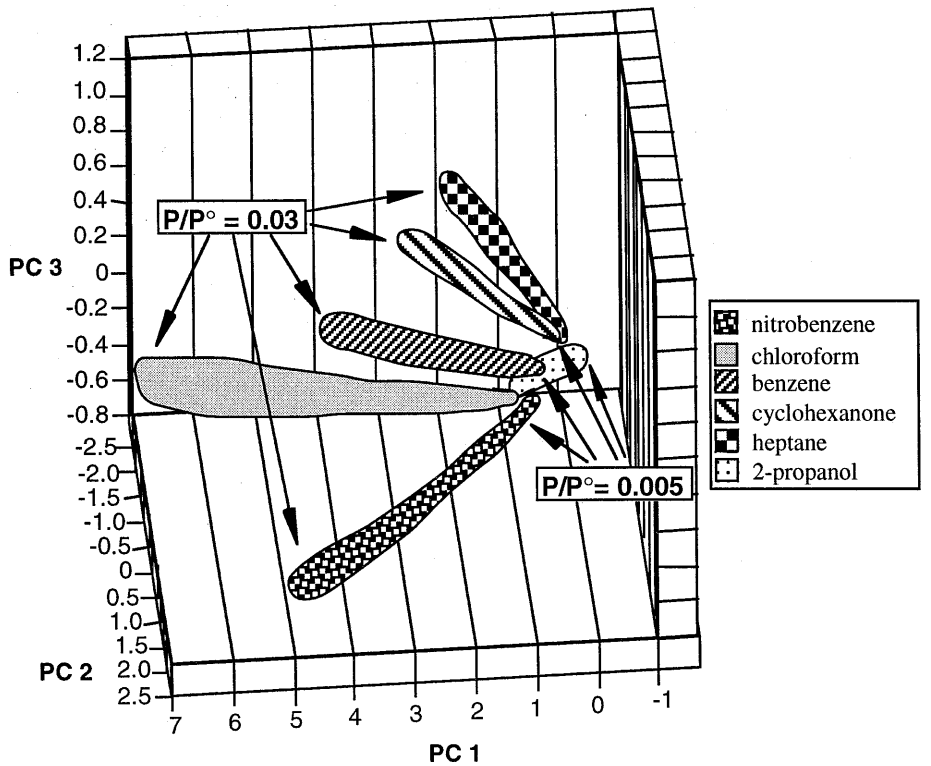
P/P° = 0.03
P/P°= 0.005
nitrobenzene
chloroform
benzene
cyclohexanone
heptane
2-propanol
PC 3
PC 2
PC 1
1.2
1.0
0.8
0.6
0.4
0.2
0
-0.2
-0.4
-0.6
-0.8
-2.5
-2.0
-1.5
-1.0
-0.5
0
0.5
1.0
1.5
2.0
2.5
7
6
5
4
3
2
1
0
-1

Figure 3.5

Figure : Histogram of the average normalized response of a 12-element array of carbon black-polymer detector films exposed to three analytes; **A**) Benzene, **B**) Chloroform, **C**) Nitrobenzene, each presented 10 times at $P/P^{\circ} = 0.005 - 0.03$ in air in six even steps. The data were normalized according to equation 3.1 in the text.

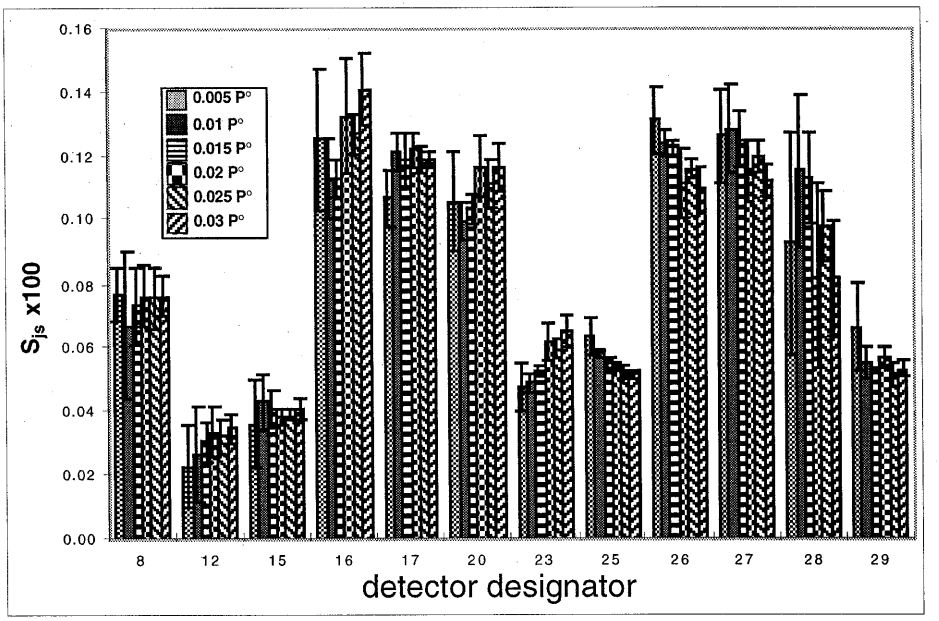
0.16
0.14
0.12
0.10
0.08
0.06
0.04
0.02
0.00
S_{js} x100
0.005 P°
0.01 P°
0.015 P°
0.02 P°
0.025 P°
0.03 P°
8
12
15
16
17
20
23
25
26
27
28
29
detector designator

Figure 3.6a

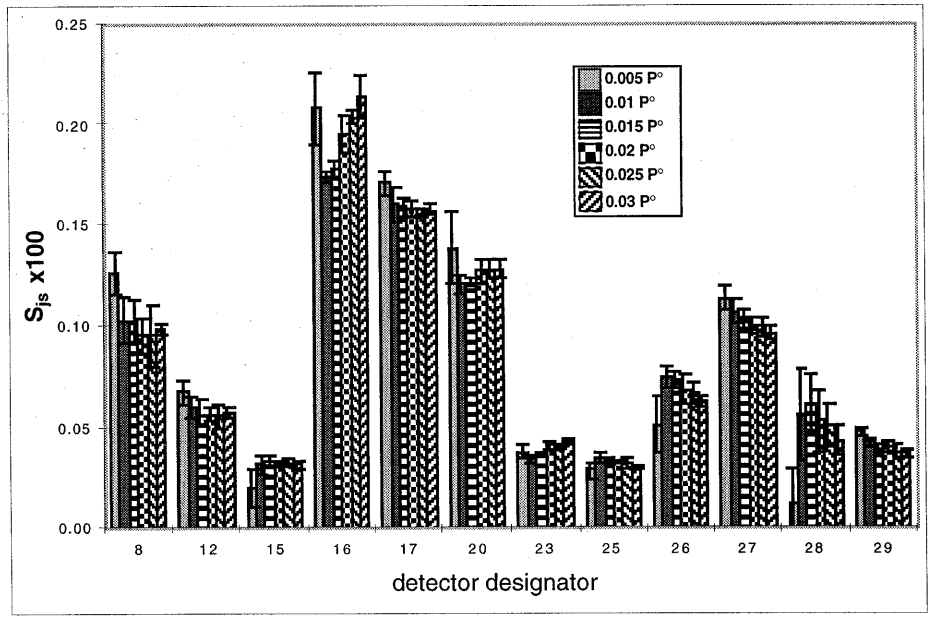
0.25
0.20
0.15
0.10
0.05
0.00
S_{js} x100
0.005 P°
0.01 P°
0.015 P°
0.02 P°
0.025 P°
0.03 P°
8
12
15
16
17
20
23
25
26
27
28
29
detector designator

Figure 3.6b

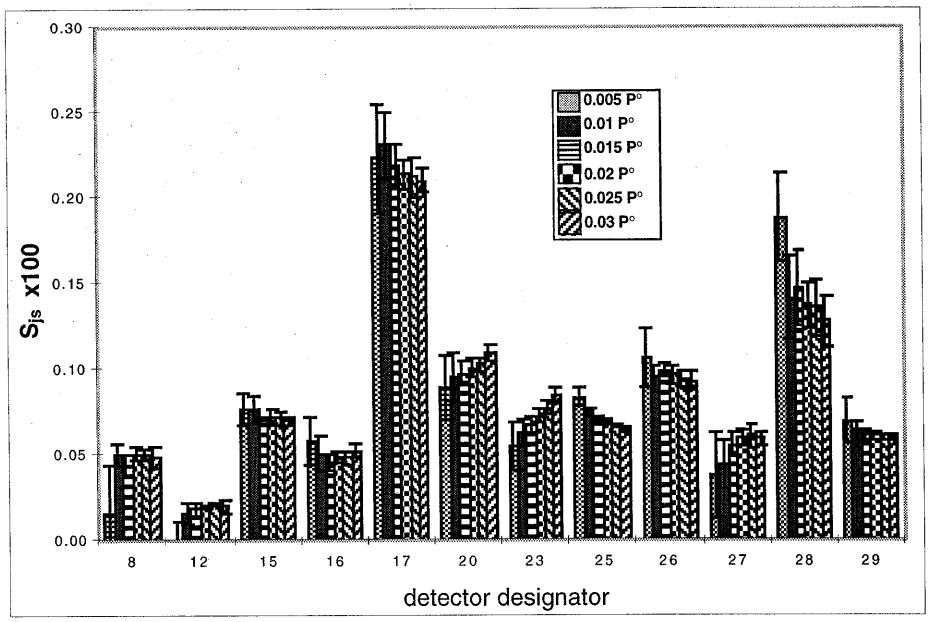
0.30
0.25
0.20
0.15
0.10
0.05
0.00
S_{js} x100
0.005 P°
0.01 P°
0.015 P°
0.02 P°
0.025 P°
0.03 P°
8
12
15
16
17
20
23
25
26
27
28
29
detector designator

Figure 3.6c

Figure 3.7: Maximum relative differential resistance responses, $\Delta R_{js,max}/R_{jb,air}$, of composite detector films consisting of carbon black and: **A**) poly(ethylene-co-vinyl acetate), **B**) poly(butadiene), **C**) poly(epichlorohydrin), when exposed to ethanol, 1-propanol, 1-butanol, 1-pentanol, 1-hexanol, and 1- heptanol each at $P/P^\circ = 0.005$ to 0.03 in six even steps in air. Each analyte was presented 10 times to the array, with the order of presentation randomized over all repetitions of all test solvents. The error bars represent 1σ values computed from 10 exposures at each P/P°.

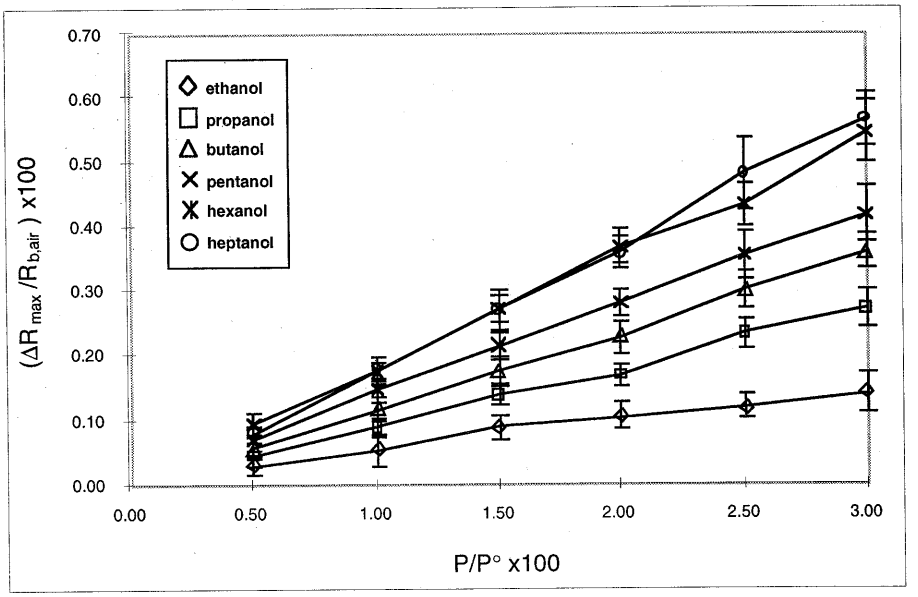
0.70
0.60
0.50
0.40
0.30
0.20
0.10
0.00
(ΔR max /R b,air) x100
ethanol
propanol
butanol
pentanol
hexanol
heptanol
0.00
0.50
1.00
1.50
2.00
2.50
3.00
P/P° x100

Figure 3.7a

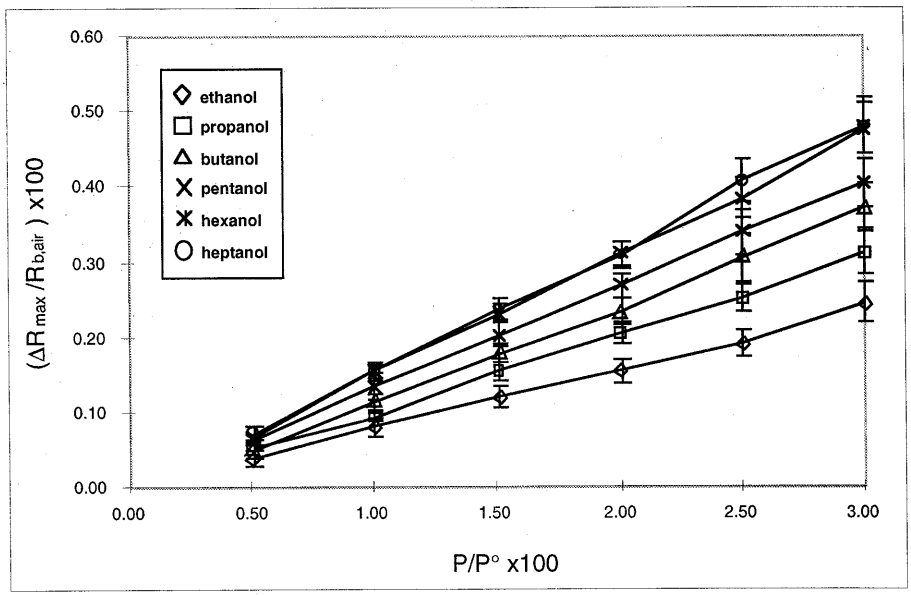
0.60
0.50
0.40
0.30
0.20
0.10
0.00
(ΔRmax /Rb,air) x100
ethanol
propanol
butanol
pentanol
hexanol
heptanol
0.00
0.50
1.00
1.50
2.00
2.50
3.00
P/P° x100

Figure 3.7b

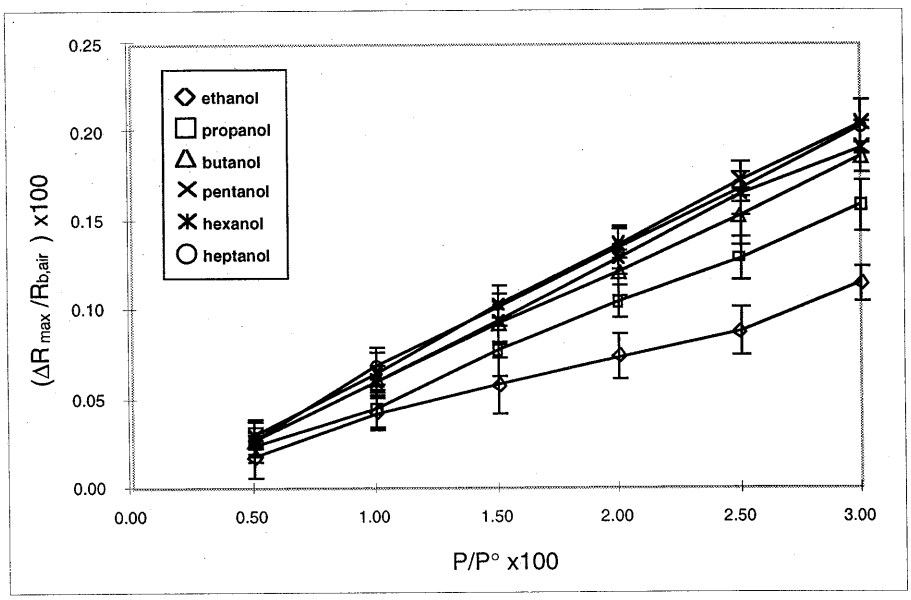
0.25
0.20
0.15
0.10
0.05
0.00
(ΔRmax /Rb,air) x100
ethanol
propanol
butanol
pentanol
hexanol
heptanol
0.00
0.50
1.00
1.50
2.00
2.50
3.00
P/P° x100

Figure 3.7c

Figure 3.8: Maximum relative differential resistance responses, $\Delta R_{js,max}/R_{jb,air}$, of composite detector films consisting of carbon black and: **A**) poly(ethylene-co-vinyl acetate), **B**) poly(butadiene), **C**) poly(epichlorohydrin), when exposed to n-dodecane, n-decane, n-nonane, n-octane, n-heptane, and n-hexane each at $P/P^\circ = 0.005$ to 0.03 in six even steps in air. **D**) Maximum relative differential resistance responses, $\Delta R_{js,max}/R_{jb,air}$, of a composite detector film consisting of carbon black and poly(ethylene oxide), when exposed to n-tetradecane, n-dodecane, n-decane, n-nonane, n-octane, and n-heptane each at $P/P^\circ = 0.005$ to 0.03 in 27 even steps in air. Each analyte was presented 10 times to the array, with the order of presentation randomized over all repetitions of all test solvents. The error bars represent 1σ values computed from 10 exposures at each P/P°.

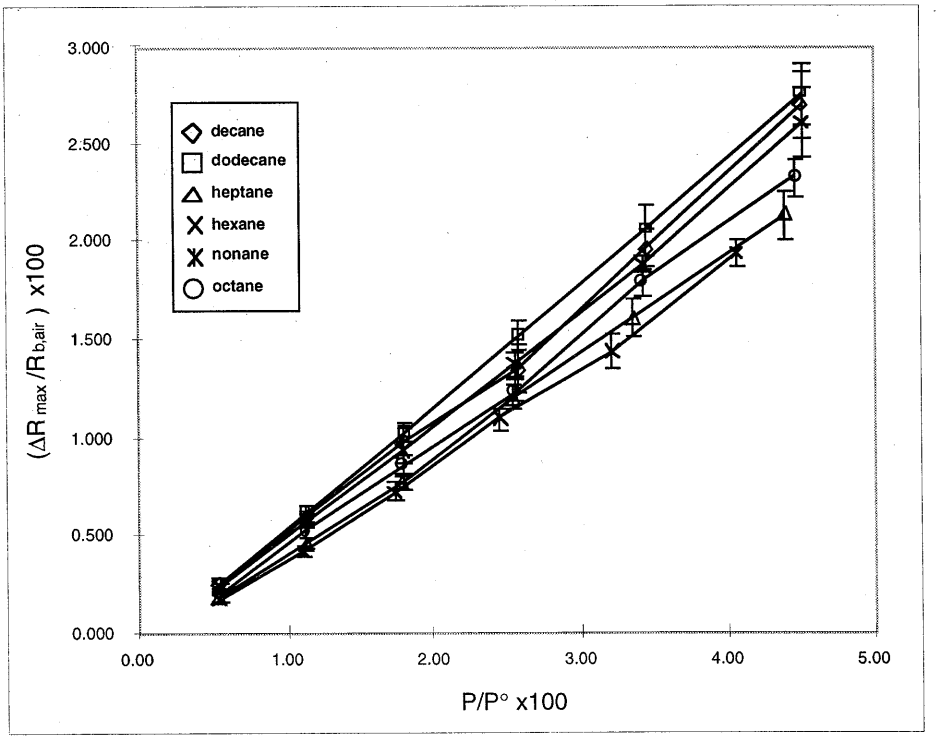
3.000
2.500
2.000
1.500
1.000
0.500
0.000
0.00
1.00
2.00
3.00
4.00
5.00
(ΔR max /R b,air) x100
P/P° x100
decane
dodecane
heptane
hexane
nonane
octane

Figure 3.8a

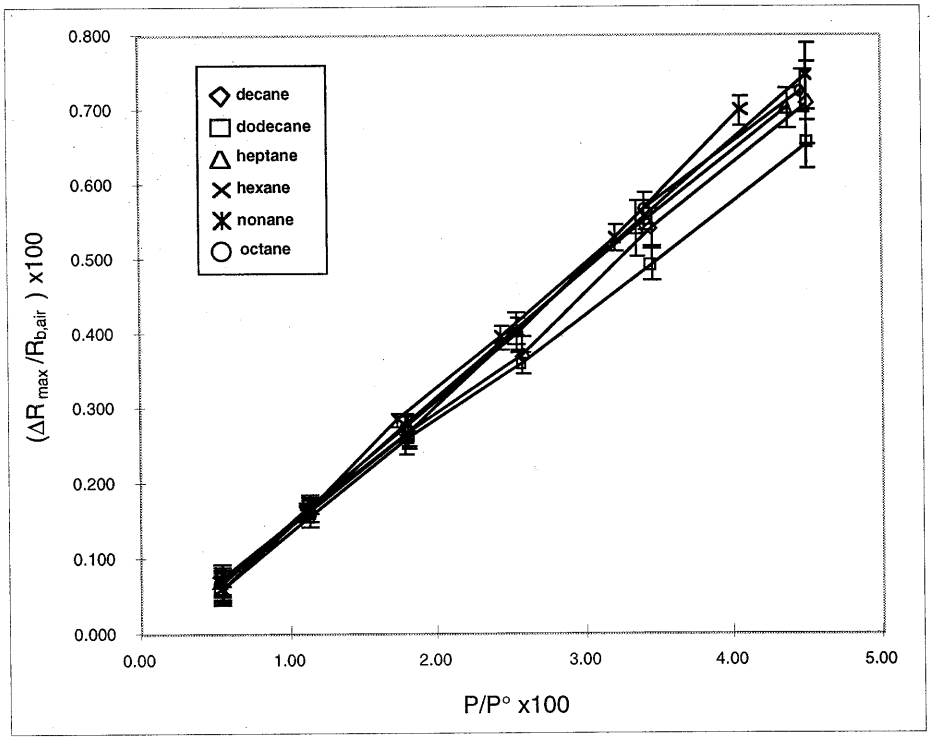
0.800
0.700
0.600
0.500
0.400
0.300
0.200
0.100
0.000
0.00
1.00
2.00
3.00
4.00
5.00
(ΔRmax /Rb,air) x100
P/P° x100
decane
dodecane
heptane
hexane
nonane
octane

Figure 3.8b

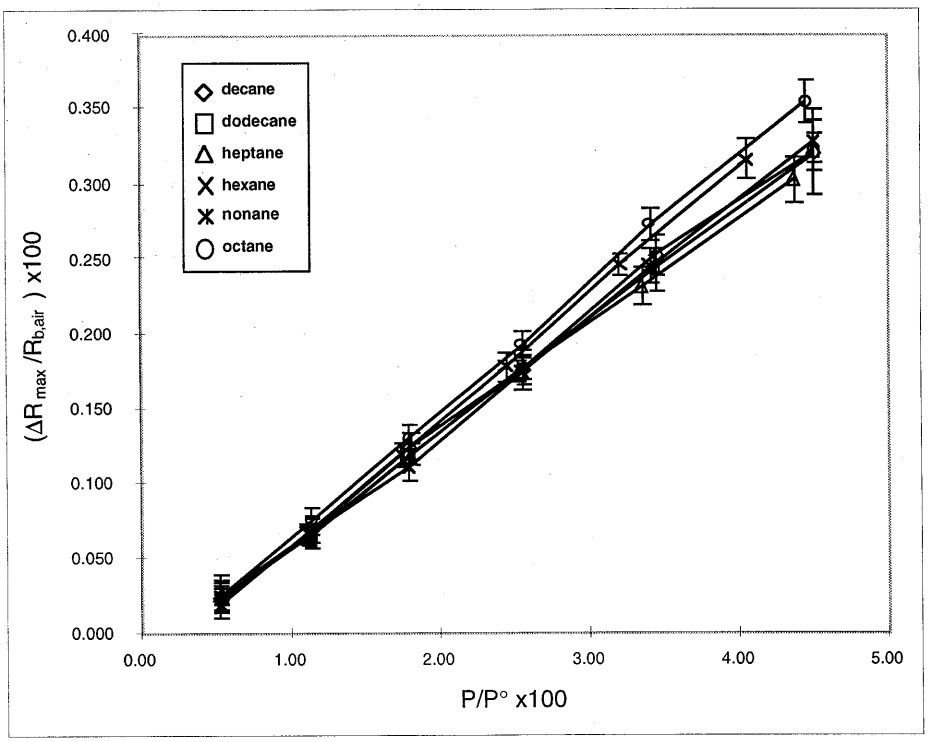
0.400
0.350
0.300
0.250
0.200
0.150
0.100
0.050
0.000
0.00
1.00
2.00
3.00
4.00
5.00
P/P° x100
(ΔRmax /Rb,air) x100
decane
dodecane
heptane
hexane
nonane
octane

Figure 3.8c

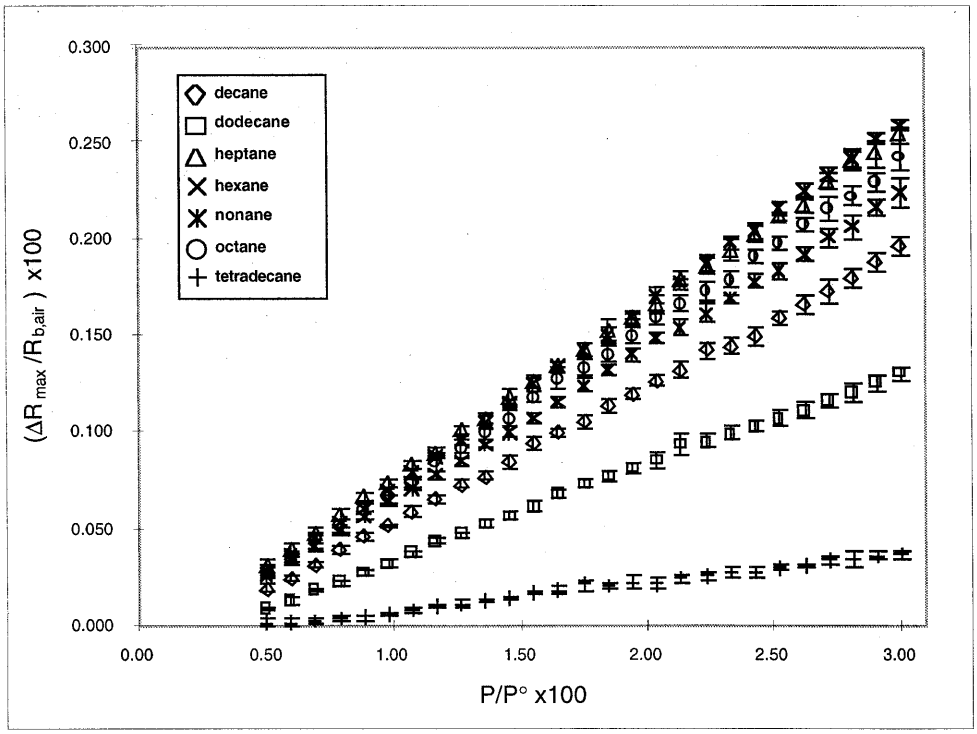
0.300
0.250
0.200
0.150
0.100
0.050
0.000
(ΔR max /R b,air) x100
decane
dodecane
heptane
hexane
nonane
octane
tetradecane
0.00
0.50
1.00
1.50
2.00
2.50
3.00
P/P° x100

Figure 3.8d

Figure 3.9: **A**) Data in principal component space from a 20-detector array exposed 10 times each to methanol, ethanol, 1-propanol, 1-butanol, 1-pentanol, 1-hexanol, 1- heptanol, and 1-octanol each at P/P° = 0.005 to 0.03 in air in 27 even steps. The first three principal components contain 99% of the total variance in the data. The ellipsoids contain 99% of the data for each analyte. **B**) Data in principal component space from a 20-detector array exposed 5 times each to n-tetradecane, n-dodecane, n-decane, n-nonane, n-octane, and n-heptane each at P/P° = 0.005 to 0.03 in air in 27 even steps. The first three principal components contain 99% of the total variance in the data. The ellipsoids contain 99% of the data for each analyte. All presentations in each set were randomized over all repetitions of all test solvents.

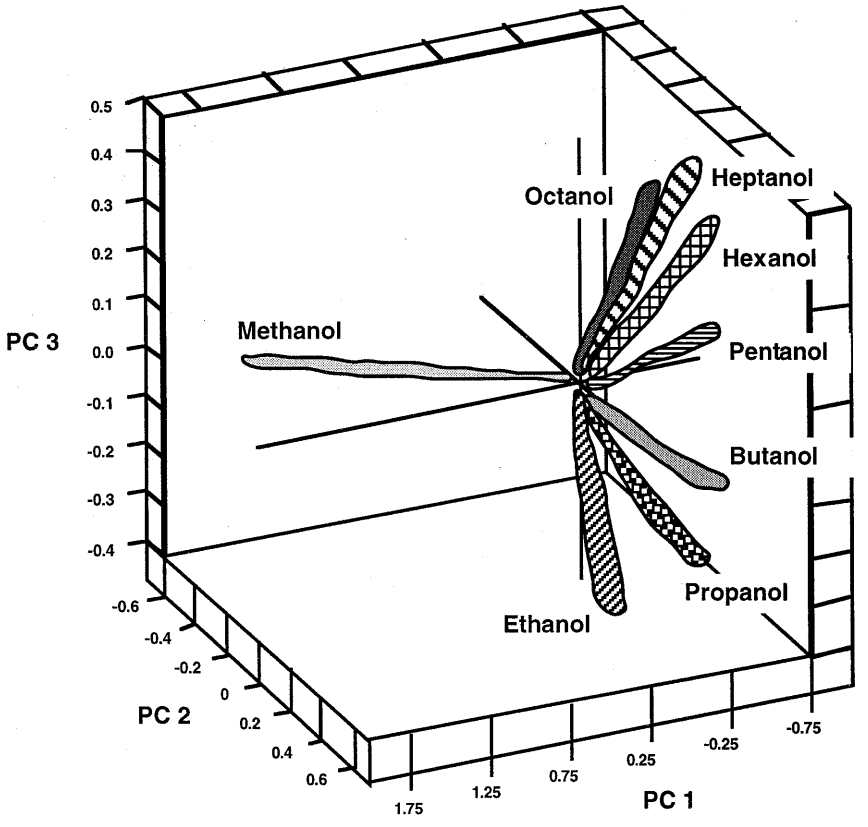
PC 3
0.5
0.4
0.3
0.2
0.1
0.0
-0.1
-0.2
-0.3
-0.4
Octanol
Heptanol
Hexanol
Methanol
Pentanol
Butanol
Propanol
Ethanol
-0.6
-0.4
-0.2
0
0.2
0.4
0.6
PC 2
1.75
1.25
0.75
0.25
-0.25
-0.75
PC 1

Figure 3.9a

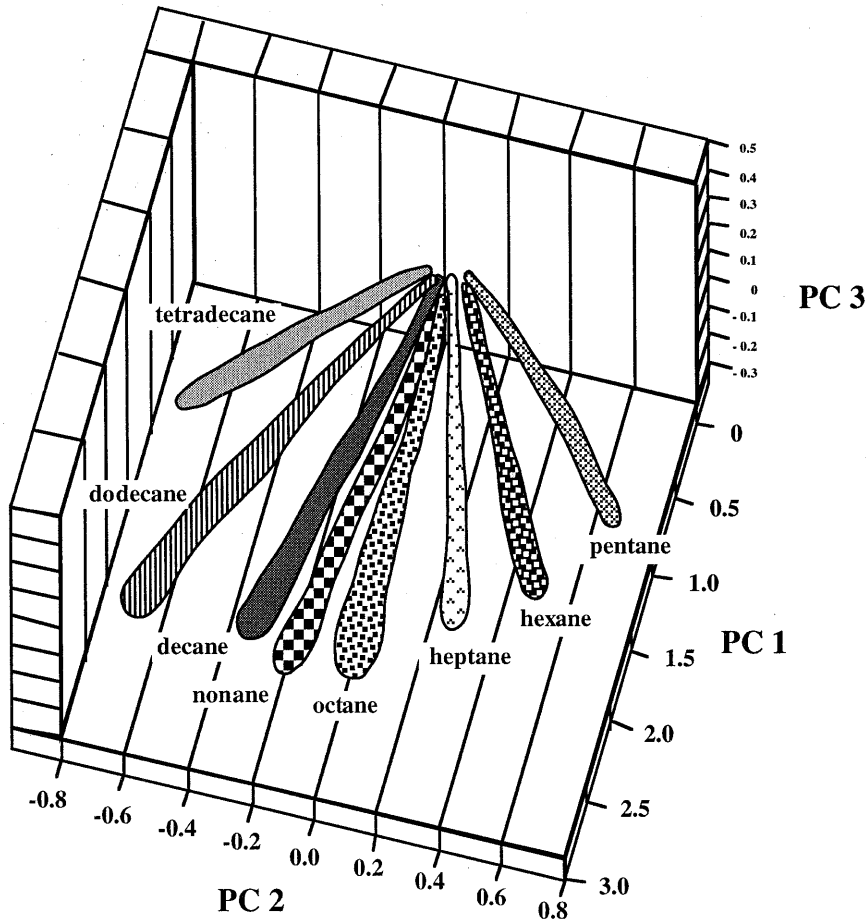
tetradecane
dodecane
decane
nonane
octane
heptane
hexane
pentane
PC 1
PC 2
PC 3
-0.8
-0.6
-0.4
-0.2
0.0
0.2
0.4
0.6
0.8
0.5
0.4
0.3
0.2
0.1
0
- 0.1
- 0.2
- 0.3
0
0.5
1.0
1.5
2.0
2.5
3.0

Figure 3.9b

Figure 3.10: Maximum relative differential resistance responses, $\Delta R_{js,max}/R_{jb,air}$, of composite detector films consisting of carbon black and: **A**) poly(ethylene-co-vinyl acetate), **B**) poly(caprolactone), when exposed to n-heptane at P/P° = 0/005 - 0/025 in air in five even steps (represented by the open symbols). Additional exposures (solid symbols) to n-heptane were performed at P/P° = 0.005, 0.01, and 0.015 while the detector film was exposed to either benzene, cyclohexanone, or 2-propanol at P/P° = 0.005, 0.01, or 0.015.

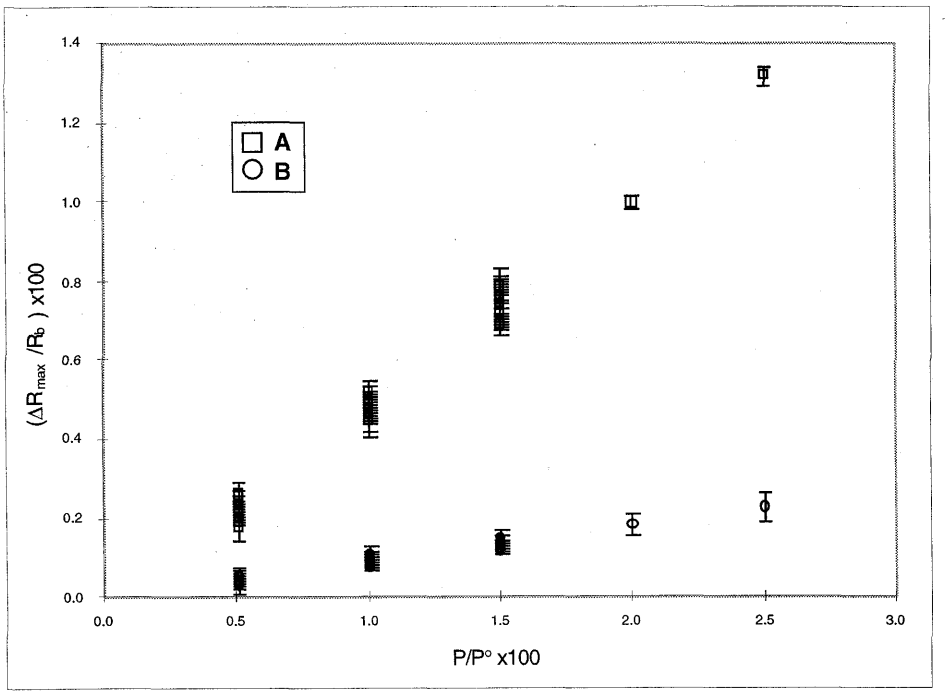

Figure 3.10

Figure 3.11: Data in principal component space from a 12-detector array exposed to n-heptane, benzene, cyclohexanone, or 2-propanol at P/P° = 0.005, 0.01, and 0.015, and to exposures of n-heptane at P/P° = 0.005, 0.01, and 0.015 while the detector film was exposed to either benzene, cyclohexanone, or 2-propanol each at P/P° = 0.005, 0.01, or 0.015. The first three principal components contain 98% of the total variance in the data. The ellipsoids contain 95% of the data for each analyte. Each analyte was presented 5 times to the array, with the order of presentation randomized over all repetitions of all exposure types.

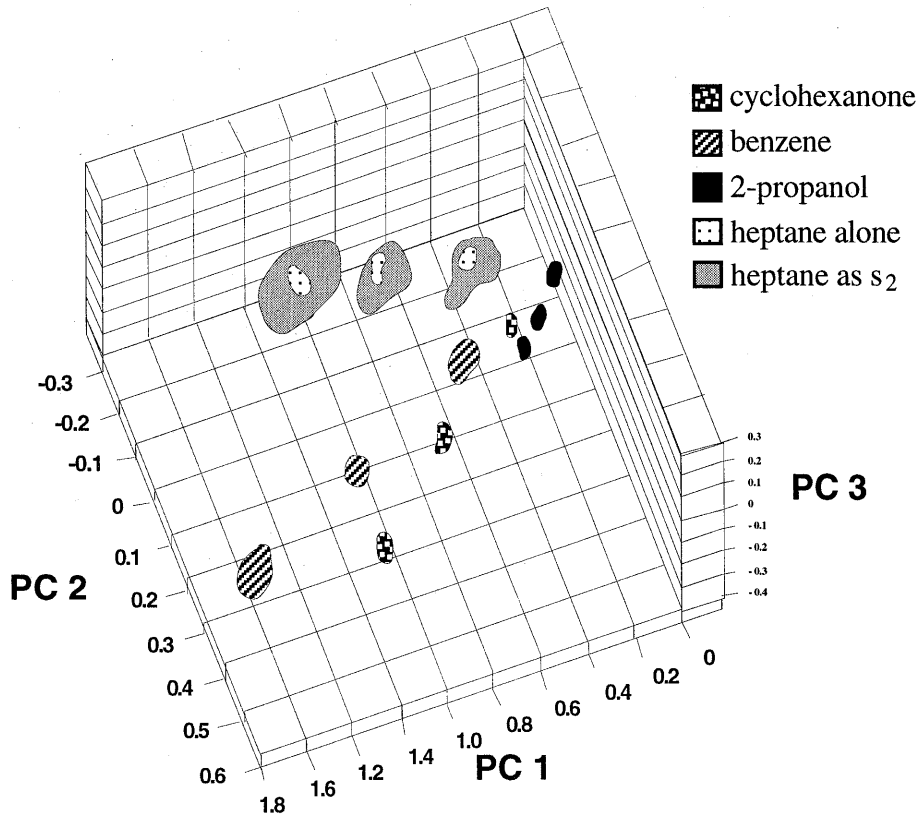
cyclohexanone
benzene
2-propanol
heptane alone
heptane as s_2
PC 1
PC 2
PC 3
-0.3
-0.2
-0.1
0
0.1
0.2
0.3
0.4
0.5
0.6
1.8
1.6
1.2
1.4
1.0
0.8
0.6
0.4
0.2
0
0.3
0.2
0.1
0
-0.1
-0.2
-0.3
-0.4

Figure 3.11

Figure 3.12: **A**) Maximum relative differential resistance responses of a poly(ethylene-co-vinyl acetate)-carbon black composite detector film when exposed to simultaneous and sequential binary mixtures of benzene at P/P° = 0.005, 0.01, or 0.015, and n-heptane at P/P° = 0.005, 0.01, or 0.015. Each of the 9 binary mixture combinations was presented 5 times to the array, with the order of presentation randomized over all repetitions. **B**) Maximum relative differential resistance responses of a poly(caprolactone)-carbon black composite detector film when exposed to simultaneous and sequential binary mixtures of chloroform at P/P° = 0.005, 0.01, or 0.015, and methanol at P/P° = 0.005, 0.01, or 0.015. Each of the 9 binary mixture combinations was presented 5 times to the array, with the order of presentation randomized over all repetitions. The error bars represent 1σ values computed from 5 exposures at each P/P°.

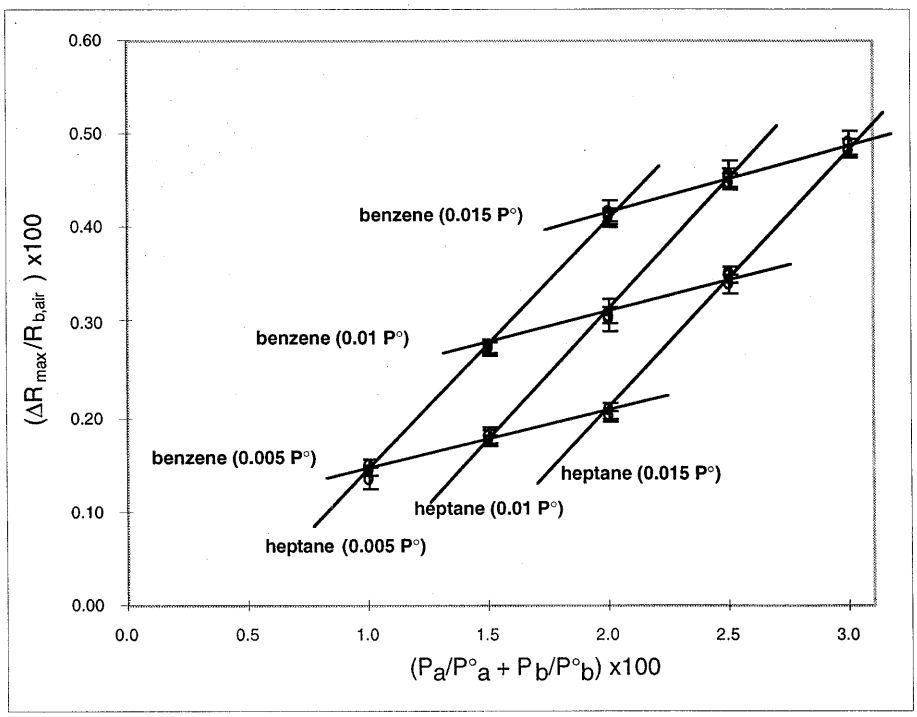
0.60
0.50
0.40
0.30
0.20
0.10
0.00
0.0
0.5
1.0
1.5
2.0
2.5
3.0
(ΔRmax/Rb,air) x100
(Pa/P°a + Pb/P°b) x100
benzene (0.015 P°)
benzene (0.01 P°)
benzene (0.005 P°)
heptane (0.015 P°)
heptane (0.01 P°)
heptane (0.005 P°)

Figure 3.12a

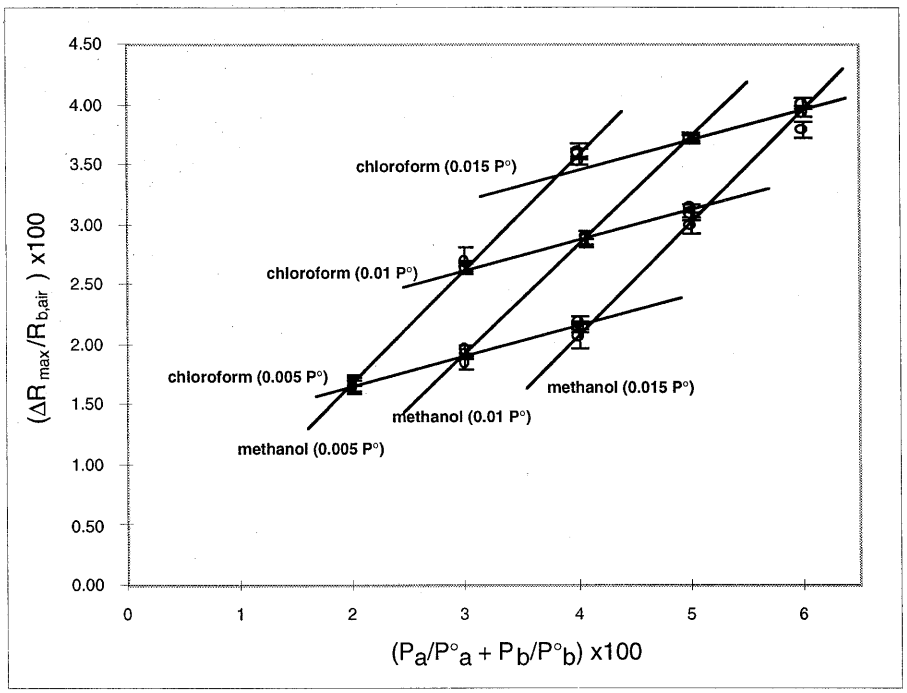
4.50
4.00
3.50
3.00
2.50
2.00
1.50
1.00
0.50
0.00
0
1
2
3
4
5
6
(ΔRmax/Rb,air) x100
(Pa/P°a + Pb/P°b) x100
chloroform (0.015 P°)
chloroform (0.01 P°)
chloroform (0.005 P°)
methanol (0.015 P°)
methanol (0.01 P°)
methanol (0.005 P°)

Figure 3.12b

Figure 3.13: Data in principal component space from a 12-detector array exposed to benzene at P/P° = 0.005-0.025 in air in five even steps, nitrobenzene at P/P° = 0.005-0.025 in air in five even steps, and binary mixtures of benzene at P/P° = 0.005, 0.01, or 0.015, and nitrobenzene at P/P° = 0.005, 0.01, or 0.015. The first three principal components contain 99.6% of the total variance in the data. The ellipsoids contain 95% of the data for each analyte. Each analyte was presented 5 times to the array, with the order of presentation randomized over all repetitions of all exposure types. The error bars represent 1σ values computed from 5 exposures at each P/P°.

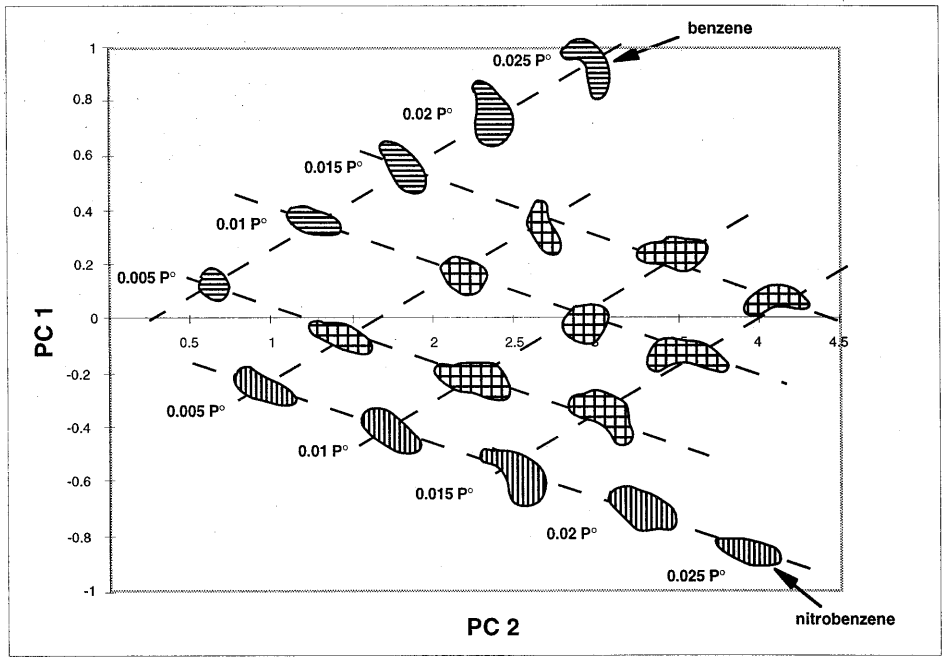
benzene
0.025 P°
0.02 P°
0.015 P°
0.01 P°
0.005 P°
0.005 P°
0.01 P°
0.015 P°
0.02 P°
0.025 P°
nitrobenzene
PC 1
PC 2
1
0.8
0.6
0.4
0.2
0
-0.2
-0.4
-0.6
-0.8
-1
0.5
1
2
2.5
4
4.5

Figure 3.13

Table 3.1: Two groups of solvents used in the 8-solvent binary mixture study and the 6-solvent binary mixture study. Binary mixtures were formed between solvents of set A and solvents of set B of each group. Solvents common to one set could not be paired.

Table 3.1

Eight solvent experiment

Set A	**Set B**
benzene	chloroform
ethyl acetate	ethanol
heptane	hexane
methanol	toluene

Six solvent experiment

Set A	**Set B**
benzene	nitrobenzene
2-propanol	chloroform
cyclohexanone	heptane

Table 3.2: The 27 types of sequential and simultaneous exposures of a binary mixture pair at $P/P^\circ = 0.005$, 0.01, and 0.015 in the 8-solvent experiment and the 6-solvent experiment. This set was repeated 5 times for each binary mixture pair.

Table 3.2

Solvent Pair Presentations

Solvent "A" @ 0.005 P° simultaneous with Solvent "B" @ 0.005 P°
Solvent "A" @ 0.005 P° simultaneous with Solvent "B" @ 0.01 P°
Solvent "A" @ 0.005 P° simultaneous with Solvent "B" @ 0.015 P°

Solvent "A" @ 0.01 P° simultaneous with Solvent "B" @ 0.005 P°
Solvent "A" @ 0.01 P° simultaneous with Solvent "B" @ 0.01 P°
Solvent "A" @ 0.01 P° simultaneous with Solvent "B" @ 0.015 P°

Solvent "A" @ 0.015 P° simultaneous with Solvent "B" @ 0.005 P°
Solvent "A" @ 0.015 P° simultaneous with Solvent "B" @ 0.01 P°
Solvent "A" @ 0.015 P° simultaneous with Solvent "B" @ 0.015 P°

Solvent "A" @ 0.005 P° followed by Solvent "B" @ 0.005 P°
Solvent "A" @ 0.005 P° followed by Solvent "B" @ 0.01 P°
Solvent "A" @ 0.005 P° followed by Solvent "B" @ 0.015 P°

Solvent "A" @ 0.01 P° followed by Solvent "B" @ 0.005 P°
Solvent "A" @ 0.01 P° followed by Solvent "B" @ 0.01 P°
Solvent "A" @ 0.01 P° followed by Solvent "B" @ 0.015 P°

Solvent "A" @ 0.015 P° followed by Solvent "B" @ 0.005 P°
Solvent "A" @ 0.015 P° followed by Solvent "B" @ 0.01 P°
Solvent "A" @ 0.015 P° followed by Solvent "B" @ 0.015 P°

Solvent "B" @ 0.005 P° followed by Solvent "A" @ 0.005 P°
Solvent "B" @ 0.005 P° followed by Solvent "A" @ 0.01 P°
Solvent "B" @ 0.005 P° followed by Solvent "A" @ 0.015 P°

Solvent "B" @ 0.01 P° followed by Solvent "A" @ 0.005 P°
Solvent "B" @ 0.01 P° followed by Solvent "A" @ 0.01 P°
Solvent "B" @ 0.01 P° followed by Solvent "A" @ 0.015 P°

Solvent "B" @ 0.015 P° followed by Solvent "A" @ 0.005 P°
Solvent "B" @ 0.015 P° followed by Solvent "A" @ 0.01 P°
Solvent "B" @ 0.015 P° followed by Solvent "A" @ 0.015 P°

Table 3.3: Correlation coefficients, intercepts, slopes, intercept errors, and errors in the slopes for three sets of analytes exposed at P/P° = 0.005-0.03.

Table 3.3

Detector designator ->		8	12	15	16	17	18	19	20	21	22	23	24
propanol	R	0.9952	0.9918	0.9896	0.9971	0.9942	0.9998	0.9997	0.9928	0.9554	0.9541	0.8924	0.9976
	intercept	-0.0459	-0.0291	-0.0129	0.0328	-0.0268	-0.0136	-0.0042	-0.0050	-0.0370	-0.0450	-0.0728	0.0025
	slope	0.0773	0.0589	0.0451	0.0945	0.1480	0.2200	0.0518	0.0428	0.0608	0.0829	0.1012	0.0567
	intercept error	0.0074	0.0074	0.0064	0.0070	0.0155	0.0044	0.0011	0.0050	0.0183	0.0253	0.0498	0.0038
	error in slope	0.0038	0.0038	0.0033	0.0036	0.0080	0.0023	0.0006	0.0026	0.0094	0.0130	0.0256	0.0020
benzene	R	0.9938	0.9964	0.9972	0.9989	0.9983	1.0000	0.9996	0.9969	0.9934	0.9900	0.9655	0.9986
	intercept	-0.0250	-0.0494	0.0057	-0.1032	0.0154	-0.0429	-0.0613	0.0453	0.1156	0.1159	0.1764	0.0365
	slope	0.3547	0.1767	0.1696	0.6225	0.5079	0.5017	0.2986	0.2030	0.4465	0.4615	0.3143	0.2075
	intercept error	0.0385	0.0147	0.0125	0.0288	0.0289	0.0047	0.0080	0.0156	0.0501	0.0640	0.0825	0.0108
	error in slope	0.0198	0.0075	0.0064	0.0148	0.0148	0.0024	0.0041	0.0080	0.0257	0.0329	0.0424	0.0056
chloroform	R	0.9998	0.9993	0.9982	0.9985	0.9994	0.9998	0.9997	0.9948	0.9944	0.9979	0.9762	0.9976
	intercept	-0.0160	-0.0192	-0.0188	-0.2922	0.0032	-0.0563	-0.0528	0.0233	0.0685	0.0712	0.0501	0.0358
	slope	0.7132	0.4158	0.2236	1.4889	1.0367	0.8509	0.2996	0.1905	0.4181	0.6415	0.3216	0.2268
	intercept error	0.0131	0.0156	0.0130	0.0784	0.0343	0.0157	0.0069	0.0190	0.0432	0.0407	0.0696	0.0154
	error in slope	0.0067	0.0080	0.0067	0.0403	0.0176	0.0081	0.0035	0.0098	0.0222	0.0209	0.0357	0.0079
cyclohexanone	R	0.6547	1.0000	0.9988	0.9999	0.9997	1.0000	0.9997	0.9989	0.9982	0.9987	0.9971	0.9992
	intercept	-0.0027	0.0000	-0.0315	-0.0226	-0.0449	-0.0668	-0.0933	0.0046	0.0714	-0.0623	0.0572	0.0082
	slope	0.0023	0.0000	0.1058	0.4025	0.3362	0.6128	0.4274	0.1681	0.3137	0.1384	0.3524	0.1907
	intercept error	0.0026	0.0000	0.0050	0.0044	0.0081	0.0059	0.0104	0.0078	0.0185	0.0069	0.0263	0.0073
	error in slope	0.0013	0.0000	0.0026	0.0022	0.0041	0.0030	0.0053	0.0040	0.0095	0.0035	0.0135	0.0037
n-heptane	R	0.7636	1.0000	0.9981	0.9998	0.9978	0.9993	0.9989	0.9984	0.9967	0.9926	0.9672	0.9988
	intercept	-0.0118	0.0000	-0.0037	-0.0332	0.0006	-0.0003	-0.0063	0.0344	0.2174	-0.0291	0.1391	0.0176
	slope	0.0105	0.0000	0.1006	0.5202	0.1333	0.1682	0.0739	0.1351	0.3387	0.1341	0.1779	0.1180
	intercept error	0.0087	0.0000	0.0061	0.0100	0.0087	0.0059	0.0033	0.0075	0.0267	0.0159	0.0455	0.0056
	error in slope	0.0044	0.0000	0.0031	0.0051	0.0045	0.0030	0.0017	0.0038	0.0137	0.0082	0.0234	0.0029
nitrobenzene	R	0.9890	0.9897	0.9965	0.9980	0.9969	0.9995	0.9987	0.9955	0.9958	0.9983	0.9942	0.9979
	intercept	-0.0470	-0.0421	0.0836	0.0190	0.2262	-0.0397	-0.0989	0.1199	0.1215	-0.0650	0.3104	0.0695
	slope	0.2957	0.1316	0.3439	0.2605	1.0431	0.5656	0.4738	0.3002	0.4776	0.3617	0.6262	0.2818
	intercept error	0.0431	0.0185	0.0282	0.0162	0.0802	0.0173	0.0238	0.0280	0.0429	0.0205	0.0659	0.0176
	error in slope	0.0221	0.0095	0.0145	0.0083	0.0412	0.0089	0.0122	0.0144	0.0220	0.0105	0.0338	0.0090
ethanol	R	0.9975	0.9961	0.9864	0.9894	0.9925	0.9980	0.9956	0.0120	0.9569	0.9859	0.9727	0.0897
	intercept	-0.0274	0.0037	0.0273	0.0140	0.0088	-0.0028	0.0024	0.0109	0.0014	0.0198	0.0005	0.0101
	slope	0.1168	0.1743	0.0290	0.0442	0.1528	0.0805	0.0367	0.0000	0.0417	0.0442	0.0586	0.0008
	intercept error	0.0081	0.0151	0.0047	0.0063	0.0184	0.0049	0.0033	0.0033	0.0123	0.0073	0.0136	0.0083
	error in slope	0.0042	0.0077	0.0024	0.0032	0.0094	0.0025	0.0017	0.0017	0.0063	0.0038	0.0070	0.0043
1-propanol	R	0.9967	0.9977	0.9840	0.9971	0.9919	0.9986	0.9990	0.9656	0.9903	0.9957	0.9929	0.8252
	intercept	-0.0080	0.0186	0.0003	-0.0020	-0.0014	-0.0046	-0.0048	0.0075	-0.0041	-0.0016	-0.0055	0.0124
	slope	0.1281	0.1536	0.0476	0.0918	0.1802	0.1045	0.0542	0.0111	0.0548	0.0426	0.0806	0.0080
	intercept error	0.0101	0.0102	0.0084	0.0069	0.0225	0.0054	0.0024	0.0029	0.0075	0.0038	0.0094	0.0053
	error in slope	0.0052	0.0052	0.0043	0.0035	0.0116	0.0028	0.0012	0.0015	0.0038	0.0020	0.0048	0.0027
1-butanol	R	0.9884	0.9909	0.9964	0.9991	0.9891	0.9995	0.9997	0.9900	0.9941	0.9436	0.9936	0.9858
	intercept	-0.0103	-0.0131	0.0170	-0.0038	-0.0192	-0.0155	-0.0031	0.0092	0.0186	0.0011	0.0447	0.0171
	slope	0.0891	0.0938	0.0559	0.1206	0.2091	0.1286	0.0629	0.0195	0.0652	0.0241	0.0936	0.0166
	intercept error	0.0133	0.0124	0.0046	0.0050	0.0303	0.0039	0.0015	0.0027	0.0069	0.0082	0.0104	0.0028
	error in slope	0.0068	0.0064	0.0024	0.0026	0.0156	0.0020	0.0008	0.0014	0.0036	0.0042	0.0053	0.0014
1-pentanol	R	0.9838	0.9818	0.9947	0.9997	0.9784	0.9999	0.9992	0.9968	0.9848	0.9597	0.9790	0.9888
	intercept	-0.0048	-0.0184	0.0028	0.0071	0.0384	-0.0021	-0.0060	0.0049	0.0189	0.0080	0.0630	0.0077
	slope	0.0535	0.0473	0.0770	0.1383	0.1986	0.1361	0.0670	0.0298	0.0823	0.0143	0.1038	0.0258
	intercept error	0.0095	0.0089	0.0077	0.0032	0.0409	0.0019	0.0026	0.0023	0.0141	0.0041	0.0211	0.0038
	error in slope	0.0049	0.0046	0.0040	0.0016	0.0210	0.0010	0.0013	0.0012	0.0073	0.0021	0.0108	0.0019
1-hexanol	R	0.9847	0.9042	0.9927	0.9986	0.9837	0.9995	0.9998	0.9995	0.9925	0.9623	0.9884	0.9716
	intercept	-0.0107	-0.0108	0.0128	0.0017	0.0427	-0.0100	-0.0036	0.0056	0.0163	0.0160	0.0674	0.0075
	slope	0.0298	0.0134	0.0909	0.1792	0.2403	0.1607	0.0703	0.0430	0.1037	0.0277	0.1097	0.0305
	intercept error	0.0051	0.0062	0.0108	0.0094	0.0428	0.0047	0.0015	0.0013	0.0124	0.0076	0.0164	0.0072
	error in slope	0.0026	0.0032	0.0055	0.0048	0.0220	0.0024	0.0008	0.0007	0.0064	0.0039	0.0084	0.0037
1-heptanol	R	0.9181	0.7070	0.9922	0.9990	0.9983	0.9994	0.9991	0.9973	0.9967	0.9639	0.9890	0.9934
	intercept	-0.0066	-0.0013	0.0191	-0.0182	0.0043	-0.0097	-0.0033	0.0088	-0.0072	0.0176	0.0294	0.0106
	slope	0.0123	0.0013	0.1028	0.1954	0.2732	0.1638	0.0691	0.0450	0.1073	0.0357	0.1102	0.0327
	intercept error	0.0052	0.0013	0.0126	0.0086	0.0156	0.0055	0.0028	0.0033	0.0086	0.0096	0.0161	0.0037
	error in slope	0.0027	0.0007	0.0065	0.0044	0.0080	0.0028	0.0014	0.0017	0.0044	0.0049	0.0082	0.0019
n-hexane	R	0.9986	0.9954	0.9968	0.9990	0.9856	0.9994	0.9999	0.9975	0.9920	0.9991	0.9859	0.9984
	intercept	-0.0101	-0.0065	-0.0276	-0.1162	-0.0362	-0.0344	-0.0262	-0.0057	0.0805	-0.0379	0.0567	-0.0033
	slope	0.0560	0.0262	0.1234	0.4980	0.1143	0.1788	0.0844	0.1214	0.4194	0.1647	0.1451	0.0961
	intercept error	0.0037	0.0031	0.0124	0.0279	0.0244	0.0074	0.0012	0.0107	0.0664	0.0085	0.0306	0.0067
	error in slope	0.0015	0.0013	0.0050	0.0112	0.0098	0.0030	0.0005	0.0043	0.0267	0.0034	0.0123	0.0027

n-heptane	R	0.9945	0.9541	0.9971	0.9997	0.8540	0.9999	0.9997	0.9912	0.9676	0.9983	0.9765	0.9972
	intercept	-0.0062	-0.0048	-0.0127	-0.1029	0.0991	-0.0175	-0.0133	0.0233	0.2930	-0.0296	0.0979	0.0080
	slope	0.0300	0.0110	0.0893	0.5117	0.0824	0.1659	0.0729	0.1123	0.3609	0.1109	0.1195	0.0946
	intercept error	0.0041	0.0045	0.0090	0.0177	0.0659	0.0037	0.0025	0.0197	0.1236	0.0085	0.0346	0.0093
	error in slope	0.0016	0.0017	0.0034	0.0067	0.0251	0.0014	0.0009	0.0075	0.0471	0.0032	0.0132	0.0035
n-octane	R	0.9953	0.8879	0.9944	0.9993	0.9931	0.9994	0.9998	0.9954	0.9952	0.9966	0.9975	0.9982
	intercept	-0.0106	-0.0013	0.0108	-0.0984	-0.0640	-0.0223	-0.0208	0.0424	0.4277	-0.0089	0.0644	0.0095
	slope	0.0153	0.0042	0.1353	0.5442	0.2374	0.1688	0.0847	0.1299	0.3384	0.0682	0.1188	0.1062
	intercept error	0.0020	0.0029	0.0192	0.0266	0.0373	0.0076	0.0025	0.0166	0.0445	0.0075	0.0113	0.0084
	error in slope	0.0007	0.0011	0.0072	0.0100	0.0140	0.0028	0.0009	0.0062	0.0167	0.0028	0.0042	0.0032
n-nonane	R	0.9478	0.8408	0.9952	0.9993	0.9930	0.9995	0.9996	0.9888	0.9474	0.9946	0.9826	0.9981
	intercept	-0.0057	-0.0015	-0.0029	-0.1037	-0.1515	-0.0294	-0.0208	0.0615	0.4170	0.0027	0.0396	0.0176
	slope	0.0052	0.0011	0.1340	0.5929	0.2444	0.1713	0.0773	0.1358	0.3227	0.0456	0.0911	0.1079
	intercept error	0.0023	0.0009	0.0177	0.0306	0.0389	0.0070	0.0030	0.0275	0.1460	0.0064	0.0230	0.0090
	error in slope	0.0009	0.0003	0.0066	0.0114	0.0145	0.0026	0.0011	0.0103	0.0545	0.0024	0.0086	0.0034
n-decane	R	0.8406	0.2328	0.9924	0.9979	0.9929	0.9988	0.9993	0.9912	0.9669	0.9854	0.9830	0.9966
	intercept	-0.0015	0.0004	0.0309	-0.1109	0.0117	-0.0162	-0.0143	0.0933	0.4940	-0.0115	-0.0025	0.0249
	slope	0.0019	0.0003	0.1459	0.6094	0.1745	0.1599	0.0756	0.1398	0.3153	0.0385	0.0830	0.1110
	intercept error	0.0016	0.0017	0.0244	0.0538	0.0282	0.0107	0.0038	0.0251	0.1119	0.0090	0.0208	0.0124
	error in slope	0.0006	0.0006	0.0091	0.0200	0.0105	0.0040	0.0014	0.0093	0.0416	0.0033	0.0077	0.0046
n-dodecane	R	0.7186	0.8800	0.9900	0.9999	0.9785	0.9997	1.0000	0.9820	0.9506	0.9491	0.9066	0.9934
	intercept	-0.0007	-0.0010	0.0877	-0.0894	0.0653	-0.0136	-0.0170	0.1451	0.3458	-0.0122	-0.0236	0.0384
	slope	0.0005	0.0008	0.1649	0.6296	0.1949	0.1478	0.0752	0.1474	0.2549	0.0109	0.0194	0.1148
	intercept error	0.0006	0.0006	0.0316	0.0120	0.0553	0.0048	0.0010	0.0381	0.1120	0.0049	0.0121	0.0179
	error in slope	0.0002	0.0002	0.0117	0.0045	0.0205	0.0018	0.0004	0.0142	0.0416	0.0018	0.0045	0.0067

Chapter 4

The Relationship Between Mass, Thickness Change, and Resistance Response for Polymer-Carbon Black Composite Chemiresistors

Abstract:

The relationships between mass uptake, thickness changes, and dc resistance changes have been investigated for carbon black-insulating polymer composite vapor detectors. Quartz crystal microbalance measurements and ellipsometry measurements have been performed simultaniously on polymer films that do not contain carbon black filler in order to relate the mass uptake and thickness change to the analyte concentration in the vapor phase. In addition, quartz crystal microbalance measurements and dc resistance measurements on carbon black composites of these same polymers have been performed simultaneously to relate the mass uptake and dc electrical resistance response to the analyte concentration in the vapor phase. Because the mass uptake for a given polymer film was not significantly affected in these test cases by the presence or absence of the carbon black filler, these measurements also yield insight into the relationships between swelling, sorption, and resistance changes of carbon black-insulating polymer composite chemiresistor vapor detectors. The data indicate that the dc resistance change is directly relateable to the thickness change of the polymers, and that a variety of analytes that produce a given thickness change produce an equated resistance change in the test set of polymers investigated in this work.

I. Introduction

Carbon black-insulating organic polymer composite films have been employed previously as components of an array of vapor detectors for use in an "electronic nose".[1] In this approach, the response of an array of broadly cross responsive vapor detectors is analyzed using standard chemometric methods to yield diagnostic patterns that allow classification and quantification of analytes in the vapor phase. Arrays of such detectors have been shown to be highly discriminating even between very structurally similar analytes, and have also been shown for many test vapors to exhibit a linear steady-state dc resistance response to analyte concentration. Thus, under these conditions the pattern type allows identification of the vapor and the steady-state pattern height allows quantification of the analyte of concern.[1-3]

The resistance response of such composites can, in general, be understood by percolation theory, which relates the resistance response of a composite of an isulating polymer filled with regions of an electrical conductor to the change in volume fraction of the conducting (filler) phase of the composite.[4-7] The goal of the present work was to elucidate the factors that control the resistance change of such films in response to a change in vapor concentration that is exposed to the detector. Unlike polymer-coated quartz crystal microbalances, where the frequency change of the detector is primarily determined by the change in mass of analyte sorbed into the polymer film, or polymer-coated surface acoustic wave devices, where changes in sorbed mass and modulus of the polymer film both contribute to the detected signal,[8] the hypothesis that was challenged in this work is that the volume change, and thus the fractional swelling, of the polymer film upon exposure to a test vapor is the key variable that determines the change in dc electrical resistance of the carbon black-polymer composite detectors.

To test this hypothesis, we have performed measurements to determine the mass uptake, thickness change, and resistance change of various composite and non-composite polymer films exposed to a variety of test organic vapors. The mass uptake and the dc electrical resistance changes of a set of carbon black-organic polymer composite films were determined on a quartz crystal microbalance (QCM). QCM measurements and thickness measurements using fixed

wavelength ellipsometry methods were then performed on clear (non-carbon black filled) films formed from the same polymers. Relationships between the two sets of measurements were facilitated because at a given analyte concentration in the vapor phase, the measured mass uptakes were very similar for polymers that did, and did not, contain the carbon black filler material.

II. Experimental

QCM crystals (10 MHz, blank dia = 13.7 mm)) with a custom electrode pattern were obtained from International Crystal Manufacturing (ICM) in Oklahoma City, OK. The standard oscillation electrodes were configured at 90° angles to make room for two other tabs that would serve as electrodes for resistance measurements of the carbon black-polymer composite films (Figure 4.1). The crystals were polished to a surface roughness of less than 5 microns, which produced a mirror-like finish on the gold electrodes. To facilitate reflection of the ellipsometer's laser beam when the crystals were used with transparent films during the thickness measurements, one oscillator electrode was larger than the other (larger electrode dia. = 7.8 mm, smaller electrode dia. = 5.1 mm). The resistance tabs were not used during the thickness vs. mass measurements on films that were not filled with carbon black. Similarly, the ellipsometer was not used during the resistance vs. mass measurements, in which optically opaque, carbon-black filled, composite films were used.

The crystals were held in a custom Teflon block by stainless steel wire spring-clips that were secured to the block by screws (Figure 4.2). The holder was 50 x 35 x 10 mm with a 5 mm cutout in the top to allow the QCM crystal to remain suspended when supported by stainless steel spring clips that were wired to the oscillator and ohmmeter circuits. This holder was placed in the custom chamber (55 x 35 x 35 mm) shown in Figure 4.3. This chamber had cutouts to allow the ellipsometer beam to reflect off the QCM surface and cutouts along the bottom to allow access for electrical connections. A hole was present in the top of the chamber to allow for leveling of the crystal by a spotting scope on the ellipsometer. This hole was blocked during vapor presentations by placing a flat glass slide over the hole. An additional hole was present to accommodate a gas

inlet for introduction of the vapor streams. The cut-outs in the chamber served as the vapor stream exit .

The vapor stream was produced by passing general laboratory compressed air through analyte solvents contained in custom bubblers. The solvents used were HPLC quality (Aldrich Chemical Co.) and were used as received. Saturation of the vapor with solvent was confirmed by mass loss experiments.[9] The solvent-saturated air was then diluted to the desired concentration with lab compressed air. The air flows through the bubbler and in the background gas were regulated by needle valves, and the flows in both streams were monitored with Gilmont rotamers (VWR Scientific). The concentration of analyte in the vapor stream was independently verified using a calibrated flame ionization detector (California Analytical, Santa Ana, CA).

Two polymers were used in this work, poly(caprolactone) (PCL) and poly(ethylene oxide) (PEO). Films of these polymers that contained carbon black were used for the resistance measurements, while transparent, pure polymer films were used for the thickness measurements. All films were cast from standard solutions that consisted of 160 mg of polymer dissolved in 20 ml of benzene to which 40 mg of carbon black was added to the solutions used to make composite films (resulting in a solution that was 20% by weight of carbon black). All solutions were sonicated for at least 5 min immediately prior to casting the films. The polymer films were spun-cast on a Headway spin caster (Headway Research, Garland, TX) at 2000 rpm and the average film thickness was obtained by profilometry (Dektak 3030, Sloan Technology Corp., Santa Barbara, CA).

The QCM crystals were weighed before and after film application using a Cahn microbalance (resolution 0.001 mg; Cahn C-35, Orion Research, Beverly, MA) to obtain the mass of the films that were deposited over the large electrode (7.8 mm diameter area) on the QCM. The PCL clear film was 19 μg in mass and 375 nm thick, while the PCL-carbon black composite film was 86 μg in mass with a baseline resistance of ≈ 12 kΩ. The PEO clear film was 57 μg in mass and 1090 nm thick, while the PEO-carbon black composite film was 9 μg in mass with a baseline resistance of ≈ 16 kΩ. Using the clear polymer film areas and the mass and thickness values

above, densities for the clear films of PEO and PCL were calculated and agreed with literature values for these polymers.

Resistance readings were measured using a Keithley 2002 digital multimeter (Cleveland, OH), and the resonant frequency of the QCM was obtained using a HP 5384A frequency counter (Palo Alto, CA). Shielded cables were used between the crystal, the oscillator circuit, and the frequency counter. Ellipsometry measurements were taken on a Gaertner L116C ellipsometer (Gaertner Scientific, Chicago, IL). Optical constants were obtained for each surface before the films were applied. The index of refraction of each polymer film was taken from the literature. The absorption coefficient for the film was obtained using the two-angle technique[10,11] which also provided an independent measurement of the index of refraction and thickness of the film. The film thicknesses obtained by ellipsometry agreed to within 10% with the values obtained by profilometry.

To initiate an experiment, a baseline value was recorded for the mass, resistance, and/or thickness of the film. The film was then exposed to analyte vapor until steady state values were reached as determined by constant output readings from the instruments. The data were recorded manually for convenience. Each thickness measurement was taken 3 - 5 times after steady state had been reached for a given vapor, and the average result was recorded for both the baseline and steady-state, solvent-exposed values of concern.

III. Results

Figure 4.4a shows the relative thickness change, $\Delta h_{max}/h_b$, of poly(caprolactone) films as a function of the analyte fractional vapor phase, P/P°. The series of test vapors used in these experiments are representative of a broad test set of analytes that has been used previously to investigate the discrimination ability of arrays of conducting polymer composite vapor detectors.[1-3] The data of Figure 4.4a are well-fit to a linear dependence of $\Delta h_{max}/h_b$ vs. P/P° (Table 4.1). Figure 4.5a shows similar data for poly(ethylene oxide) films.

Figures 4.4b and 4.5b depict the steady-state relative differential resistance responses, $\Delta R_{max}/R_b$, of carbon-black filled poly(caprolactone) and poly(ethylene oxide) films, respectively,

as a function of the analyte concentration, for the same set of test analytes. Over the concentration ranges probed in the experiment, the data are well-fit by straight lines passing though the origin (Table 4.1).

Figures 4.6a and 4.6b depict the relative mass uptake, $\Delta m_{max}/m_b$, of poly(caprolactone) films as a function of the analyte concentration in the vapor phase. Figures 4.7a and 4.7b depict the same data for poly(ethylene oxide) films. Data are depicted for films of polymer that were, and were not, respectively, filled with carbon black. Again the data are well-fit by straight lines over the analyte concentration range of experimental interest (Table 4.1), indicating a relatively constant gas-polymer partition coefficient over the analyte concentration range probed in these experiments. For all the solvents, the relative mass uptake of the pure polymer films was the same as the mass uptake of the analogous carbon black filled composite, to within the error in the measurements. For example, Figure 4.8 depicts the relative mass uptake as a function of the fractional vapor pressure for $CHCl_3$ for poly(caprolactone) and poly(ethylene oxide) carbon black containing and carbon black free films.

IV. Discussion

Figure 4.9a depicts a plot of the dc relative differential resistance change of the poly(caprolactone) film, from electrical measurements, as a function of the fractional swelling of the polymer, as determined by optical ellipsometry measurements. The same analysis for a second poly(caprolactone) film is shown in Figure 4.9b to illustrate the variance in the data. For both polymer systems, the slopes and intercepts of the $\Delta R_{max}/R_b$ vs. P/P° data for the composite films were used to predict what value of $\Delta R_{max}/R_b$ would be expected for the P/P° values used in measurement by the non-filled polymer films. Likewise, the slopes and intercepts of the $\Delta h_{max}/h_b$ vs. P/P° data for the non-filled polymer films were used to predict what value of $\Delta h_{max}/h_b$ would be expected for the P/P° values used in measurement by the composite films. The predicted values of $\Delta R_{max}/R_b$ were then plotted vs. the predicted $\Delta h_{max}/h_b$ values at the corresponding fractional vapor pressure of the analyte. As displayed in Figure 4.9, the data are linear and roughly fall on the same line for all of the test vapors investigated in this work. In each film some solvents do not

lie on the common line, but this is presumed to be due to experimental error in the delivery of the vapor. It is clear that regardless of the analyte used, a given fractional thickness change of the polymer produces a given steady-state relative differential resistance response of the corresponding carbon-filled composite, at least for the polymer-analyte combinations explored in this work. Thus, the hypothesis of concern -- that volumetric film swelling is the key variable determining $\Delta R_{max}/R_b$ in the composite carbon black-insulating polymer detectors -- seems to be confirmed from the data obtained in this work, at least for the analytes and polymers investigated to date. Also, this shows that the relationship between thickness change and steady-state relative differential resistance change is linear, at least over the range of analyte concentrations investigated in this work.

One complicating factor is that the thickness measurements obtained in this work were performed on pure polymeric materials, while the $\Delta R_{max}/R_b$ measurements were performed on carbon black-filled polymer composites. The assumption made above in interpreting the data of Figure 4.9 is that the volumetric swelling of the polymer is similar whether or not the material is loaded with carbon black. Given the linear relationship deduced between $\Delta h_{max}/h_b$ and $\Delta R_{max}/R_b$, and the low intuitive likelihood that, over a range of analytes and concentrations, two separate functional dependencies of swelling on analyte concentration would precisely counteract each other to yield the data of Figure 4.9, this assumption seems quite reasonable. Given the linear dependence of $\Delta R_{max}/R_b$ on P/P° that has been observed for other test analytes,[12] it seems reasonable to assume that the relationship between relative volumetric swelling and relative differential resistance measurements is extendible, at least to first order, for those composite-analyte combinations as well.

An independent check on the validity of the relationship between swelling in the carbon-black filled composites and the pure polymer films is available through the QCM mass uptake measurements. The relationship between $\Delta R_{max}/R_b$ vs. $\Delta m_{max}/m_b$ and $\Delta h_{max}/h_b$ vs. $\Delta m_{max}/m_b$ is linear as seen in Figure 4.10 for PCL and Figure 4.11 for PEO (See also Table 4.1). The slopes and intercepts of the $\Delta R_{max}/R_b$ vs. $\Delta m_{max}/m_b$ data for the composite films were used to predict

what value of $\Delta R_{max}/R_b$ would be expected for the $\Delta m_{max}/m_b$ values measured for the non-filled polymer films at the various analyte concentrations used in the measurements. Likewise, the slopes and intercepts of the $\Delta h_{max}/h_b$ vs. $\Delta m_{max}/m_b$ data for the non-filled polymer films were used to predict what value of $\Delta h_{max}/h_b$ would be expected for the $\Delta m_{max}/m_b$ values measured for the composite films at the various analyte concentrations used in the measurements. The predicted value of $\Delta R_{max}/R_b$ was then plotted vs. the predicted $\Delta h_{max}/h_b$ values at the corresponding fractional vapor pressure of the analyte. As displayed in Figure 4.12, the data are linear and roughly fall on the same line for all of the test vapors investigated in this work. This strongly implies the presence of a correlation between volume change and resistance change in these composite films. This is a stronger indicator than the correlation through P/P° because the $\Delta m_{max}/m_b$ for each presentation for each film was taken simultaneously with the $\Delta R_{max}/R_b$ and $\Delta h_{max}/h_b$ measurements. The fractional vapor pressure correlation presented above was less precise due to variance in the flow system, whereas any changes in the concentration of the exposed analyte would be reflected in the $\Delta m_{max}/m_b$ as well.

Further support for the swelling-induced resistance change hypothesis can be obtained by investigating the relationship between $\Delta R_{max}/R_b$ and $\Delta h_{max}/h_b$ as a function of analyte density. As seen in Figures 4.13 and 4.14, the slopes of the $\Delta h_{max}/h_b$ vs. $\Delta m_{max}/m_b$ lines and the $\Delta R_{max}/R_b$ vs. $\Delta m_{max}/m_b$ lines depend linearly on the density (as measured in the pure liquid phase) of the sorbing species. These data are in agreement with recently reported results that were obtained in parallel with our study, in which the relative differential resistance response of carbon black filled poly(ethylene oxide) composites was shown to correlate with the density of the gaseous analyte (as measured in its pure liquid phase).[13]

These data support the hypothesis that the resistance response is primarily induced by a change in volume of the film, as reflected in the thickness change. A straight line of any slope for $[(\Delta m_{max}/m_b)/(\Delta R_{max}/R_b)]$ vs. density that goes through the origin would imply a precise correlation between the density and the detector response. The $[(\Delta m_{max}/m_b)/(\Delta R_{max}/R_b)]$ ratio for hexafluorobenzene is larger in all cases most likely because the molecules do not chemisorb into

the polymer matrix in proportion to the amount that physisorbs because molecular interactions between the perfluoroinated analyte and the polymer chains are not likely to be sufficiently favorible energetically to disrupt the polymer inter-chain interactions. This will cause an increase in mass response for hexafluorobenzene (due to adsorption) without a concomitant increase in resistance or thickness response (which requires absorbtion), leading to larger $[(\Delta m_{max}/m_b)/(\Delta R_{max}/R_b)]$ and $[(\Delta m_{max}/m_b)/(\Delta h_{max}/h_b)]$ ratios for that solvent.

Generally, the slope of the line for the thickness response vs. the density is about an order of magnitude larger than the slope of the line for the related resistance response measurements. In both the thickness and resistance measurements the mass uptake is similar, therefore the difference in slopes is due to differences in relative response between the thickness and resistance measurements. In all cases, the relative differential resistance response is greater than the relative thickness change for a given relative mass change. This finding is consistent with percolation theory, which relates the fractional volume change of a conductor in a composite with a fractional resistivity change of that composite for a given initial conductor volume fraction. We are unable to make direct comparisons with percolation theory because we do not have a complete understanding of the morphology of the carbon black in the composites; however, these data are consistent with reasonable values for the variables in the percolation theory equation for high conductivity carbon black.[14-16]

An implication of these findings is that low density analytes will cause a larger resistance response in our detectors for a given mass uptake. We have shown in prior work that the amount of analyte that sorbs into these detector films is a function of the fraction of vapor pressure of the analyte.[17] This fractional vapor pressure argument accounts for most of the response by a detector to an analyte, but the differences in response by a detector to a set of analytes are due to differences in chemical affinity between the polymer film and the analytes as well as the molecular properties of the analytes such as their molecular volume. Therefore, a lower density analyte will be easier to detect at lower levels of sorption (mass uptake) than high density analytes.

These findings suggest design guidelines for producing optimal detectors and vapor sampling systems for tasks in which the analyte is not available in large concentrations (for example, low vapor pressure analytes). In an optimal system, the greatest amount of analyte-laden sample should impinge on the smallest area possible, and this area should correspond to the smallest detector area that is feasible. These findings make clear the need for the greatest volume change within the detector film for a sensing event to be recorded. The best way to cause the largest possible swelling of the detector films, in the absence of pre-concentration, is to cause the low concentration vapor stream to have direct contact with a small film area.

In conclusion, we have shown that our composite detectors respond based on the volume change of the composite film as evidenced by a linear dependence on the analyte densities by the slopes of the lines for the thickness and resistance responses vs. mass uptake and by a linear relationship between percent resistance change and percent thickness change when these two are correlated by the percent mass uptake. Additionally, we have developed a single element densiometer that can be used to characterize one molecular characteristic of exposed analytes.

VI. REFERENCES

1)Lonergan, M. C.; Severin, E. J.; Doleman, B. J.; Beaber, S. A.; Grubbs, R. H.; Lewis, N. S. *Chemistry of Materials* **1996**, *8*, 2298.

2)Freund, M. S.; Lewis, N. S. *Proceedings of the National Academy of Sciences* **1995**, *92*, 2652-2656.

3)Doleman, B. J.; Lonergan, M. C.; Severin, E. J.; Vaid, T. P.; Lewis, N. S. *Anal. Chem.* **1998**, *70*, 4177-4190.

4)Anderson, J. E.; Adams, K. M.; Troyk, P. R. *Journal of Non-Crystalline Solids* **1991**, *131*, 587-592.

5)Ast, D. G. *Physical Review Letters* **1974**, *33*, 1042-1045.

6)Godovski, D. Y.; Koltypin, E. A.; Volkov, A. V.; Moskvina, M. A. *Analyst* **1993**, *118*, 997-999.

7)Kirkpatrick, S. *Reviews of Modern Physics* **1973**, *45*, 574-588.

8)Grate, J. W.; Klusty, M.; McGill, R. A.; Abraham, M. H.; Whiting, G.; Andonian-Haftvan, J. *Analytical Chemistry* **1992**, *64*, 610-624.

9)Atkins, P. W. *Physical Chemistry*; W.H. Freeman and Co.: New York, NY, 1994.

10)Comfort, J. C.; Urban, F. K.; Barton, D. *Thin Solid Films* **1996**, *291*, 51.

11)Urban, F. K. *Applied Surface Science* **1988**, *33*, 934.

12)Severin, E. J.; Doleman, B. J.; Lewis, N. S. *manuscript in preparation.* **1999**.

13)Swann, M. J.; Glidle, A.; Cui, L.; Barker, J. R.; Cooper, J. M. *Chemical Communications* **1998**, 2753-2754.

14)Ali, M. H.; AboHashem, A. *Journal Of Materials Processing Technology* **1997**, *68*, 163.

15)Ali, M. H.; AboHashem, A. *Journal Of Materials Processing Technology* **1997**, *68*, 168.

16)Ali, M. H.; Abohashem, A. *Plastics Rubber and Composites Processing and Applications* **1995**, *24*, 47.

17)Doleman, B. J.; Severin, E. J.; Lewis, N. S. *Proceedings of the National Academy of Sciences of the United States of America* **1998**, *95*, 5442-5447.

Figure 4.1: Custom 10 MHz QCM crystal with oscillation electrodes and tabs for reading the composite film resistance. Shaded areas indicate regions coated with Au. The larger electrode was used to facilitate ellipsometry measurements. The smaller back electrode is shown with solid lines.

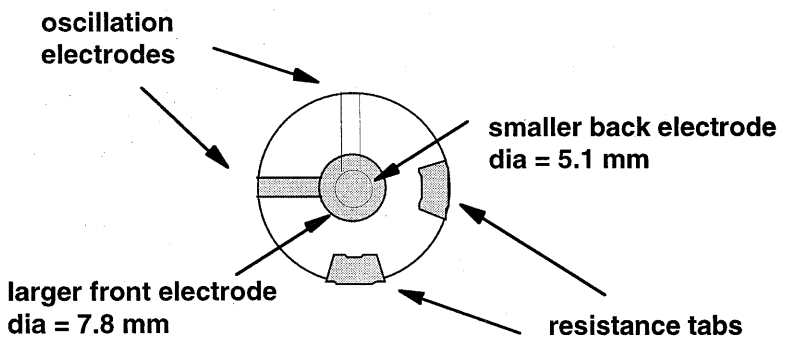
oscillation
electrodes
smaller back electrode
dia = 5.1 mm
larger front electrode
dia = 7.8 mm
resistance tabs

Figure 4.1

Figure 4.2: Custom Teflon crystal holder (top and side views). The holder was 50 x 35 x 10 mm with a 5 mm cutout in the top to allow the QCM crystal to remain suspended when supported by stainless steel spring clips which were wired to the oscillator and ohmmeter circuits (see Experimental).

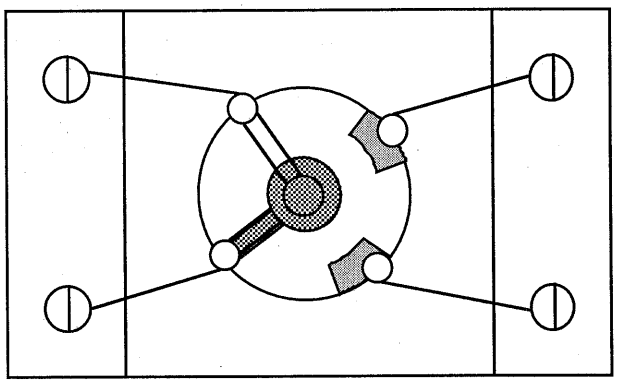

Top View

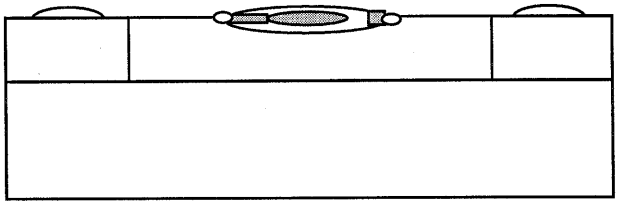

Side View

Figure 4.2

Figure 4.3: Custom sample chamber (55 x 35 x 35 mm). This chamber had cutouts to allow the ellipsometer beam to reflect off the QCM surface and cutouts along the bottom to allow access for the wires. A hole was present in the top of the chamber to allow for leveling of the crystal by a spotting scope on the ellipsometer. This hole was blocked during vapor presentations by placing a flat glass slide over the hole. An additional hole was present to accommodate a gas inlet for introduction of the vapor streams. The cut-outs in the chamber served as the vapor stream exit.

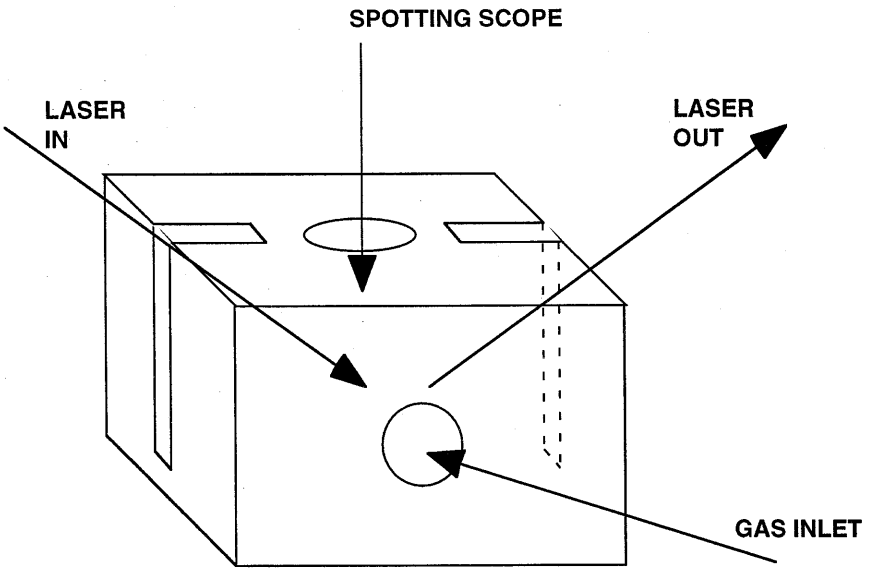

Figure 4.3

Figure 4.4: (**A**) Differential thickness increase for a carbon black free PCL film vs. fraction of analyte vapor pressure exposed to the film. (**B**) Differential relative resistance increase in a PCL-carbon black composite vs. fraction of analyte vapor pressure exposed to the film.

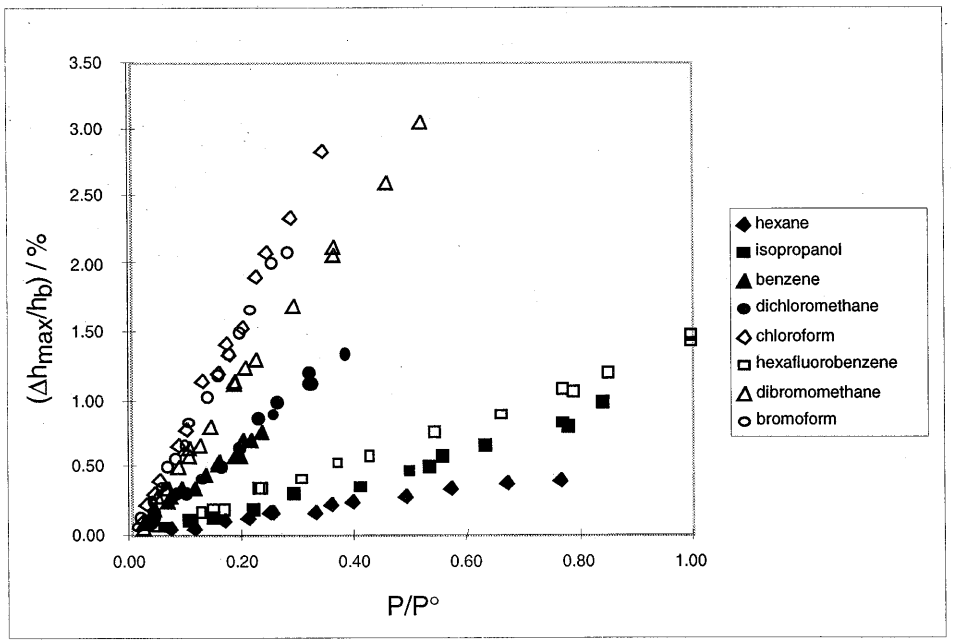
3.50
3.00
2.50
2.00
1.50
1.00
0.50
0.00
0.00
0.20
0.40
0.60
0.80
1.00
(Δhmax/hb) / %
P/P°
hexane
isopropanol
benzene
dichloromethane
chloroform
hexafluorobenzene
dibromomethane
bromoform

Figure 4.4a

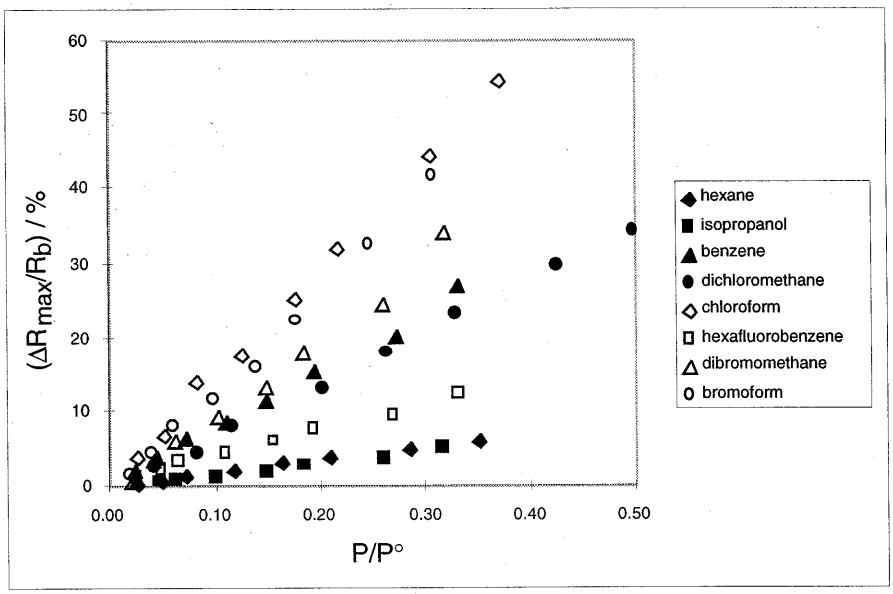
60
50
40
30
20
10
0
0.00
0.10
0.20
0.30
0.40
0.50
(ΔRmax/Rb) / %
P/P°
hexane
isopropanol
benzene
dichloromethane
chloroform
hexafluorobenzene
dibromomethane
bromoform

Figure 4.4b

Figure 4.5: (**A**) Differential thickness increase for a carbon black free PEO film vs. fraction of analyte vapor pressure exposed to the film. (**B**) Differential relative resistance increase in a PEO-carbon black composite vs. fraction of analyte vapor pressure exposed to the film.

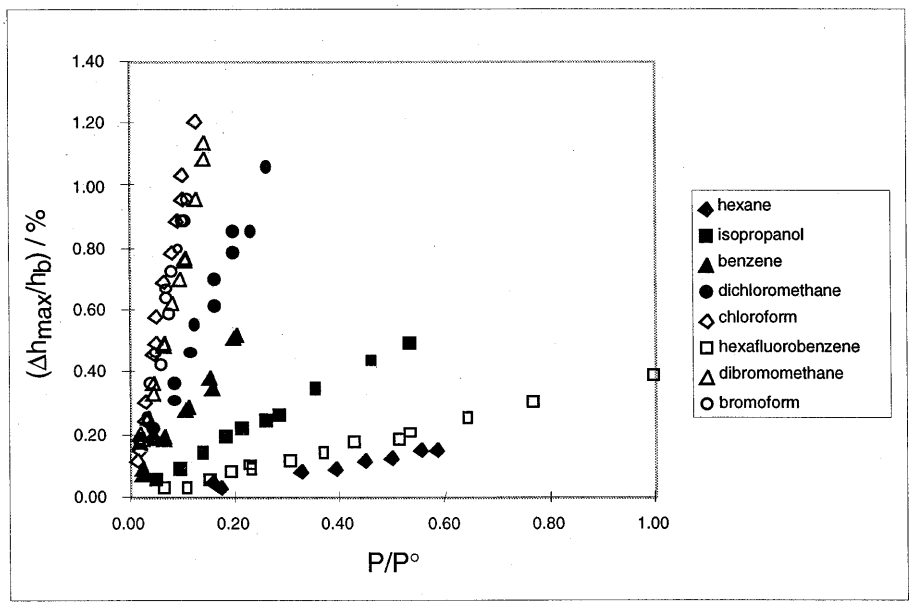
1.40
1.20
1.00
0.80
0.60
0.40
0.20
0.00
0.00
0.20
0.40
0.60
0.80
1.00
(Δhmax/hb) / %
P/P°
hexane
isopropanol
benzene
dichloromethane
chloroform
hexafluorobenzene
dibromomethane
bromoform

Figure 4.5a

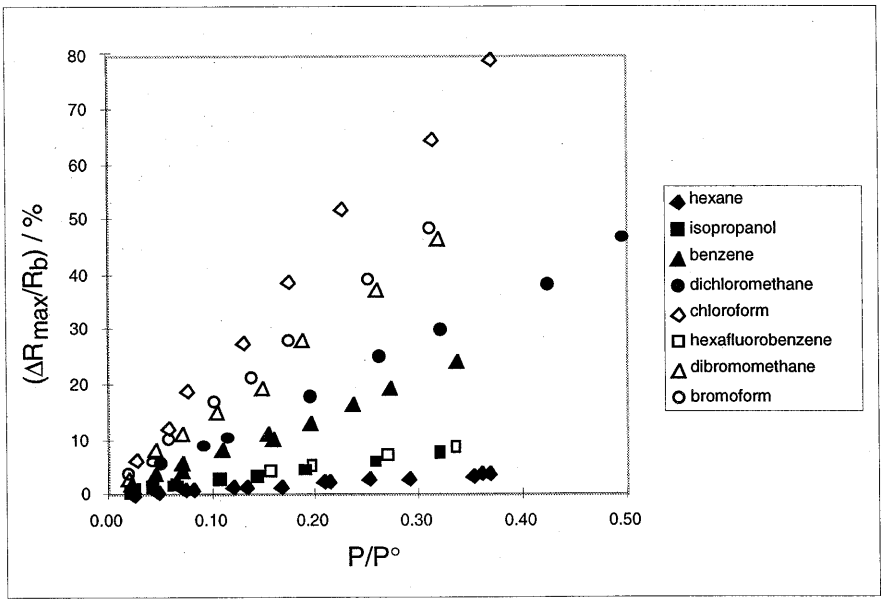
80
70
60
50
40
30
20
10
0
0.00
0.10
0.20
0.30
0.40
0.50
(ΔR max/Rb) / %
P/P°
hexane
isopropanol
benzene
dichloromethane
chloroform
hexafluorobenzene
dibromomethane
bromoform

Figure 4.5b

Figure 4.6: Differential relative mass increase vs. fraction of analyte vapor pressure exposed to the film for (**A**) PCL carbon black free and (**B**) PCL carbon black containing films.

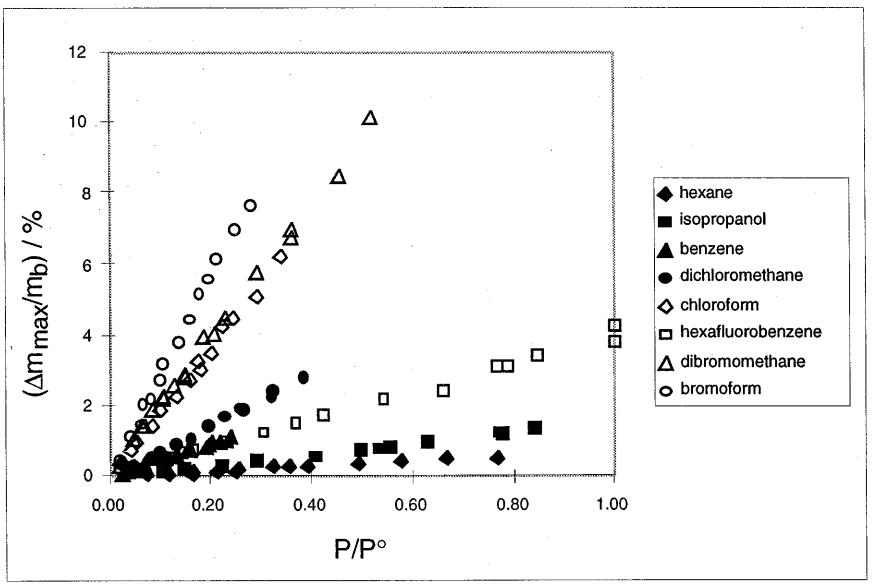
12
10
8
6
4
2
0
0.00
0.20
0.40
0.60
0.80
1.00
P/P°
(Δm max/mb) / %
hexane
isopropanol
benzene
dichloromethane
chloroform
hexafluorobenzene
dibromomethane
bromoform

Figure 4.6a

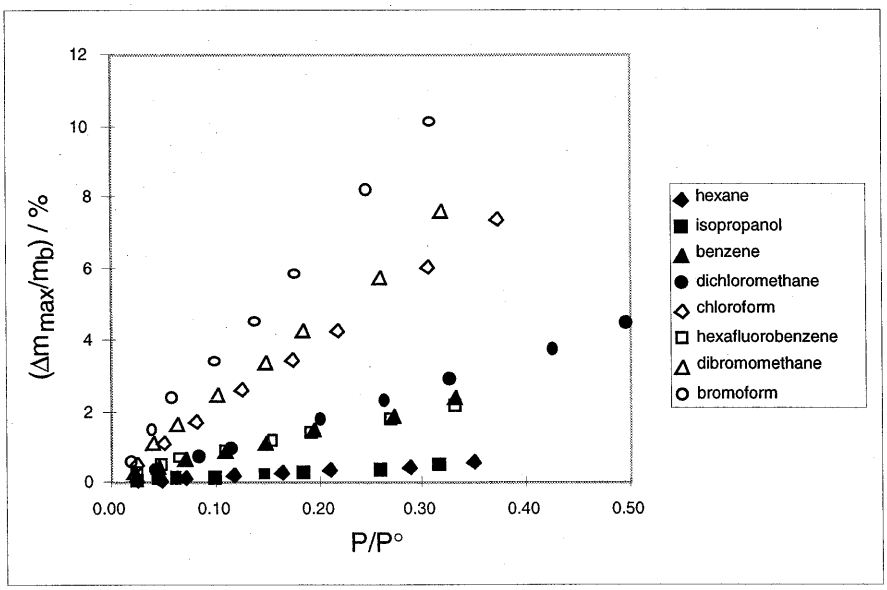
12
10
8
6
4
2
0
0.00
0.10
0.20
0.30
0.40
0.50
P/P°
(Δm max/mb) / %
hexane
isopropanol
benzene
dichloromethane
chloroform
hexafluorobenzene
dibromomethane
bromoform

Figure 4.6b

Figure 4.7: Differential relative mass increase vs. fraction of analyte vapor pressure exposed to the film for (**A**) PEO carbon black free and (**B**) PEO carbon black containing films.

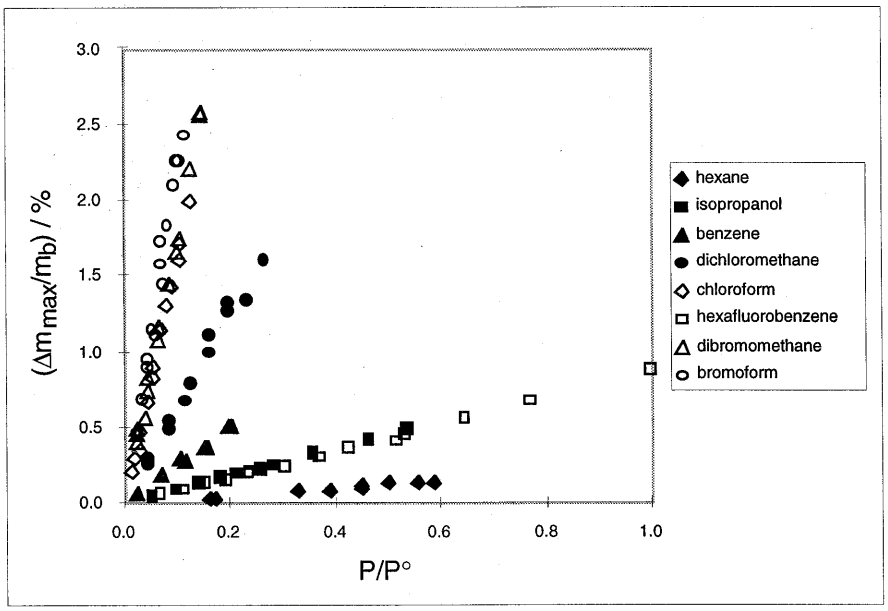
3.0
2.5
2.0
1.5
1.0
0.5
0.0
(Δm max/mb) / %
0.0
0.2
0.4
0.6
0.8
1.0
P/P°
hexane
isopropanol
benzene
dichloromethane
chloroform
hexafluorobenzene
dibromomethane
bromoform

Figure 4.7a

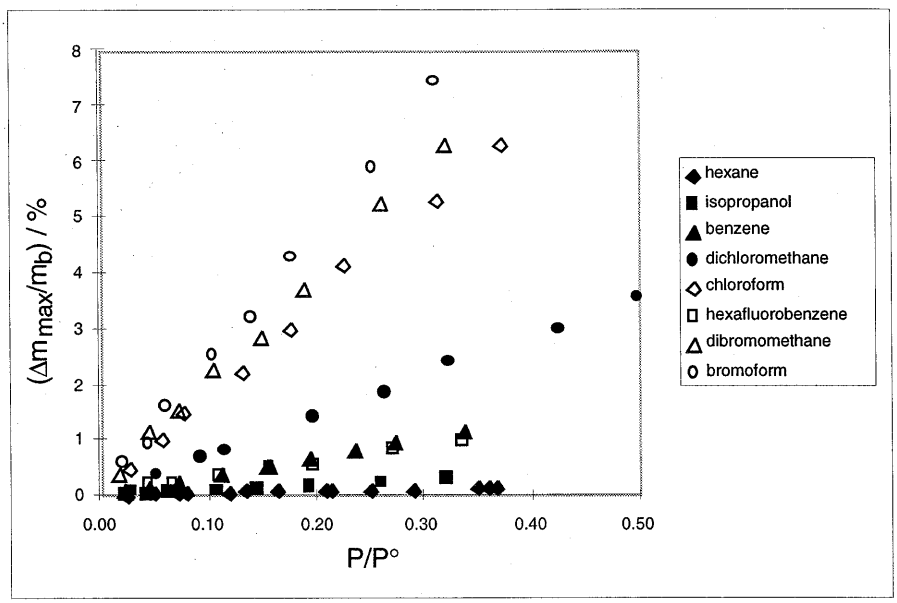
8
7
6
5
4
3
2
1
0
0.00
0.10
0.20
0.30
0.40
0.50
P/P°
(Δm max/mb) / %
hexane
isopropanol
benzene
dichloromethane
chloroform
hexafluorobenzene
dibromomethane
bromoform

Figure 4.7b

Figure 4.8: Differential relative mass increase vs. fraction of analyte vapor pressure exposed to the film for (**A**) PCL-carbon black containing film and carbon black free film and for (**B**) PEO-carbon black containing film and carbon black free film.

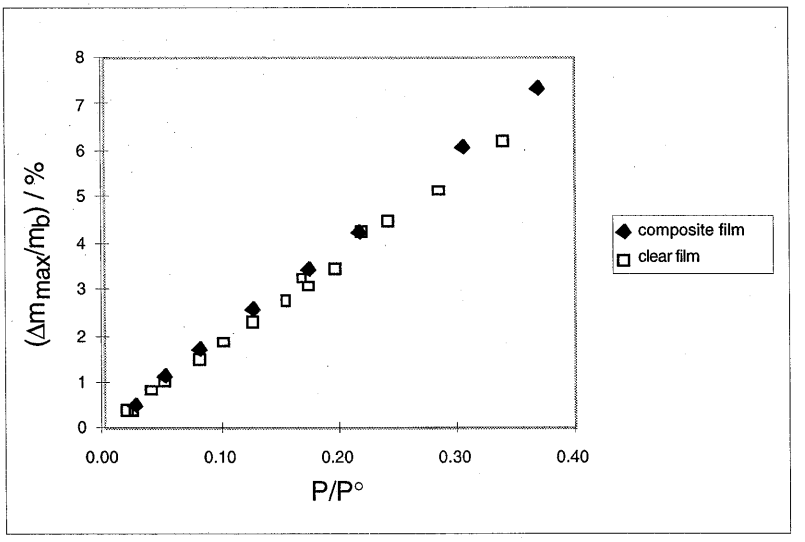
8
7
6
5
4
3
2
1
0
0.00
0.10
0.20
0.30
0.40
P/P°
(Δm max/mb) / %
composite film
clear film

Figure 4.8a

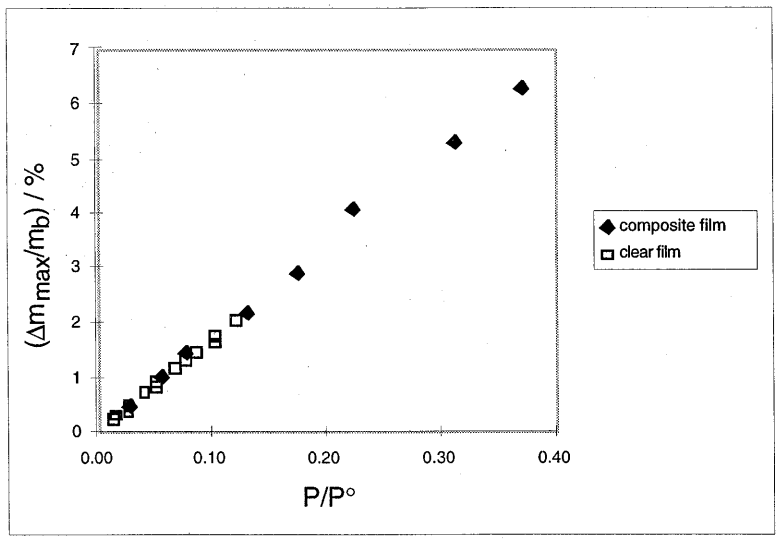
7
6
5
4
3
2
1
0
0.00
0.10
0.20
0.30
0.40
P/P°
(Δmmax/mb) / %
composite film
clear film

Figure 4.8b

Figure 4.9: Relative resistance increase for a PCL-carbon black composite film verses relative thickness increase for a PCL clear film when both films were exposed to various anlaytes at various frational vapor pressures, correlated by the analyte fractional vapor pressure for two separate (**A** & **B**) PCL films.

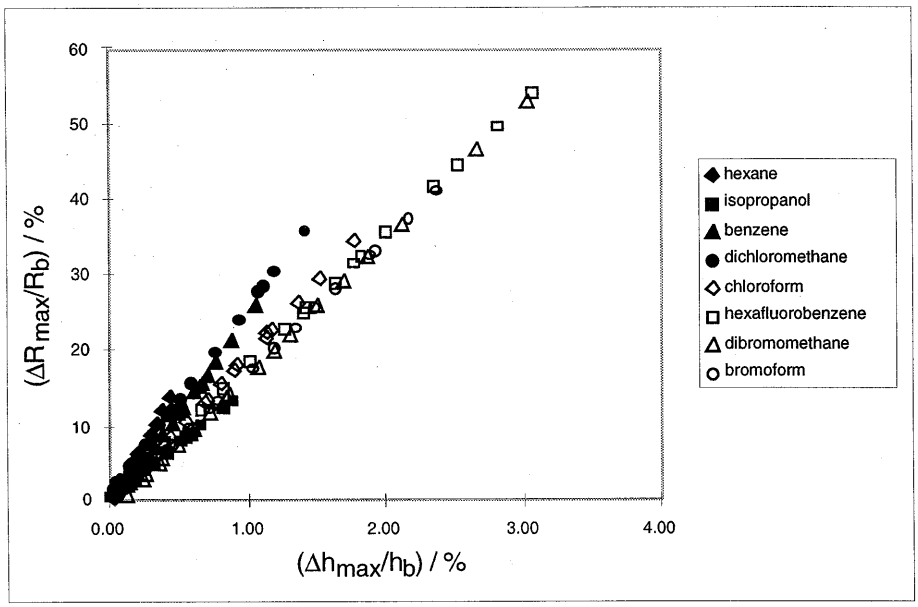
60
50
40
30
20
10
0
0.00
1.00
2.00
3.00
4.00
(ΔRmax/Rb) / %
(Δhmax/hb) / %
hexane
isopropanol
benzene
dichloromethane
chloroform
hexafluorobenzene
dibromomethane
bromoform

Figure 4.9a

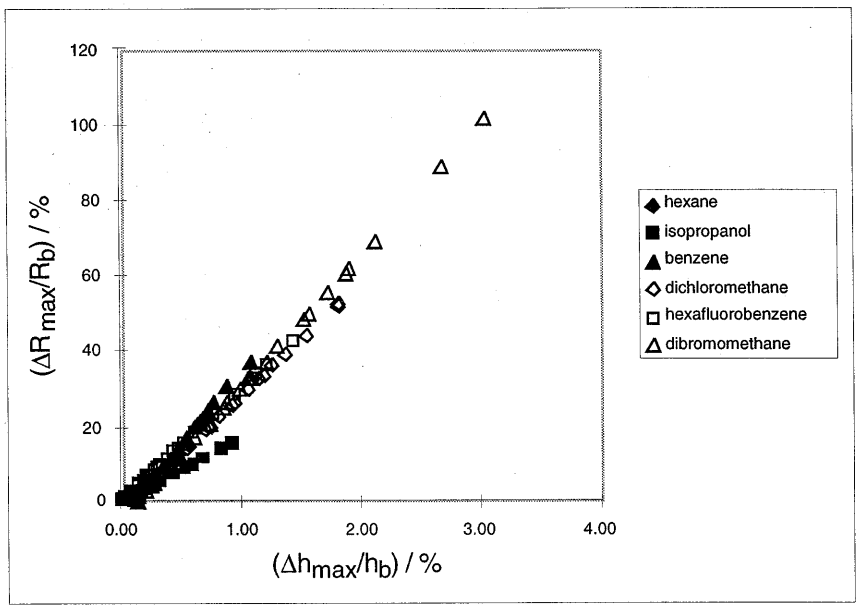
120
100
80
60
40
20
0
0.00
1.00
2.00
3.00
4.00
(ΔRmax/Rb) / %
(Δhmax/hb) / %
hexane
isopropanol
benzene
dichloromethane
hexafluorobenzene
dibromomethane

Figure 4.9b

Figure 4.10: (**A**) Differential relative thickness increase vs. differential relative mass increase for a PCL film when exposed to various analyte fractional vapor pressures. (**B**) Differential relative resistance increase vs. differential relative mass increase for a PCL film when exposed to various analyte fractional vapor pressures.

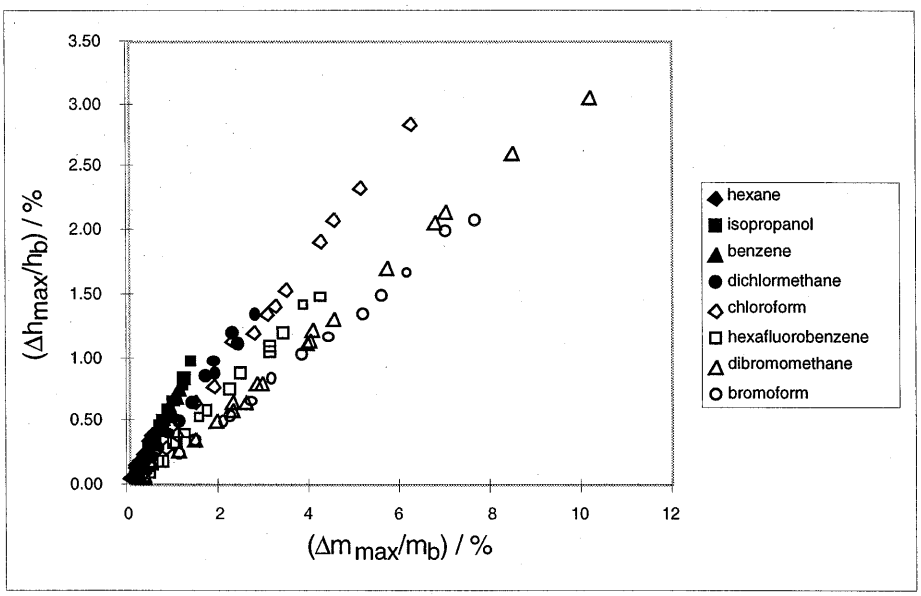
3.50
3.00
2.50
2.00
1.50
1.00
0.50
0.00
0
2
4
6
8
10
12
(Δhmax/hb) / %
(Δmmax/mb) / %
hexane
isopropanol
benzene
dichlormethane
chloroform
hexafluorobenzene
dibromomethane
bromoform

Figure 4.10a

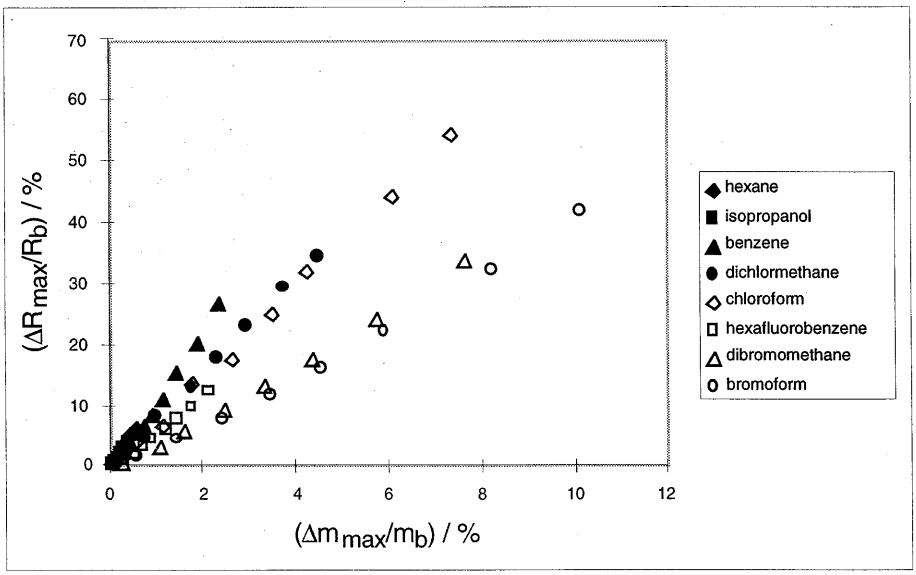
70
60
50
40
30
20
10
0
0
2
4
6
8
10
12
(ΔRmax/Rb) / %
(Δmmax/mb) / %
hexane
isopropanol
benzene
dichlormethane
chloroform
hexafluorobenzene
dibromomethane
bromoform

Figure 4.10b

Figure 4.11: (**A**) Differential relative thickness increase vs. differential relative mass increase for a PEO film when exposed to various analyte fractional vapor pressures. (**B**) Differential relative resistance increase vs. differential relative mass increase for a PEO film when exposed to various analyte fractional vapor pressures.

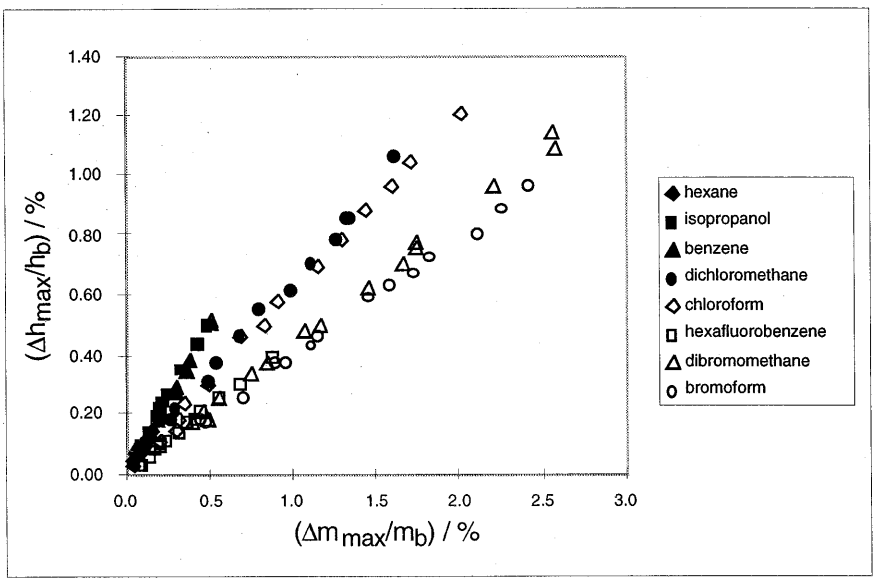
1.40
1.20
1.00
0.80
0.60
0.40
0.20
0.00
0.0
0.5
1.0
1.5
2.0
2.5
3.0
(Δhmax/hb) / %
(Δmmax/mb) / %
hexane
isopropanol
benzene
dichloromethane
chloroform
hexafluorobenzene
dibromomethane
bromoform

Figure 4.11a

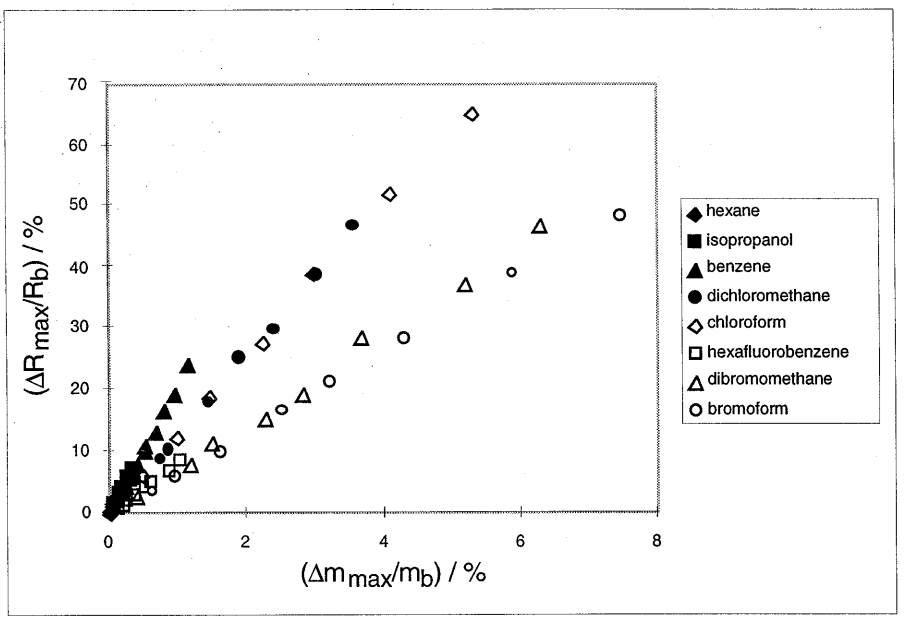
70
60
50
40
30
20
10
0
0
2
4
6
8
(ΔRmax/Rb) / %
(Δmmax/mb) / %
hexane
isopropanol
benzene
dichloromethane
chloroform
hexafluorobenzene
dibromomethane
bromoform

Figure 4.11b

Figure 4.12: Relative resistance increase for a polymer-carbon black composite film verses relative thickness increase for a polymer clear film when both films were exposed to various anlaytes at various frational vapor pressures, correlated by the relative mass increase in each film recorded during those analyte exposures for for (**A**) PCL and for (**B**) PEO films.

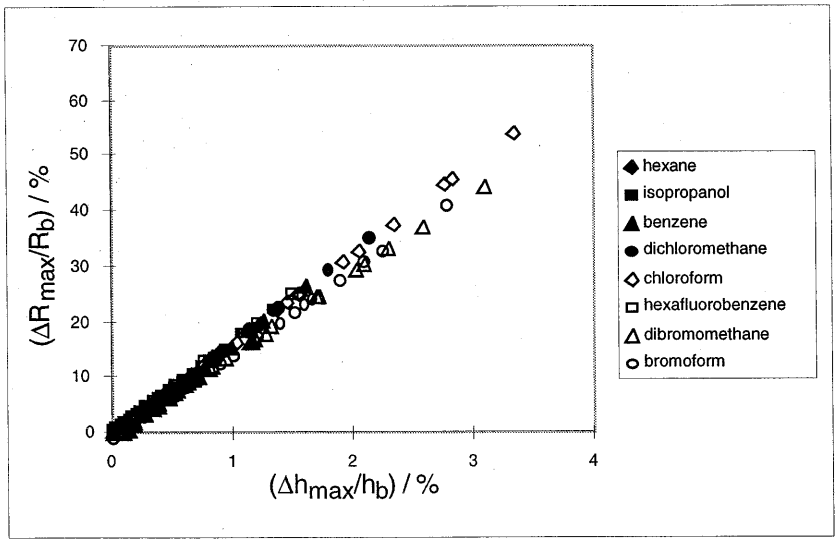
70
60
50
40
30
20
10
0
0
1
2
3
4
(ΔRmax/Rb) / %
(Δhmax/hb) / %
hexane
isopropanol
benzene
dichloromethane
chloroform
hexafluorobenzene
dibromomethane
bromoform

Figure 4.12a

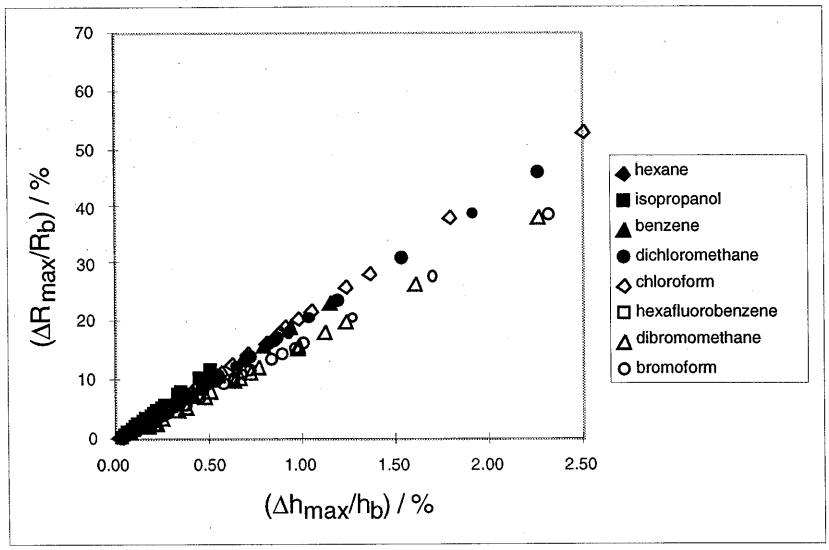
70
60
50
40
30
20
10
0
0.00
0.50
1.00
1.50
2.00
2.50
(ΔRmax/Rb) / %
(Δhmax/hb) / %
hexane
isopropanol
benzene
dichloromethane
chloroform
hexafluorobenzene
dibromomethane
bromoform

Figure 4.12b

Figure 4.13: (**A**) Value of the slope of the line corresponding to $[(\Delta m_{max}/m_b)/(\Delta h_{max}/h_b)]$ for a clear PCL film for various analyte presentations at various analyte fractional vapor pressures vs. the analyte liquid-phase density for the exposed analyte. (**B**) Value of the slope of the line corresponding to $[(\Delta m_{max}/m_b)/(\Delta R_{max}/R_b)]$ for a PCL-carbon black composite film for various analyte presentations at various analyte fractional vapor pressures vs. the analyte liquid-phase density for the exposed analyte.

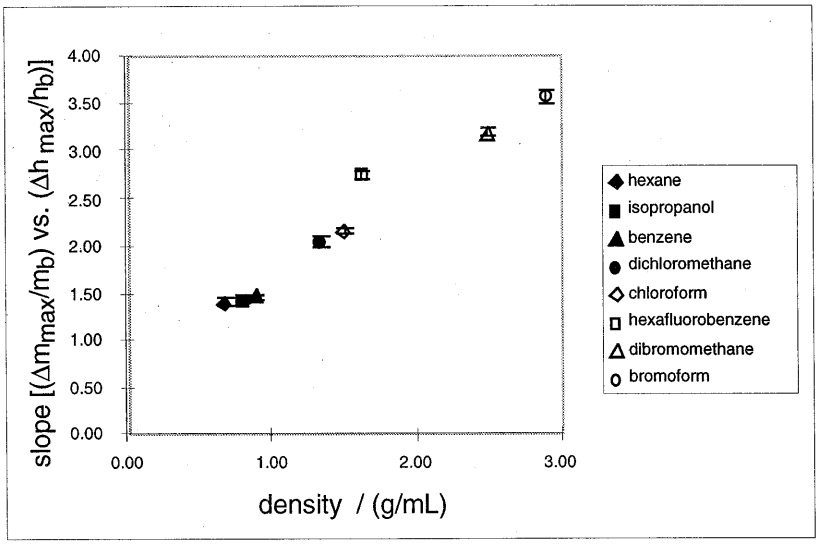
slope [(Δm max/mb) vs. (Δh max/hb)]
4.00
3.50
3.00
2.50
2.00
1.50
1.00
0.50
0.00
0.00
1.00
2.00
3.00
density / (g/mL)
hexane
isopropanol
benzene
dichloromethane
chloroform
hexafluorobenzene
dibromomethane
bromoform

Figure 4.13a

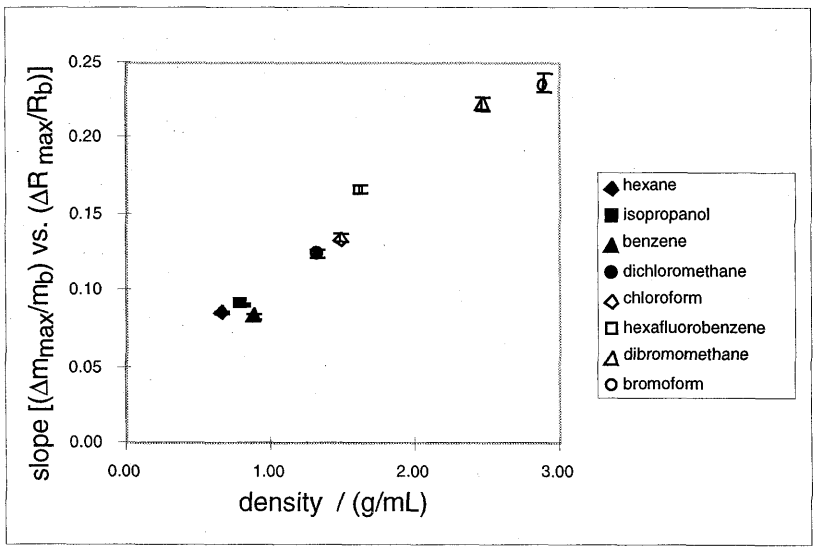
slope [(Δm max/mb) vs. (ΔR max/Rb)]
0.25
0.20
0.15
0.10
0.05
0.00
0.00
1.00
2.00
3.00
density / (g/mL)
hexane
isopropanol
benzene
dichloromethane
chloroform
hexafluorobenzene
dibromomethane
bromoform

Figure 4.13b

Figure 4.14: (**A**) Value of the slope of the line corresponding to $[(\Delta m_{max}/m_b)/(\Delta h_{max}/h_b)]$ for a clear PEO film for various analyte presentations at various analyte fractional vapor pressures vs. the analyte liquid-phase density for the exposed analyte. (**B**) Value of the slope of the line corresponding to $[(\Delta m_{max}/m_b)/(\Delta R_{max}/R_b)]$ for a PEO-carbon black composite film for various analyte presentations at various analyte fractional vapor pressures vs. the analyte liquid-phase density for the exposed analyte.

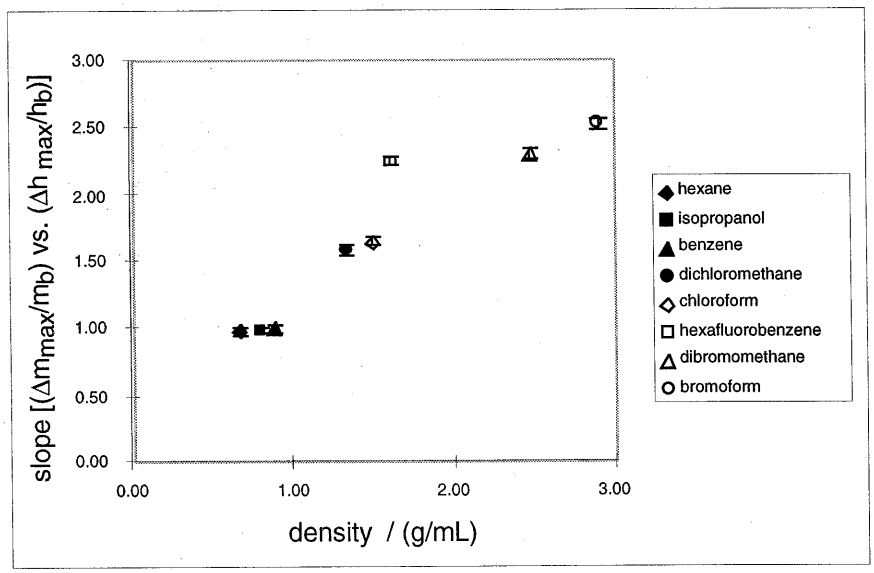
3.00
2.50
2.00
1.50
1.00
0.50
0.00
0.00
1.00
2.00
3.00
slope [(Δm max/mb) vs. (Δh max/hb)]
density / (g/mL)
hexane
isopropanol
benzene
dichloromethane
chloroform
hexafluorobenzene
dibromomethane
bromoform

Figure 4.14a

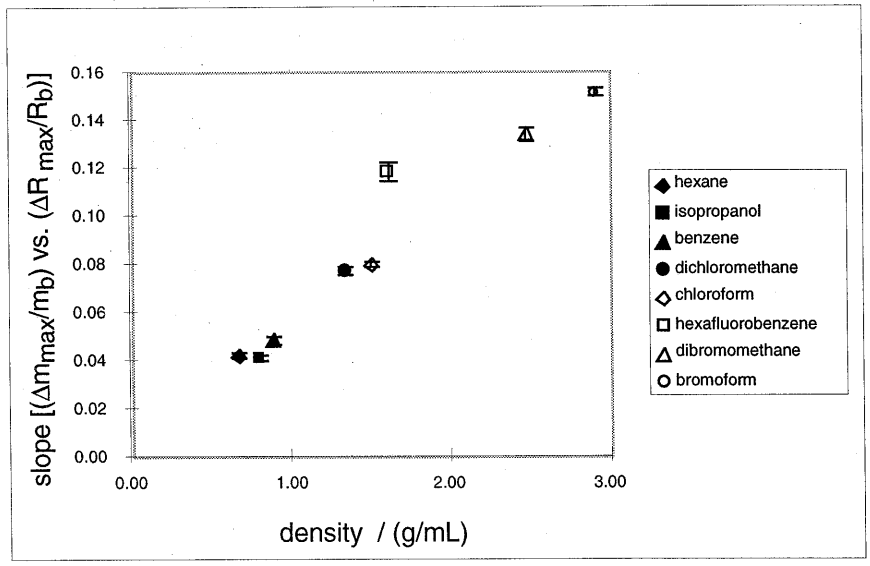
slope [(Δm max/m b) vs. (ΔR max/R b)]
0.16
0.14
0.12
0.10
0.08
0.06
0.04
0.02
0.00
0.00
1.00
2.00
3.00
density / (g/mL)
hexane
isopropanol
benzene
dichloromethane
chloroform
hexafluorobenzene
dibromomethane
bromoform

Figure 4.14b

Table 4.1: Correlation coefficients, slopes, intercepts, intercept error, and slope error for the eight solvents and two polymer systems used in this work. Differential relative mass increase vs. analyte fractional vapor pressure (wt/VP), differential relative resistance increase vs. analyte fractional vapor pressure (R/VP), differential relative thickness increase vs. analyte fractional vapor pressure (A/VP), differential relative resistance increase vs. differential relative mass increase (R/wt), and differential relative thickness increase vs. differential relative mass increase (A/wt) are tabulated.

Table 4.1:

PCL	wt/VP					R/VP					R/wt				
composite film	R	intcpt	slp	intcpt err	slp error	R	intcpt	slp	intcpt err	slp error	R	intcpt	slp	intcpt err	slp error
hexane	0.9997	0.00	1.55	0.003	0.014	0.9989	0.00	17.99	0.066	0.344	0.9991	0.01	11.61	0.059	0.197
isopropanol	0.9934	0.01	1.46	0.012	0.069	0.9933	0.04	15.93	0.130	0.754	0.9999	-0.05	10.88	0.018	0.070
benzene	0.9976	0.16	6.47	0.033	0.183	0.9968	0.40	76.98	0.456	2.520	0.9987	-1.52	11.89	0.330	0.252
dichloromethane	0.9998	-0.03	8.91	0.020	0.068	0.9993	-0.60	71.15	0.317	1.099	0.9987	-0.38	7.98	0.420	0.165
chloroform	0.9998	0.08	19.64	0.033	0.164	0.9988	0.21	145.40	0.604	2.962	0.9984	-0.38	7.40	0.694	0.170
hexafluorobenzene	0.9937	0.23	5.82	0.048	0.268	0.9969	0.78	35.03	0.203	1.124	0.9987	-0.58	5.99	0.158	0.127
dibromomethane	0.9974	-0.02	23.46	0.119	0.690	0.9960	-1.31	105.29	0.668	3.861	0.9991	-1.23	4.49	0.319	0.079
bromoform	0.9989	0.17	32.57	0.104	0.631	0.9982	-1.16	137.74	0.558	3.375	0.9983	-1.88	4.22	0.558	0.101

PCL	wt/VP					A/VP					A/wt				
clear film	R	intcpt	slp	intcpt err	slp error	R	intcpt	slp	intcpt err	slp error	R	intcpt	slp	intcpt err	slp error
hexane	0.9981	0.01	0.78	0.005	0.013	0.9909	0.02	0.55	0.008	0.021	0.9926	0.01	0.70	0.007	0.024
isopropanol	0.9971	-0.01	1.57	0.017	0.034	0.9932	-0.03	1.10	0.019	0.037	0.9987	-0.02	0.70	0.008	0.010
benzene	0.9956	0.08	4.43	0.017	0.116	0.9928	0.05	3.02	0.015	0.101	0.9967	0.00	0.68	0.011	0.015
dichloromethane	0.9992	-0.05	7.54	0.018	0.082	0.9963	-0.03	3.65	0.018	0.084	0.9950	0.00	0.48	0.020	0.013
chloroform	0.9984	0.00	18.31	0.051	0.292	0.9967	-0.03	8.43	0.033	0.189	0.9984	-0.03	0.46	0.023	0.007
hexafluorobenzene	0.9973	0.07	3.92	0.042	0.075	0.9984	-0.02	1.43	0.012	0.021	0.9985	-0.04	0.36	0.011	0.005
dibromomethane	0.9980	0.24	18.82	0.066	0.284	0.9989	-0.01	5.88	0.015	0.064	0.9993	-0.08	0.31	0.012	0.003
bromoform	0.9977	-0.02	28.44	0.080	0.536	0.9977	-0.05	7.94	0.022	0.151	0.9981	-0.04	0.28	0.020	0.005

PEO	R/VP					wt/VP					R/wt				
composite film	R	intcpt	slp	intcpt err	slp error	R	intcpt	slp	intcpt err	slp error	R	intcpt	slp	intcpt err	slp error
hexane	0.9990	-0.02	9.89	0.025	0.117	0.9985	0.00	0.41	0.001	0.006	0.9970	-0.06	23.83	0.044	0.479
isopropanol	0.9992	0.11	22.57	0.048	0.305	0.9972	0.01	0.93	0.004	0.023	0.9979	-0.02	24.13	0.079	0.527
benzene	0.9963	0.13	69.49	0.358	2.006	0.9996	0.01	3.37	0.005	0.031	0.9967	-0.07	20.59	0.342	0.561
dichloromethane	0.9991	0.50	91.89	0.464	1.615	0.9993	0.06	7.08	0.031	0.109	0.9986	-0.20	12.97	0.591	0.284
chloroform	0.9975	1.34	210.58	1.260	6.096	0.9985	0.09	16.82	0.077	0.375	0.9991	0.16	12.52	0.758	0.213
hexafluorobenzene	0.9997	0.25	24.76	0.047	0.259	0.9979	0.05	2.94	0.014	0.079	0.9968	-0.12	8.37	0.157	0.272
dibromomethane	0.9975	0.47	143.09	0.726	4.176	0.9985	0.16	19.26	0.076	0.438	0.9985	-0.73	7.43	0.586	0.168
bromoform	0.9992	0.40	155.11	0.420	2.510	0.9989	0.10	23.53	0.076	0.456	0.9998	-0.24	6.59	0.235	0.058

PEO	A/VP					wt/VP					A/wt				
clear film	R	intcpt	slp	intcpt err	slp error	R	intcpt	slp	intcpt err	slp error	R	intcpt	slp	intcpt err	slp error
hexane	0.9922	0.00	0.26	0.004	0.011	0.9975	0.00	0.26	0.002	0.006	0.9945	0.00	1.01	0.004	0.036
isopropanol	0.9980	0.02	0.92	0.006	0.020	0.9986	0.01	0.90	0.005	0.017	0.9989	0.01	1.01	0.004	0.017
benzene	0.9929	0.03	2.41	0.013	0.102	0.9966	0.02	2.44	0.009	0.071	0.9963	0.01	0.99	0.010	0.030
dichloromethane	0.9892	0.04	3.88	0.028	0.182	0.9916	0.02	6.20	0.040	0.256	0.9970	0.02	0.63	0.015	0.015
chloroform	0.9957	0.02	9.94	0.018	0.267	0.9975	0.02	16.42	0.022	0.336	0.9983	0.01	0.61	0.011	0.010
hexafluorobenzene	0.9981	0.00	0.39	0.003	0.007	0.9986	-0.01	0.88	0.007	0.013	0.9989	0.01	0.44	0.003	0.006
dibromomethane	0.9974	0.03	7.48	0.013	0.150	0.9978	0.06	17.24	0.027	0.316	0.9985	0.00	0.43	0.010	0.006
bromoform	0.9905	0.01	8.61	0.023	0.331	0.9905	0.02	21.85	0.059	0.840	0.9986	0.00	0.39	0.009	0.006

Chapter 5

Temperature Dependence of Differential Resistance Responses Exhibited by Carbon Black-Polymer Composite Chemiresistors

Abstract:

The temperature dependence of the differential resistance response of various conducting polymer composite chemiresistors has been investigated in the presence of eight organic vapors. Increases in the temperature relative to the ambient temperature caused decreases in the differential resistance response of the detectors, as expected from thermodynamic arguments, indicating a general strategy of lowering the temperature of the detectors relative to the temperature of the analyte vapor to achieve increased sensitivity. Additionally, different response patterns for the set of solvents were obtained at different temperatures. In general, combinations of compositionally different detectors maintained at different temperatures will produce more information from a given detector array than measurements at a single temperature, and such arrays can therefore be usefully exploited for the purpose of detection, identification, and quantification, of a particular analyte.

I. Introduction

The signal transduction mechanism of the composite insulator/conductor detectors developed recently in our laboratory exploits the change in electrical properties of the detector materials that are caused by exposure to an analyte of interest.[1] These changes are presumably induced by swelling of the polymer composite by the analyte, producing a change in the resistance of the composite film.[2,3] The signatures of the differential resistance responses produced by an array of compositionally different detectors is then used to identify and quantify the analyte.

Since the vapor must partition into the detector film in order to affect its electrical characteristics, any physical perturbation that can affect the vapor/composite partitioning process, either through modifying its magnitude or its time-dependence, can be exploited to add additional analytical information to the output of the detector array. The partitioning of the vapor into the film has thermodynamic and kinetic components, and both of these are, in general, expected to be dependent on temperature.

Since these detectors are used in an array to produce a pattern that is diagnostic of a particular analyte, one could envision use of an array of compositionally identical detectors at different temperatures as an alternative to, or in combination with, use of a array of compositionally different detectors at a common temperature, in order to generate a differential output response of a detector array for the purpose of identifying, classifying, and quantifying an analyte. The purpose of this study was to demonstrate that temperature can be used to affect the output properties of conducting polymer composite detectors, and to probe differences that can be induced through variation in the temperature of typical conducting polymer composite detector elements.

II. Experimental

Poly(ethylene-co-vinyl acetate) (PEVA), poly(ethylene oxide) (PEO), and poly(4-vinyl phenol) (P4VP) were used to form the detector composites used in this work. Solutions of 150 mg of each polymer in benzene were mixed with 50 mg of carbon black to form suspensions which were used to cast the composite films, which are assumed to be 25% carbon black by

weight. The suspensions were sonicated at least 5 min prior to casting onto 5 x 25 mm glass substrates which had evaporated gold tabs as electrical contacts. To the underside of the glass slide (the side without the polymer film) was affixed nickel-chromium heating wire using low vapor pressure/high temperature epoxy. The wire was bent into a zig-zag shape and affixed so that the main heating area was directly opposite the region between the gold tabs. A plain (not coated with gold or polymer) glass slide of the same dimension as the substrate slide was then attached the underside of the heating wire. In this configuration the heating wire was sandwiched between two glass slides. A thin thermocouple was glued to the second glass slide on the opposite side from the heating wire. In this manner, the temperature detection was made at a similar orientation to the heater as the polymer composite film.

The current for all the resistive heaters was supplied by a common power supply. The resistive heaters were wired in parallel with the power supply. A rheostat was in series with each branch of the parallel circuit to control the amount of current to each heater, and subsequently its temperature, which was measured by the attached thermocouples. The temperatures were not monitored continuously, but were recorded before an experiment began and at selected times during the experiment. Once equilibrium was reached, the temperature of the detector/heater did not deviate more than 0.1°C over the course of minutes and did not deviate more than 1°C over the course of each experiment (about 3 hours).

Multiple copies of each detector/heater were made and placed into a flow chamber. The heated detectors of each type were set to different temperatures; PEVA was maintained at 23°C, 46°C, and 55°C; PEO was maintained at 22°C, 47°C, 57°C; and P4VP was maintained at 23°C, 38°C, 43°C. Five detectors were made using poly(ethylene oxide), of which two were heated. Four detectors were made using poly(ethylene-co-vinyl acetate), of which two were heated. Four detectors were made using poly(4-vinyl phenol), of which two were heated.

In these experiments, exposures were made to eight solvents: benzene, chloroform, toluene, cyclohexane, hexane, 2-propanol, ethanol, and methanol. Six trials were performed by alternating between heating the detectors and leaving them at room temperature (which was 22°C ±

1°C). Three sets of exposures were performed at room temperature and three at elevated temperatures. For each set of detector temperatures, each solvent was exposed at a concentration of 900 ppm, three times, in a random order. The average of these three trials was taken and the standard deviation calculated. Between trials the detectors were allowed enough time to equilibrate to the new temperature as determined by the thermocouple values. The differential resistance responses from the three trials of a particular temperature for each solvent were averaged.

For the data presented in Figure 5.3, ten poly(α-methylstyrene) composite films were made as above and then were directly attached to peltier heaters with spring clips. An additional blank glass substrate was attached to each peltier heater with an attached thermocouple located in the same spatial relationship to the heater as the detector film. This allowed the temperature of the film to be monitored. The detector films were equilibrated to 15.5°C, 16.5°C, 18°C, 25°C, 30°C, 40°C, 50°C, 60°C, 70°C. Ethyl acetate, chloroform, and benzene, at 4% of their equilibrium vapor pressures, were presented to the films four times each, in a random order. A presentation consisted of 30 s of background air to obtain a baseline resistance, followed by 60 s of exposure to an analyte, and finally an additional 60 s of background gas to remove the analyte from the film.

III. Results and Discussion

The differential relative resistance responses, expressed as percent, corresponding to the heated detectors are shown in Figure 5.1. The non-heated sensors were included in the experiment to correct for any variance in the flow system. The non-heated detectors gave the same response, within error, during the trials conducted at room temperature and during the trials in which detectors were heated. Additionally, the differential resistance responses of the non-heated detectors were similar to the differential resistance responses obtained by the detectors fitted with wire heaters when they were equilibrated to room temperature. The main comparison is between the room temperature and heated trials for those detectors fitted with wire heating elements. As can be seen in Figure 5.1, the over-all response of a given detector decreases as temperature increases in accord with the expected decrease in gas/polymer partition coefficient with increasing

temperature. In addition, the error bars became larger at the higher temperatures as the signal became smaller relative to the noise.

It has been reported, through gas chromatography studies, that the temperature dependence of the partition coefficient, K, at low vapor concentrations and over finite temperature ranges, can be described by the Arrhenius-type relationship,[4]

$$K = Ae^{-\Delta H_s/RT} = Ae^{(-\Delta H_c + \Delta H_m)/RT} \qquad (5.1)$$

were the preexponential term A is, to a first approximation, independent of temperature,[5] ΔH_S is the heat of sorption, R is the gas constant, T is the absolute temperature, ΔH_C is the molar heat of condensation, and ΔH_M is the partial molar heat of mixing, which is ideally zero but generally is positive for real solvent-polymer mixtures.[4] ΔH_C is related to the vapor pressure of the solvent via the Clausius-Clapeyron equation,[6] and ΔH_M is related to the difference in cohesive energies between the vapor and the polymer.[5] The absolute value of ΔH_C is usually larger than ΔH_M,[4] consistent with the general observation that the amount an analyte vapor sorbs into a polymer decreases exponentially with increasing temperature.[4] To the extent that ΔH_S values differ among vapors partitioning into polymer coatings, the pattern of relative differential responses obtained from an array of sensors will vary with temperature. This is seen to be the case in this system in Figures 5.2 & 5.3.

Because of the differences in over-all height of the absolute responses between the room temperature data and the heated data, the differences in response patterns are difficult to visualize from the plots shown in Figure 5.1. Therefore, the patterns were normalized by adding all the responses by a detector to the eight solvents at a given temperature and dividing this sum by each response at that temperature. This normalization process highlights the differences in the pattern of responses at different temperatures rather than the over-all height differences. Figure 5.2 shows the normalized patterns for the heated detectors.

In general, the fingerprints for the various vapors were similar at the different temperatures because the temperature differentials between heated and non-heated detectors were only about 20°C; however, slight differences begin to emerge at larger temperature differentials (See Figure

5.2). For example, for the PEVA detector film, benzene gives a larger differential resistance response than cyclohexane in the 23°C film, but for the films held at 46°C and 55°C this is reversed. In the case of the PEO detector film, the magnitude of the response to benzene vapor for a 22°C detector relative to chloroform increases for a 57°C detector. Additionally, the relative magnitude of the cyclohexane response increases with temperature for the PEO film. Since the detector response is expected to have an exponential dependence on temperature, higher temperature differentials were probed for a poly(α-methylstyrene) film exposed to ethyl acetate, chloroform, and benzene at 4% of their vapor pressure. Arrhenius plots show a fit with average correlation coefficients of 0.99 (Figure 5.3). All solvents show a positive slope corresponding to a negative heat of sorption. Additionally, the magnitude of response by a detector of this composition maintained at 40°C ($1/T \approx 0.0032$) and exposed to benzene and ethyl acetate are the same, but are different from chloroform. In contrast, the magnitude of response by a detector of this composition maintained at 25°C ($1/T \approx 0.00335$) exposed to chloroform and benzene are the same, but are different from ethyl acetate. Therefore, this detector composition maintained at two temperatures is able to distinguish three analytes. In these non-isothermal conditions where the detector is a different temperature than the ambient gas, ΔH_C makes the biggest contribution to ΔH_S in equation 5.1. Since ΔH_C is negative,[6] the negative correlation to temperature by the response is expected. This supports the proposed dependence of the resistance response on temperature.

Temperature variation between detector films can be used to an advantage in other applications of these detector arrays, since lowering the temperature of an array element will, in general, increase the signal and therefore increase the sensitivity of the detector to the desired analyte. Thus, an array of compositional identical detectors, each held at a different temperature during a measurement period, could be used to produce signals above a threshold value at different concentrations of the vapor, thereby aiding in quantifying various ranges of the vapor concentration while still maintaining a linear concentration vs. vapor concentration response (in the small swelling regime) for an individual detector. In addition, the differential response of

compositional identical detectors at various temperatures can be used to provide classification and identification information as the basis for the output signature of the detector array.

IV. Conclusion

In general, combinations of compositional different detectors maintained at different temperatures will produce more information from a given detector array than measurements at a single temperature, and such arrays can therefore be usefully exploited for the purpose of detection, identification, and quantification, of a particular analyte.

V. References

1)Lonergan, M. C.; Severin, E. J.; Doleman, B. J.; Beaber, S. A.; Grubbs, R. H.; Lewis, N. S. *Chemistry of Materials* **1996**, *8*, 2298.

2)Anderson, J. E.; Adams, K. M.; Troyk, P. R. *Journal of Non-Crystalline Solids* **1991**, *131*, 587-592.

3)Godovski, D. Y.; Koltypin, E. A.; Volkov, A. V.; Moskvina, M. A. *Analyst* **1993**, *118*, 997-999.

4)Zellers, E. T.; Han, M. W. *Analytical Chemistry* **1996**, *68*, 2409-2418.

5)Hiemenz, P. C. *Polymer Chemistry; The Basic Concepts*; Marcel Dekker, Inc.: New York, NY, 1984.

6)Atkins, P. W. *Physical Chemistry*; W.H. Freeman and Co.: New York, NY, 1994.

Figure 5.1: Relative differential resistance responses for the detectors used in this work at the indicated temperatures. **A**) PEVA **B**) PEO **C**) P4VP

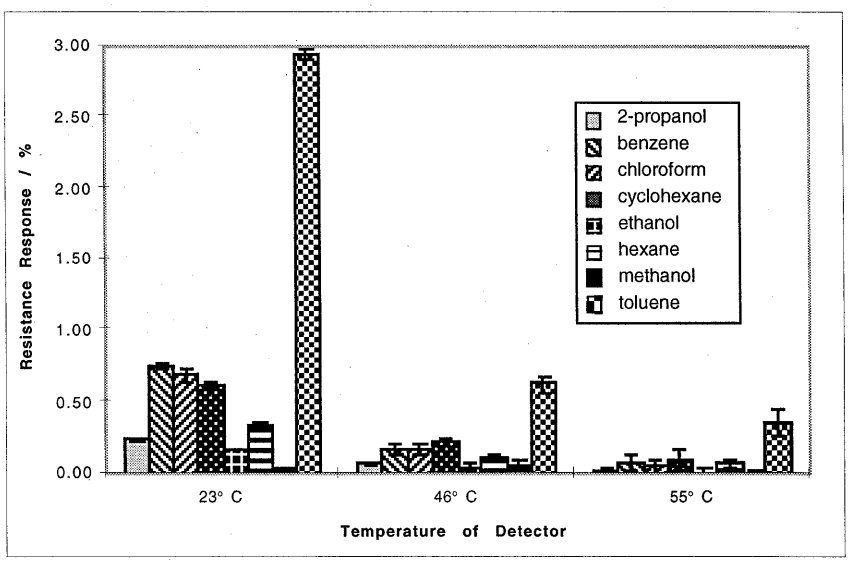
3.00
2.50
2.00
1.50
1.00
0.50
0.00
Resistance Response / %
2-propanol
benzene
chloroform
cyclohexane
ethanol
hexane
methanol
toluene
23° C
46° C
55° C
Temperature of Detector

Figure 5.1a

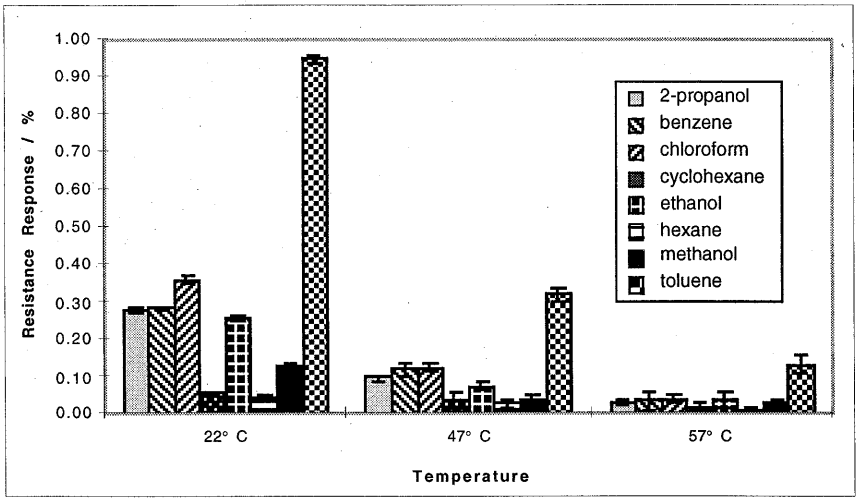
1.00
0.90
0.80
0.70
0.60
0.50
0.40
0.30
0.20
0.10
0.00
Resistance Response / %
22° C
47° C
57° C
Temperature
2-propanol
benzene
chloroform
cyclohexane
ethanol
hexane
methanol
toluene

Figure 5.1b

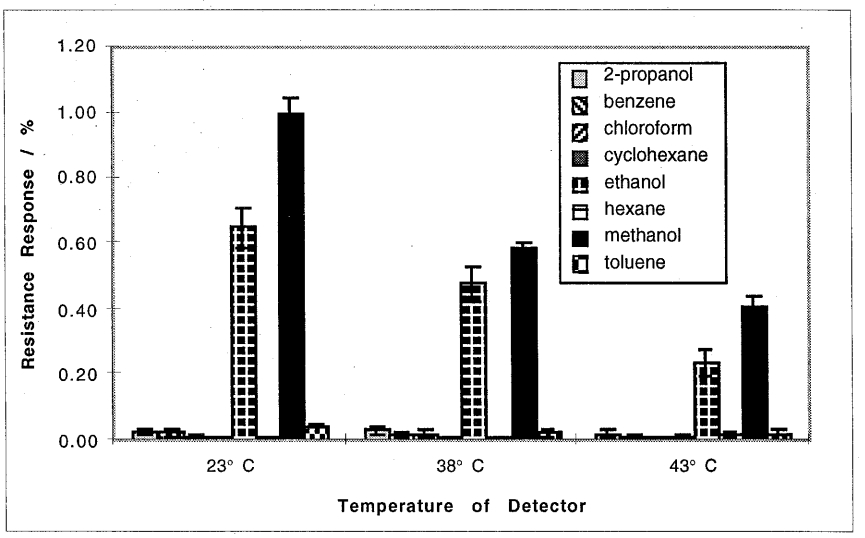
1.20
1.00
0.80
0.60
0.40
0.20
0.00
Resistance Response / %
2-propanol
benzene
chloroform
cyclohexane
ethanol
hexane
methanol
toluene
23° C
38° C
43° C
Temperature of Detector

Figure 5.1c

Figure 5.2: Normalized relative differential resistance responses for the detectors used in this work at the indicated temperatures. **A**) PEVA **B**) PEO **C**) P4VP **D**) P4VP scaled to highlight the variance in the data.

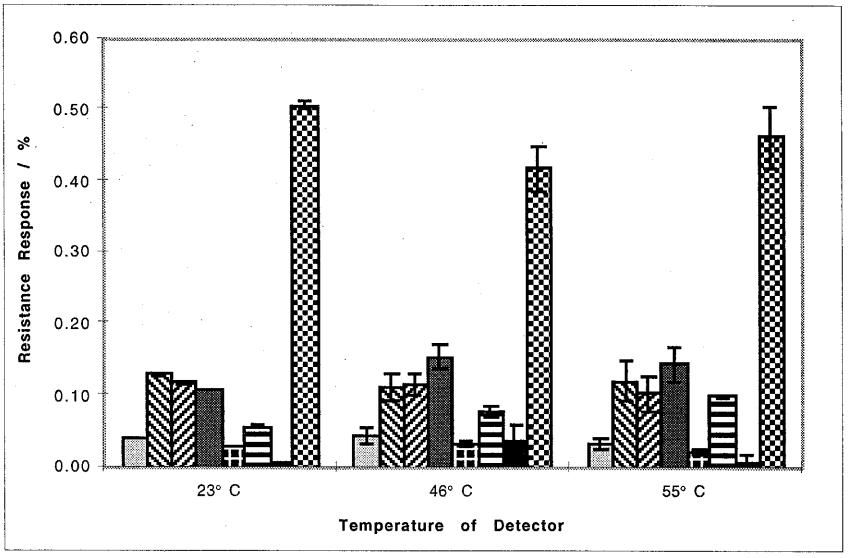
0.60
0.50
0.40
0.30
0.20
0.10
0.00
Resistance Response / %
23° C
46° C
55° C
Temperature of Detector

Figure 5.2a

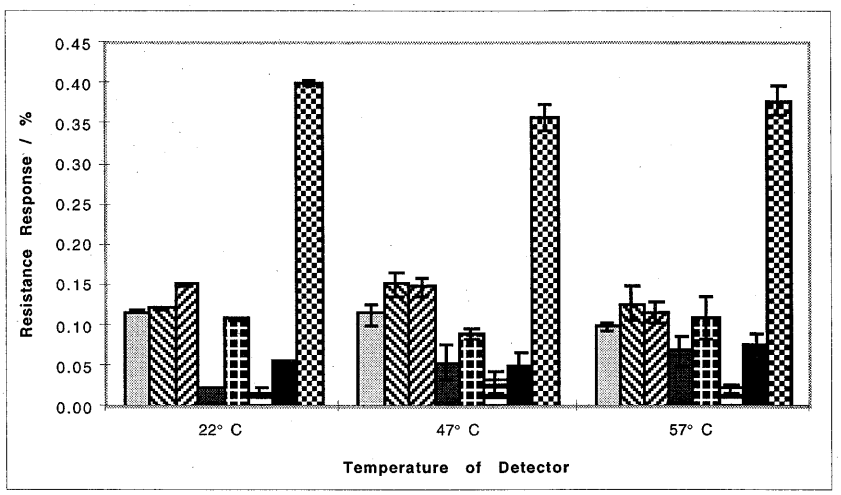
0.45
0.40
0.35
0.30
0.25
0.20
0.15
0.10
0.05
0.00
Resistance Response / %
22° C
47° C
57° C
Temperature of Detector

Figure 5.2b

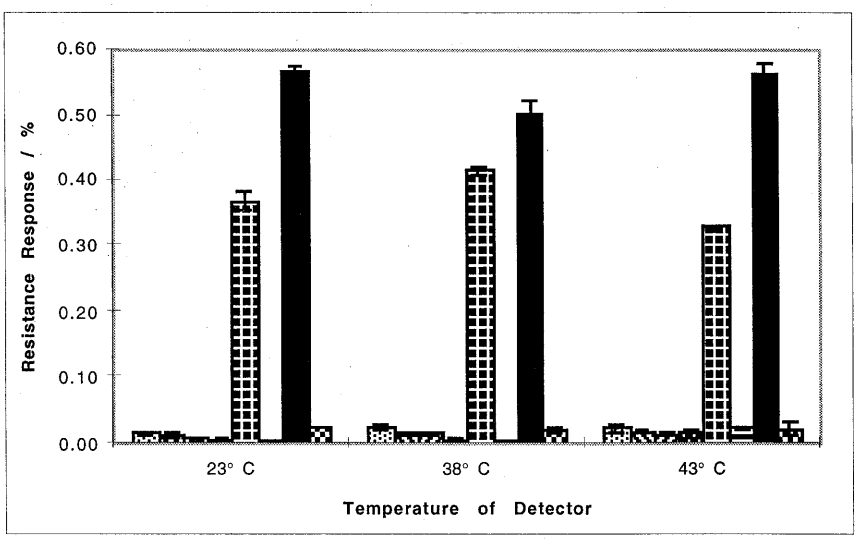
0.60
0.50
0.40
0.30
0.20
0.10
0.00
Resistance Response / %
23° C
38° C
43° C
Temperature of Detector

Figure 5.2c

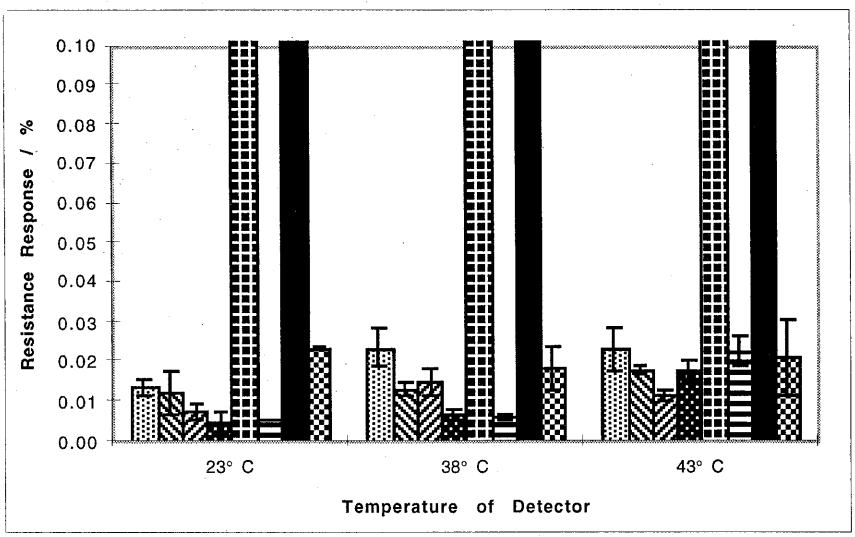
0.10
0.09
0.08
0.07
0.06
0.05
0.04
0.03
0.02
0.01
0.00
Resistance Response / %
23° C
38° C
43° C
Temperature of Detector

Figure 5.2d

Figure 5.3: The natural log of the relative resistance response of poly(α-methylstyrene) verses the inverse of temperature for three solvents at ten different temperatures. Each data point is the average of four exposures of each solvent. The lines represent a best fit through the data. The data for ethyl acetate has a slope of 2847 and an R^2 value of 0.997; the data for chloroform has a slope of 2758 and an R^2 value of 0.999; the data for benzene has a slope of 2237 and an R^2 value of 0.999. This data is courtesy of Dr. Greg Sotzing.

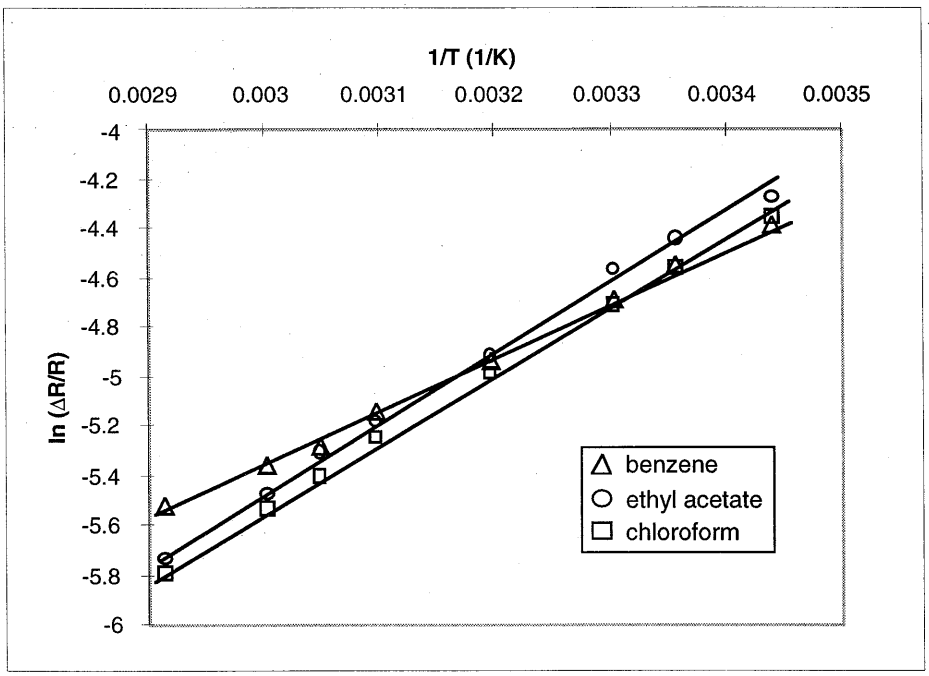
1/T (1/K)
0.0029
0.003
0.0031
0.0032
0.0033
0.0034
0.0035
-4
-4.2
-4.4
-4.6
-4.8
-5
-5.2
-5.4
-5.6
-5.8
-6
ln (ΔR/R)
benzene
ethyl acetate
chloroform

Figure 5.3

Chapter 6

Enantiomeric Resolution of Gaseous Analytes Using Carbon Black-Chiral Polymer Composite, Chemically Sensitive Resistors

Abstract:

Carbon black-chiral polymer composites were used to provide diagnostic differential resistance responses in the presence of enantiomers of chiral gaseous analytes. Vapors of (+)-2-butanol and (-)-2-butanol, (+)-α-pinene and (-)-α-pinene, (+)-epichlorohydrin and (-)-epichlorohydrin, and methyl-(+)-2-chloropropionate and methyl-(-)-2-chloropropionate were generated and passed over a chemically sensitive carbon black-poly(R-3-hydroxybutyrate-*co*-R-3-hydroxyvalerate) (77% butyrate) composite resistor. Each enantiomer of a pair produced a unique relative differential resistance change on the chiral detector, whereas both enantiomers of a set produced identical signals for achiral carbon black-poly(ethylene-*co*-vinyl acetate) (82% ethylene) detectors.

I. Introduction

We have previously reported the use of carbon black-polymer composites for array-based vapor sensing applications.[1] In such an array, no individual detector responds solely to a specific molecule, but the collective response of the entire array of detectors yields a unique fingerprint for the vapor of interest. Such arrays are often referred to as "electronic noses" and are not designed in advance to perform a specific task, but are instead developed to classify, identify, and quantify vapors based on pattern recognition algorithms.[2-7] This approach to vapor sensing takes advantage of the collective output of an array of broadly responsive detectors. In the polymer composite array configuration, the signal transduction is extremely simple: swelling of the polymeric phase of the composite, in the presence of a vapor, leads to an increase in the electrical resistance of the composite, which is monitored using simple electronics.

An ideal detector array would produce a unique signature for every molecule to which it was exposed. In order to make progress toward such a system, it is necessary to include detectors that probe important, but possibly subtle, molecular parameters such as chirality. None of the polymer based conducting composite detectors reported to date are chiral, so enantiomers would not be differentiable on arrays of such achiral detectors. We demonstrate herein the use of chiral polymers in carbon black-polymer composites to achieve such enantiomeric identification. The materials described herein represent additional detector elements that would be part of a larger detector array, thus broadening the discrimination ability of such arrays towards chiral analytes.[1]

II. Experimental

The carbon black used in the composites was Black Pearls 2000, a furnace black material donated by Cabot Co. (Billerica, MA). The polymer used in the chiral composites was poly(R-3-hydroxybutyrate-*co*-R-3-hydroxyvalerate) (77% butyrate), and was obtained from the Goodfellow Corp. (Berwyn, PA). (See Figure 6.2) The achiral polymer used for control experiments was poly(ethylene-*co*-vinyl acetate) (82% ethylene) (Polysciences Inc.; Warrington, PA). The enantiomeric pairs examined were: (+)-2-butanol and (-)-2-butanol (Aldrich; Milwaukee, WI), (+)-α-pinene and (-)-α-pinene (Fluka; Ronkonkoma, NY), (+)-epichlorohydrin and (-)-

epichlorohydrin (Aldrich), and methyl-(+)-2-chloropropionate and methyl-(-)-2-chloropropionate (Aldrich). (See Figure 6.2)

An apparatus that provided known partial pressures of the vapors was constructed of general laboratory glassware. This consisted of a bubbler made from small 12 mL centrifuge tubes with conical bottoms that were filled to a depth of 3 cm (ca. 2 mL). Into the 1.5 cm diameter mouth of the tube was affixed a two-hole rubber stopper. In each hole was a 5 mm outer diameter glass tube, one of which extended to the bottom of the bubbler and served as the gas inlet, the other of which extended past the stopper by only a few mm and served as the gas exit. The carrier gas was nitrogen obtained from a commercial gas supply tank. The measurements were performed at room temperature, which was 23 ± 1 °C.

The carrier gas was introduced through the glass tube which extended to the bottom of the bubbler apparatus, and was bubbled through the solvent, thus saturating it with the solvent vapor. The saturated vapor was carried out of the bubbler, diluted by blending with a controlled background flow of pure carrier gas, and then introduced into a sensing chamber. This chamber consisted of a glass tube (22 cm long with a 2.6 cm inner diameter) to which inlet and outlet sidearms had been attached. The detectors were introduced into the chamber through a 24/40 standard taper ground glass opening attached at one end of the chamber. The chamber was then sealed with a ground-glass stopper through which electrical lead wires for the detectors had been sealed. The gas flow rates were controlled using needle valves and stopcocks.

To prepare the detector substrates, two parallel bands of gold, 50-100 nm thick and separated by 5 mm, were deposited onto conventional 7.5 cm x 2.5 cm glass slides. The slides were then cut into strips to produce 0.7 cm x 2.5 cm pieces of glass, with each strip of glass having one pair of Au leads spaced 5 mm apart.

The detectors were made from a solution of the polymer into which carbon black had been suspended. 125 mg of the polymer was dissolved in 10 mL of tetrahydrofuran, and carbon black (42 mg) was then suspended in this solution, to produce a composition of 75% polymer and 25% carbon black by weight of solids. A single solution that contained the polymer and the carbon

black was used to prepare all the detectors of a given composition that were used in this work. Detectors used to analyze pinene vapors were fabricated slightly differently, having films made from a suspension with a carbon black loading of 30% by weight of solids. In both cases, an aliquot of the suspension was spin coated, at 1000 rpm, onto a glass substrate using a Headway (Garland, TX) spin coater, and the resulting film was allowed to dry in air. One coating of the suspension was applied to each substrate, yielding a film thickness of ≈1 micron as determined by atomic force microscopy, except for pinene detectors, for which six coats of suspension were applied, producing films ≈6 micron in thickness. The detectors with extra coatings gave higher signal-to-noise when used for pinene.

The dc resistance of each detector was determined as a function of time using a simple two-point resistance configuration. Contacts were made to the gold lines by pressure-contacting electrical leads using flat-jawed alligator clips. Resistance data were acquired using a Hydra 2620A Data Acquisition Unit (John Fluke Mfg. Co.; Everett, WA) which was interfaced to a personal computer. All of the films had resistance values below the 10 MΩ limit of the Hydra 2620A.

To initiate an experiment, five copies of a given detector type were placed into the glass chamber and a background flow of nitrogen was introduced until the resistance of the detectors stabilized. Solvent vapor streams were then passed over the detectors. The background and analyte flow rates were monitored using two flow meters (Gilmont Instruments, Inc.) which had limits of 0.2 L min^{-1} to 15.0 L min^{-1} and 0.0015 L min^{-1} to 0.310 L min^{-1} respectively. In a typical experiment, resistance data on the detectors were collected for 150 s with just the background gas flowing (typically about 1 - 2 L min^{-1}) to serve as a baseline. This was followed by a 150 s data collection while the detectors were exposed to the analyte vapor stream (typically about 200 - 300 mL min^{-1}). The detectors were then given 200 - 300 s to recover during which pure background gas was passed through the chamber. The exposure times varied somewhat, but steady-state values of resistance change were always reached for any given exposure time. Resistances for all detectors in a given trial were monitored contemporaneously through the use of

the multiplexing capabilities of the Hydra voltmeter. Results were obtained by running two trials (except for epichlorohydrin for which three trials were run) of five exposures each, with the trials performed on different days. Each analyte was exposed to five copies of the detector simultaneously and the results were averaged to obtain the reported data set. In the case of epichlorohydrin, a third trial was run using 300 s exposure and recovery times to investigate whether longer time cycles produced different response signals, but the data were essentially identical to those obtained using the shorter detector cycle times described above. The exposures were made at the following concentrations: epichlorohydrin, 3 parts per thousand (ppth); α-pinene, 1 ppth; methyl-2-chloropropionate, 2 ppth; and 2-butanol, 4 ppth. Concentrations were calculated by diluting saturated gas streams to known volumes, and the analyte concentrations were determined from measurements of the flow rate of the gas and the rate of mass loss of the solvent.[1]

The achiral control detectors were made from benzene solutions of poly(ethylene-*co*-vinyl acetate) (82% ethylene) into which carbon black had been suspended. The same type of carbon black was used as for the chiral detector fabrication. Glass slides, containing gold contacts, were coated by dipping the slide into the suspension. Three coatings were applied to each slide. The polymer concentration was 10 mg mL^{-1} and the carbon black loading was 30% by weight of solids. Results were obtained by running one trial of four (for epichlorohydrin and methyl-2-chloropropionate) or five (for 2-butanol and α-pinene) exposures. Each analyte was exposed to five detectors simultaneously and the results were averaged to obtain the reported data set. The control exposures were made at the following concentrations: epichlorohydrin, 4 ppth; α-pinene, 1 ppth; methyl-2-chloropropionate, 3 ppth; and 2-butanol, 4 ppth.

III. Results and Discussion

Figure 6.1 represents a typical response of a chiral detector to 2-butanol. All the detectors displayed an increase in resistance upon exposure to the vapor, and returned to their baseline values after the vapor was removed. In all of the experiments performed, the change in resistance was quite rapid, taking less than 20 s to reach 75% of the final resistance value (taken after 150 s). The responses were analyzed by calculating the maximum differential response value, ΔR_{max},

observed during the exposure period and dividing it by the baseline value of the resistance, R_b, (taken as the resistance value just before the exposure began) and expressed as a percent change in resistance, Q:

$$Q = (\Delta R_{max}/R_b)*100 \qquad (4.1)$$

$Q_{(+)}$ and $Q_{(-)}$ correspond to the percent relative differential resistance response for the (+) and (-) enantiomers respectively. A representative data set, for the enantiomers of 2-butanol, is presented in Table 6.1, while Table 6.2 summarizes the data for all of the enantiomers studied in this work.

As reported in Tables 1 and 2, statistically significant differences in detector response were observed when enantiomers of a given analyte were exposed to the chiral carbon black-polymer composite detectors. In contrast, no statistically significant difference in response was observed when achiral detectors were exposed to these same enantiomers. The magnitude of the differentiation between enantiomers can be quantified by considering the relative difference in response, Q_{rel}, between the enantiomers:

$$Q_{rel} = [\Delta Q_{(+/-)}/Q_{(-)}] \qquad (4.2)$$

where $\Delta Q_{(+/-)}$ is the difference in percent response of a detector when exposed to the (+) and (-) enantiomers of an analyte, respectively. As defined, $\Delta Q_{(+/-)}$ was always positive because in our samples $Q_{(+)}$ was always greater than $Q_{(-)}$.

In gas chromatography, the partition coefficient, K, is defined as $K = C_s/C_v$, where C_s is the concentration of solute in the sorbent phase and C_v is the concentration in the vapor phase, at equilibrium. In our experimental protocol, C_v is constant since the vapor stream is continuously being replenished by the vapor generation apparatus. Therefore, we can define a ratio, α, of the partition coefficients between the two enantiomers, as follows:

$$\alpha = K_1/K_2 = [C_s/C_v]_1/[C_s/C_v]_2 = [C_s]_1/[C_s]_2 \qquad (4.3)$$

To remain consistent with the gas chromatography literature, K_1 is defined as the larger partition coefficient, ensuring that α is greater than one.[8] This corresponds to the analyte which gave the largest response, which, in this work, was always the (+) enantiomer.

The differences in steady-state response for each of the enantiomeric pairs can be attributed to the differences in the free energy, ΔG, of sorption for each enantiomer into the chiral carbon black-polymer composite (i.e., $(\Delta G_1 - \Delta G_2)$, or $\Delta_{1,2}(\Delta G)$). The difference in ΔG of sorption is related to the ratio of the partition coefficients as expressed below:[8]

$$\Delta_{1,2}(\Delta G) = -RT \ln(\alpha) \qquad (4.4)$$

We have shown that the composite chemiresistor detectors respond linearly to gaseous analyte concentrations over at least a factor of 10^2 in concentration, therefore C_s is proportional to Q.[1,9] And, since the vapor concentrations of each enantiomer of an analyte were identical, with only the amount sorbing into the polymer matrix being different, we can relate α to $Q_{(+)}$ and $Q_{(-)}$ as follows:

$$\alpha = [C_s]_1/[C_s]_2 = Q_{(+)}/Q_{(-)} \qquad (4.5)$$

The values of $\Delta_{1,2}(\Delta G)$ calculated using the percent response data and the relationships of eq 6.2 - 6.5 are given in Table 6.2. These values are similar to the minimum values (ca. -0.1 kJ mol^{-1}) observed for enantiomers in chiral gas chromatography.[8]

In summary, we have shown that the resistance response of carbon black-polymer composite detectors can be extended to differentiate between enantiomers in the vapor phase. This behavior increases the number of molecular characteristics of a vapor-based analyte that can be probed by a carbon black-polymer composite sensor. The enhancement in classification ability arising from the use of these chiral detectors in an array configuration will be highly task-dependent, and quantification of the separation ability of enantiomers in specific application scenarios will be reported separately.

IV. References

(1) Lonergan, M. C.; Severin, E. J.; Doleman, B. J.; Beaber, S. A.; Grubbs, R. H.; Lewis, N. S. *Chem. Mater.* **1996**, *8*, 2298.

(2) Zaromb, S.; Stetter, J. R. *Sens. Actuators* **1984**, *6*, 225.

(3) Lundstrom, I.; Erlandsson, R.; Frykman, U.; Hedborg, E.; Spetz, A.; Sundgren, H.; Welin, S.; Winquist, F. *Nature* **1991**, *352*, 47.

(4) Shurmer, H. V.; Gardner, J. W. *Sens. Actuators B* **1992**, *8*, 1.

(5) Gardner, J. W.; Bartlett, P. N. *Sens. Actuators B* **1994**, *18*, 211.

(6) Gardner, J. W.; Hines, E. L.; Tang, H. C. *Sens. Actuators B* **1992**, *9*, 9.

(7) Nakamoto, T.; Fukuda, A.; Moriizumi, T. *Sens. Actuators B* **1993**, *10*, 85.

(8) Schurig, V. *J. Chromatogr. A* **1994**, *666*, 111.

(9) Severin, E. J.; Doleman, B. J.; Lewis, N. S. to be submitted

Table 6.1: Representative Data[b] for the (+) and (-) Enantiomers of 2-Butanol.

Table 6.1

Trial 1 Detector #	Q(-)a	Q(+)a	ΔQ(+/-)	Qrel	α	Δ1,2(ΔG) kJ/mol
1	3.41(0.01)	3.60(0.03)	0.19	5.5%	1.06	-0.133
2	3.29(0.02)	3.52(0.03)	0.23	7.0%	1.07	-0.167
3	2.89(0.02)	3.10(0.02)	0.21	7.3%	1.07	-0.174
4	2.96(0.02)	3.17(0.03)	0.21	7.0%	1.07	-0.166
5	2.75(0.03)	2.97(0.04)	0.22	8.0%	1.08	-0.189
	Average across five sensors =		0.21(0.02)	7.0(0.9)%	1.07(0.01)	-0.17(0.02)

Trial 2 Detector #	Q(-)a	Q(+)a	ΔQ(+/-)	Qrel	α	Δ1,2(ΔG) kJ/mol
1	2.71(0.04)	2.97(0.04)	0.26	9.5%	1.10	-0.224
2	2.59(0.02)	2.87(0.04)	0.28	11%	1.11	-0.253
3	2.55(0.03)	2.79(0.04)	0.24	9.5%	1.10	-0.224
4	2.62(0.03)	2.86(0.04)	0.24	9.2%	1.09	-0.216
5	2.49(0.03)	2.73(0.04)	0.24	9.6%	1.10	-0.225
	Average across five sensors =		0.25(0.02)	9.7(0.6)%	1.10(0.01)	-0.23(0.01)

Control Detector #	Q(-)a	Q(+)a	ΔQ(+/-)
1	2.71(0.02)	2.73(0.06)	0.02
2	2.50(0.01)	2.50(0.01)	0.00
3	2.58(0.03)	2.56(0.02)	-0.02
4	3.02(0.03)	3.04(0.01)	0.02
	Average across five sensors =		0.00(0.02)

[a] $Q_{(+)}$ and $Q_{(-)}$ correspond to the percent relative differential resistance change averaged over five exposures for the (+) and (-) enantiomers, respectively. α is defined as K_1/K_2, where K_1 is defined as the larger partition coefficient.

[b] The numbers in parentheses are estimated standard deviations.

Table 6.2: Differences in Percent Response[a], $\Delta Q_{(+/-)}$, Observed for Chiral Detectors During Exposure to the (+) and (-) Enantiomers of Four Test Vapors.

Table 6.2

Analyte	Trial	ΔQ(+/-)	Qrel	Avg α	Avg Δ1,2(ΔG) kJ/mol
2-Butanol	Trial 1	0.21(0.02)	7.0(0.9)%	1.07(0.01)	-0.17(0.02)
	Trial 2	0.25(0.02)	9.8(0.6)%	1.10(0.01)	-0.23(0.01)
	control	0.02(0.01)			
α-Pinene	Trial 1	0.15(0.01)	7.6(1.5)%	1.08(0.01)	-0.18(0.03)
	Trial 2	0.15(0.04)	8.0(1.1)%	1.08(0.01)	-0.19(0.02)
	control	0.02(0.01)			
Epichlorohydrin	Trial 1	0.22(0.01)	6.9(0.6)%	1.07(0.01)	-0.16(0.02)
	Trial 2	0.19(0.03)	5.6(0.6)%	1.06(0.01)	-0.13(0.01)
	Trial 3	0.24(0.03)	7.1(1.2)%	1.07(0.01)	-0.17(0.03)
	control	0.03(0.03)			
Methyl-2-	Trial 1	0.26(0.03)	9.1(1.2)%	1.09(0.01)	-0.21(0.03)
chloropropionate	Trial 2	0.26(0.01)	8.9(0.6)%	1.09(0.01)	-0.21(0.01)
	control	0.02(0.01)			

[a] The values tabulated are the percent response values that were averaged over five nominally identical detectors, each of which had been exposed four (for epichlorohydrin and methyl-2-chloropropionate) or five (for 2-butanol and α-pinene) times to the analyte vapor. The other quantities were calculated using the formulas and definitions given in the text.

Table 6.2

Figure 6.1: A typical chiral detector response upon exposure to 5 ppth of (+)-2-butanol.

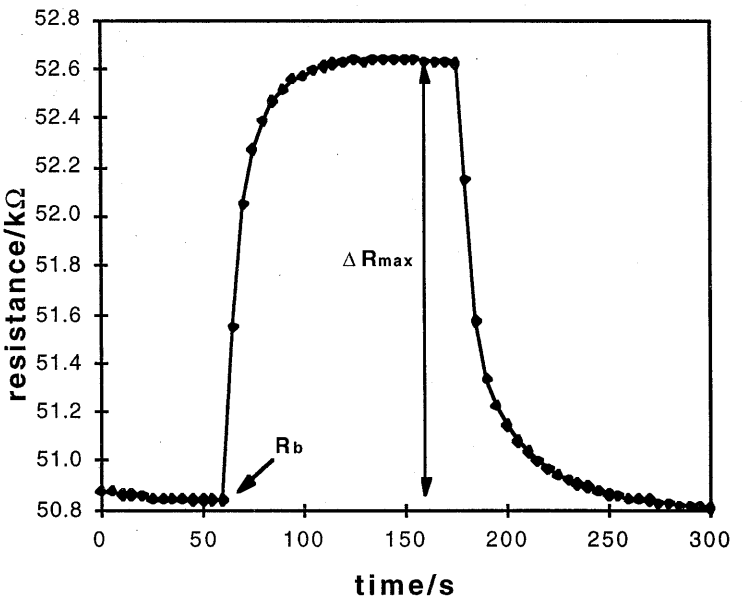
52.8
52.6
52.4
52.2
52.0
51.8
51.6
51.4
51.2
51.0
50.8
resistance/kΩ
ΔRmax
Rb
0
50
100
150
200
250
300
time/s

Figure 6.1

Figure 6.2: Structures of the chiral polymer and analytes used in this work (only (+) analytes shown).

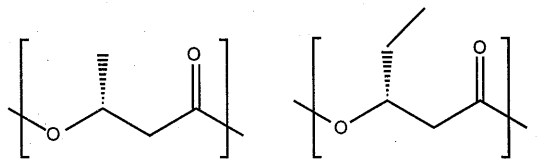

poly((R)-3-hydroxybutyrate-*co*-(R)-3-hydroxyvalerate)
77% butyrate

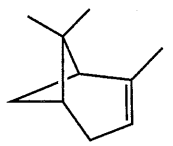

(R)-(+)- α-pinene

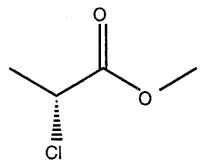

methyl (R)-(+)-2-chloropropionate

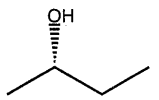

(S)-(+)-2-butanol

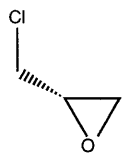

(S)-(+)-epichlorohydrin

Figure 6.2

Chapter 7

Miscellaneous Applications of the Sensor System

Note: These items are included for completion, in order to illustrate the breadth of applications to which this system can be applied.

Chapter 7, Part A

Carbon Black-Polymer Composite Detector Response To Solid-Generated Vapors

Abstract:

The head space vapors from six solids (naphthalene, vanillin, indole, 2,4-dinitrotoluene, 4-nitrotoluene, and military grade TNT) were individually exposed to a nine unit carbon black-polymer composite detector array. The differential relative resistance change by each of the nine detector films upon exposure to the test analyte vapors were sufficiently unique to allow complete classification of those analytes.

I. Introduction

The detection of ultra-trace analytes is a continuing challenge in the field of chemical sensors. Many vapor detection tasks involve detecting a vapor signature generated from a solid sample. These tasks can involve high vapor pressure solids like naphthalene-like or indole-like compounds or can involve ultra-low vapor pressure solids such as 2,4,6-trinitrotoluene (TNT). Particularly useful would be the development of sensors for the detection of TNT and 2,4-dinitrotoluene (DNT) which are the principal constituents of the nearly 120 million unexploded land mines worldwide.[1] The huge difficulty of locating land mines in diverse environments around the world is complicated by inefficient detection using metal detectors because of the large number of false alarms caused by the metal detritus of war. Dogs can detect and identify the odor signature of land mines and are the best mine detectors in the arsenal of methods used to locate inplaced mines. However, they are expensive to train and maintain, and they need rest approximately every 15 min. Additionally, a skilled (and expensive) human trainer is needed for every 1-3 dogs. Direct methods of TNT/DNT detection have been developed for the goal of better land mine detectors, including neutron activation analysis, electron capture detection, ion mobility spectroscopy, biosensors, and fluorescent polymer film chemosensors.[2,3] However, there still exists the need for real time TNT sensors that are low cost and have low complexity.

Depending on the detection scheme, the diverse environments in which land mines are found can add noise to a characteristic land mine vapor signature. This chemical "clutter" includes water, fuel spills, and sewage. The "clutter" problem exists even for analyte specific detection schemes which only show response to TNT or DNT since inplaced land mines are often found in former battle zones, which are characterized by trace amounts of explosives scattered over a large area as a result of exploded ordinance. Additionally, land mines are found in agriculture sites where there may be large amounts of nitrogen based fertilizers which could foul certain detection strategies. In these environments, methods of detection which can cancel out the ambient conditions would find great use.

There is a general interest in the ability to detect and identify the vapor signatures of solids for applications other than land mine detection such as the identification and grading of non-liquid foodstuffs such as coffee beans and spices, as well as the detection of contraband drugs. In this section we show the detection and identification of the vapors of six solids using a nine detector array.

II. Experimental

The composite films used in this work are made from (with designator number): 1, poly(styrene-co-allyl alcohol); 2, poly(α-methylstyrene); 3, poly(N-vinylpyrrolidone); 4, poly(sulfone); 5, poly(caprolactone); 6, poly(ethylene-co-vinyl acetate); 7, poly(ethylene oxide); 8, poly(ethylene-co-vinyl acetate); 9, poly(ethylene-co-vinyl acetate). With the exception of detectors #8 and #9, 160 mg of each of these polymers was dissolved in 20 ml of benzene, chloroform, or THF depending on the solubility of the polymer. To these solutions was added 40 mg of carbon black (BP2000, Cabot Co., Billerica, MA) to make suspensions that were 20% by weight carbon black. In the case of detector #8, 168 mg of polymer and 32 mg of carbon black were used to form a suspension that was 16% by weight carbon black. In the case of detector #9, 166 mg of polymer and 34 mg of carbon black was used to form a suspension that was 17% by weight carbon black. All polymers were obtained from Aldrich or Polysciences Inc. and used as received. The resulting suspensions were sonicated for 5 - 10 min immediately prior to casting the composite films. The detectors were made from substrates consisting of 15 pF capacitors that had been ground down and polished to expose their interdigitated electrodes. The composite films were dip-coated onto these substrates until a baseline resistance of ca 100 kΩ was achieved.

The detectors were plugged into a standard ribbon cable connector which was connected to Keithley 7011, 10 x 10 multiplexer card which was inserted in to a Keithley 7001 multiplexer. The two-probe electrical resistance of the composite was monitored with a Keithley 2002 digital multimeter through the multiplexer. The data collection system and data storage was controlled by custom LabVIEW software (see chapter 8).

The six volatile solids were placed in petri dishes (2" in diameter) and were covered when not in use to reduce dilution of the head-space vapor. In a typical exposure, a baseline resistance was established by placing the detector array in an empty petri dish to simulate the sampling environment. This step was performed because some detector film resistance values decrease upon being placed near the petri dish presumably because of a decreased humidity in the vicinity of the dish. This effect was greater for detectors made from polar polymers. The sensors were held near the empty dish for 60 s to collect a baseline resistance, then moved to the dish containing the analyte. The brief transient response which occurred upon going from the empty petri dish to the analyte containing dish was disregarded during data work-up. During an exposure, the cover on the petri dish was moved aside slightly (70% of the dish was still covered during exposure to reduce air flow which would cause dilution) and the detector array was held over the analyte (within 5 mm of the powder in all cases) for a period of 120 s. The detector array was held in the open air for an additional 60 s to allow off-gassing of the analyte.

The substances probed were (with vapor pressures): 2,4,6-trinitrotoluene (2 ppb); 2,4-dinitrotoluene (10 ppb); vanillin (1 ppm); indole (15 ppm); 4-nitrotoluene (212 ppm); and naphthalene (324 ppm). All solids were obtained from Aldrich with the exception of a sample of military grade TNT which was obtained from the USMC (Camp Pendelton, CA). The analytes were exposed to the detector array four times in a random order which included two blanks consisting of sodium chloride and clean, dry sand; both of which caused no response in the detectors. The data were normalized to account for concentration differences between exposures to the same analyte. This normalization was done by dividing the individual detector response to a particular analyte exposure by the sum of responses by all the detectors to that same exposure.

III. Results and Discussion

All six test substances produced discernible differential relative response patterns; however, not all detectors responded to all analytes. The histogram of the normalized differential relative responses is shown in Figure 7A.1. Detectors 6, 8, and 9, which were made from poly(ethylene-co-vinyl acetate) and differing amounts of carbon black, gave the best responses to all the test

vapors, with the largest response among this set occurring in the 16% carbon black composite. This is in agreement with percolation theory which would predict that the composite with the smaller volume fraction of conductor would be nearer to its percolation threshold and so would give larger resistance change for small conductor volume fraction changes.[4,5]

Principal component analysis was performed on the data shown in Figure 7A.1 to aid the visualization of the pattern differences. Figure 7A.2 shows PC 1 and PC 2 resulting from this analysis. These two principle components contain 99% of the variance in the data. Each spheroid in Figure 7A.2 encloses 99% of the data for the analyte indicated. Clearly, each analyte is differentiated (including the military grade TNT) and is therefore resolved by these detectors. It has been reported that DNT is the primary component of the odor signature of military grade TNT used in land mines;[3] however, in this test the two substances produced distinguishable signatures. This may be due to the higher quality of US military TNT; however, the presence of other non-explosive impurities that may have significant vapor pressures is not precluded. Provided the vapor signature of the TNT is constant, the identity of the sub-component of that signature which is most responsible for the detector response is irrelevant.

We have shown in other work that the signal response by our detectors is, to a first order, a function of the fractional vapor pressure of the analyte that is presented to the detector.[6] The vapor signatures generated from these solids may be at low concentrations but will be at high fractions of their equilibrium vapor pressure. Therefore, provided the analyte can be transported to the detector film, it will be sorbed into the film and cause a response. In this work, diffusion in air was the transport mechanism (the sensors were held as close to the solid as possible without touching it); however, if these detectors are to be used for general solid-source vapor detection, then analyte transport schemes that preserve the original concentration of analyte must be employed.

IV. Conclusions

These results indicate that the vapor signature from certain sufficiently volatile solids are detectable by these detectors. The response pattern generated by the array is of sufficient intensity to visualize the clusters of similar vapor presentations in principal component space. This extends

the vapor detection-vapor identification tasks to which these polymer-carbon black composite detector arrays can be applied to include such useful problems such as explosive and drug detection, or quality control for aromatic foodstuffs such as coffee, herbs, and spices.

References

1)Rouhi, A. M. *Chemical & Engineering News* **1997**, *75*, 14.

2)Yang, J. S. S. T. M. *Journal Of the American Chemical Society* **1998**, *120*, 11864.

3)Kolla, P. *Angewandte Chemie-International Edition In English* **1997**, *36*, 801.

4)Anderson, J. E.; Adams, K. M.; Troyk, P. R. *Journal of Non-Crystalline Solids* **1991**, *131*, 587-592.

5)Godovski, D. Y.; Koltypin, E. A.; Volkov, A. V.; Moskvina, M. A. *Analyst* **1993**, *118*, 997-999.

6)Doleman, B. J.; Severin, E. J.; Lewis, N. S. *Proceedings of the National Academy of Sciences of the United States of America* **1998**, *95*, 5442-5447.

Figure 7A.1: Normalized differential resistance change relative to baseline, $\Delta R_{max}/R_b$, obtained by an array of 9 polymer/carbon black composite detectors to headspace vapor signature presentations of six solid analytes. Four exposures of each analyte type was performed in a random order and the results normalized then averaged. Note that not all sensors responded to all analytes.

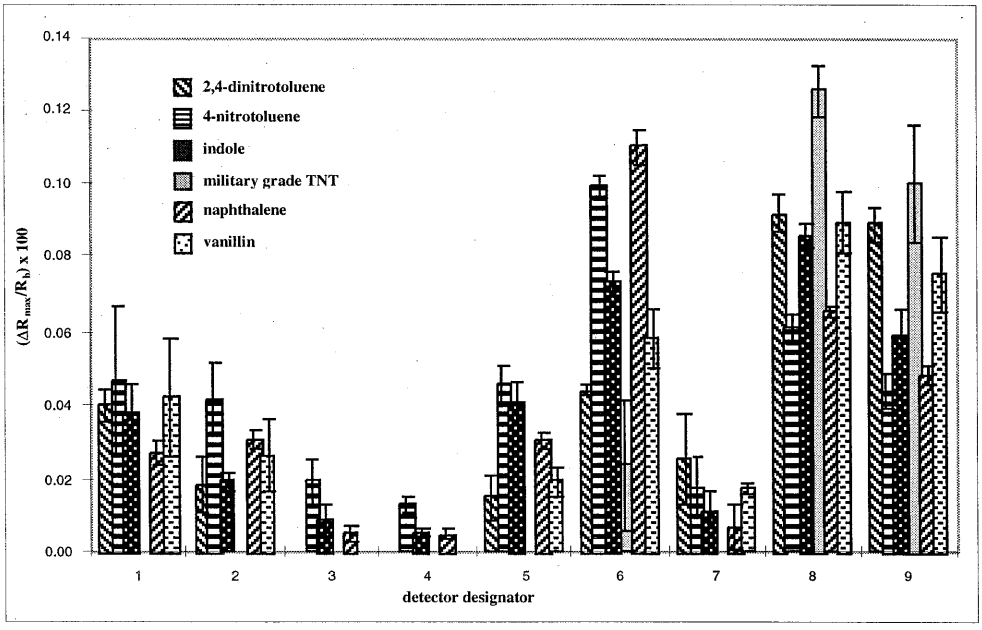
0.14
0.12
0.10
0.08
0.06
0.04
0.02
0.00
$(\Delta R_{max}/R_b) \times 100$
2,4-dinitrotoluene
4-nitrotoluene
indole
military grade TNT
naphthalene
vanillin
1
2
3
4
5
6
7
8
9
detector designator

Figure 7A.1

Figure 7A.2: Normalized results from the exposure of the 9-element array to the headspace vapor signature indicated as represented in the first two dimensions of principal component space. These two principal components contain 99% of the total variance in the data.

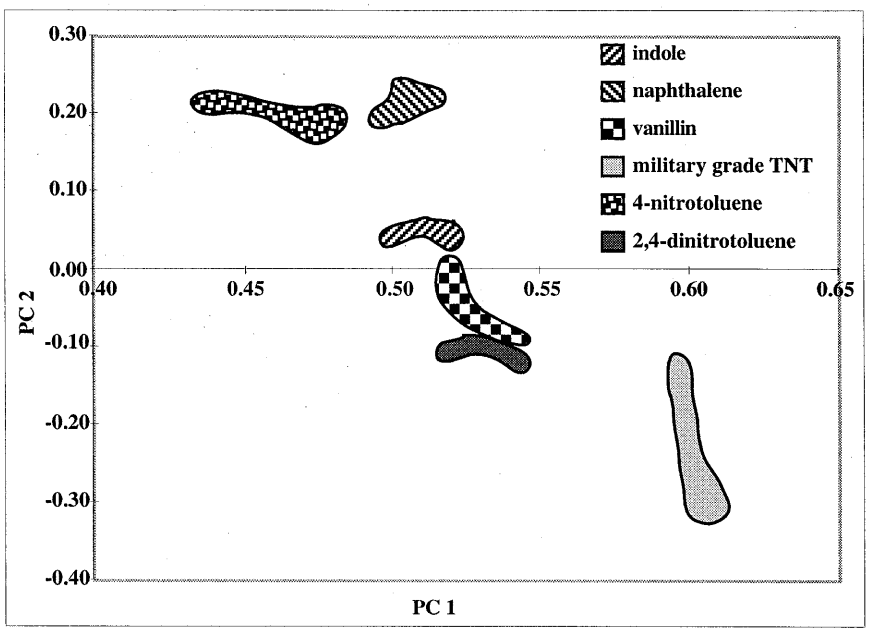
0.30
0.20
0.10
0.00
-0.10
-0.20
-0.30
-0.40
0.40
0.45
0.50
0.55
0.60
0.65
PC 2
PC 1
indole
naphthalene
vanillin
military grade TNT
4-nitrotoluene
2,4-dinitrotoluene

Figure 7A.2

Chapter 7, Part B

Tracking The Decay Of Fish With A Polymer-Carbon Black Composite Vapor Detector Array

Abstract:

The decay of a saltwater fish was tracked over six days with a carbon black-polymer composite detector array. A distinctive normalized response pattern associated with the spoiling fish emerged during the time period. Principal component analysis showed that the data moved in a roughly linear fashion in principal component space as time progressed indicating that the response patterns changed with the changing vapor signature and became more distinctive of the decaying fish. Additionally, the differential relative resistance responses increased in intensity relative to a water saturated background concomitant with decreased signal variance as decay progressed and the vapor signature stabilized and intensified.

I. Introduction

Odor is one of the most important freshness determinants for the food industry. Off-odors are a common cause of spoilage in all branches of the food industry and the economic consequences can be serious. Rapid, effective means of identifying the cause of the odor, troubleshooting the problem, and thereby being able to effect solutions with minimum delay are essential.[1] The seafood industry is acutely aware of the need for maintaining product quality. There are changes in seafood that occur not only during but also before and after processing.[2] Because of the global nature of the industry, uniform standards for seafood freshness are needed. The U.S. imports large quantities of seafood from other countries.[3] While some of these countries have advanced food preservation technologies and handling systems, many others do not. Consequently, quality standards may be difficult to implement on a worldwide basis, particularly if the analysis techniques are expensive or complex. Therefore, both industry and regulatory agencies seek methods to directly measure volatile compounds associated with food spoilage.

The initial quality loss in fish is mainly due to the breakdown of nucleotides. It has been shown that volatile sulfides such as hydrogen sulfide, dimethyl sulfide and methyl mercaptan are produced by bacterial enzymes acting on sulfur containing amino acids such as cysteine.[3] One characteristic feature of spoilage is the production of volatile bases, ammonia, trimethylamine, dimethylamine, and methylamine.[4] After death, bacterial action rapidly converts trimethylamine oxide, a naturally occurring osmotic pressure regulator, to trimethylamine (TMA), a volatile base largely responsible for the characteristic odor of dead fish.[4] Therefore, in decaying fish (and other meats) ammonia, amines, and volatile sulfur compounds are produced. If these substances could be measured or detected easily, then important parameters such as time elapsed since catching, and shelf life, could be determined.[3]

Typically, odor and malodor are assessed by human sensory panels. The biggest disadvantage in this approach is that it involves a trained panel of humans to smell each sample, which is expensive and time consuming.[3] Additionally, the throughput of sensory panels is inadequate for use in modern fish processing and handling sites. Moreover, sensory panels are

subject to fatigue, resulting poor product assessment.[5] Other methods of assessment include gas and liquid chromatography, steam distillation, TMA-specific electrodes, and bacterial sensors. All these methods suffer from drawbacks such as low throughput (requiring several minute per sample analysis), and high expense of equipment maintenance and a well-trained staff, which would restrict the use of these methods becoming worldwide.[4] There is a demand, therefore, for methods to objectively measure fish and other food odor quality by detecting and quantifying important volatile compounds.

In this study, a type of saltwater mackerel was allowed to decay in a sample chamber and the head space vapor was flushed over the detector array to monitor the odor signature over six days during which time the fish completely decayed. No individual detector element used here is particularly attuned to the basic amines or other volatile components found in the vapor signature of rotting fish, however in spite of this lack of specificity by the detectors to the task, the detector array used in this work was able to distinguish and track the vapor signature of the decomposing fish.

II. Experimental

The polymers used in the composite films with their position in the array are listed here: 1) poly(vinyl chloride-co-vinyl acetate), 2) poly(vinyl acetate), 3) poly(N-vinyl pyrrolidone), 4) poly(methyl methacrylate), 5) poly(bisphenol A carbonate), 6) poly(styrene-co-maleic anhydride), 7) poly(caprolactone), 8) poly(ethylene oxide), 9) poly(sulfone), 10) poly(vinyl butyral), 11) poly(vinylidene chloride-co-acrylonitrile), 12) poly(methyl vinyl ether-co-maleic anhydride), 13) poly(ethylene-co-vinyl acetate), 14) poly(4-vinyl phenol), 15) poly(α-methyl styrene), 16) poly(styrene-co-allyl alcohol). Composite films were cast from solutions of 160 mg of the insulating polymer dissolved in 20 ml of THF, benzene, or dichloromethane depending on the solubility of the polymer. To this solution was added 40 mg of highly conductive carbon black (BP2000, Cabot Corp., Billerica, MA). The resulting suspension was sonicated for 5 - 10 min immediately prior to casting the composite films. The detectors were made from substrates consisting of 15 pF capacitors that had been ground down and polished to expose their

interdigitated electrodes. The composite films were dip-coated onto these substrates until a baseline resistance of ca 100 kΩ was achieved.

The detectors were plugged into a standard ribbon cable connector which was connected to Keithley 7011, 10 x 10 multiplexer card which was inserted in to a Keithley 7001 multiplexer. The two-probe electrical resistance of the composite was monitored with a Keithley 2002 digital multimeter through the multiplexer. The data collection system and data storage was controlled by custom LabVIEW software (see chapter 8).

A fresh King fish (*Scomberomorus cavalla*, a type of saltwater mackerel) was purchased from a local grocery store and placed in a 1 L glass jar to which gas inlet and outlet tubes were attached. The fish was allowed to decay naturally over six days during which time the head space was sampled consecutively 5 - 6 times (over about 15 min) each day with the sampling sessions occurring at roughly 24 hour intervals. In a typical experiment, nitrogen gas which was saturated with water vapor was passed over the detector array for 60 s at 300 ml/min to establish a baseline resistance value. To collect a sample, the 300 ml/min flow was diverted through the 1 L vessel containing the fish for 2 min. This head space sample was immediately passed over a detector array after leaving the fish sample chamber. The flow rates of the sample and background gas streams were controlled using Gilmont rotamers (VWR Scientific) and needle valves. The resistance of each detector in the array was monitored with a Hydra 2620A data acquisition unit (John Fluke Mfg. Co.) interfaced to a personal computer which multiplexed through the detectors and measured and stored their dc resistance values.

III. Results and Discussion

The response patterns by the detector array over the six day period are shown in Figure 7B.1. The pattern for water is shown in Figure 7B.1a. When the sample of fresh fish was blanked against a water background, the detector array gave a response pattern that was quite noisy due to insufficient analyte concentration from the fresh fish to cause reproducible responses in the detectors relative to the water background (Figure 7B.1b).

Over the course of the six day experiment, the smell of the fish was quite evident to the human nose after the first day but it was not until day four that a distinctive pattern in the detector array had emerged. Of course, humans have had evolutionary pressure to become highly sensitized to the odor of spoiled food. Figures 7B.1c - f correspond to the detector array responses recorded on day three through day six, respectively. These response data were normalized to eliminate errors due to differences in concentration between exposures. Therefore, the changing patterns are illustrative of a change in the vapor composition rather than simply a change in concentration of the same composition. Figure 7B.1d shows the array response at day six. Note that detector films numbered 3, 6, 11, and 12 (see Experimental section) are increasing relative to the other sensors with time and spoilage. By day six the pattern is quite strong and is less noisy than the samples taken in prior days.

Principal component analysis was performed on the data shown in Figure 7B.1 to aid the visualization of the pattern differences. Figure 7B.2 shows PC 1 and PC 2 resulting from this analysis. These two principle components contain 89% of the variance in the data. The spheroid for fresh fish is large, indicating a large amount of noise in the data relative to the spheroid corresponding to day six, which has a smaller diameter in principal component (PC) space indicating less variance in the signal from each detector. The data spheroids move linearly in PC space in the direction of increased spoilage corresponding to an increase in the characteristic signature of the decaying fish. Since the spheroids contain 95% of the PC points, the decreasing size of the spheroids with time illustrates the decreasing standard deviation in the responses from individual detectors due to increased signal strength over the six day period.

The background flow stream in these experiments was humidified to amplify the signal due to the spoiling fish relative to that for water. As dry air passes over the fish, it becomes saturated with water since the fish is wet and contains body fluids that seeped out over the course of the six day experiment. By the last day of the experiment the sample jar was roughly half filled with fluid (ca 500 ml) all originating from within the fish. We have shown in other work (see chapter 3) that mixtures of analytes cause an additive response in these detectors.[6] The method of canceling out

the baseline ambient (in this case water) does nothing more than amplify the difference between that particular ambient and the sample. There is no new information available in this technique; it simply allows the differences in response patterns to become more obvious. The signals associated with the decaying fish are still present in an non-canceled data set, but those signals are small additional responses on top of an already large response attributed to the ambient water. Detectors with low noise in a stable ambient could produce patterns in which the differences due to the analyte of interest are easily seen. However, in our system, canceling out the ambient allows easier visualization of the response patterns due to the test analyte. This background ambient canceling technique works well for detection tasks characterized by a small response signal superimposed onto a large response signal due to ambient conditions.

IV. Conclusions

There has been evolutionary pressures on the mammalian nose to develop a high sensitivity to the by-products of spoiling food such as amines and thiols. However, by comparison, the polymers used to form the detector array used in this experiment were not specifically designed for the detection of volatile amines or sulfur, yet were still able to classify the decay of the sample. This work illustrates an application of our technology to the detection and identification of the causes of malodors. With sufficient knowledge of polymer-analyte interactions, and the development of sensors designed to give large responses to amines and sulfides, these detector arrays could be developed to identify the cause of a malodor in everything from carpet samples to "sick office syndrome" to spoiling food. Additionally, and perhaps more importantly, these detector arrays could be used to determine when the malodorous substance is no longer present.

V. References

1)Dainty, R. H. *International Journal of Food Microbiology* **1996**, *33*, 19 - 33.

2)Wiese-Lehigh, P. L.; Marshall, D. L. *Determination of Shrimp Freshness Using Impedance Technology*; American Chemical Society: Washington DC, 1993.

3)Strachan, N. J. C.; Nicholson, F. J. *International Journal of Food Science and Technology* **1992**, *27*, 261 - 269.

4)Sadok, S.; Uglow, R. F.; Haswell, S. J. *Analytica Chimica Acta* **1996**, *321*, 69 - 74.

5)Zhang, H.-Z.; Lee, C.-T. *Gas Chromatography - Mass Spectrometry Analysis of Volatile Flavor Compounds in Mackerel for Assessment of Fish Quality*; American Chemical Society: Washington D. C., 1997.

6)Severin, E. J.; Doleman, B. J.; Lewis, N. S. *manuscript in preparation.* **1999**.

Figure 7B.1: The normalized relative differential responses expressed as percent obtained by an array of 16 polymer/carbon black composite detectors. Sensor designators refer to the numbers given for each polymer in the Experimental section. **A**) The normalized response pattern for saturated water vapor; **B**) the normalized response pattern for a fresh King fish with saturated water vapor as the ambient; **C**) the normalized response pattern for the same fish after three days with saturated water vapor as the ambient; **D**) the normalized response pattern for the same fish after four days with saturated water vapor as the ambient; **E**) the normalized response pattern for the same fish after five days with saturated water vapor as the ambient; **F**) the normalized response pattern for the same fish after six days with saturated water vapor as the ambient.

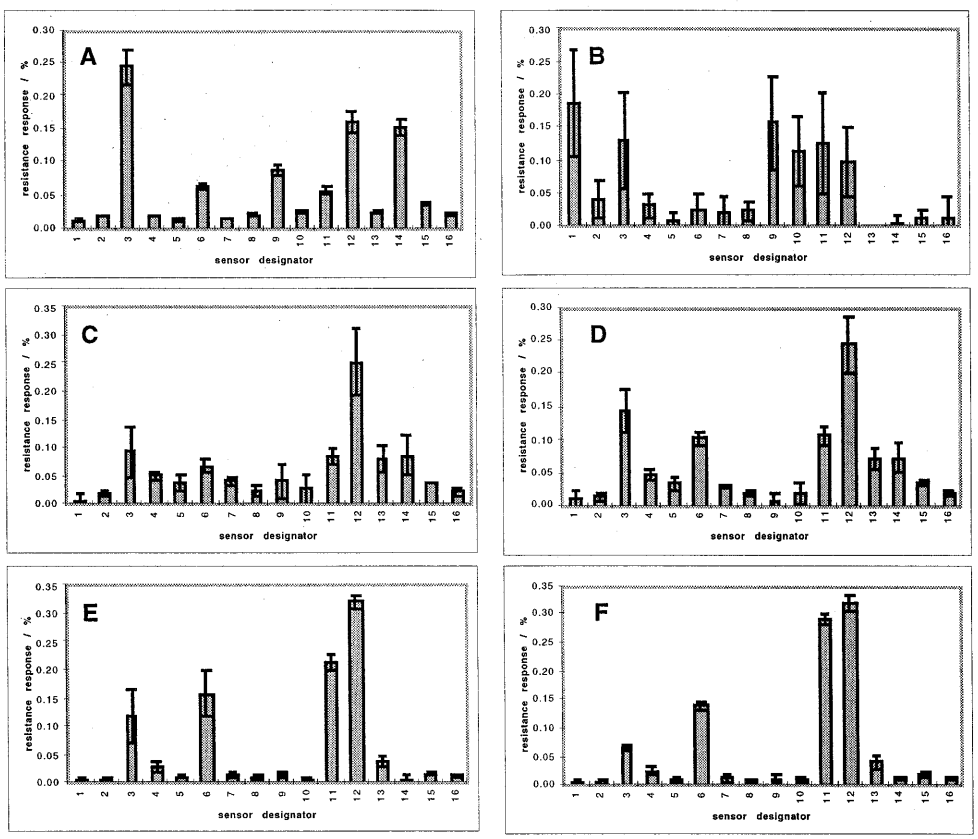

Figure 7B.1

Figure 7B.2: Normalized results from the exposure of the 16-element array to water and to the spoiling fish over six days as represented in the first two dimensions of principal component space. These two principal components contain 89% of the total variance in the data.

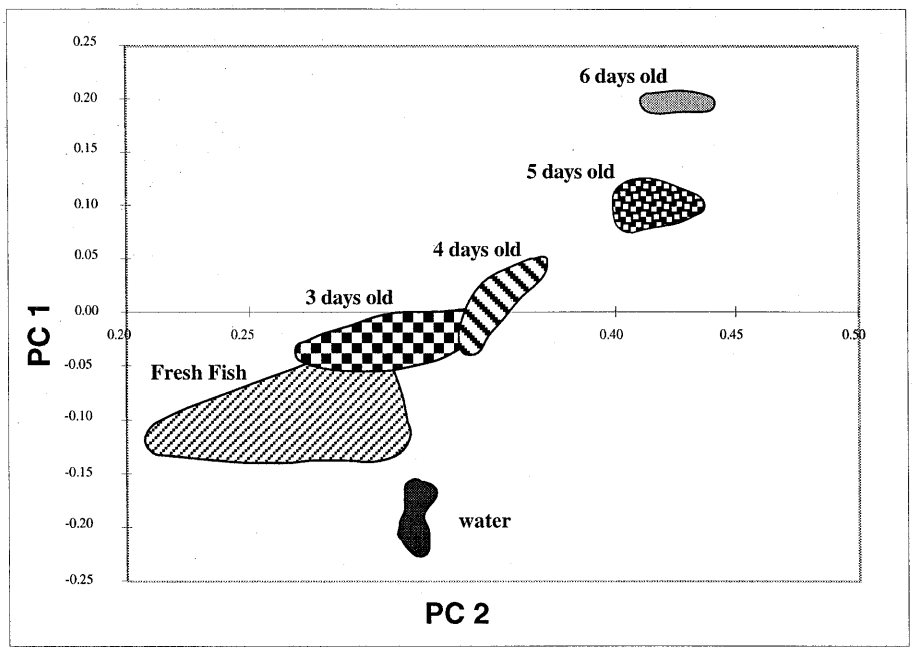
0.25
0.20
0.15
0.10
0.05
0.00
-0.05
-0.10
-0.15
-0.20
-0.25
0.20
0.25
0.40
0.45
0.50
PC 1
PC 2
6 days old
5 days old
4 days old
3 days old
Fresh Fish
water

Figure 7B.2

Chapter 8

An Automated Vapor-Generation and Data-Collection Instrument For the Evaluation Of Chemiresistor Vapor Detectors

Abstract:

An automatic vapor delivery system has been built which can generate up to 8 different vapors from neat-liquid bubbler sources. These vapors can be delivered to a test chamber at concentrations from saturated to 0.02% of saturation at programmable flow rates. Additionally, mixtures of two vapors can be generated. The resistance responses of up to 80 chemiresistors can be recorded with 9-digit accuracy up to resistance values of 1 GΩ. The system is fully automated using a personal computer which controls the entire system, permitting unattended operation during elaborate vapor exposure and data collection sequences. Parameters describing the duration and test conditions of vapor presentations are stored in the computer along with the sensor responses to the presentations. The fully automated character of this instrument affords many advantages including unattended operation during long sequences of tests, reduced operator exposure to toxic chemicals, and improved measurement precision.

I. Introduction

In the last number of years, interest in sensor development has grown tremendously, particularly in the field of "electronic noses." Necessary to this development has been the design and implementation of vapor delivery systems. This is often left to investigator ingenuity and may be hindered by a lack of engineering expertise required to build a successful system.

Proper flow system design is crucial for a successful sensor characterization program. Many questions concerning new sensor systems deal with concentration dependence, temperature dependence, reproducibility issues, and longevity issues. Paramount to the proper interpretation of experimental data is the assumption that analyte vapors are delivered as specified. Additionally, proper characterization of robust sensor systems require repeated exposures of a given analyte at a given concentration which simply cannot be adequately performed manually. An automatic delivery and data collection system is required.

Herein is described a system that will deliver any of eight solvent vapors from concentrations ranging from saturated to 0.02% of saturation in a carrier gas background flow. Additionally, this system allows delivery of a binary mixture of vapors from any one of a bank of four bubbler sources with any one of another bank of four bubbler sources. The two components of these mixtures can be delivered simultaneously or sequentially. All analyte presentations are completely controlled by a personal computer according instructions input by the user. The fully automated character of this instrument affords many advantages including unattended operation during long sequences of tests, reduced operator exposure to toxic chemicals, and improved measurement precision. This instrument is extremely valuable for the complete development and characterization of prototype chemical vapor detectors.

II. Overview of system

Dynamic methods of generating vapors that involve the addition of calibrated amounts of a vapor to a flowing system of carrier gas are preferred over static methods, particularly for dilute vapors. Dynamic methods minimize the effects of wall absorption on calibration accuracy and a wide range of concentrations can be prepared by simple manipulation of the gas flow rates.[1] The

gas stream output of the instrument reported here can be switched (under computer control) between the generated vapor stream and clean air so that the baseline drift and reversibility of the detectors can be recorded. Additionally, the flow rate of the generated diluted vapor stream can be regulated to a constant value regardless of the gas flow rates required to affect the desired dilution. This capability allows the investigation of the dependence (if any) that delivery flow rates have on sensor performance.

The vapor generation and sensor evaluation system consists of a flow system to generate and deliver vapor streams to the test chamber and a data collection system to record data from the detectors. The general schematic of the system is illustrated in Figure 8.1. The carrier gas was oil-free air, obtained from the general compressed air lab source at 40 psi, containing 1.10 ± 0.15 ppth (parts per thousand) of water vapor. The compressed air is ducted through a set of mass flow controllers which regulate the flow, in terms of (mL/min), that is delivered to the system. The air stream is split into two branches, one for the background/diluting gas and one for the sample gas. The background gas flow rate is controlled by a mass flow controller (MFC) with a range of 0 - 50 L/min after which it is mixed with saturated analyte vapor, then passed to the sample chamber. The analyte gas stream passes through an MFC with a range of 0-500 mL/min whereupon it is passed to a set of neat-liquid bubblers. The gas becomes saturated with analyte vapor corresponding to the liquid in the bubbler. This saturated analyte vapor stream is then delivered to a 3-way valve. The two channels of the 3-way valve correspond to waste and to the diluting gas flow going to the sensor chamber. If the exposure is not yet required, the saturated vapor is passed out of the system to a fume hood. When the exposure is to begin, the normally open-to-waste 3-way valve closes and the analyte stream is blended with the background flow, whereupon it becomes diluted to the desired concentration determined by the volume/min ratio of the two streams. The combined flow is mixed by turbulence in the gas lines leading to the sample chamber. Further mixing of the combined streams occurs just prior to encountering the test sensors by passing through a set of 1 mm pore stainless steel screens.

While the vapor-generation system is operating, the data logging system is reading resistance values from each of the test detectors. The central control computer is interfaced with the data collection system through an IEEE general purpose interface board (GPIB). The dc resistance of each chemiresistor is read sequentially with a Keithley 2002 digital multimeter (DMM) by multiplexing through the chemiresistors (up to 80) with a Keithley 7001 multiplexing system (MUX). The resistance data from all detectors is initially stored in the DMM. When a complete set of data are recorded, corresponding to one pass through the set of detectors, those data are sent to the control computer where they are stored in a tab-delimited text file. The use of the GPIB communications protocol combined with the use of the DMM affords great flexibly to the system. Many other components can be incorporated into the system such as thermocouples, pressure gauges, frequency counters, etc. The system is therefore expandable and malleable to meet future measurement needs of the user.

The central computer controls the entire system through the GPIB board mentioned above and two I/O boards. Analog voltage from three channels of an A/D board supply the control signals for the three MFCs and digital signals from a separate digital output board control which bubblers receive gas flow. The central computer also regulates the interaction between the DMM and the MUX and synchronizes these devices with the sequence of vapor presentations. The timing and sequence of all tasks are dictated by a method file (described below) that is input by a user. This allows completely automated operation of the instrument for an unlimited amount of time.

III. Flow system

The eight bubblers were made from glass and built in the chemistry department's in-house glass shop. Glass was used because of its ease of fabrication which was important in the early design stages. Additionally, glass is easy to clean and to observe contamination that might accumulate in the system. These are illustrated in Figure 8.2. The drain holes at the bottom are closed with Kontes Teflon valves. The valves used are not terminated with O-rings but seal with Teflon-glass contact. It was found that the viton O-rings decomposed in a number of solvents used in the system. The only O-rings used are higher on the valve stem and provide a snug fit and

final sealing. The solvent reservoir bulb at the top of the bubbler was made from a standard, 24/40 joint, 3-neck, 500 ml flask. One neck was removed and a 1/2 inch tube was attached to which a PTFE swage-type fitting was connected to join with the gas delivery tubing. The center neck accommodated the gas dispersion frit on the end of a glass tube that was long enough to reach the bottom of the bubbler. The final neck was used to fill the bubbler and on which, during vapor delivery, a rubber septum was fitted. The septum closed the fill-port during gas delivery , but it also served as a last-resort pressure relief valve. The septum would blow off before any other part of the system would fail.

All tubing used in the system was either PTFE or stainless steel. The gas delivery tubes from the compressed air source to the MFCs are steel to accommodate the source air pressure (30-40 psi). Tubing running from the MFCs and to and from the solenoids, bubblers, and chamber are 1/8" i/d PTFE from VWR and the stainless was 1/4" id from Caltech's central supply warehouse. All fittings used to connect the PTFE tubing to the bubblers, the steel tubing, and the Teflon solenoid blocks were from Cole-Parmer and were either PFE or PTFE.

Pressurized gas enters the delivery tube of the bubbler and is forced out the gas dispersion frit which was of coarse porosity. This pore size in the frit was a compromise between creating small bubbles in the analyte liquid and reducing line pressure by not constricting the gas flow more than necessary. A fine porosity frit would have provide smaller bubbles thus allowing a shorter solvent head through which the bubbles rise and become saturated, but would limit the flow rate of delivery since the back pressures would become too great and system rupture would occur. It was found by mass loss experiments[2] that a solvent height of 12" was required for the bubbles produced from the coarse frit to become saturated. The large globe at the top of the bubbler acts as a solvent reservoir so that the solvent level inside the bubbler does not fall below 12" due to evaporation during an experiment.

The solenoid valves were from ASCO/ANGAR (Cedar Knolls, NJ) and were installed into Teflon blocks to create a 1 x 4 manifold. They could only handle 30 psi, so to ensure that they were not damaged by an accidental over-pressure event, check valves set to 29 psi were installed

upstream of the solenoid manifolds for emergency pressure relief. Two solenoids per bubbler were configured (one upstream and one downstream of each bubbler) to prevent cross-contamination between delivery lines. A rotary 3-way valve, obtained from the same company and which has the same pressure limits, was configured to deliver the analyte vapor stream to waste as the default setting. When the 3-way valve is activated, the analyte stream is delivered into the main carrier gas. Each solenoid required a 12 V power supply and each drew about 300 mA when open. The power supply for all the solenoids was a 10 amp/12 V system.

Three MFCs were used; one to control the background/diluting gas and two to control the gas flow to the solvent bubblers. All mass flow controllers used in the system were purchased from MKS (Andover, MA). The MFC used for the background/dilution flow has a flow range from 0-50 L/min while the solvent delivery MFCs have a flow range of 0-500 mL/min. These devices have an accuracy of 1% of full scale but a repeatability of 0.2% of reading. For example, the limit of accuracy is 5 mL/min for the smaller MFCs, but the repeatability at that flow rate is 0.01 mL/min. Because of the high degree of repeatability, the lower flow range of the MFC could be utilized if independently characterized.

To characterized the MFCs, floating ball rotamers (Gilmont) were used on the exit of the system. The rotamers had an accuracy of 5% of full scale but had smaller ranges so that the overall accuracy was greater when they were combined. The MFCs were activated in the 0-10 mL/min range and the reading from the rotamers was recorded. Since the MFCs are calibrated in terms of Standard conditions of 0°C and 1 atm, while rotamers react to real conditions, the rotamer values were correlated to the desired MFC reading, after converting to STP conditions. From the experimental data, calibration curves for the low flow range of each MFC were generated and the coefficients from the calibration fitting are listed in Table 8.1. These coefficients are used by the user when developing a method file to determine the voltages that will be applied to the MFCs.

Each MFC has connections for an analog signal input, as well as +15 V, -15 V, common ground, and signal ground. The signal ground and common ground were connected together and were grounded to the casing of the MFC. The power supply for the three MFCs was a ± 15 V

surplus power supply from C & H Supply (Pasadena, CA). The MFCs require a 15 min warm up period to operate at published specifications, but in this system they are left powered continuously. The signal input is supplied from the analog output board (described below) in the main computer and consisted of a 0-5 V analog signal.

There is an additional correction that must be made to the voltage values supplied in the method file. When a volume of gas becomes saturated with a vapor it will expand to a new volume at constant pressure. This expansion must be accounted for in the voltage supplied to the MFC. This expansion will be a fractional increase based on the total pressure and the vapor pressure of the solvent.

$$V_f = V_d + \left[\frac{(V_d \bullet VP)}{(P - VP)}\right] \qquad (8.1)$$

were V_f is the final volume exiting the bubbler in the time unit used (usually per min), V_d is the volume actually delivered to the bubbler, VP is the vapor pressure of the solvent, and P is the pressure of the system. For example, with an external pressure of 760 Torr benzene vapor (VP = 82 Torr) will expand a volume of gas by a factor of 0.121 which means that a flow of 100 mL/min entering the bubbler will exit at 112 mL/min.

IV. Electronics

The control computer was a Dell OptiPlex Pentium computer running Windows 95 software. To control the analog signals supplied to the MFCs three analog lines were routed from a AT-AO-6 (National Instruments) D/A board that was installed into the computer mother board. The digital control signals routed to the solenoid relay board were produced by a PC-LPM-16 (National Instruments) digital output board installed into the computer mother board. All communications between the control computer and the Keithley data collection system were routed through a GPIB board (National Instruments) in the central computer.

Specifications and settings on the hard drive: drive 0; Type : Auto or 55; Cyls: 525; Heads: 255; Write Precompt: -1 or none; LZ or Park Place: 525; Sect: 63; Size: 4318; Ctrl Byte: 8; Step Rate: 220; IRQ avail. (originally) = 5,10,11,12,15.

There are three analog output channels on the AT-AO-6 control card. Channel 0 controls the large Mass Flow Controller used for the background flow by sourcing voltage to the signal input pins on the MFC. Input values are 0-5 which correspond to the amount of volts delivered. The input values have an allowed precision corresponding the resolution of the MFC as described above. Channel 1 is the 0-500 mL/min mass flow controller connected to bubblers 1-4. Channel 2 is the 0-500 mL/min mass flow controller connected to bubblers 5-8. Two digital lines from this board are used to provide power to the relay board (digital line 0) and to provide an activation signal to the relay which controls the 3-way valve (digital line 1).

Settings and specifications on the AT-AO-6 board: Win95 device manager designation: device 2; "W21" = open; "W24" = open; "W22" = 5, Direct Memory Access (DMA) = channel 5; "W23": Group 1 = 10, Group 2 = 9 (i.e. the interrupts are #10 and #9); In/Out address = HEX 1C0; Dip switch positions: A5 = 1, A6 = 0, A7 = 0, A8 = 0, A9 = 1.

The eight remaining digital control signals for bubblers 1-8 that are routed to the relay board come from the PC-LPM-16 board. This board can output a voltage from 0-10 V or from $\pm$ 5 volts. Driving the line high can produce +5 or +10 volts. The board is set to deliver +5 volts (see settings below). On this board channels 0-7 are routed to the relays which open the solenoids regulating bubblers 1-8. Since this board was designed to output all 8 TTL voltages simultaneously, corresponding to an 8 bit number, each digital line is not directly addressable. The board only accepts a whole number which it converts into a binary array. In order to cause the board to power up only those lines necessary to open the proper solenoids, an Arabic number must be supplied that converts to the desired pattern of high and low voltages. Therefore, in the program listed in the appendix, the binary array, which the user supplies to indicate which bubblers should be open, is translated into a Arabic number which is passed to the board,

whereupon it is converted back into an 8 element binary array. The corresponding 8 digital lines are driven high.

Settings and specifications on the PC-LPM-16 board: "W3" = Interrupt = #5; "W1" (closed across BC) = ± 5 volts output; "W2" (closed across BC) = ± 5 volts output, In/Out address = HEX 260; Dip switch positions: A9 = 1, A8 = 0, A7 = 0, A6 = 1, A5 = 1.

All communication with the data logging system was routed through a National Instruments general purpose interface board (GPIB). This board was designated: GPIB 0, "controller in charge". There are two devices connected to the GPIB system. "Device 16" is the Keithley 2002 digital multimeter and "Device 7" is the Keithley 7001 multiplexer which contains two 7011 cards each currently wired as two 1 x 40 matrixes, but through software control they operate as one 1x 80 matrix. The board can be configured with software defined settings that are set by the factory ("PCIIa"), or can be configured by the user ("PCII") which is how it is configured in this system.

Settings and specifications on the GPIB board: "A11" = 1, Interrupt = 7, (jumped across #7); Direct Memory Access (DMA) = 1 (i.e., DRQ = 1, DRCK = 1); Set to chip 7210; "A10" = 1; In/Out Address = 2B8; Dip switch positions: A3 = 1, A4 = 1, A5 = 1, A6 = 0, A7 = 1, A8 = 0, A9 = 1.

The power to each solenoid was controlled via a relay board that received a 5 V signal from the central control computer (see below) The relay board was a National Instruments relay board (Austin, TX) and into it were installed DC5 relays. The relay board required 5 V for its power supply and this power came from the central computer. The two solenoids upstream and downstream of each bubbler were controlled by one relay. This was a fail-safe measure to avoid the possible situation of the solenoids being opened independently through user error while the MFCs were delivering gas. There were a total of 9 relays; eight for the 16 solenoids that controlled the gas inlets and outlets for the 8 bubblers, and one relay for the 3 way valve.

The relay modules are "default closed" relays, i.e., the switch is closed (allowing electricity to flow to the solenoid valves) when the control voltage is removed from the relay. The relays must be actively opened (electrical connection broken) with a 5 V TTL signal, otherwise the solenoids

get power all the time and are driven open continuously. The digital lines go from a digital output board (described below) in the control computer to each of the relays on the relay board. They are hard wired to the screw terminals of the relay board rather than via the alternative ribbon cable connector. The power for the relay board comes from the computer as well, namely, digital channel 0 from the AT-AO-6 board.

Since these relays are default-closed (electrically connected), a signal must be sent to them to open. Therefore, if the relay board was simply powered on with no signal to the relay modules, all the solenoids would open. One reason that the power to the relay board comes from the computer rather than from an independent 5 V source is so that the system can be shut down by computer control thus avoiding the need for the user to directly power-down the voltage supply to the solenoids. In the LabVIEW software this is reflected in the usage of 1 s and 0s in the sub-routine called "Timed analog/digital.vi" that might not seem intuitive. One would expect that a "1" in the software would imply an open solenoid (i.e., closed relay). Unfortunately, this is not the case, often a "1" is sent to specifically close the solenoid (i.e., open the relay).

The resistance values are read by a Keithley 2002 digital multimeter DMM that has an upper range of 1 GΩ with 9 digits of resolution. The multimeter reads each sensor in turn as controlled by a Keithley 7001 multiplexing system. The multiplexer has two 40 channel Keithley 7011 cards in it, making it capable of scanning 80 channels. The data collected from one scan of the sensors is stored in the 2002 and once all channels have been read the data is sent over a GPIB line to the central computer where it is saved in an appropriately labeled file. Instructions in Keithley's command language are sent by the LabVIEW program to set-up and run the data logging and multiplexing systems. These will be described in the software section.

V. Calibrating

The system gas output was checked for linearity with a flame ionization detector from California Analytical instruments (Santa Ana, CA). Four toluene standards were purchased from Scott Specialty Gases in concentrations of 996 ppm, 200 ppm, 99.2 ppm, and 50.6 ppm. The FID was checked for linearity with these standards and its output calibrated for concentration. The flow

system was checked by placing toluene liquid in bubbler #7 to check the MFC that delivered air to bubblers 5 - 8 and in bubbler #3 to check the MFC that delivered air to bubblers 1 - 3. It was found that the output of the flow system was linear with an R^2 of 0.99. Additionally it was found that there was no flow dependence on the way in which the concentration was achieved, i.e., no difference was found between 100 mL/min blended into 10 L/min and 200 mL/min blended into 20 L/min. The output of the system was reproducible to within 5% of the flow.

VI. Software

To operate the system, a user creates a tab-delimited text file (usually from a spreadsheet program like Excel) which contains the instructions to operate the system. This method file has 16 columns, one for each controlled device, and as many rows as required for the experiment. Each row consists of a set of instructions that will configure the system in the particular manner the user chooses for the amount of time the user chooses. The settings on each row are the state the instrument is in for the time period that is indicated in column 3 of that particular row (see below). When the user requires the system to change configuration by opening a different bubbler or changing the flow through a MFC the user must have a row of commands corresponding to the new desired set-up. Each row of the method file changes the settings of the various components of the system for the time period specified. This makes for a complex, but very flexible, system that can be configured in any way desired by the user. The following is a description of what element of the system each column controls. In all cases a "0" indicates "False" and a "1" indicates "True." The descriptions are for one row of the method file.

Column 1) This cell determines if the data from the data log system is to be saved to a file during the events executed on this line. Value: 0 (False) or 1 (True).

Column 2) The suffix of the name given to the file saved. This must have a value even if the data is not being saved. The value must be a number, not text. The text prefix comes in the front panel of the LabVIEW program (see appendix). Value: Any number such that the total number of characters in the prefix from the LabVIEW front panel and this suffix number will not exceed 8 (the limit for many DOS applications).

Column 3) The number of seconds before the LabVIEW command program goes to the next command row. Value: Any positive whole number.

Column 4) The voltage applied to the 0-50 L/min MFC that delivers the background flow. This voltage must be corrected according to the calibration curves created for the MFC. Value: 0-5

Column 5) The voltage applied to the 0-500 mL/min MFC that controls bubblers 5-8 (counting from the right). This voltage must be corrected according to the calibration curves created for the MFC and must reflect the volume increase by the solvent (see below). Value: 0-5

Column 6) The voltage applied to the 0-500 mL/min. MFC that controls bubblers 1 - 4 (counting from the right). This voltage must be corrected according to the calibration curves created for the MFC and must reflect the volume increase by the solvent (see below). Value: 0-5

Column 7) This is always 1. It means power is being delivered to the relay board.

Column 8) This controls the 3-way valve. A value of 0 means that the flow is directed to waste, and a value of 1 means the flow is directed toward the background flow which, once mixed, will flow over the sensors.

Column 9-16) Control for bubblers #1-8, respectively. Values for columns 9-16 are either 1 or 0, which stand for Open or Closed.

As an example of the use of the system, a fragment from a method file is shown in Table 8.2. In this fragment the experiment begins with the system blowing 30 L/min (a 3 in column 4 associated with the background flow) through the system for 1800 seconds (1800 in the column for time, column 3). This is often done at the beginning of an experiment to settle the sensors in the system. Note that in this fragment no data is being saved (a zero in column 1). Then the system opens bubbler #1 (a 1 in column 9) and blows 100 mL/min through it for 30 s, with the flow going to waste because the 3-way valve is not open. During this time period the data is being saved to a file whose suffix is the number one (a 1 in the "name" column, column 2). This period is used to collect baseline values for the sensors and to equilibrate the delivery tubes with the analyte. After 30 s the next line is read and the system keeps everything the same except that the 3-way valve is opened (column 7) to allow the analyte to mix with the background flow which is

reduced to keep the total flow constant. The data file with the suffix of number one is appended with the data from this exposure of the analyte to the detectors. This goes on for 60 seconds, at which time the next line is read and the system stops the flow through the bubbler and closes the solenoids. The data file is still appended during this 90 s off-gas period. The program does basically the same thing for bubbler #6. A 30 s baseline collection is followed by a 60 s exposure of 476 mL/min of saturated analyte vapor blended into 19.5 L/min background flow, followed by 90 s of recovery. This is saved in a file whose suffix is the number two. The final exposure in the example is a mixture of two analytes at the same flow rates as above, except that the reduction in background flow accounts for both analyte flows. Note that the first analyte is exposed for 60 s since it is continually flowing while the second analyte is started. The second analyte only flows for 30 s before both are shut off during the recovery period of 90 s.

This method file system is quite powerful. Since every element of the system can be independently controlled at any time interval, there are no limits on the types of experiments that can be performed. The only challenge is creating an accurate method file that reflects the desired experiments.

The LabVIEW program (called "NOSE") that controls the system is made up of two sub-systems. One sub-system controls the data logging system and the other controls the solenoids and MFCs. The appendix contains the entire program.

In the control software there are variables supplied by the user. These cannot be altered after the program starts because they are involved in the set-up of the instrument. The user defined variables are: the file prefix, the expected upper limit of resistance, the expected lower limit of resistance, the digits of resolution, the channels to scan, the delay between scans (if any), and the path name for data files.

The initial step when any method file is loaded is to set up the Keithley data logging system with the particular configuration defined by the user on the LabVIEW front panel. The script that does this set-up is detailed in the next section. After the data logging system is configured, the "Nose" program begins to read the user's method file line by line. Each row in the method file is

read off as a one dimensional 16 element array. The elements of the array are routed to the appropriate parts of the control program (see appendix). The functions of each of the 16 elements are detailed in the method file section (see above). (An important point to remember while reading the program, is that LabVIEW defines the first element of an array as position zero and the second element of the array as one, etc.)

The control program instructs the data logging system (see Keithley section below) to multiplex through the detectors to read and save the resistance data from each element. This process is completely controlled by the Keithley system, independent of the control computer, based on the set-up instructions. Once the resistance values of all the specified elements have been saved in the DMM memory, the DMM sends a command to the central computer indicating this state. The central computer then requests the data which is sent over the GPIB line. This data is saved in a data file defined by the prefix name on the "Nose" front panel and the suffix value supplied in the method file (column 2). Upon completion of the data transfer, the DMM clears its memory and waits for the next initiate command from the central computer. This process of multiplex, data storage, data transfer, clear buffer, and re-initiate continues for the number of seconds specified in the method file (column 3). The next line in the method file is then read, and the system is reconfigured to the new settings. Once configuration is complete (usually < 1 s), the data collection process starts again.

The state of the solenoids and MFCs during the data collection is dictated by the user's method file. The data collection is independent of the state of the flow system. To review: 1) the data collection system is configured; 2) the first line of the method file is read; 3) the data collection cycle begins and continues for the number of seconds specified; 4) the next line of the method file is read and the system re-configured; 5) data collection begins again.

After all the lines in the method file are finished, the "Nose" control program re-sets the data collection system into a stand-by mode, turns off all MFCs, closes all solenoids, and powers down the relay board. This configures the instrument such that no components of the system have any

control voltages supplied to them. This allows the computer to be powered down or the system to be left for indefinite periods of time if necessary.

Keithley instruments have a custom command syntax that must be used to communicate with these devices. In order to set up the data logging system the LabVIEW "Nose" control program (described above) sends a series of configuration commands in the Keithley command syntax to the DMM and MUX. This set-up sequence assume the Keithley units are in the configuration they have when powered-up. After the initial set-up of the two instruments, the DMM and MUX interact with the central computer as described in the previous section. The commands that are sent to the data logging system from the "Nose" program to initiate a (multiplex)/(store data)/(send data) sequence are outlined below. Italicized words below are values input by the user on the "Nose" front panel. They are inserted into this command script by the "Nose" program before being sent to the data logging system.

Set-up 2002

*RST
*CLS
:SENS1:FUNC 'RES'
:SENS1:RES:NPLC 1
:SENS1:RES:DIG *resolution value*
:SENS1:RES:RANG:AUTO 1
:SENS1:RES:RANG:AUTO:ULIM *expected upper limit*
:SENS1:RES:RANG:AUTO:LLIM *expected lower limit*
:ROUT:SCAN:EXT (@ *channel list*)
:ROUT:SCAN:EXT:FUNC: (@ *channel list*), 'RES'
:TRIG:COUN *number of channels*
:ARM:SOUR IMM
:ARM:COUN 1
:ARM:TCON:DIR ACC
:ARM:LAY2:COUN INF
:ARM:LAY2:TCON:DIR ACC
:TRIG:SOURCE TLINK
:TRIG:TCON:PROT ASYN
:TRIG:TCON:DIR ACC
:TRIG:TCON:ASYN:ILIN 2
:TRIG:TCON:ASYN:OLIN 1
:ROUT:SCAN:LSEL EXT
:INIT:CONT ON
:TRAC:EGR COMP
:TRAC:POIN:AUTO 1
:TRAC:FEED SENS
:TRAC:FEED:CONT NEXT
*SRE 1
:STAT:MEAS:ENAB 640
:STAT:MEAS:PTR 512
:STAT:MEAS:NTR 128
:ABOR

Set Up 7001

*CLS
:INIT:CONT OFF
:ARM:SOUR IMM
:ARM:COUN 1
:ARM:TCON:DIR ACC
:ARM:LAY2:SOUR IMM
:ARM:LAY2:COUN 1
:ARM:LAY2:TCON:DIR ACC
:TRIG:SOUR TLIN
:TRIG:COUN:AUTO 1
:TRIG:TCON:PROT ASYN
:TRIG:TCON:ASYN:ILIN 1
:TRIG:TCON:ASYN:OLIN 0
:TRIG:TCON:DIR SOUR
:ROUT:SCAN (@ *channel list*)
:ABOR

After this set-up, a while loop in the "Nose" program runs until a timer equals the time set by the user method file. The first sub-routine in the "Nose" program is called "SCAN CHAN" which initiates scanning through the resistors. The resistance values are automatically stored in the DMM.

Send 7001; :INIT

During scanning, the DMM is asked by the "Nose" program over and over again if its data storage buffer is full (the buffer size set by the number of resistors indicated on the "Nose" front panel).

Send 2002; :STAT:MEAS?

This query continues until the DMM returns the status register value 512 which means the data storage buffer is full. When 512 is returned the DMM is commanded to send the contents of the buffer.

Send 2002; :TRAC:DATA?

The contents of the buffer are saved by the central computer in a file designated by the user in the method file and the "Nose" front panel. The DMM is commanded to clear the contents of the data buffer.

Send 2002; :TRAC:CLE; :TRAC:FEED:CONT NEXT

The DMM is then queried if the data buffer is clear.

Send 2002; :STAT:MEAS?

When status register 128 is returned indicating the buffer has been cleared, the "Nose" program returns to the sub-routine "SCAN CHAN" and sends the next initiation command.

Send 7001; :INIT

When the last line of the method file is complete, commands are sent to the DMM and the MUX to reset their configuration to the state they are in when powered-up. Send 2002; *CLS; *RST

Send 7001; *CLS; *RST; :OPEN ALL

VI. Conclusions

The flow system described here greatly simplifies the process of evaluating custom vapor sensitive detectors. Now it is possible to collect resistance values and generate variable concentrations of analyte vapor over long periods of time with little user monitoring or input. Furthermore, the system described is very flexible and modular which allows custom experiments, of a nature unknown at the present, to be performed.

VII. References

1)Grate, J. W.; Ballantine, D. S.; Wohltjen, H. *Sensors and Actuators* **1987**, *11*, 173.

2)Atkins, P. W. *Physical Chemistry*; W.H. Freeman and Co.: New York, NY, 1994.

Figure 8.1: Illustrative overview of the main components of the automated detector evaluation system.

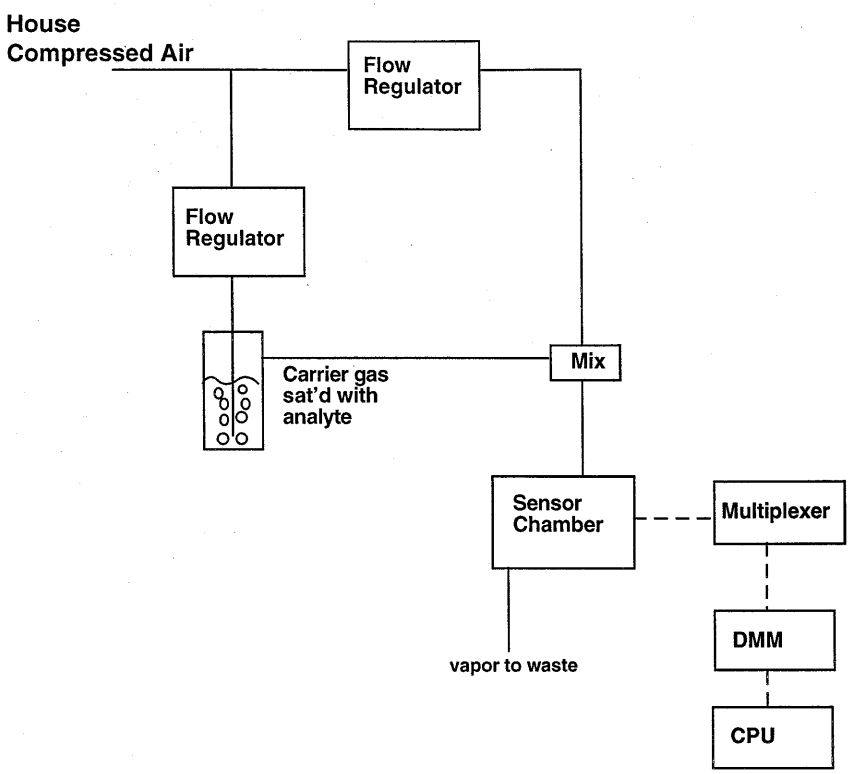
House
Compressed Air
Flow
Regulator
Flow
Regulator
Carrier gas
sat'd with
analyte
Mix
Sensor
Chamber
Multiplexer
DMM
CPU
vapor to waste

Figure 8.1

Figure 8.2: Detailed schematic of the gas delivery lines for the automated vapor generation system.

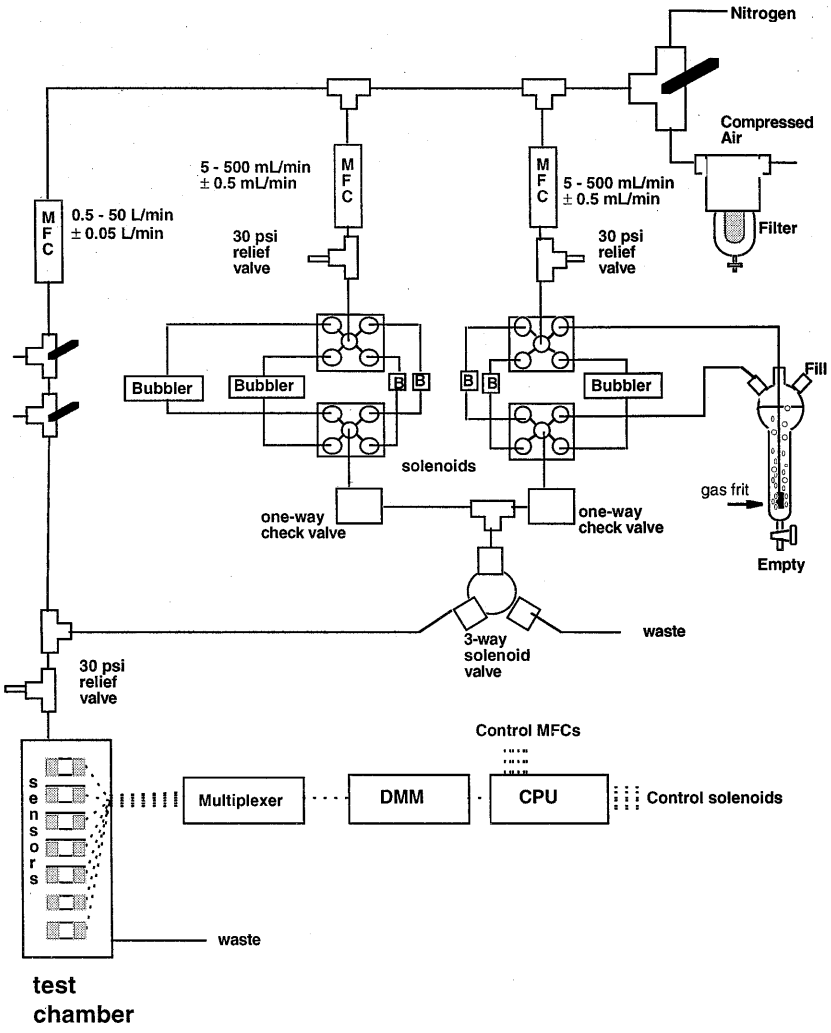
Nitrogen
Compressed Air
Filter
5 - 500 mL/min ± 0.5 mL/min
MFC
0.5 - 50 L/min ± 0.05 L/min
30 psi relief valve
Bubbler
B
solenoids
one-way check valve
Fill
gas frit
Empty
3-way solenoid valve
waste
Control MFCs
Multiplexer
DMM
CPU
Control solenoids
sensors
test chamber

Figure 8.2

Figure 8.3: Detailed schematic of the wiring and communication lines for the automated vapor generation system.

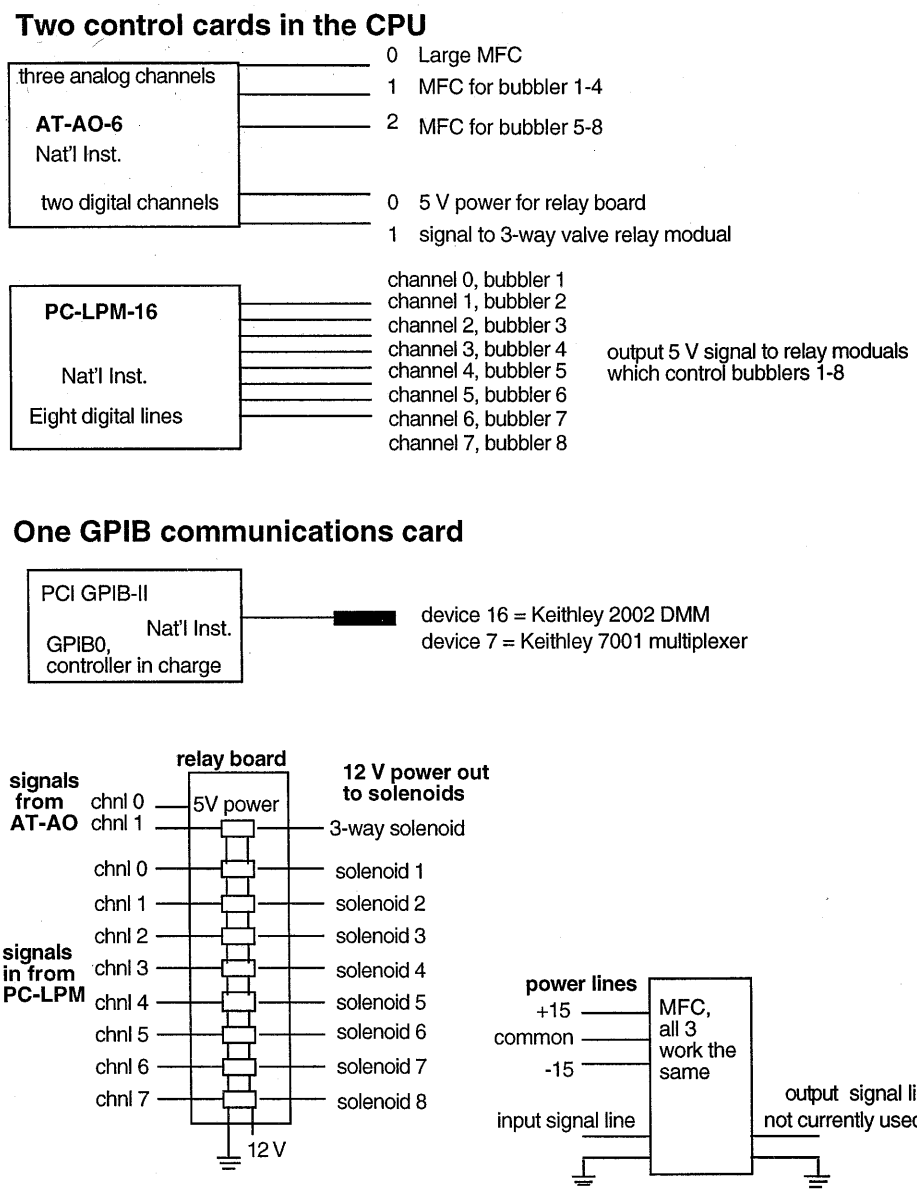
Two control cards in the CPU
three analog channels
AT-AO-6
Nat'l Inst.
two digital channels
0 Large MFC
1 MFC for bubbler 1-4
2 MFC for bubbler 5-8
0 5 V power for relay board
1 signal to 3-way valve relay modual
PC-LPM-16
Nat'l Inst.
Eight digital lines
channel 0, bubbler 1
channel 1, bubbler 2
channel 2, bubbler 3
channel 3, bubbler 4
channel 4, bubbler 5
channel 5, bubbler 6
channel 6, bubbler 7
channel 7, bubbler 8
output 5 V signal to relay moduals which control bubblers 1-8
One GPIB communications card
PCI GPIB-II
Nat'l Inst.
GPIB0, controller in charge
device 16 = Keithley 2002 DMM
device 7 = Keithley 7001 multiplexer
relay board
signals from AT-AO
chnl 0
chnl 1
5V power
12 V power out to solenoids
3-way solenoid
chnl 0
chnl 1
chnl 2
chnl 3
chnl 4
chnl 5
chnl 6
chnl 7
signals in from PC-LPM
solenoid 1
solenoid 2
solenoid 3
solenoid 4
solenoid 5
solenoid 6
solenoid 7
solenoid 8
12 V
power lines
+15
common
-15
MFC, all 3 work the same
input signal line
output signal line
not currently used

Figure 8.3

Table 8.1: Calibration correction equation and coefficients for the three mass flow controllers used in the described system.

$\mathbf{Y} = A + B*(\mathbf{X}) + C*(\mathbf{X}^2)$

X is the flow rate desired from the MFC

Y is the voltage applied to the MFC to achieve the desired flow

	A	**B**	**C**
Background MFC	1.06E-02	9.91E-05	-1.33E-10
MFC for bubblers #1 - #5	1.99E-02	1.00E-02	1.15E-06
MFC for bubblers #5 - #8	6.32E-02	1.00E-02	7.47E-07

Table 8.2: A short excerpt from a typical method file used by the "NOSE" control program determine the status of all the components in the system during an automated vapor delivery and data collection sequence.

Table 8.2

save?	name	seconds	bkgrd	left MFC	Right MFC	relay	3-way	# 1	# 2	# 3	# 4	# 5	# 6	# 7	# 8
0	999	1800	3.00	0.00	0.00	0	0	0	0	0	0	0	0	0	0
1	1	30	2.00	0.00	1.00	1	0	1	0	0	0	0	0	0	0
1	1	60	1.99	0.00	1.00	1	1	1	0	0	0	0	0	0	0
1	1	90	2.00	0.00	0.00	1	0	0	0	0	0	0	0	0	0
1	2	30	2.00	4.76	0.00	1	0	0	0	0	0	0	1	0	0
1	2	60	1.95	4.76	0.00	1	1	0	0	0	0	0	1	0	0
1	2	90	2.00	0.00	0.00	1	0	0	0	0	0	0	0	0	0
1	3	60	2.00	4.76	1.00	1	0	1	0	0	0	0	1	0	0
1	3	30	1.99	0.00	1.00	1	1	1	0	0	0	0	0	0	0
1	3	30	1.94	4.76	1.00	1	1	1	0	0	0	0	1	0	0
1	3	90	2.00	0.00	0.00	1	0	0	0	0	0	0	0	0	0

Appendix

Control Program for Automated

Vapor Generation And Data collection system

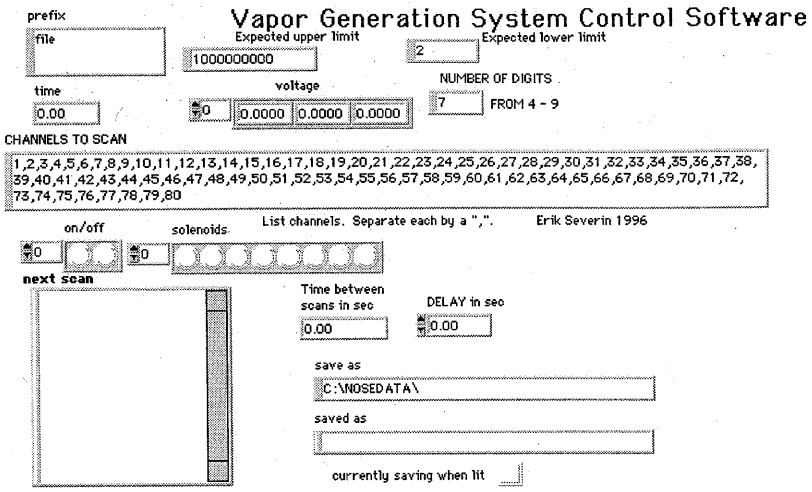
prefix
file
Vapor Generation System Control Software
Expected upper limit
1000000000
Expected lower limit
2
time
0.00
voltage
0
0.0000
0.0000
0.0000
NUMBER OF DIGITS
7
FROM 4 - 9
CHANNELS TO SCAN
1,2,3,4,5,6,7,8,9,10,11,12,13,14,15,16,17,18,19,20,21,22,23,24,25,26,27,28,29,30,31,32,33,34,35,36,37,38,
39,40,41,42,43,44,45,46,47,48,49,50,51,52,53,54,55,56,57,58,59,60,61,62,63,64,65,66,67,68,69,70,71,72,
73,74,75,76,77,78,79,80
List channels. Separate each by a ",".
Erik Severin 1996
on/off
solenoids
0
0
next scan
Time between
scans in sec
0.00
DELAY in sec
0.00
save as
C:\NOSEDATA\
saved as
currently saving when lit

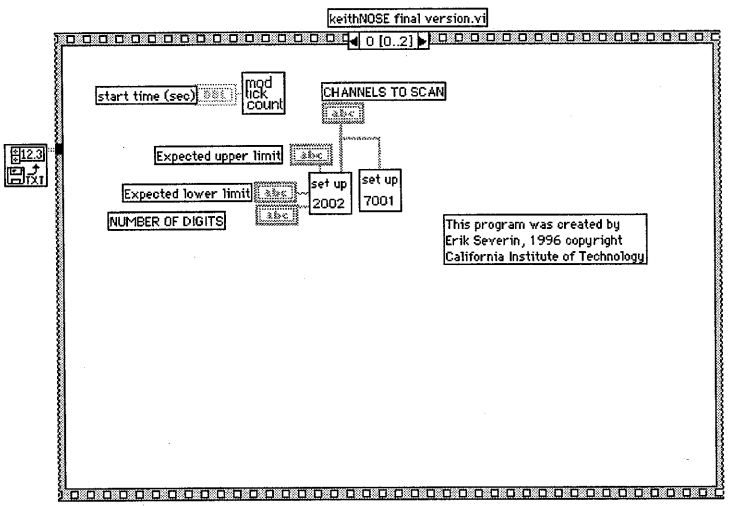
keithNOSE final version.vi
0 [0..2]
start time (sec)
mod tick count
CHANNELS TO SCAN
Expected upper limit
Expected lower limit
NUMBER OF DIGITS
set up 2002
set up 7001
This program was created by
Erik Severin, 1996 copyright
California Institute of Technology

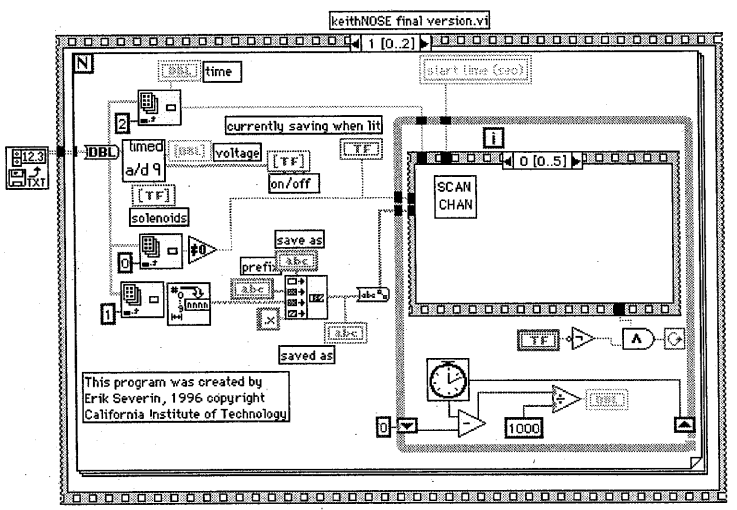
keithNOSE final version.vi
1 [0..2]
time
start time (sec)
currently saving when lit
timed a/d 9
voltage
on/off
solenoids
save as
prefix
saved as
0 [0..5]
SCAN CHAN
1000
This program was created by
Erik Severin, 1996 copyright
California Institute of Technology

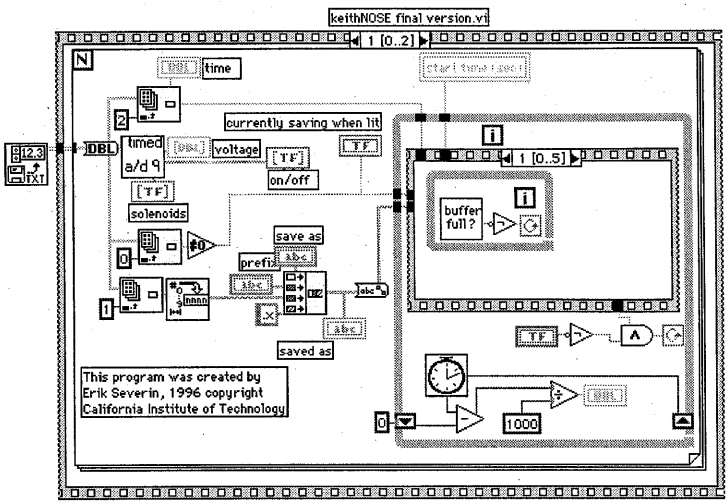
keithNOSE final version.vi
1 [0..2]
time
start time (sec)
currently saving when lit
timed a/d 9
voltage
on/off
solenoids
save as
prefix
saved as
1 [0..5]
buffer full?
This program was created by
Erik Severin, 1996 copyright
California Institute of Technology
1000

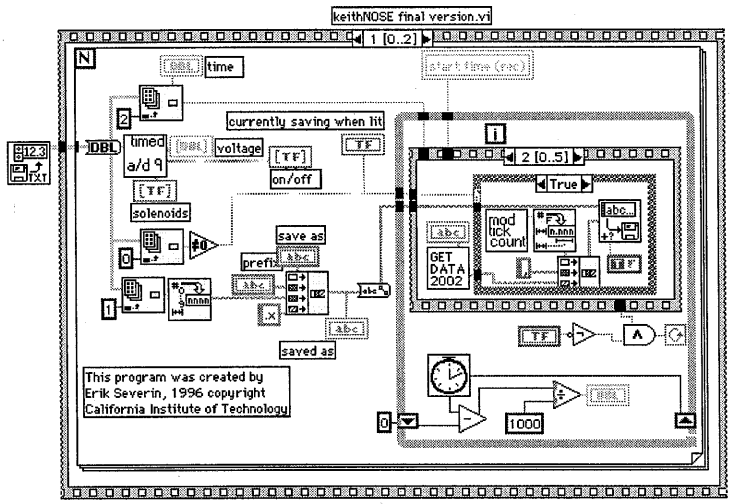
keithNOSE final version.vi
1 [0..2]
time
start time (sec)
currently saving when lit
timed a/d 9
voltage
on/off
solenoids
save as
prefix
saved as
2 [0..5]
True
mod tick count
GET DATA 2002
This program was created by
Erik Severin, 1996 copyright
California Institute of Technology
1000

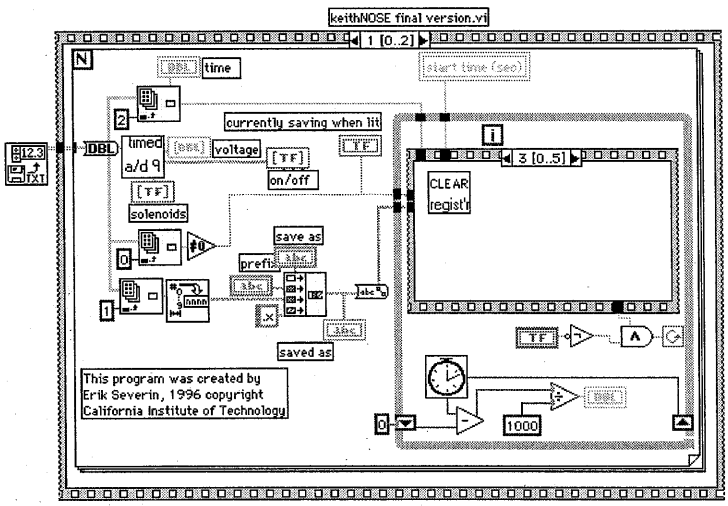
keithNOSE final version.vi
1 [0..2]
time
start time (sec)
currently saving when lit
timed a/d 9
voltage
on/off
solenoids
save as
prefix
saved as
3 [0..5]
CLEAR regist'
This program was created by
Erik Severin, 1996 copyright
California Institute of Technology
1000

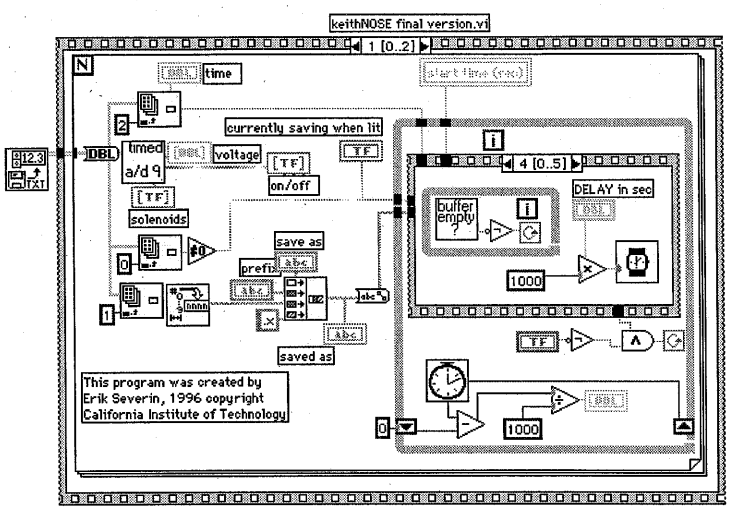
keithNOSE final version.vi
1 [0..2]
time
currently saving when lit
timed a/d 9
voltage
on/off
solenoids
save as
prefix
saved as
4 [0..5]
buffer empty
DELAY in sec
1000
This program was created by
Erik Severin, 1996 copyright
California Institute of Technology

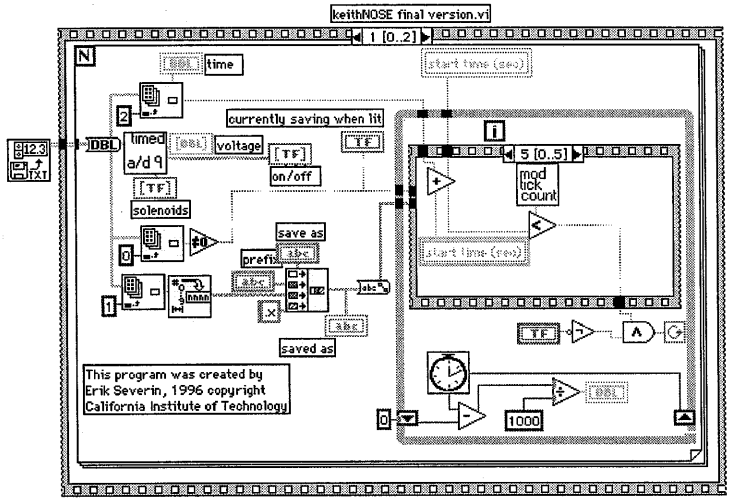
keithNOSE final version.vi
1 [0..2]
time
currently saving when lit
timed a/d 9
voltage
on/off
solenoids
save as
prefix
saved as
5 [0..5]
mod tick count
1000
This program was created by
Erik Severin, 1996 copyright
California Institute of Technology

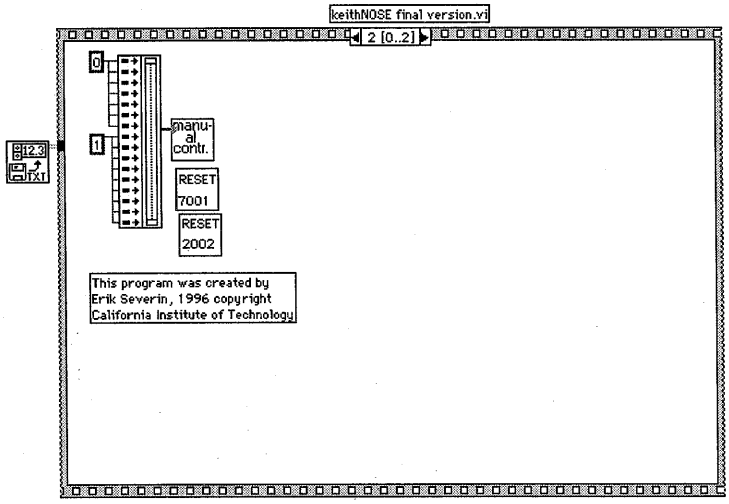
keithNOSE final version.vi
2 [0..2]
manu-al contr.
RESET 7001
RESET 2002
This program was created by
Erik Severin, 1996 copyright
California Institute of Technology

****

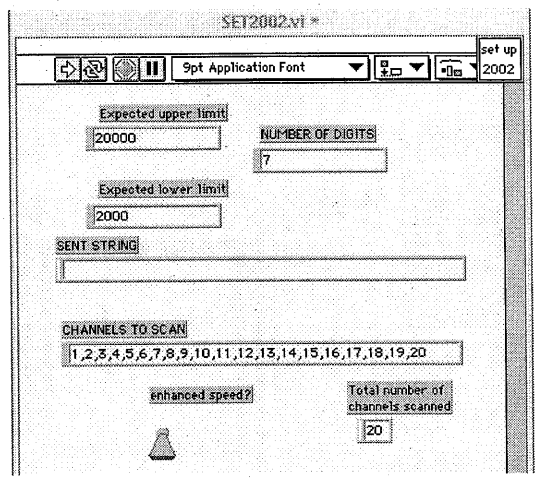
SET2002.vi *
9pt Application Font
set up 2002
Expected upper limit
20000
NUMBER OF DIGITS
7
Expected lower limit
2000
SENT STRING
CHANNELS TO SCAN
1,2,3,4,5,6,7,8,9,10,11,12,13,14,15,16,17,18,19,20
enhanced speed?
Total number of channels scanned
20

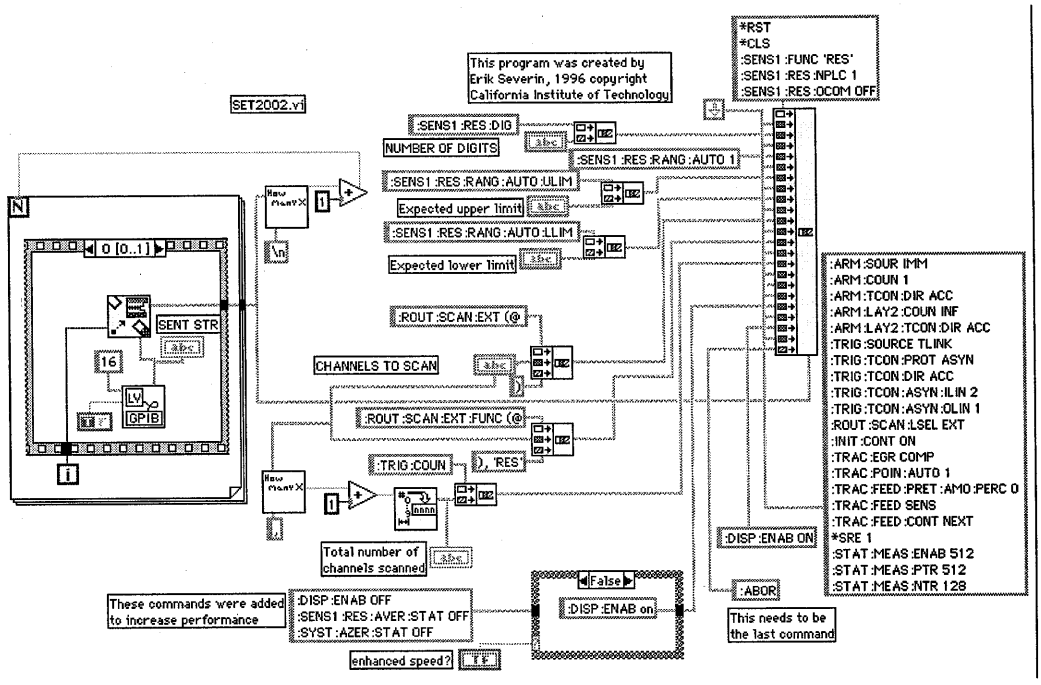
This program was created by
Erik Severin, 1996 copyright
California Institute of Technology
SET2002.vi
*RST
*CLS
:SENS1 :FUNC 'RES'
:SENS1 :RES :NPLC 1
:SENS1 :RES :OCOM OFF
:SENS1 :RES :DIG
NUMBER OF DIGITS
:SENS1 :RES :RANG :AUTO 1
:SENS1 :RES :RANG :AUTO :ULIM
Expected upper limit
:SENS1 :RES :RANG :AUTO :LLIM
Expected lower limit
:ROUT :SCAN :EXT (@
CHANNELS TO SCAN
:ROUT :SCAN :EXT :FUNC (@
:TRIG :COUN
), 'RES'
Total number of channels scanned
These commands were added to increase performance
:DISP :ENAB OFF
:SENS1 :RES :AVER :STAT OFF
:SYST :AZER :STAT OFF
enhanced speed?
False
:DISP :ENAB on
:DISP :ENAB ON
:ABOR
This needs to be the last command
:ARM :SOUR IMM
:ARM :COUN 1
:ARM :TCON :DIR ACC
:ARM :LAY2 :COUN INF
:ARM :LAY2 :TCON :DIR ACC
:TRIG :SOURCE TLINK
:TRIG :TCON :PROT ASYN
:TRIG :TCON :DIR ACC
:TRIG :TCON :ASYN :ILIN 2
:TRIG :TCON :ASYN :OLIN 1
:ROUT :SCAN :LSEL EXT
:INIT :CONT ON
:TRAC :EGR COMP
:TRAC :POIN :AUTO 1
:TRAC :FEED :PRET :AMO :PERC 0
:TRAC :FEED SENS
:TRAC :FEED :CONT NEXT
*SRE 1
:STAT :MEAS :ENAB 512
:STAT :MEAS :PTR 512
:STAT :MEAS :NTR 128
SENT STR
16
GPIB
0 [0..1]

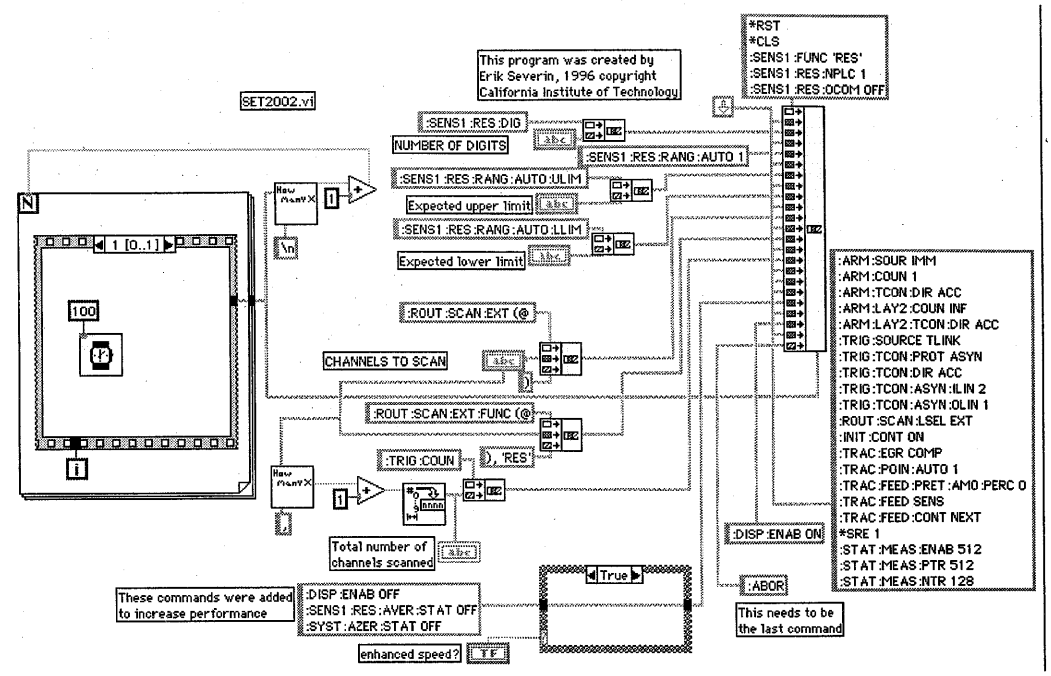
SET2002.vi
This program was created by
Erik Severin, 1996 copyright
California Institute of Technology
*RST
*CLS
:SENS1 :FUNC 'RES'
:SENS1 :RES :NPLC 1
:SENS1 :RES :OCOM OFF
:SENS1 :RES :DIG
NUMBER OF DIGITS
:SENS1 :RES :RANG :AUTO 1
:SENS1 :RES :RANG :AUTO :ULIM
Expected upper limit
:SENS1 :RES :RANG :AUTO :LLIM
Expected lower limit
:ROUT :SCAN :EXT (@
CHANNELS TO SCAN
:ROUT :SCAN :EXT :FUNC (@
:TRIG :COUN
), 'RES'
Total number of
channels scanned
:ARM :SOUR IMM
:ARM :COUN 1
:ARM :TCON :DIR ACC
:ARM :LAY2 :COUN INF
:ARM :LAY2 :TCON :DIR ACC
:TRIG :SOURCE TLINK
:TRIG :TCON :PROT ASYN
:TRIG :TCON :DIR ACC
:TRIG :TCON :ASYN :ILIN 2
:TRIG :TCON :ASYN :OLIN 1
:ROUT :SCAN :LSEL EXT
:INIT :CONT ON
:TRAC :EGR COMP
:TRAC :POIN :AUTO 1
:TRAC :FEED :PRET :AMO :PERC 0
:TRAC :FEED SENS
:TRAC :FEED :CONT NEXT
*SRE 1
:STAT :MEAS :ENAB 512
:STAT :MEAS :PTR 512
:STAT :MEAS :NTR 128
:DISP :ENAB ON
:ABOR
This needs to be
the last command
These commands were added
to increase performance
:DISP :ENAB OFF
:SENS1 :RES :AVER :STAT OFF
:SYST :AZER :STAT OFF
True
enhanced speed?
TF

****

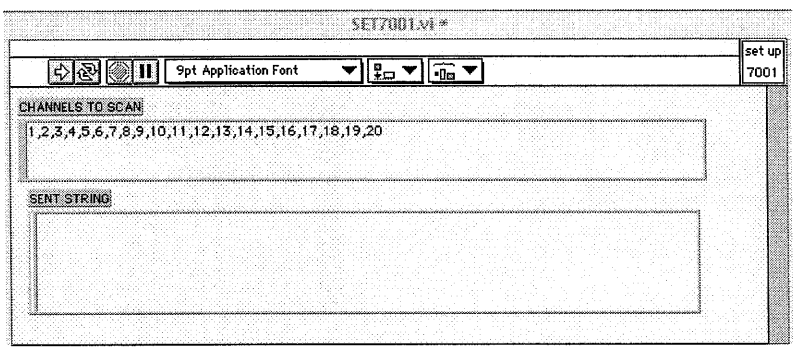
SET7001.vi *
9pt Application Font
set up
7001
CHANNELS TO SCAN
1,2,3,4,5,6,7,8,9,10,11,12,13,14,15,16,17,18,19,20
SENT STRING

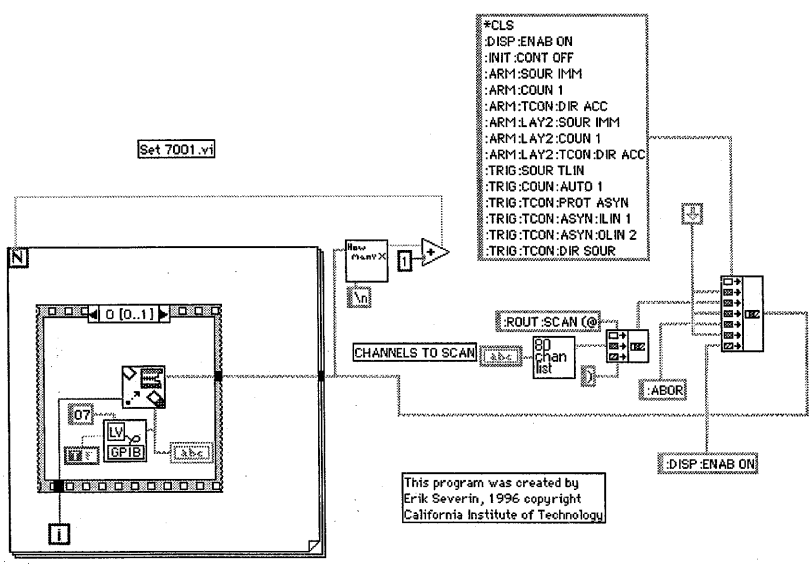
Set 7001.vi
*CLS
:DISP :ENAB ON
:INIT :CONT OFF
:ARM :SOUR IMM
:ARM :COUN 1
:ARM :TCON :DIR ACC
:ARM :LAY2 :SOUR IMM
:ARM :LAY2 :COUN 1
:ARM :LAY2 :TCON :DIR ACC
:TRIG :SOUR TLIN
:TRIG :COUN :AUTO 1
:TRIG :TCON :PROT ASYN
:TRIG :TCON :ASYN :ILIN 1
:TRIG :TCON :ASYN :OLIN 2
:TRIG :TCON :DIR SOUR
:ROUT :SCAN (@
CHANNELS TO SCAN
80
chan
list
:ABOR
:DISP :ENAB ON
This program was created by
Erik Severin, 1996 copyright
California Institute of Technology

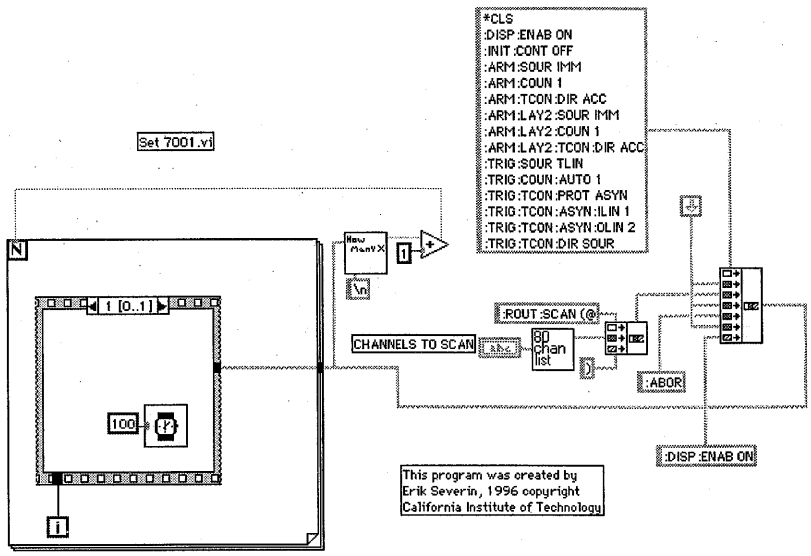
*CLS
:DISP:ENAB ON
:INIT:CONT OFF
:ARM:SOUR IMM
:ARM:COUN 1
:ARM:TCON:DIR ACC
:ARM:LAY2:SOUR IMM
:ARM:LAY2:COUN 1
:ARM:LAY2:TCON:DIR ACC
:TRIG:SOUR TLIN
:TRIG:COUN:AUTO 1
:TRIG:TCON:PROT ASYN
:TRIG:TCON:ASYN:ILIN 1
:TRIG:TCON:ASYN:OLIN 2
:TRIG:TCON:DIR SOUR
Set 7001.vi
1 [0..1]
100
CHANNELS TO SCAN
:ROUT:SCAN (@
80 chan list
:ABOR
:DISP:ENAB ON
This program was created by
Erik Severin, 1996 copyright
California Institute of Technology

****

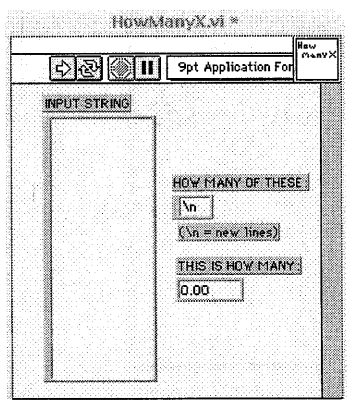
HowManyX.vi *
9pt Application Fon
INPUT STRING
HOW MANY OF THESE
\n
(\n = new lines)
THIS IS HOW MANY
0.00

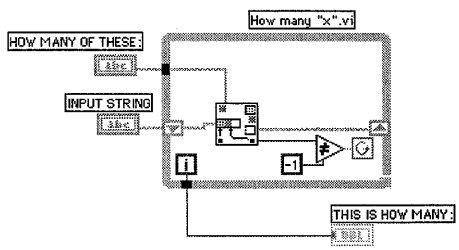
How many "x".vi
HOW MANY OF THESE
INPUT STRING
-1
THIS IS HOW MANY

****

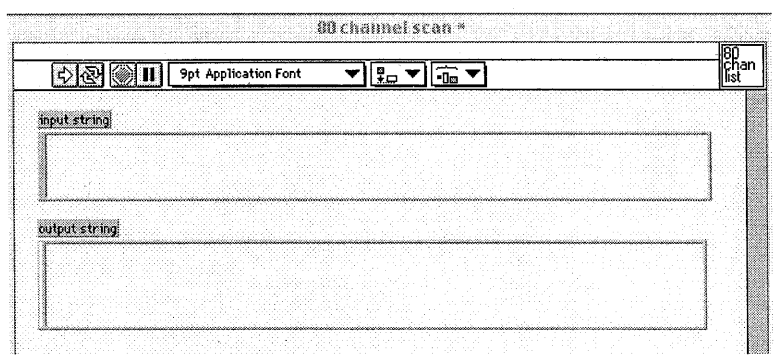
80 channel scan *
9pt Application Font
80 chan list
input string
output string

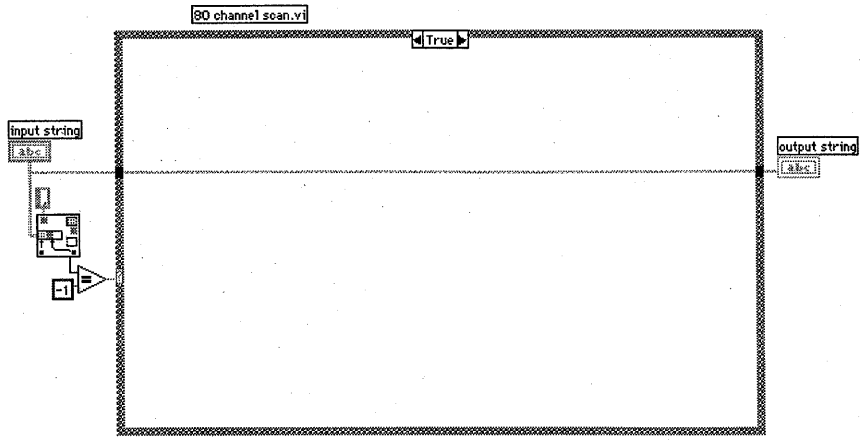
80 channel scan.vi
True
input string
output string
-1

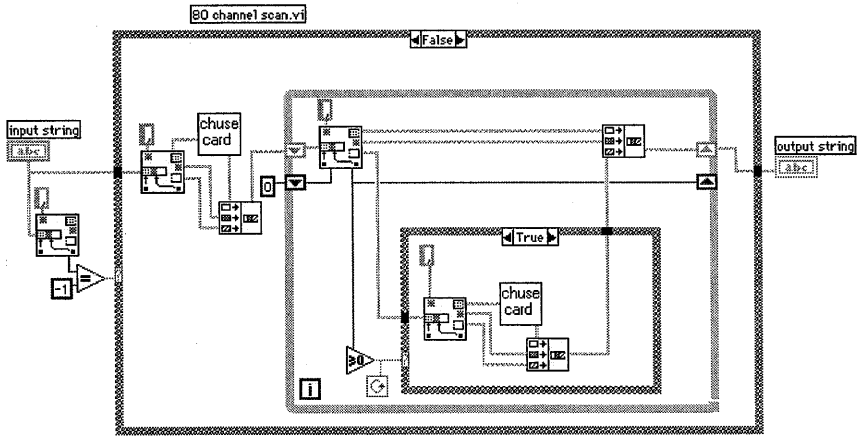
80 channel scan.vi
False
input string
chuse card
0
output string
True
chuse card
-1

****

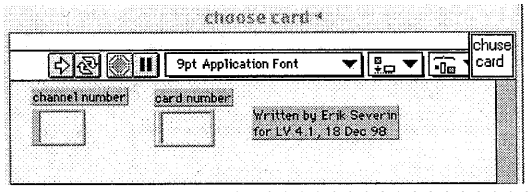
choose card
9pt Application Font
chuse card
channel number
card number
Written by Erik Severin
for LV 4.1, 18 Dec 98

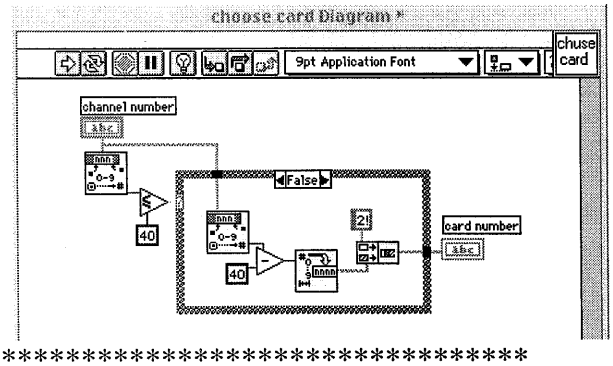
choose card Diagram
9pt Application Font
chuse card
channel number
False
40
2
40
card number

****

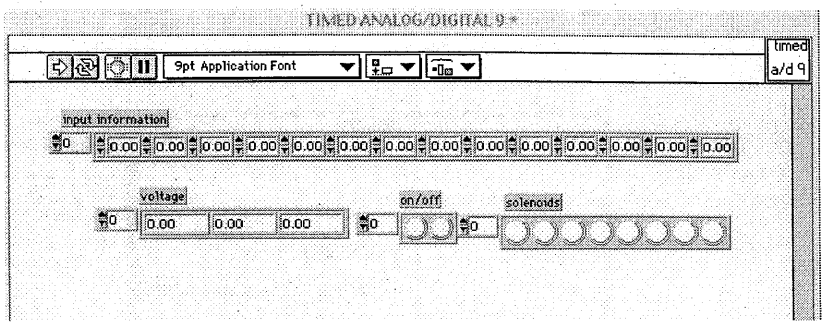
TIMED ANALOG/DIGITAL 9 *
9pt Application Font
timed a/d 9
input information
voltage
on/off
solenoids

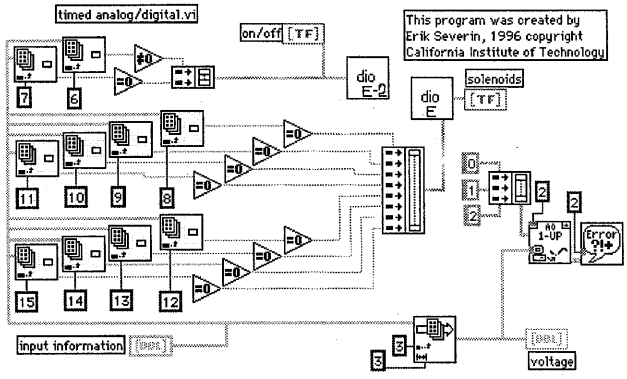
timed analog/digital.vi
on/off [TF]
This program was created by Erik Severin, 1996 copyright California Institute of Technology
dio E-2
dio E
solenoids
[TF]
1-UP
error
input information
[DBL]
voltage

****

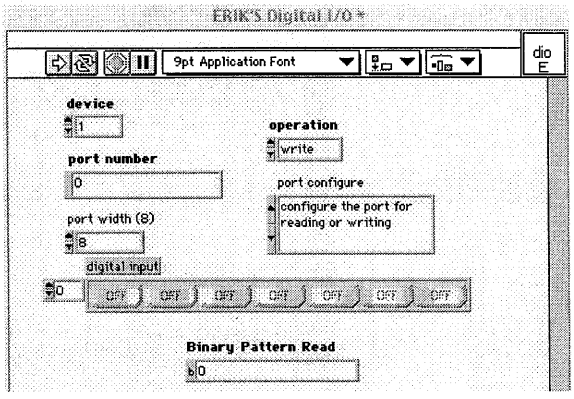
ERIK'S Digital I/O *
9pt Application Font
dio E
device
operation
write
port number
port configure
configure the port for reading or writing
port width (8)
digital input
OFF
Binary Pattern Read

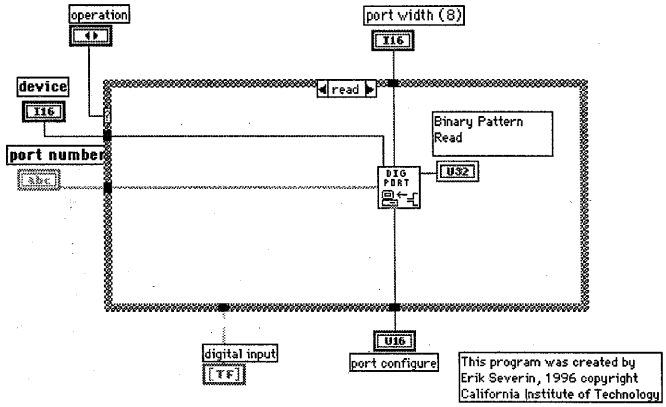
operation
port width (8)
I16
device
read
port number
Binary Pattern Read
DIG PORT
U32
digital input
TF
U16
port configure
This program was created by Erik Severin, 1996 copyright California Institute of Technology

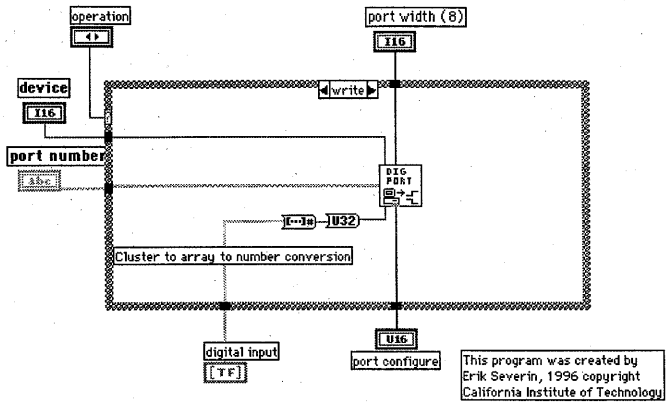
operation
port width (8)
I16
device
I16
write
port number
DIG PORT
U32
Cluster to array to number conversion
digital input
TF
U16
port configure
This program was created by
Erik Severin, 1996 copyright
California Institute of Technology

****

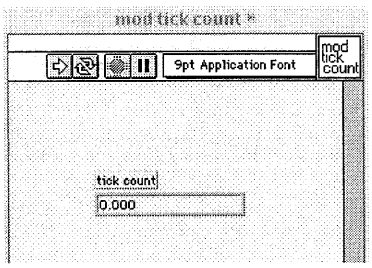
mod tick count *
9pt Application Font
mod tick count
tick count
0.000

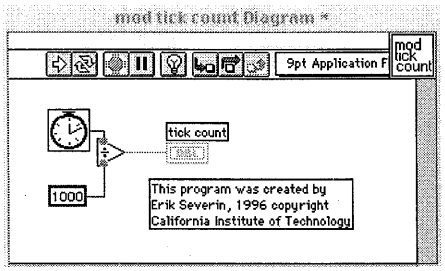
mod tick count Diagram *
9pt Application F
mod tick count
tick count
1000
This program was created by
Erik Severin, 1996 copyright
California Institute of Technology

****

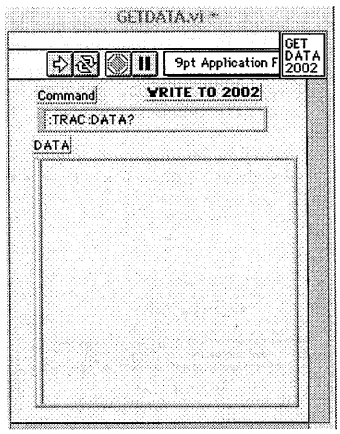
GETDATA.vi *
9pt Application F
GET DATA 2002
Command
WRITE TO 2002
:TRAC:DATA?
DATA

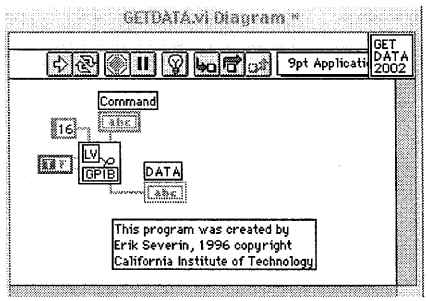
GETDATA.vi Diagram *
9pt Applicatn
GET DATA 2002
Command
16
LV
GPIB
DATA
This program was created by
Erik Severin, 1996 copyright
California Institute of Technology

****

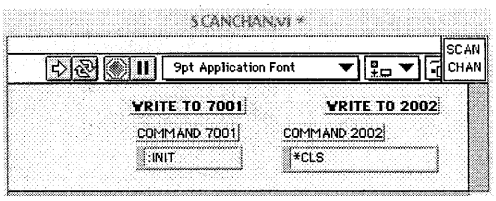
SCANCHAN.vi *
9pt Application Font
SCAN CHAN
WRITE TO 7001
WRITE TO 2002
COMMAND 7001
:INIT
COMMAND 2002
*CLS

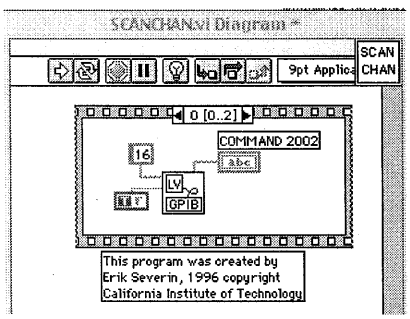
SCANCHAN.vi Diagram *
9pt Applica
SCAN CHAN
0 [0..2]
COMMAND 2002
16
LV
GPIB
This program was created by
Erik Severin, 1996 copyright
California Institute of Technology

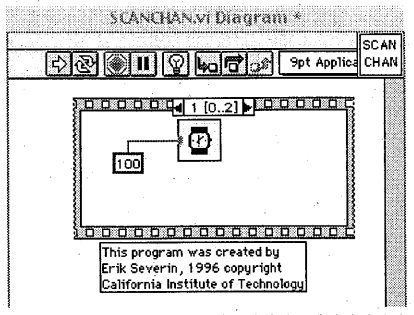
SCANCHAN.vi Diagram *
SCAN CHAN
1 [0..2]
100
This program was created by
Erik Severin, 1996 copyright
California Institute of Technology

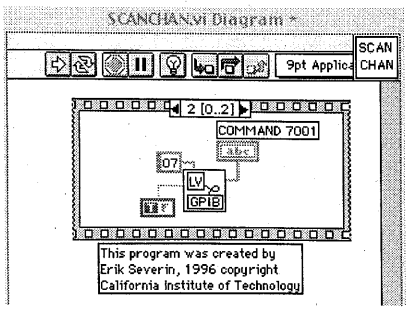
SCANCHAN.vi Diagram *
SCAN CHAN
2 [0..2]
COMMAND 7001
07
GPIB
This program was created by
Erik Severin, 1996 copyright
California Institute of Technology

****

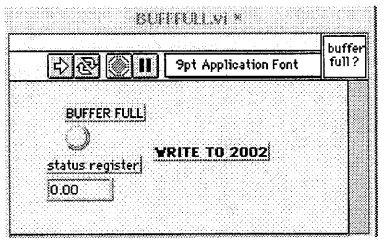
BUFFFULL.vi *
9pt Application Font
buffer full ?
BUFFER FULL
status register
WRITE TO 2002
0.00

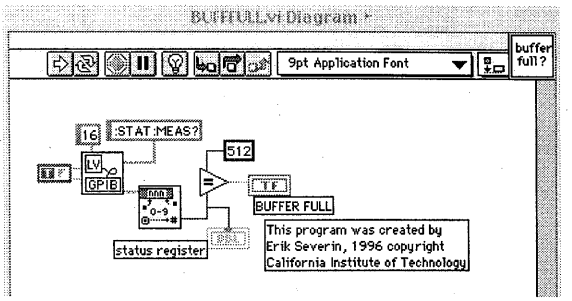
BUFFFULL.vi Diagram *
9pt Application Font
buffer full ?
16
:STAT:MEAS?
512
TF
BUFFER FULL
status register
This program was created by
Erik Severin, 1996 copyright
California Institute of Technology

****

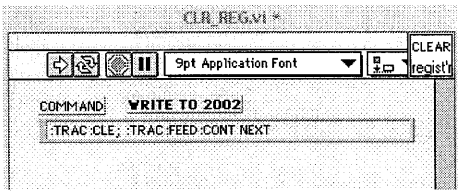
CLR_REG.vi *
9pt Application Font
CLEAR regist'r
COMMAND
WRITE TO 2002
:TRAC:CLE ; :TRAC:FEED:CONT NEXT

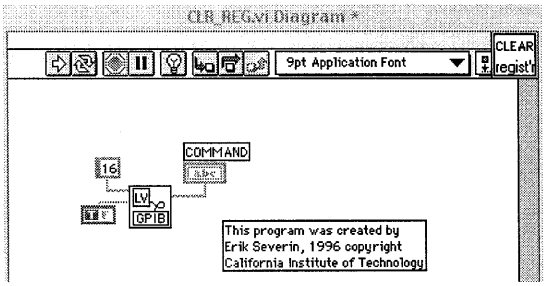
CLR_REG.vi Diagram *
9pt Application Font
CLEAR regist'r
16
COMMAND
This program was created by
Erik Severin, 1996 copyright
California Institute of Technology

****

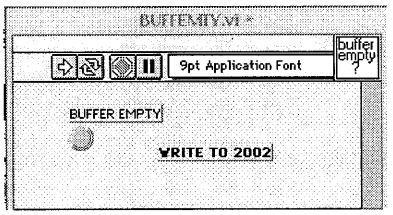
BUFFEMTY.vi *
9pt Application Font
buffer empty ?
BUFFER EMPTY
WRITE TO 2002

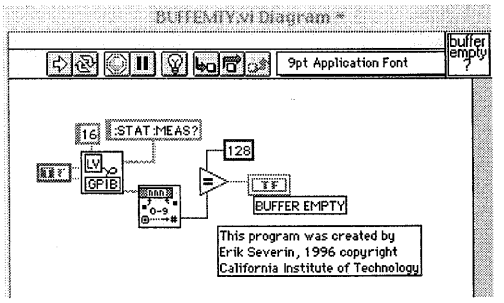
BUFFEMTY.vi Diagram *
9pt Application Font
buffer empty ?
16
:STAT:MEAS?
128
TF
BUFFER EMPTY
This program was created by
Erik Severin, 1996 copyright
California Institute of Technology

****

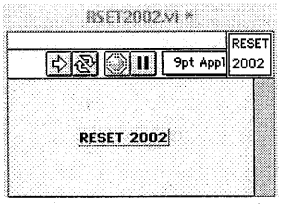
RSET2002.vi *
9pt Appl
RESET 2002
RESET 2002

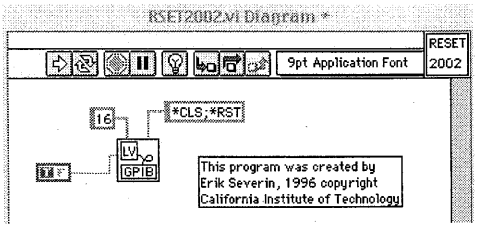
RSET2002.vi Diagram *
9pt Application Font
RESET 2002
16
*CLS;*RST
This program was created by
Erik Severin, 1996 copyright
California Institute of Technology

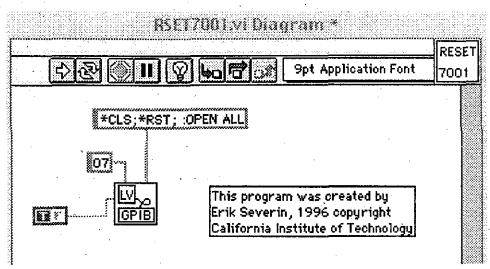
RSET7001.vi Diagram *
9pt Application Font
RESET 7001
*CLS;*RST; :OPEN ALL
07
GPIB
This program was created by
Erik Severin, 1996 copyright
California Institute of Technology

****

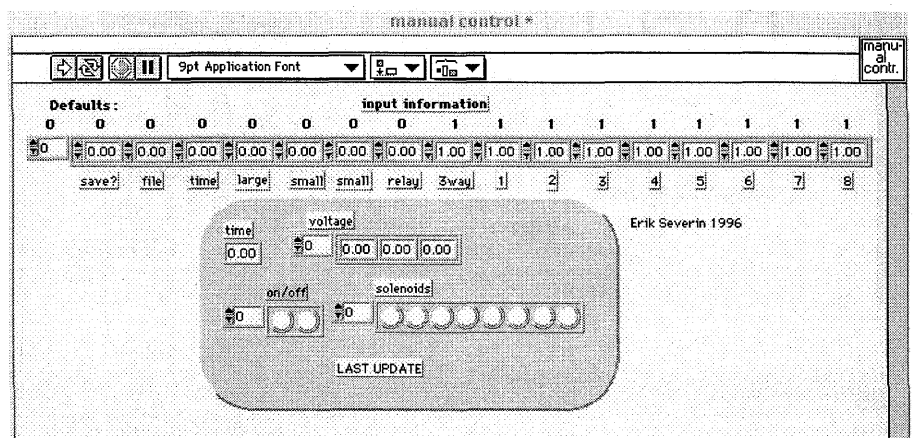
manual control *
9pt Application Font
manu-al contr.
Defaults :
input information
save?
file
time
large
small
small
relay
3way
time
voltage
on/off
solenoids
LAST UPDATE
Erik Severin 1996

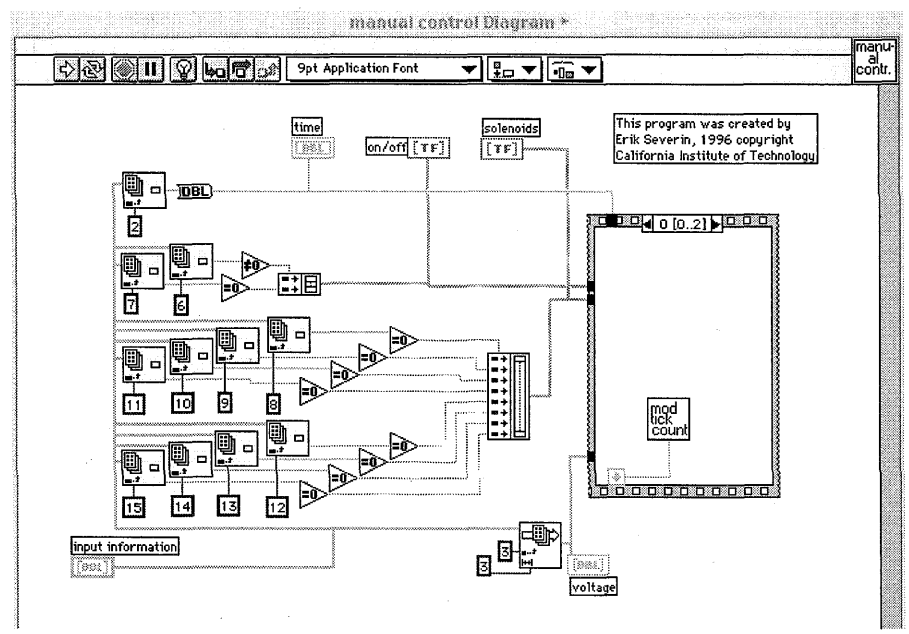
manual control Diagram *
9pt Application Font
manu-al contr.
time
on/off
solenoids
This program was created by
Erik Severin, 1996 copyright
California Institute of Technology
DBL
TF
0 [0..2]
mod tick count
input information
voltage

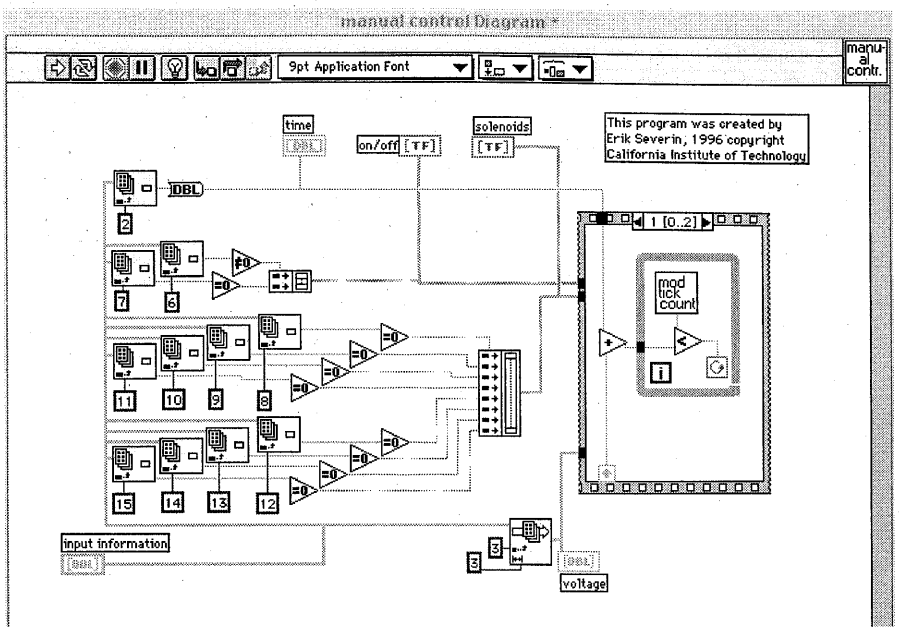
manual control Diagram *
9pt Application Font
manu-
al
contr.
time
DBL
on/off
TF
solenoids
TF
This program was created by
Erik Severin, 1996 copyright
California Institute of Technology
DBL
2
7
6
1 [0..2]
mod
tick
count
11
10
9
8
15
14
13
12
input information
DBL
3
DBL
voltage

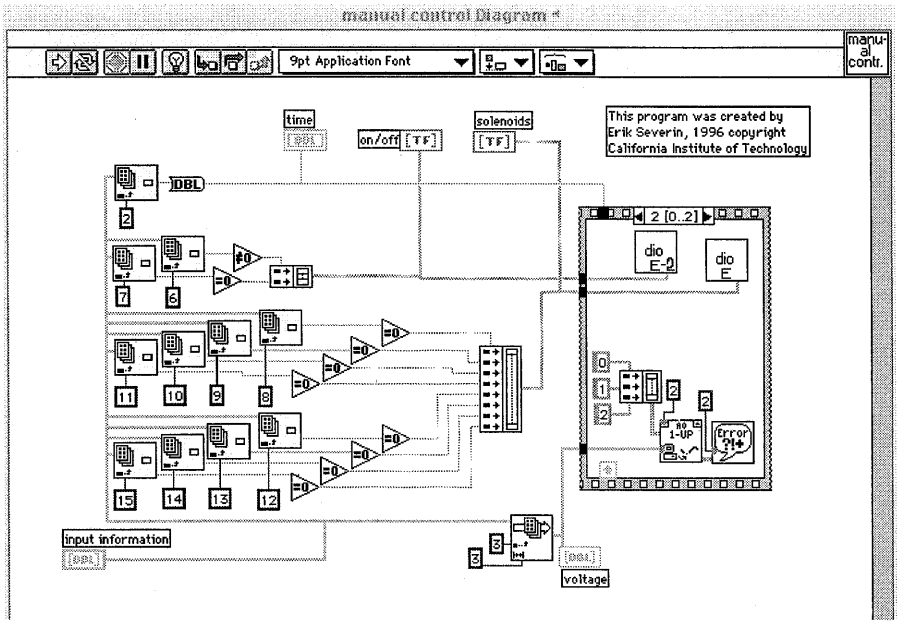
manual control Diagram *
9pt Application Font
manu-
al
contr.
time
DBL
on/off
TF
solenoids
TF
This program was created by
Erik Severin, 1996 copyright
California Institute of Technology
DBL
2
7
6
2 [0..2]
dio
E-0
dio
E
11
10
9
8
15
14
13
12
0
1
2
2
2
1-UP
error
input information
DBL
3
DBL
voltage

****

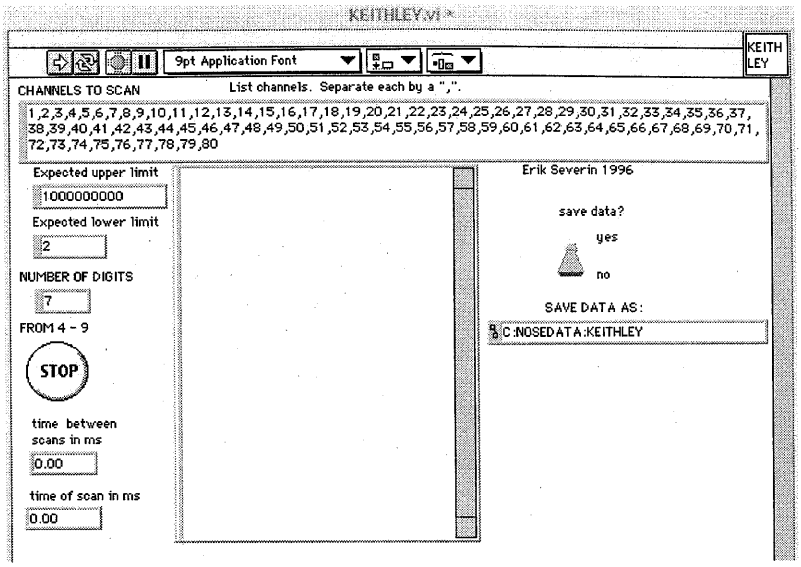
KEITHLEY.vi *
9pt Application Font
KEITH LEY
CHANNELS TO SCAN
List channels. Separate each by a ",".
1,2,3,4,5,6,7,8,9,10,11,12,13,14,15,16,17,18,19,20,21,22,23,24,25,26,27,28,29,30,31,32,33,34,35,36,37,38,39,40,41,42,43,44,45,46,47,48,49,50,51,52,53,54,55,56,57,58,59,60,61,62,63,64,65,66,67,68,69,70,71,72,73,74,75,76,77,78,79,80
Expected upper limit
1000000000
Expected lower limit
2
NUMBER OF DIGITS
7
FROM 4 - 9
STOP
time between scans in ms
0.00
time of scan in ms
0.00
Erik Severin 1996
save data?
yes
no
SAVE DATA AS:
C:\NOSEDATA\KEITHLEY

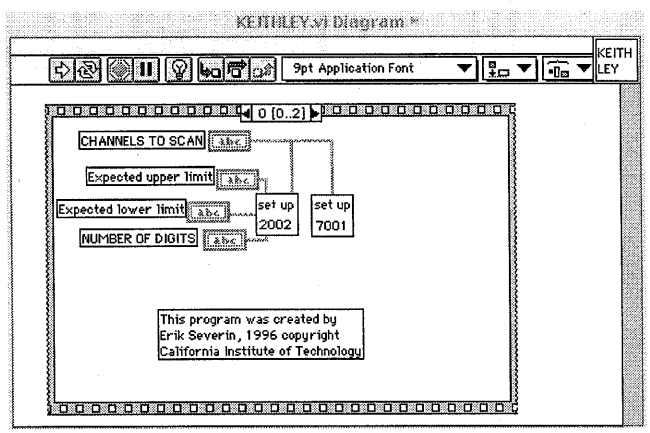
KEITHLEY.vi Diagram *
9pt Application Font
KEITH LEY
0 [0..2]
CHANNELS TO SCAN
Expected upper limit
Expected lower limit
NUMBER OF DIGITS
set up 2002
set up 7001
This program was created by Erik Severin, 1996 copyright California Institute of Technology

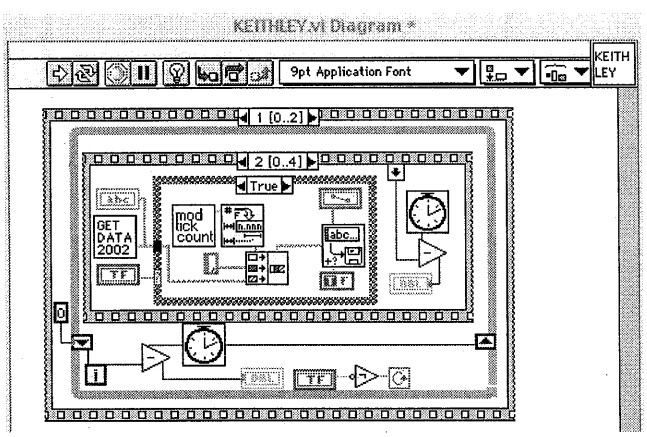
KEITHLEY.vi Diagram *
9pt Application Font
KEITH LEY
1 [0..2]
2 [0..4]
True
GET DATA 2002
mod tick count
TF

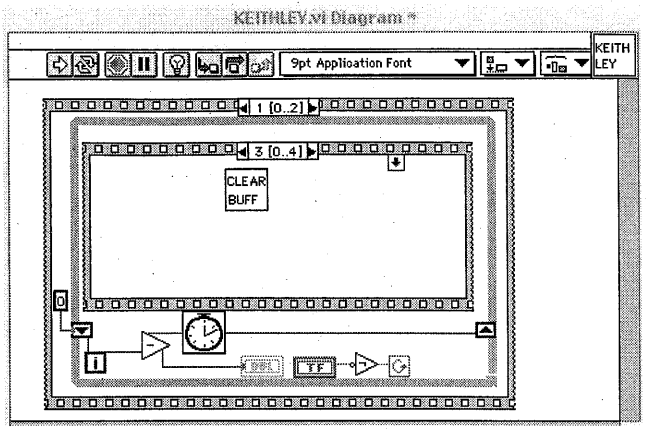
KEITHLEY.vi Diagram *
9pt Application Font
KEITH LEY
1 [0..2]
3 [0..4]
CLEAR BUFF
0
i
DBL
TF

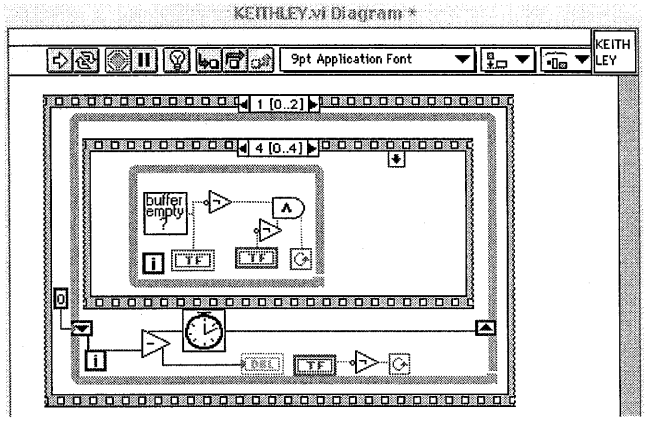
KEITHLEY.vi Diagram *
9pt Application Font
KEITH LEY
1 [0..2]
4 [0..4]
buffer empty ?
i
TF
0
DBL

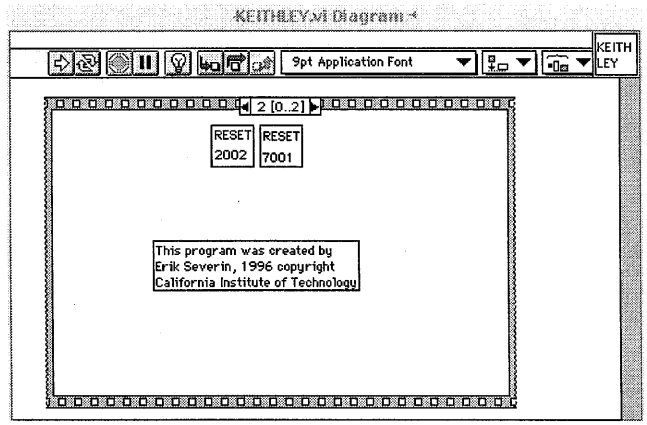
KEITHLEY.vi Diagram *
9pt Application Font
KEITH LEY
2 [0..2]
RESET 2002
RESET 7001
This program was created by
Erik Severin, 1996 copyright
California Institute of Technology

****